# THE ROLE OF PERIODONTAL INFECTION IN THE PATHOGENESIS OF ALZHEIMER'S DISEASE

by

Shalini Kanagasingam

(G20736001)

A thesis submitted in partial fulfilment of the requirements
for the degree of Doctor of Philosophy
at the University of Central Lancashire

May 2025

## RESEARCH STUDENT DECLARATION FORM

**Type of Award** _____**PhD**_____
**School** _____**Medicine & Dentistry**___

**1. Concurrent registration for two or more academic awards**

I declare that while registered as a candidate for the research degree, I have not been a registered candidate or enrolled student for another award of the University or other academic or professional institution.

**2. Material submitted for another award**

I declare that no material contained in the thesis has been used in any other submission for an academic award and is solely my own work

**3. Collaboration**

Where a candidate's research programme is part of a collaborative project, the thesis must indicate in addition clearly the candidate's individual contribution and the extent of the collaboration. Please state below:

I declare that the following work was undertaken in collaboration:

- Transmission Electron Microscope (TEM) work was outsourced to Dr Christopher Von Ruhland, Central Biotechnology Services Cardiff University due to lack of facilities at UCLAN.
- Dr Sasanka S. Chukkapalli, Department of Oral Biology, University of Florida provided the db/db mouse brains with periodontal infection and *P. gingivalis* conditioned medium.

**4. Use of a Proof-reader**

No proof-reading service was used in the compilation of this thesis.

**Signature of Candidate**

**Print name: SHALINI KANAGASINGAM**

# ABSTRACT

**BACKGROUND**: Alzheimer's disease (AD) is a neurodegenerative disease clinically presenting with deterioration in memory and, neuropathologically by the presence of insoluble amyloid-beta (Aβ) plaques and phosphorylated tau (p-Tau) binding neurofibrillary tangles (NFTs).

**AIM:** This study was aimed at investigating the complex interaction between periodontitis, its pathogens, especially *Porphyromonas gingivalis* and mechanisms of AD hallmark lesion pathogenesis.

**METHODOLOGY:** The experimental protocols used include light microscopy, scanning electron microscopy (SEM), transmission electron microscopy (TEM), immunohistochemical staining, *in vitro* cell culture using SH-SY5Y cell line challenged with *P. gingivalis* (Pg381) conditioned medium in the presence and absence of cytokines and immunoblotting. An obese, diabetic (db/db) mouse model inoculated with *P. gingivalis* and *Fusobacterium nucleatum* were assessed via light microscopy and immunostaining to assess for neuroinflammation. Antibacterial assays for *P. gingivalis* were performed to assess if gingipains-fragmented tau peptides displayed antimicrobial properties. Circular dichroism (CD) was undertaken to assess tau peptide secondary structure. Paired helical/straight filament (PHF/SF) formation with implications for the NFT lesion was evaluated using TEM and polarising light microscopy.

**RESULTS:** SEM demonstrated a polymicrobial biofilm with extracellular polymeric substance (EPS) and water channels within the calculus. Immunohistochemistry on rehydrated paraffin wax embedded calculus and diseased tooth sections confirmed the presence of Aβ TEM revealed electron dense fibrils of variable sizes, similar to human Aβ fibrils. Western blotting of the cell lysates with selected APP antibodies demonstrated variable molecular weight bands corresponding to full length APP, C99 and C83 dimerized fragments. Anti-Aβ antibody detected statistically significant increase in Aβ40/42 levels in experimental groups with *P. gingivalis* and cytokines. TEM examination of supernatants demonstrated insoluble $A\beta_{40}$ and $A\beta_{42}$ fibrils. No Aβ plaques were detected in the db/db mice, however neuroinflammation was confirmed by immunohistochemistry in the infected groups. Phosphorylated tau peptide A showed significant antimicrobial activity against planktonic *P. gingivalis*. The CD results demonstrated that phosphorylated and non-phophorylated tau peptide A adopted mainly-β pleated sheet structures. The peptides investigated appeared fibrillar, with helical twists under TEM. Tau peptides were birefringent.

**CONCLUSIONS:** This study detected both soluble and insoluble Aβ fibrils within the EPS of periodontal and endodontic natural biofilm, strongly suggesting its role as a host antimicrobial peptide. However, its potential risk for cross-seeding into the brain may have implications to AD development. *P. gingivalis* infection in the presence of pro-inflammatory cytokines elevated the production of Aβ. Periodontitis and comorbidities of obesity and diabetes can instigate neuroinflammation. Phosphorylation of tau peptides physically changed their tertiary structure into PHFs with potential for self-aggregation and binding to the NFT lesion. These findings support the bidirectional relationship between periodontal disease and AD.

# TABLE OF CONTENTS


| | |
|---|---|
| **ABSTRACT** | 2 |
| **TABLE OF CONTENTS** | 3 |
| **Acknowledgements** | 9 |
| Funding, Awards & Publications | 10 |
| List of Figures | 12 |
| List of Tables | 16 |
| List of Abbreviations | 18 |
| **CHAPTER 1: INTRODUCTION** | 23 |
| 1.1 Alzheimer's Disease | 25 |
| 1.1.1 Epidemiology of AD | 26 |
| 1.1.2 Pathophysiology of AD | 27 |
| 1.2 Periodontitis | 32 |
| 1.2.1 Epidemiology of periodontitis | 33 |
| 1.2.2 *Porphyromonas gingivalis* | 33 |
| 1.3 Microbiota of periodontal and endodontic disease | 38 |
| 1.4 Periodontitis and AD | 44 |
| 1.4.1 Bacteraemia | 44 |
| 1.4.2 Inflammatory mechanisms and comorbidities in periodontitis and AD | 45 |
| 1.4.3 Epidemiological evidence linking periodontitis and AD | 48 |
| 1.5 Originality, Hypothesis and Overall Aims and Objectives | 52 |
| **CHAPTER 2: *EX VIVO* DETECTION OF AMYLOID-BETA IN ORAL BIOFILM OF EXTRACTED HUMAN TEETH WITH ENDODONTIC AND PERIODONTAL DISEASE** | 55 |
| 2.1 Introduction | 56 |
| 2..1.1 Hypothesis | 60 |
| 2.1.2 Aims & Objectives | 61 |
| 2.1.3 Ethical Approval | 61 |
| 2.1.4 Funding award | 62 |
| 2.2 Materials & Methods | 63 |
| 2.2.1 Specimen collection | 64 |

| | |
|---|---|
| 2.2.2 Preparation of specimens | 66 |
| 2.2.3 Tissue Morphology and Biofilm Detection under Light Microscopy | 67 |
| 2.2.4 Immunohistochemical microscopy | 70 |
| 2.2.5 Biofilm morphology and characteristics under electron microscopy | 72 |
| 2.3 Results | 79 |
| 2.3.1 Collection of extracted teeth | 79 |
| 2.3.2 Collection of calculus on root surfaces | 82 |
| 2.3.3 Light microscopy investigation of extracted teeth and calculus | 82 |
| 2.3.4 Immunohistochemical light microscopy investigation of extracted teeth and calculus | 85 |
| 2.3.5 Correlative light and electron microscopy of semi-thin Araldite sections | 89 |
| 2.3.6 Light microscopy of immunocolloidal gold silver staining (IGSS) of LR White resin embedded gutta percha biofilm sections. | 90 |
| 2.3.7 SEM imaging of extracted teeth | 91 |
| 2.3.8 SEM imaging of calculus | 94 |
| 2.3.9 Morphological visualisation and immunochemistry investigations under TEM | 96 |
| 2.3.10 Combinations of morphological and immunochemical investigative images for comparison across the various experimental techniques utilised | 99 |
| 2.4 Discussion | 101 |
| 2.4.1 Challenges, strengths and limitations of study | 104 |
| 2.4.2 Clinical relevance | 107 |
| 2.4.3 Future studies | 109 |
| 2.5 Conclusion | 111 |
| **CHAPTER 3: *PORPHYROMONAS GINGIVALIS* CONDITIONED MEDIUM *IN VITRO* CHALLENGE OF SH-SY5Y CELLS INDUCES AMYLOIDOGENIC PROCESSING OF THE AMYLOID-B PRECURSOR PROTEIN** | 112 |
| 3.1 Introduction | 118 |
| 3.1.1 Hypothesis | 118 |
| 3.1.2 Aims & Objectives | 118 |
| 3.1.3 University approvals | 118 |
| 3.2 Materials & Methods | 119 |

| | |
|---|---|
| 3.2.1 Source of reagents | 119 |
| 3.2.2 *P. gingivalis* conditioned medium as source of crude virulence factors | 120 |
| 3.2.3 *In vitro* cell culture | 121 |
| 3.2.4 Cell lysate preparation | 123 |
| 3.2.5 Protein assay | 124 |
| 3.2.6 Western blot of cell lysates | 126 |
| 3.2.7 TEM detection of Aβ fibrils | 128 |
| 3.2.8 Statistical Analysis | 129 |
| 3.3 Results | 130 |
| 3.3.1 Western blot: Rabbit anti-APP C-terminal antibody | 130 |
| 3.3.2 C99 bands densitometry analysis | 131 |
| 3.3.3 C83 bands densitometry analysis | 132 |
| 3.3.4 Western blot: Rabbit anti-APP N-terminal antibody | 133 |
| 3.3.5 C99 bands densitometry analysis | 134 |
| 3.3.6 Western blot: Mouse anti-Aβ (clone 6e10) antibody | 135 |
| 3.3.7 Aβ1-40 densitometry analysis | 136 |
| 3.3.8 Aβ1-42 densitometry analysis | 137 |
| 3.3.9 Aβ1-40/42 relative abundance densitometry analysis | 137 |
| 3.3.10 TEM detection of Aβ fibril formation in supernatants | 139 |
| 3.4 Discussion | 140 |
| 3.4.1 Challenges, strengths and limitations | 147 |
| 3.4.2 Clinical relevance | 149 |
| 3.4.3 Future work | 151 |
| 3.5 Conclusion | 151 |
| **CHAPTER 4: *P. GINGIVALIS* (W83) AND *F. NUCLEATUM* (ATCC 49256) INFECTION INDUCES ALZHEIMER'S DISEASE-LIKE PATHOPHYSIOLOGY IN OBESE AND DIABETIC MICE** | 152 |
| 4.1 Introduction | 153 |
| 4.1.1 Hypothesis | 159 |
| 4.1.2 Aims & Objectives | 159 |
| 4.1.3 University Approvals | 159 |
| 4.3 Materials & Methods | 160 |

| | |
|---|---|
| 4.3.1 Source of Reagents | 161 |
| 4.3.2 db/db mice and infection regime | 161 |
| 4.3.3 Formalin fixed tissue processing | 162 |
| 4.3.4 Tissue sectioning | 163 |
| 4.3.5 Methenamine silver impregnation | 163 |
| 4.3.6 Immunohistochemistry | 164 |
| 4.4 Results | 165 |
| 4.4.1 Preserved histology of the temporal lobe of infected db/db mice and a mouse model for AD | 165 |
| 4.4.2 Immunohistochemistry | 166 |
| 4.5 Discussion | 170 |
| 4.5.1 Challenges, strengths and limitations | 174 |
| 4.5.2 Clinical relevance | 176 |
| 4.5.3 Future work | 176 |
| 4.6 Conclusion | 177 |
| **CHAPTER 5: ANTIMICROBIAL PROPERTIES, AND PAIRED HELICAL FILAMENT STRUCTURES OF SELECTED TAU PEPTIDES FRAGMENTED BY GINGIPAINS** | 179 |
| 5.1 Introduction | 180 |
| 5.1.1 Hypothesis | 185 |
| 5.1.2 Aims & Objectives | 185 |
| 5.1.3 Ethical Approval | 186 |
| 5.1.4 Funding Award | 186 |
| 5.2 Materials & Methods | 187 |
| 5.2.1 Source of reagents | 188 |
| 5.2.2 *Porphyromonas gingivalis* cultures | 188 |
| 5.2.3 Assessment of the putative gingipain binding tau hexapeptide motif antimicrobial activity on *P. gingivalis* | 190 |
| 5.2.4 Circular dichroism spectroscopy for assessment of the secondary structure of tau peptide A (non-phosphorylated and phosphorylated) | 193 |
| 5.2.5 TEM | 193 |
| 5.2.6 Statistical analysis | 194 |
| 5.3 Results | 195 |

| | |
|---|---|
| 5.3.1 Anaerobic growth of P. gingivalis ATCC 33277 from in TSB culture | 196 |
| 5.3.2 Assessment of the putative gingipain binding hexapeptide motif antimicrobial activity on *P. gingivalis* ATCC 33277 | 196 |
| 5.3.3 Assessment of the secondary structure of the soluble peptide A in non-phosphorylated and phosphorylated forms using Circular Dichroism (CD) | 203 |
| 5.3.4 Transmission Electron Microscopy (TEM) detection of helical twists to indicate pair helical filaments in vitro | 205 |
| 5.4 Discussion | 207 |
| 5.3.1 Challenges, strengths and limitations | 212 |
| 5.3.2 Clinical relevance | 213 |
| 5.3.3 Future work | 214 |
| 5.5 Conclusion | 215 |
| **CHAPTER 6: BIREFRINGENCE OF GINGIPAINS FRAGMENTED TAU PEPTIDES** | 216 |
| 6.1 Introduction | 217 |
| 6.1.1 Hypothesis | 220 |
| 6.1.2 Aims and Objectives | 220 |
| 6.1.3 Ethical Approval | 220 |
| 6.1.4 Funding award | 220 |
| 6.2 Materials & Methods | 221 |
| 6.2.1 Source of reagents | 221 |
| 6.2.2 Congo red staining and polarising light microscopy | 221 |
| 6.3 Results | 222 |
| 6.4 Discussion | 224 |
| 6.4.1 Challenges, strengths and limitations | 225 |
| 6.4.2 Clinical relevance | 226 |
| 6.4.3 Future work | 227 |
| 6.5 Conclusion | 227 |
| **CHAPTER 7: GENERAL DISCUSSION & CONCLUSION** | 228 |
| 7.1 Rationale for research: AD and Recognised Risk Factors | 229 |
| 7.2 Aβ expression in human oral tissues | 232 |
| 7.3 *P. gingivalis*, cytokines and amyloidogenic processing | 235 |

| | |
|---|---|
| 7.4 Periodontitis, AD and associated comorbidities | 238 |
| 7.5 *P. gingivalis* and Tau peptides | 239 |
| 7.6 Clinical implications of research findings | 245 |
| 7.7 Future Directions | 245 |
| 7.8 Thesis Conclusion | 249 |
| **REFERENCES** | 250 |

# ACKNOWLEDGEMENTS

I would like to record my gratitude to some amazing people for their unwavering support, encouragement, and guidance throughout the course of this PhD. Completing this thesis has been a challenging and deeply rewarding journey, and I am truly grateful to all those who have stood by my side and kept my spirits up.

Firstly, I would like to thank my initial supervisory team, Professor Richard Welbury and Dr Sim Singhrao for your infinite patience and kindness. I shall genuinely miss our time together at UCLAN, getting through all the official PhD meetings and also finding time for my much-needed therapy/motivational sessions. Sim, I have never known a more passionate and hardworking researcher. Thank you so much for accommodating my crazy teaching and clinical schedule and facilitating my laboratory work during the evenings and weekends. I have such happy memories of the fun times we had in the lab. Your dedication and curiosity for AD research continues to inspire me to this day!

To my current supervisory team, Dr Flavio Pisani and Dr Nadia Shah, thank you very much for getting me to the finish line while having to juggle your own ever-increasing academic workload. I am eternally grateful for all the precious time spent sitting with me to guide me through my final stages of writing and constantly checking on my wellbeing throughout the past 2 years. To Dr Marta Krysmann, my RDT, you have taught me to keep calm and carry on. Thank you for sharing your scientific expertise as well as always keeping me in a positive mindset.

I owe a huge thank you to my long-suffering family who have endured my many absences, distractions, and total preoccupation with work. To my amazing (and super patient) husband Ali, my incredibly resilient daughter, Ava, thank you for sorting out everything else in life to allow me the time and headspace to get this thesis done. To my devoted parents in Malaysia and loving in-laws in London, your constant support, encouragement, and prayers have kept me going.

To my dearest friends (and colleagues) - Shareen, Rachel, Maria, Kartina, Kate and Steve- thank you for your kindness, encouragement, and constant offers to lend a hand (as well as feed me!). Your friendship has meant the world to me during some of the most testing phases of this process.

Finally, to my forever faithful, furry sidekick Luna, thank you for staying curled up by my side through the many long nights spent writing this thesis- couldn’t have asked for a better writing companion!

# FUNDING, AWARDS & PUBLICATIONS

Funding

- ODRT OHI (PREVISER) AWARD 2018-2020, Oral and Dental Research Trust, £5000.00
- TCWhite Young Researcher Award 2018-2020, RCPS Glasgow, £10,000.00

Awards

- British Endodontic Society Spring Meeting POSTER PRIZE Winner 2024
- 3 Minute Thesis (3MT) UCLan People's Choice Winner and VITae Round Runner Up (2020)

PhD research-related publications:

1. Singhrao, S.K., Consoli, C., Dennison, S.R., **Kanagasingam**, S. and Welbury, R. (2024). *Porphyromonas gingivalis* LPS and *Actinomyces naeslundii* Conditioned Medium Enhance the Release of a Low Molecular Weight, Transcriptionally Active, Fragment of Glycogen Synthase-3 Kinase in IMR-32 Cell Line. *Journal of Alzheimer's Disease Reports,* 8(1), pp.1055-1067.

2. **Kanagasingam, S**. (2023). Ignoring oral health can put general health at risk. *Journal of General Practice Nursing (GPN),* 9(4), pp.26-28.

3. **Kanagasingam, S**., von Ruhland, C., Welbury, R. and Singhrao, S.K. (2022). Ex vivo Detection of Amyloid-β in Naturally Formed Oral Biofilm. *Journal of Alzheimer's Disease Reports,* 6(1), pp.757-773.

4. **Kanagasingam, S**., von Ruhland, C., Welbury, R. and Singhrao, S.K. (2022). Antimicrobial, Polarizing Light, and Paired Helical Filament Properties of Fragmented Tau Peptides of Selected Putative Gingipains. *Journal of Alzheimer's Disease,* 89(4), pp.1279-1291.

5. **Kanagasingam, S**., von Ruhland, C., Welbury, R., Chukkapalli, S.S. and Singhrao, S.K. (2022). *Porphyromonas gingivalis* conditioned medium induces amyloidogenic processing of the amyloid -β precursor protein upon in vitro infection of SH-SY5Y cells. *Journal of Alzheimer's Disease Reports,* 6(1), pp.577-587.

6. Bahar, B., **Kanagasingam, S**., Tambuwala, M.M., Aljabali, A.A.A., Dillon, S.A., Doaei, S., Welbury, R., Chukkapalli, S.S. and Singhrao, S.K. (2021). *Porphyromonas gingivalis* (W83) Infection Induces Alzheimer's Disease-Like Pathophysiology in Obese and Diabetic Mice. *Journal of Alzheimer's Disease*, 82(3), pp.1259-1275.

7. **Kanagasingam, S**., Chukkapalli, S.S., Welbury, R. and Singhrao, S.K. (2020). *Porphyromonas Gingivalis* Is a Strong Risk Factor for Alzheimer's Disease. *Journal of Alzheimer's Disease Reports*, 4(1), pp.501-511.

8. Contributed book chapter to 'Periodontitis as a risk factor for Alzheimer's disease - the experimental journey so far, with hope of therapy. (2021). *Advances in Experimental Medicine and Biology*. ISSN 0065-2598.'

# List of Figures


| Figure No | Figure title | Page |
|---|---|---|
| 1.1 | Evolution of research on the association between periodontitis and Alzheimer's Disease from 2000 to 2023 | 25 |
| 1.2 | Amyloid Cascade Hypothesis | 29 |
| 1.3 | Schematic representation of tau oligomer propagation | 30 |
| 1.4 | Structure of *P. gingivalis* | 35 |
| 1.5 | Percentage of prevalence of *P. gingivalis* detected in primary endodontic infections | 40 |
| 1.6 | Endodontic-periodontal disease | 43 |
| 1.7 | Periodontal bacteria can spread via different routes | 47 |
| 1.8 | How periodontal pathogen can invade the bloodstream and gain access to the brain via multiple routes | 48 |
| 2.1 | Flowchart of methods used for specimen preparation and imaging techniques | 64 |
| 2.2 | Workflow of Grocott's Gomori Methanamine silver staining | 69 |
| 2.3 | Flowchart showing the numbers and grouping of the extracted teeth | 80 |
| 2.4 | Photos showing a selection of the freshly extracted human teeth collected for the study | 69 |
| 2.5 | Calculus deposits on the root surfaces of extracted teeth | 80 |
| 2.6 | Tooth sections and calculus specimens embedded in paraffin wax set in moulds | 81 |
| 2.7 | Gram stain of tooth sections from Group B and root calculus | 83 |
| 2.8 | Grocott-Gomori's methenamine silver impregnation of root calculus | 85 |
| 2.9 | Immunohistochemical staining of tooth sections with Anti-β-Amyloid antibody | 87 |

| | | |
|---|---|---|
| 2.10 | Immunohistochemical staining of calculus sections with Anti-β-Amyloid antibody and Anti-Escherichia coli lipopolysaccharide | 89 |
| 2.11 | Light microscopy of gutta percha from a failed root treatment with periodontal disease (Group C) stained with Toluidine Blue | 90 |
| 2.12 | Light microscopy of immunocolloidal gold silver staining (IGSS) for Anti-Aβ antibody, Mouse (clone 6e10) of LR White resin embedded gutta percha biofilm sections | 90 |
| 2.13 | Selection of teeth from Groups A-C prepared for SEM imaging | 91 |
| 2.14 | SEM images of the extracted tooth with primary root canal infection and periodontal disease | 92 |
| 2.15 | SEM images of extracted tooth with secondary root canal infection and periodontal disease | 93 |
| 2.16 | SEM imaging of the calculus deposits from the external tooth root surface | 94 |
| 2.17 | SEM imaging of root calculus microorganisms | 95 |
| 2.18 | TEM High resolution ultrastructure images from teeth in Group B (primary root canal infection with periodontitis) in araldite resin. | 97 |
| 2.19 | TEM ultrastructure of a specimen of gutta percha and biofilm from failed root canal treatment and periodontal disease, Group C which were embedded in Araldite resin | 98 |
| 2.20 | Ultrastructure of a specimen of gutta percha and biofilm from failed root canal treatment, Group C which were embedded in Araldite resin | 99 |
| 2.21 | Morphological and immuno-staining investigations with light microscopy and SEM imaging | 100 |
| 3.1 | APP processing and cleavage to produce Aβ proteins via the non-amyloidogenic and amyloidogenic pathways | 115 |
| 3.2 | Graph of protein assay data | 121 |
| 3.3 | Immunoblot of the cell lysate with Rabbit anti-APP C-terminal antibody | 127 |
| 3.4 | Densitometric analysis of the cell lysate immunoblotted with anti-APP C-terminal antibody C99 | 128 |

| | | |
|---|---|---|
| 3.5 | Densitometrical analysis of the cell lysate immunoblotted with anti-APP C-terminal antibody C83 | 129 |
| 3.6 | Immunoblot of the cell lysate with Rabbit anti-APP N-terminal antibody | 134 |
| 3.7 | Densitometric analysis of the cell lysate immunoblotted with anti-APP N-terminal antibody C | 135 |
| 3.8 | Immunoblot of the cell lysate with mouse anti-Aβ antibody | 136 |
| 3.9 | $A\beta_{1-40}$ densitometry | 138 |
| 3.10 | $A\beta_{1-42}$ densitometry | 138 |
| 3.11 | $A\beta_{1-40/42}$ relative abundance densitometry | 139 |
| 3.12 | TEM ultrastructural morphological analysis of the supernatant from SH-SY5Y | 140 |
| 3.13 | Cleavage of APP by two proteases (β- and γ-secretases) liberate Ab from APP. | 144 |
| 4.1 | Common pathways of aging-associated disorders highlight the increased risk of AD by the combination of obesity, diabetes, cardiovascular disease and aging | 155 |
| 4.2 | Mice brain tissue sections | 166 |
| 4.3 | Rehydrated paraffin wax tissue sections underwent immunostaining with rabbit anti-Iba-1 antibody to detect activated microglia | 167 |
| 4.4 | Rehydrated paraffin wax tissue sections underwent immunostaining with Anti-GFAP immunostaining to identify astrocytes | 168 |
| 4.5 | Rehydrated paraffin wax tissue sections were immunostained with Mouse anti-tau (AT8) to detect NFTs | 169 |
| 4.6 | A schematic outline of 4 major pathways including PI3K/AKT, MAPK, TNF and insulin signalling impacted by *P. gingivalis* W83 infection in the db/db mice | 173 |
| 5.1 | Schematic diagram showing tau domain organization | 181 |
| 5.2 | Tau phosphorylation and formation of NFTs within neurons | 184 |

| | | |
|---|---|---|
| 5.3 | Diagram illustrating the serial dilution protocol used for *P. gingivalis* | 190 |
| 5.4 | Tau peptides designated as A-G (non-phosphorylated) were commercially synthesized and supplied by Severn Biotech Ltd (Kidderminster, UK) in their purified crystallised (powder) form with/without post-translational modification | 191 |
| 5.5 | The blood agar plates showing the control plate | 197 |
| 5.6 | Bar chart showing the growth of viable *P. gingivalis* ATCC 33227 (CFU/mL) in different concentrations | 199 |
| 5.7 | Bar chart showing mean colony forming units of *P. gingivalis* at varying concentrations of phosphorylated tau peptide A | 200 |
| 5.8 | Bar chart showing phosphorylated peptide B demonstrated statistically significant differences (p= 0.00001) antimicrobial action against *P. gingivalis* as compared to the control group | 200 |
| 5.9 | Bar chart showing mean colony forming units of *P. gingivalis* ATCC 33277 at varying concentrations of phosphorylated peptide C | 197 |
| 5.10 | Circular dichroism spectroscopic analysis of non-phosphorylated tau peptide A | 198 |
| 5.11 | Displays of non-phosphorylated tau peptide B, phosphorylated tau peptide B | 201 |
| 6.1 | Images showing the topographic representation of Braak stages 0 according to the original histopathologic descriptions | 218 |
| 6.2 | Congo Red staining and polarizing light microscopy illustrations | 223 |
| 7.1 | Potentially modifiable risk factors for dementia | 231 |
| 7.2 | Schematic drawing shows Aβ aggregation | 232 |
| 7.3 | The impact of chemotactic and pro-inflammatory cytokines on APP and Aβ peptide | 231 |
| 7.4 | The bar charts show the frequency of fibrillar tau pathology in the human brain across the decades of lifespan | 237 |
| 7.5 | Proposed strategies to address the challenges of multi-morbidity in periodontitis and AD, by engaging with medical and dental professionals in both settings. | 241 |

# List of Tables


| Table No | Table title | Page |
|---|---|---|
| 1 | Summary of characteristics and critical findings of longitudinal studies on oral health and cognitive status | 51 |
| 3.1 | The constituents of DMEM including relevant additives | 122 |
| 3.2 | Summary of treatments carried out on SH-SY5Y, CRL-2266™ cell line | 122 |
| 3.3 | List of lysis buffer components | 124 |
| 3.4 | Lysis buffer with protease inhibitors added to 48 mL of final buffer from Table 3.3, for the preparation of cell lysates | 124 |
| 3.5 | Protein assay data | 125 |
| 3.6 | Antibodies used in the experimental work, including their sources and relevant working dilutions | 128 |
| 3.7 | P. gingivalis virulence factors and its functions | 141 |
| 3.8 | Cytokines used in this study (IL-1β, IL-6 and TNF-α) and their potential influence on periodontitis and AD | 142 |
| 4.1 | Key features of Metabolic Syndrome, MetS, including dysglyceamia and at least 2 other factors | 154 |
| 4.2 | Transgenic mouse models for investigations into obesity and diabetes | 156 |
| 4.3 | Transgenic mouse models commonly used for investigations into AD | 157 |
| 5.1 | Initial non-phosphorylated peptide toxicity prediction carried out by Severn Biotech Ltd., UK | 187 |
| 5.2 | Reagents and amounts used to produce TSB | 189 |
| 5.3 | Tau peptides (A-G) of interest in this study | 192 |

| | | |
|---|---|---|
| 5.4 | Enumeration for the 25-hour broth P. gingivalis cfu/mL counts with each dilution to determine the optimal dilution for use with the surface drop method | 196 |
| 5.5 | Number of colonies for non-phosphorylated peptide A and control groups, with the average number of colonies and results of the Mann-Whitney U test | 197 |
| 5.6 | Number of colonies for phosphorylated peptide A and control groups, with the average number of colonies and results of the Mann-Whitney U test | 198 |
| 5.7 | Number of colonies for phosphorylated peptide B and control groups, with the average number of colonies and results of the Mann-Whitney U test | 200 |
| 5.8 | Number of colonies for phosphorylated peptide C and control groups, with the average number of colonies and results of the Mann-Whitney U test | 202 |
| 5.9 | Secondary structure determination using Circular Dichroism of tau peptide A in its non- phosphorylated and phosphorylated states | 204 |

# List of Abbreviations

| | |
|---|---|
| Aα | alpha amyloid |
| Aβ | beta amyloid |
| AAALAC | Association for the assessment and accreditation of laboratory animal care international |
| AD | Alzheimer ‘s disease |
| AMP | antimicrobial peptides |
| ApoE | apolipoprotein E |
| APP | amyloid precursor protein |
| ATP | Adenosine triphosphate |
| AWERB | Animal Welfare Ethical Review Board |
| BBB | Blood Brain Barrier |
| BSA | bovine serum albumin |
| C/O | Care of |
| CD | Circular Dichroism |
| CFU | colony- forming unit |
| $cm^3$ | centimeters cubed |
| CNS | Central nervous system |
| CRISPR | Clustered Regularly Interspaced Short Palindromic Repeats |
| CSF | cerebrospinal fluid |
| DNA | Deoxyribonucleic acid |
| EDTA | Ethylenediaminetetraacetic acid |
| EMEM | Eagle‘s minimal essential medium |

| | |
|---|---|
| FBS | foetal calf serum |
| FimA | fibrillin |
| *F. nucleatum* | *Fusobacterium Nucleatum* |
| g | grams |
| H/E | Haematoxylin and Eosin |
| HRP | horse radish peroxidase |
| IACUC | Institutional Animal Care and Use Committee |
| Ig | immunoglobulins |
| IGF-1 and IGF-2 | Insulin-like growth factors 1 and 2 |
| IL-1β | interleukin 1β |
| IL-2 | interleukin 2 |
| IL | interleukin |
| IL-6 | interleukin 6 |
| IMR32 | Human neuroblastoma cell line |
| INF-γ | Interferon gamma |
| M | Molar |
| mA | Milliamps |
| MAC | membrane attack complex |
| MAPK | Mitogen-activated protein kinases |
| MBL | mannose binding lectin |
| MCI | mild cognitive impairment |
| mg | Milligram |
| MHC | major histocompatibility complex |
| mL | Millilitre |

| | |
|---|---|
| mM | Millimolar |
| mm2 | Millimetre squared |
| MTA | material transfer agreement |
| Na2S | Sodium Sulfide |
| NaCl | Sodium Chloride |
| NaOH | Sodium Hydroxide |
| NFTs | neurofibrillary tangles |
| ng | nanogram |
| NGS | next generation sequencing |
| NMWL | nominal molecular weight limit |
| NO | Nitric Oxide |
| No. | number |
| OD | optical density |
| OMVs | outer membrane vesicles |
| PAMP | pathogen associated molecular pattern |
| PAS | periodic acid- Schiff |
| PBS | phosphate buffered saline |
| PCR | polymerase chain reaction |
| PD | periodontal disease |
| *P. gingivalis* | *Porphyromonas gingivalis* |
| PHF's | paired helical filaments |
| PNS | peripheral nervous system |
| p-Tau | hyperphosphorylated Tau protein |
| PVDF | polyvinylidene difluoride |

| | |
|---|---|
| Rgps | arginine specific gingipains |
| ROS | reactive oxygen species |
| Rpm | revolutions per minute |
| rRNA | Ribosomal ribonucleic acid |
| SDS | Sodium dodecyl sulphate |
| SEM | Scanning Electron Microscope |
| SF | Straight Filaments |
| SDS PAGE | Sodium dodecyl sulphate polyacrylamide gel electrophoresis |
| TAE | Buffer solution containing a mixture of Tris base, acetic acid and |
| TEM | Transmission electron microscopy |
| TNF-α | tumor necrosis factor α |
| TSB | tryptic soy broth |
| U | Unit |
| UCLan | University of Central Lancashire |
| UK | United Kingdom |
| USA | United States of America |
| V | volts |
| W | watts |
| w/v | % weight per volume |
| µM | micromolar |
| α | Alpha |
| β | Beta |
| γ | Gamma |
| µg | micrograms |

| | |
|---|---|
| µL | microliter |
| µM | micromolar |

# CHAPTER 1

# INTRODUCTION

# INTRODUCTION

The bidirectional relationships between oral health and systemic health have become the focus of research in recent years, especially in association with chronic non-communicable diseases (NCDs) including cardiovascular disease, diabetes mellitus, respiratory diseases, rheumatic diseases and neurodegenerative diseases (Jin et al., 2016; Meurman & Bascones-Martinez 2021; Botelho et al., 2022). Periodontal and endodontic disease are chronic oral infections with similar pathogens, inflammatory mediators and biological pathways connecting both diseases to systemic health (Costa et al., 2014; Rosen et al., 2017; Niazi & Baksh 2022).

Research interest in the connection of periodontitis and Alzheimer's Disease (AD) has increased significantly over the past decade, as described in recent bibliometric and network analysis studies (Matta-Pacheco et al., 2024; Villar et al., 2024). The Systematic Literature Network Analysis (SLNA) by Villar et al. (2024) analysed records identified through Scopus, compiled the number of relevant articles from the year 2000 to 2023. Figure 1.1 illustrates the overall increasing trend, peaking circa 2020-2022, which confirms the growing interest in this important topic (Villar et al.; 2024). Matta-Pacheco et al. (2024) recognised the contributions of researchers at the University of Central Lancashire with the most publications, based on metadata extraction.

The landscape of oral healthcare provision has changed over the years, from 'drilling and filling' to a focus on preventative measures and tooth preservation. There is increasing awareness about the impact of oral diseases on patients' overall health amongst dental professionals. This puts the onus on the dental team to play an active role in educating patients on the importance of maintaining oral health as this is a modifiable risk factor for many systemic conditions, including dementia (Akl et al., 2021). The topic of periodontitis and AD

presents a novel multi-disciplinary research opportunity as a better understanding of the complex interplay between the two diseases and ultimately influences prevention and targeted therapies.

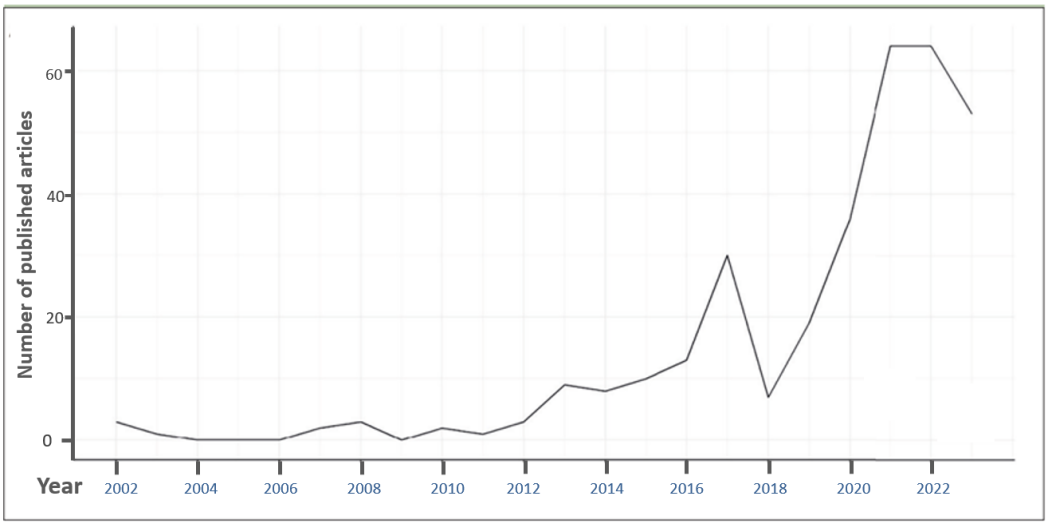


**Figure 1.1:** Evolution of research focused on the association between periodontitis and AD from 2000 to 2023, showing an increasing trend over the years (adapted from Villar et al., 2024)

## 1.1 Alzheimer's Disease

Alzheimer's Disease (AD) was first described by German neuropathologist, Alois Alzheimer, a progressive neurodegenerative disease. The overarching term 'dementia' refers to a group of symptoms including impairments to memory, language, problem-solving and thinking skills, which impacts daily activities. The other types of dementia include vascular dementia, Lewy body dementia and frontotemporal dementia. AD is the most common cause of dementia, accounting for 60% to 80% of dementia cases (2024 Alzheimer's disease facts and figures, www.alz.org). The diagnosis of AD is defined by the detection of extra-neuronal aggregations of amyloid-beta (Aβ) and intraneuronal aggregations of neurofibrillary tangles (NFTs) in the brain, together with clinical signs of cognitive deficit (Hyman et al., 2012). Taking into account recent developments in the biomarker field, Jack et al. (2018) proposed the 'ATN framework',

whereby biomarkers are grouped into A (amyloid), T (phosphorylated tau) and N (neurodegeneration, measured by total tau). The progression of AD begins with biological αchanges in the brain, even in the absence of clinical symptoms, and advances to pathological brain changes accompanied by cognitive impairment and physical disability (Sperling et al., 2011). This framework facilitates diagnosis before the stage of AD-associated dementia, meaning it would be possible for individualised risk-profiling in patients with mild cognitive impairment (Jack et al., 2018).

### 1.1.1 Epidemiology of AD

AD can be further classified as early-onset (before the age of 65), late-onset (after the age of 65) and familial, which is a rare, inherited form of AD affecting younger individuals. Late-onset AD is also known as sporadic AD, denoting a lack of family history or inherited genetic predisposition. In 2018, dementia prevalence was estimated at 50 million people worldwide. This figure is projected to triple in 2050, meaning 153 million of the global population, two-thirds of whom would be living in low to middle income countries (Alzheimer's Disease International. World Alzheimer Report 2018). Every 5 years after the age of 65, the incidence of AD doubles. Age-related incidence rates significantly increase from less than 1% per year before the age of 65, to 6% yearly after the age of 85. AD incidence is reported to be higher for females compared to males (Qiu et al., 2009).

In general, AD patients have a shorter life expectancy compared to the general population. Studies based in the USA and Europe have reported that the average survival times post dementia diagnosis is within a range of 3-6 years (Prince et al., 2016; Mayeda et al., 2017). In a Dutch study involving almost 4500 dementia patients, the median survival time was similar

in patients with late-onset dementia and younger, early-onset dementia (Rhodius-Meester et al., 2018).

AD is a multifactorial disease with the strongest risk factors associated with aging (above 65 years of age) and the APOE gene, which is associated with the Alipoprotein E protein. This protein is involved with lipid metabolism and cholesterol transport (van de Lee et al., 2018). The APOE gene has three common alleles namely allele APOE ε2 (which has a protective role), allele APOE ε3 (most prevalent, neutral effect on AD risk) and risk allele APOE ε4 (Farrer et al., 1997). Carriers who are homozygous for APOE ε4 would have a 50% risk of AD by 85 years of age, this is in contrast with non-carriers who would have an estimated risk of less than 10% at the same age (van der Lee et al., 2018). On the other hand, familial AD is associated with mutations in the Aβ precursor protein (APP), presenilin genes PSEN1 and PSEN2 (Lambert et al., 2011). In comparison, sporadic AD has a strong link to genetics (APOE ε4) as well as environmental factors (Serrano-Pozo et al., 2021).

### 1.1.2 Pathophysiology of AD

A number of hypotheses have been discussed to explain AD pathogenesis, including the Amyloid Cascade, Tau hyperphosphorylation, neurotransmitters and oxidative stress (Glenner et al., 1984; Frost et al., 2009). The 'Infection Model' for AD proposes that bacteria and viruses may play a role in the development and progression of AD (Zhao et al., 2024).

(i) Amyloid Cascade Hypothesis

This hypothesis as first described by Hardy and Allsop (1991), postulated that Aβ deposition was the primary cause of neurodegenerative processes in AD. The Aβ peptides are cleaved from the transmembrane protein, Amyloid Precursor Protein (APP), which is expressed in many tissues, particularly in neuron synapses. APP plays an important role in the regulation of

neuronal excitability and synaptic plasticity, especially in the cerebral cortex (Lee et al., 2020). APP is cleaved by α-secretase via the non-amyloidogenic pathway or by β-secretase, through the amyloidogenic pathway. This generates α- and β-C terminal fragments (CTFs). Subsequent processing involves intramembrane cleavage of the CTFs by γ-secretase, producing Aβ peptides, including the 42-amino-acid $A\beta_{42}$ which was the isoform associated with amyloid senile plaques in AD (Castellani et al., 2019).

Figure 1.2 illustrates the central steps of the Amyloid Cascade Theory, showing how aberrant proteolytic processing of the APP triggers downstream neurodegenerative events characteristic of AD. APP, shown on the neuronal membrane, is cleaved sequentially by β-secretase (BACE1) and the γ-secretase complex (PSEN1, PSEN2, nicastrin and APH-1), producing the Aβ peptides—particularly $A\beta_{42}$, which is prone to misfolding. The diagram describes how Aβ monomers aggregate into soluble oligomers and eventually fibrils, with APOE4 enhancing aggregation propensity. These oligomeric and fibrillar species accumulate as extracellular senile plaques and drive neurotoxicity, synaptic dysfunction, leading to neuronal death (Castellani et al., 2019).

From the inception of the Amyloid Cascade Hypothesis, there has been criticism, fuelled by limited results from anti-Aβ therapeutic strategies as well as the weak correlation between the lowering of cerebral Aβ levels and progression of cognitive decline (Ricciarelli & Fedele, 2017). This suggests that Aβ accumulation may be necessary but not sufficient for neurodegeneration. The model also struggles to account for early tau pathology, neuroinflammation, and vascular dysfunction, which often precede or progress independently of amyloid changes (Selkoe & Hardy, 2016). Moreover, population studies detected a pathological Aβ burden in about 60% of individuals aged above 85 years, were in fact, cognitively intact (Jack et al. 2019; Knopman et al., 2021). These inconsistencies indicate that AD is likely driven by multiple interacting pathways rather than a linear amyloid-first

mechanism (Selkoe & Hardy, 2016). This has led researchers to consider alternative hypotheses for AD pathophysiology.

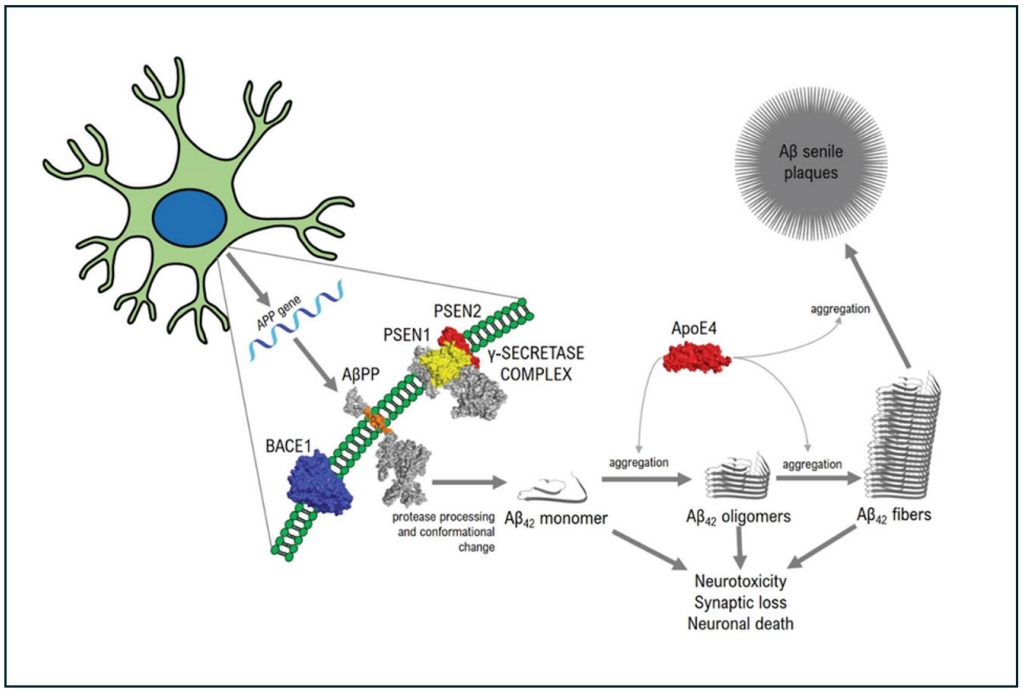


**Figure 1.2: The Amyloid Cascade Hypothesis** postulates that the Amyloid Precursor Protein (APP) gene expression causes protease processing by β-secretase 1 (BACE1) and γ-secretase complex which includes Presenilin 1 (PSEN1), Presenilin 2 (PSEN2), nicrastrin and Anterior Pharynx Defective 1 (APH-1). Following the release of the pathogenic insoluble $A\beta_{42}$ peptide, it goes through conformational change, assembling into oligomers and protofibrils (>100 kDa). These are neurotoxic, and continued aggregation eventually leads to deposition of senile plaques (Image credit: Castellani et al., 2019).

(ii) Tau Hyperphosphorylation Hypothesis

In healthy neurons, tau is a microtubule-bound protein which provides stabilization and aids in cytoplasmic transportation within neurons. In AD, tau can undergo abnormal phosphorylation, causing it to lose its ability to bind to microtubules, resulting in disassembly. The free misfolded tau protein subsequently aggregates into paired helical filaments (PHFs) and straight filaments (SFs). These eventually form intraneuronal fibrillary deposits i.e. neurofibrillary tangles (NFTs). Accumulation of NFTs can cause the reduction the number of neuronal synapses, cause

neurotoxicity and cause cellular dysfunction (Callahan et al. 1999, Fan et al. 2020). Interestingly, the quantity of hyperphosphorylation of tau (also known as tau oligomers) has been correlated to the degree of severity of AD (Mocanu et al. 2008). Tau oligomers are reported to be toxic and have the ability to spread between cells, potentiating neuronal damage (Gerson et al. 2014). Phosphorylated tau exhibited seeding activities which had the propensity to convert normal tau into cytotoxic species, contributing to fibrillization (Liu et al. 2020). Some researchers have argued that tau phosphorylation is the primary driver of AD neurodegeneration, instead of Aβ (Shafiei et al. 2017, Roda et al. 2022). Refer Figure 1.3.

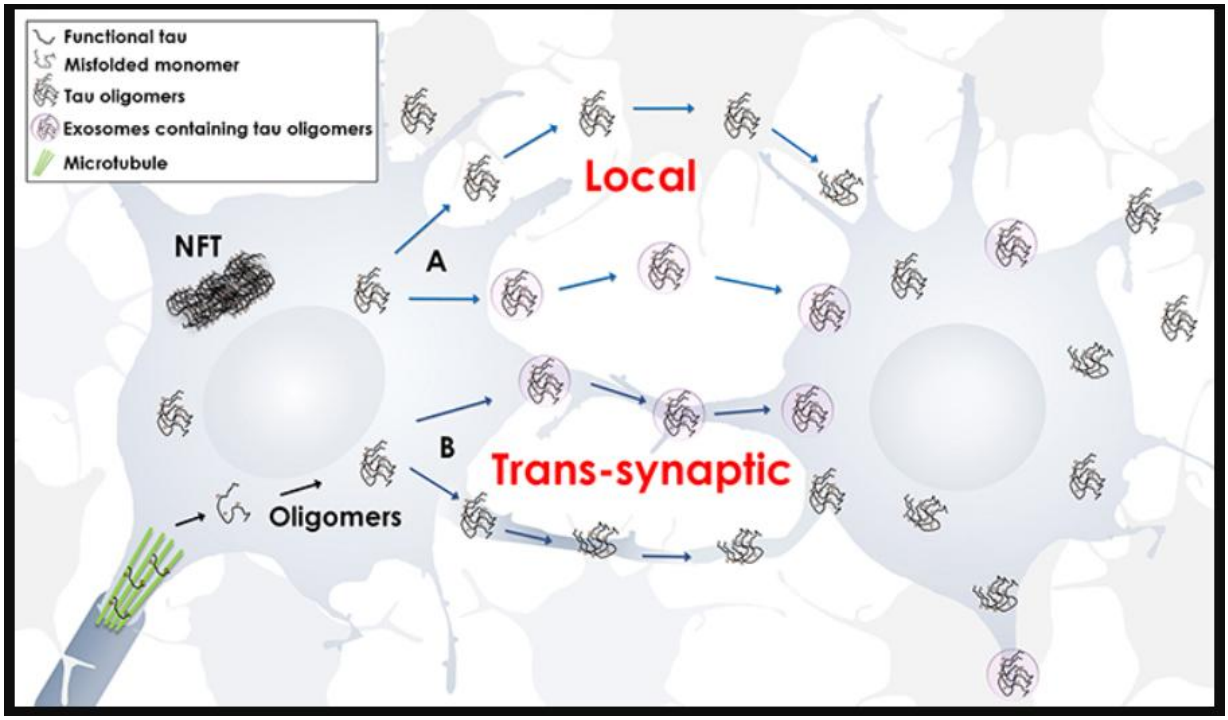


**Figure 1.3:** Schematic representation of tau oligomer propagation. Tau oligomers can spread from one neuron to another, via in local transmission. Whereas trans-synaptic transmission involved tau oligomers within exosomes which pass across the synapse of two neighbouring neurons (Image credit: Shafei et al. 2017).

(iii) Infection Model for AD

The biofilm concept of AD Aβ plaques arising from the bacterial virulence factors was proposed as an alternative platform for answering the fundamental question of microbes playing a role in AD development (Friedland 2015; Allen et al., 2016; Miklossy, 2016). It proposes that some prokaryotic cells may produce functional amyloid to support the extracellular polymeric substances (EPS) secreted by microbes to improve the biofilm's structural integrity (Epstein et al., 2008; Dueholm et al., 2013). The prokaryotic functional amyloids could range from structural components namely, fimbriae, to curli and other cellular appendages (Larsen et al., 2007; Dueholm et al., 2013). Functional amyloids are protein fibrils that adopt the same cross-β structural architecture as pathological amyloids but are intentionally produced and tightly regulated to support normal biological functions, such as bacterial biofilm formation. Their existence demonstrates that amyloid formation is not inherently toxic. Toxicity in AD arises when amyloid-β or tau aggregate without regulation, generating intracellular oligomers that disrupt neuronal homeostasis. Functional amyloids such as bacterial curli provide mechanistic insights into nucleation and seeding. These processes underpin the potential prion-like spread of tau and Aβ pathology in AD (Fowler et al., 2007).

What was surprising was the discovery of prokaryotic Aβ fibres crossing the blood-brain barrier (BBB) with the potential towards forming pathological Aβ plaques seen in AD. To explain the plausibility of such a phenomenon taking place, Friedland (2015), proposed the "molecular mimicry theory". whereby curli fibres would act as a 'template' for cross seeding the human Aβ as a potential trigger for AD pathology. Friedland suggested that curli fibres undergo conformational change, they become incorporated by host Aβ and subsequently aggregate with Aβ plaques (Friedland, 2015). This has not been validated experimentally yet,

however there is evidence that *Escherichia coli* (K99) LPS's curli have been shown to localise to Aβ plaques in AD brains (Zhan et al., 2016; 2018).

Spirochetes and non-spirochetes are amongst the multiple microorganisms identified from AD brain specimens. The biofilm concept for AD considers Aβ "senile" plaques (composed of $A\beta_{1-42}$) as miniature biofilm structures (Allen 2016; 2017). In support, Miklossy (2016) demonstrated the biological characteristics of an *in vitro* spirochaetal biofilm in the context of AD. From the biofilm model of senile plaques perspective, Aβ may be serving as an EPS macromolecule in AD and is likely to involve prokaryotic curli fibre contribution and other amyloid-like proteins linking Aβ plaques as an innate immune response to trap and kill bacteria (Soscia et al., 2010; Kumar et al., 2016). The latter idea of Aβ as an antimicrobial has evolved into the antimicrobial protection hypothesis for AD plaque lesion formation (Moir et al., 2018) and strongly supports the plausibility of microbes in general and *P gingivalis* infection driving deposition of Aβ in the brain as indicated by the *in vivo* findings of Ilievski et al., (2018).

## 1.2 Periodontitis

Periodontitis involves the progressive destruction of gingival tissue, periodontal ligament and alveolar bone, due to chronic multifactorial inflammatory changes within the periodontium, as a result of the host response to pathogens (Hajishengallis & Lamont, 2016; Xu et al., 2020). Clinical signs of deepening periodontal pockets, gingival recession, loss of alveolar bone, tooth mobility and eventually, tooth loss (Hajishengallis et al. 2012). Based on Dewhirst et al. (2010) there are 687 predominant species in the oral cavity (Human Oral Microbiome Database, www.homd.org). Identification of bacteria based on cultural and culture-independent molecular studies using 16S rRNA gene comparative analyses (Krishnan *et al.* 2017).

Approximately 400–500 oral taxa have been detected in the subgingival crevice alone (Paster et al, 2001; Aas et al, 2005).

Of the 700 bacterial species identified in the oral cavity, more than 400 have been detected in subgingival plaque and periodontal pockets (Paster et al. 2006). The understanding of how dental plaque shifts from a microbiome (healthy biofilm) to a diseased state (pathobiome, or biofilm with more numbers of pathogens) have changed over time (Rosier et al. 2014). In a healthy site, a greater ratio and diversity of commensals (species of non-disease-causing microbes) to a lesser number of pathogens is present. Changes to the local environment (dysbiosis), shifts the balance within the microbial community favouring greater numbers of a pathogen compared to commensals, resulting in disease (Kumar et al. 2006). As periodontitis develops, a transition occurs from Gram positive bacteria to the more virulent Gram negative population, including filaments, rods and spirochetes. The oral flora implicated are the 'red complex' consisting of *Porpyromonas gingivalis*, *Tannerella forsythia* and *Treponema denticola* as well as the orange complex, examples of which are *Fusobacterium nucleatum*, *Prevotella intermedia*, *Eikenella corrodens* and *Campylobacter rectus*. The orange complex are the precursor to the red complex as they serve a 'bridging' function as early colonisers, facilitating more pathogenic bacteria to thrive in the periodontal biofilm (Kametani et al. 2024).

Periodontitis is associated with a decrease in microbial diversity, which may be the result of bacteria being able to manipulate the local immune function because of limited availability of nutrients at the periodontal pocket (Dewhirst et al. 2010, Camelo-Castillo et al. 2015). The ecology of the gingival crevice is unique as it is constantly bathed in GCF which contains serum factors and immunoglobulins. In periodontal lesions, the crevice becomes a pocket and site becomes highly anaerobic. The flow of GCF is increased in gingivitis and significantly

more in periodontitis, delivering humoral and cellular defence factors to combat microbial insult. Paradoxically, proteins and glycoproteins from GCF can provide substrates for bacterial metabolism e.g. transferrin and haemoglobin, immunoglobulins (Huynh et al., 2014).

### 1.2.1 Epidemiology of periodontitis

Based on data from the Global Burden of Disease (GBD), periodontitis was recognised as a significant public health burden of non-communicable diseases (Kassebaum et al., 2014; Wu et al. 2022). A systematic review and meta-analysis of epidemiological studies carried out by Trindade et al. (2023) covering the period between 2011 and 2020, estimated pooled prevalence of periodontitis as nearly 60% of the studied population. This is an alarmingly high prevalence, especially considering that the authors reported a substantial prevalence of 24% of severe periodontal disease. Not dissimilar to the Wu et al. (2022) GBD statistics, the Trindade et al. (2023) meta-analysis showed the highest prevalence in the older age group, 65 years and older.

### 1.2.2 *Porphyromonas gingivalis*

*Porphyromonas gingivalis* is a Gram negative, obligate anaerobic, non-motile, asaccharolytic rod or coccobacillus, able to trigger tissue disruption and sustain inflammation in periodontal tissues (Xu et al., 2020). It is considered the keystone microbiological agent causing periodontitis, belonging to the red complex family as discussed previously (Socransky et al. 1998). *P. gingivalis* can cause an imbalance in the host's response, leading to dysbiosis and irreversible tissue destruction in periodontitis (Hajishengallis & Lamont, 2016; Xu et al., 2020).

The mechanisms by which *P. gingivalis* manifests its virulence behaviour, have been investigated in several *in vivo* and *in vitro* studies. The recognised virulence factors include the bacterium's release of proteinases, known as 'Gingipains', the release of Lipopolysaccharides

(LPS), the presence of fimbriae, its capsule structure, the presence of adhesin domains and the production of Outer Membrane Vesicles, OMVs (Xu et al., 2020; Zhang et al., 2021; Mysak et al. 2014; Zheng et al., 2021; Bodet et al., 2007; How et al.,2016), Figure 1.4.

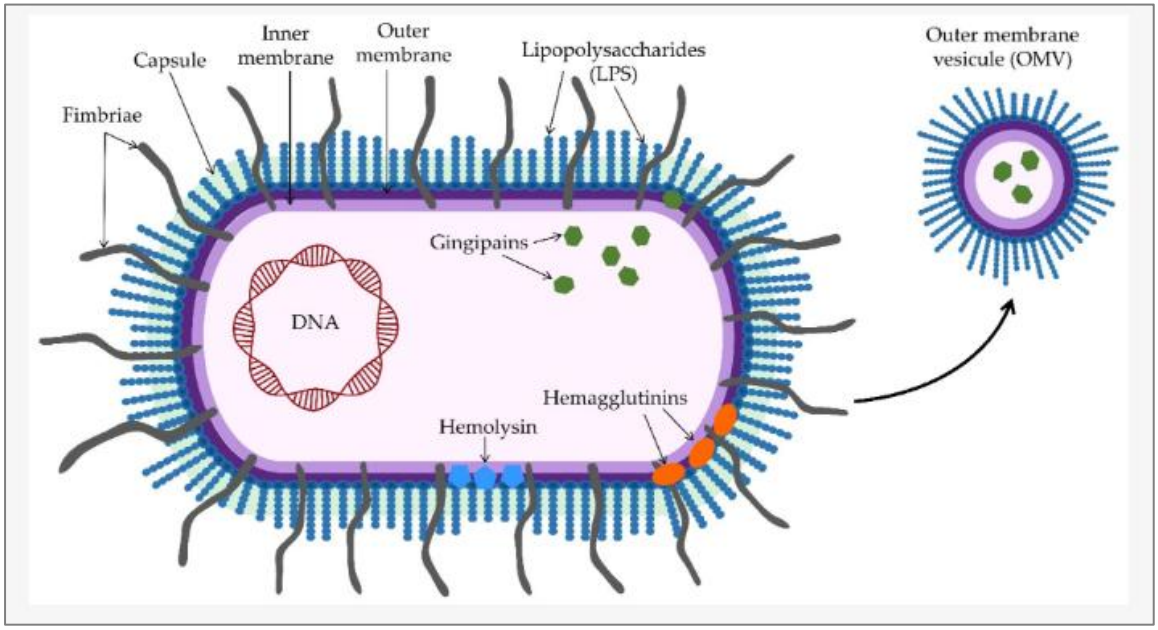


**Figure 1.4:** Structure of *P. gingivalis* shows the most significant virulence factors, which include gingipains, LPS, fimbriae, capsule, the presence of adhesin domains (hemagglutinin and hemolysin) and OMV (Image credit: Aleksijevic et al., 2022).

(i) Proteinases (Gingipains)

Gingipains are 'cysteine proteinases', which cleave the peptide and polypeptide bonds present on the host's epithelial cell surfaces causing their detachment from the connective tissue (Bostanci & Belibasakis, 2012). They also contribute to the degradation of several proteins in the host's immune system as complement, integrins, cytokines (Kristoffersen at al., 2015) and collagen allowing the penetration of *P. gingivalis* in the deeper tissues. The main isotypes of gingipains are arginine-Gingipain A (Rgp-A), arginine-Gingipain B (Rgp-B) and Lysine-Gingipain (Kgps) (Zhang et al. 2021). Gingipains may affect AD by enhancing the effect of

polymorphic complement gene defects as documented by The Genome-Wide Association Studies (GWAS) (Lambert et al. 2009, Lambert et al. 2013, Morgan 2018). It is also possible that gingipains, together with the defective complement component genes, aggravate and sustain AD through ineffective clearance of cellular debris, which in turn, aids the accumulation of hallmark proteins. Tau protein that associates with NFTs in AD brains is said to be a substrate for gingipains (Dominy et al., 2019).

(ii) Lipopolysaccharides (LPS)

Lipopolysaccharides (LPS) is the most representative component of *P. gingivalis* outer cell membrane, and it acts as an MAMP or microbe-associated molecular patterns, which sets off the host's immune responses (Xu et al., 2020). Different acylations (presence of tetra- and penta-acylated lipid A structures) in LPS allows *P. gingivalis* to modulate its interactions with the host immune system by changing the relative proportions of the lipid A forms. The heterogeneity of lipid A structures can differentially activate signalling pathways as well as control cytokine production through interactions with TLR-2 and TLR-4 as IL-1, IL-6, IL-8 and TNF-alpha (Curtis et al., 2011, Zhang et al., 2021).

(iii) Capsule

The *P. gingivalis* capsule is a dense outer layer made of polysaccharide which masks the cell surface, thereby evading the host's immune response by reducing the intensity of the inflammatory response. This ensures the bacteria's survival under adverse conditions (Xu et al., 2020). The capsule offers protection from opsonisation and phagocytosis (Bostanci & Belibasakis, 2012). *P. gingivalis* exhibits three types of surface glycans i.e. O-LPS, A-LPS and K-antigen capsule, which accounts for strain serotype specificity. The *P. gingivalis* strain W83 is associated with severe periodontitis, while ATCC 33277 strain does not possess a capsule,

leading to a more localized abscess (Vernal et al., 2014). This may not disseminate in animal infection models (Monasterio et al., 2019).

(iv) Fimbriae

Fimbriae are thin filaments that extend beyond the outer membrane of the *P. gingivalis* cell surfaces. They are composed of two parts; Mfa1 and FimA protein subunits (Jia et al., 2019) and they help *P. gingivalis* to adhere to host cells, co-aggregating with other bacteria in the biofilm structure and to invade host cells (Jia et al., 2019). There are two types of fimbriae according to their length i.e. long fimbriae (major) are able to evade the complement system, while the short ones (minor) promote osteoclastic differentiation of stem cells leading to bone resorption (Jia et al., 2019, Aleksijevic et al., 2022).

(v) Adhesin domains

*P. gingivalis*' survival and virulence is dependent on iron availability. This leads the bacterium to acquire iron from the heme group in salivary and crevicular hemoproteins and erythrocytes. (Smalley et al., 1998). *P. gingivalis* can extract the heme binding it with its adhesins, as Hemaglutinin (HGP44), hemolysin and Hemoglobin receptor protein (HbR) (Smalley & Olczak, 2017). However, *P. gingivalis* is unable to provide itself a constant supply of adhesins. They are produced through the catabolic activity of gingipains to produce gingipains-adhesins complexes on the cell surface and on the outer membrane vesicles (Smalley and Olczak, 2017), while at the same time, adhesins are required for the maturation of its cell surface proteins as gingipains and fimbrilin (Nhien et al., 2010).

(vi) Outer Membrane Vesicles (OMVs):

A typical *P. gingivalis* feature is the production of Outer Membrane Vesicles (OMVs). They mainly contain LPS, gingipains, phospholipids, C-terminal domain proteins, DNA and RNA and they are localised on the cell surfaces by type IX secretion system of the patient (Zhang et al., 2021). Their specific role is still under investigation, however the main tasks are assisting with bacterial co-aggregation within the biofilm and supporting the quorum sensing (Bonnington & Kuehn, 2014), nutrient seeking and supporting via the heme provision (Zhang et al., 2021) and cell invasion by endocytosis therefore damaging and triggering apoptosis (Cecil et al., 2019).

## 1.3 Microbiota of periodontal and endodontic disease

*P. gingivalis* can also participate in endodontic disease, a polymicrobial infection of the root canal due to caries, cracks, traumatic injuries or advanced periodontal disease which create pathways for bacteria to enter the root canal system. Successive inflammatory responses within the infected pulp tissue causes an inflammatory lesion in the periapical tissues termed 'Apical Periodontitis' (Nair, 2004). In parallel with periodontitis, apical periodontitis also poses a considerable global health burden. A systematic review and meta-analysis concluded that half the adult population worldwide have at least one tooth with apical periodontitis (Tiburcio-Machado et al., 2020).

Previously. culture dependant and culture independent molecular biology studies have detected *P. gingivalis* with a prevalence of up to 29% and as high as 72% respectively in the cases of primary endodontic infection. The microbial profile of primary infected root canals (untreated canals) consists of 10–30 species per canal, predominantly anaerobic bacteria (Siqueira 2009, Munson et al., 2002). Gram-negative bacteria detected in primary endodontic infections

include *Fusobacterium, Porphyromonas, Prevotella, Parvimonas, Tannerella, Treponema, Dialister, Filifactor, Actinomyces* and *Pseudoramibacter*, suggesting an overlap of bacterial genera with other periodontal disease (Munson et al., 2002, Siqueira et al., 2008).

Periodontal and endodontic infections are both polymicrobial biofilm-mediated diseases dominated by anaerobic communities from similar phyla e.g. *Firmicutes*, *Bacteroidetes, Fusobacteriota, Actinobacteriota*. Next-generation sequencing studies show that endodontic infections are dominated by obligate anaerobes such as *Fusobacterium, Prevotella, Porphyromonas, Parvimonas* and *Olsenella*, whereas periodontal pockets—chronically exposed to saliva and gingival crevicular fluid—are characterised by red-complex species (*Porphyromonas gingivalis*, *Tannerella forsythia*, *Treponema denticola*) alongside *Aggregatibacter actinomycetemcomitans*. (Siqueira & Rocas, 2022, Baksh et al. 2023, Park et al,, 2025). High-resolution profiling of persistent endodontic infections demonstrated that root canal microbiota differed from sulcular communities which exhibited more *Streptococcus* and *Actinomyces*, yet several taxa are shared, supporting microbial migration along anatomical communications in endo-perio lesions (Gomes et al.,2015, Siqueira & Rocas, 2022). Siqueira and Rôças (2022) reported that high-throughput molecular studies revealed marked inter-individual heterogeneity driven by microbial succession, ecological pressures and treatment history (Figure 1.5).

These biofilms act as chronic reservoirs of virulence factors (LPS, proteases, outer-membrane vesicles) capable of inducing episodic bacteraemia and low-grade systemic inflammation, with both periodontal and endodontic infections contributing to a cumulative “oral inflammatory burden” (Gomes et al. 2015, Bakhsh et al., 2023). For periodontitis, robust epidemiological data show independent associations with cardiovascular disease, diabetes, chronic respiratory

disease, adverse pregnancy outcomes, multiple cancers, metabolic syndrome, neurodegenerative and autoimmune conditions, and indicate that periodontal therapy can improve glycaemic control and surrogate cardiovascular risk markers (Herrera et al., 2024, Isola et al., 2025). Longitudinal biomarker studies nevertheless show that successful endodontic treatment can significantly reduce serum and salivary inflammatory and cardiovascular-risk biomarkers (e.g. hs-CRP, ADMA, MMP-2), underscoring that chronic endodontic lesions also contribute meaningfully to systemic inflammatory load (Al-Abdulla et al., 2023)

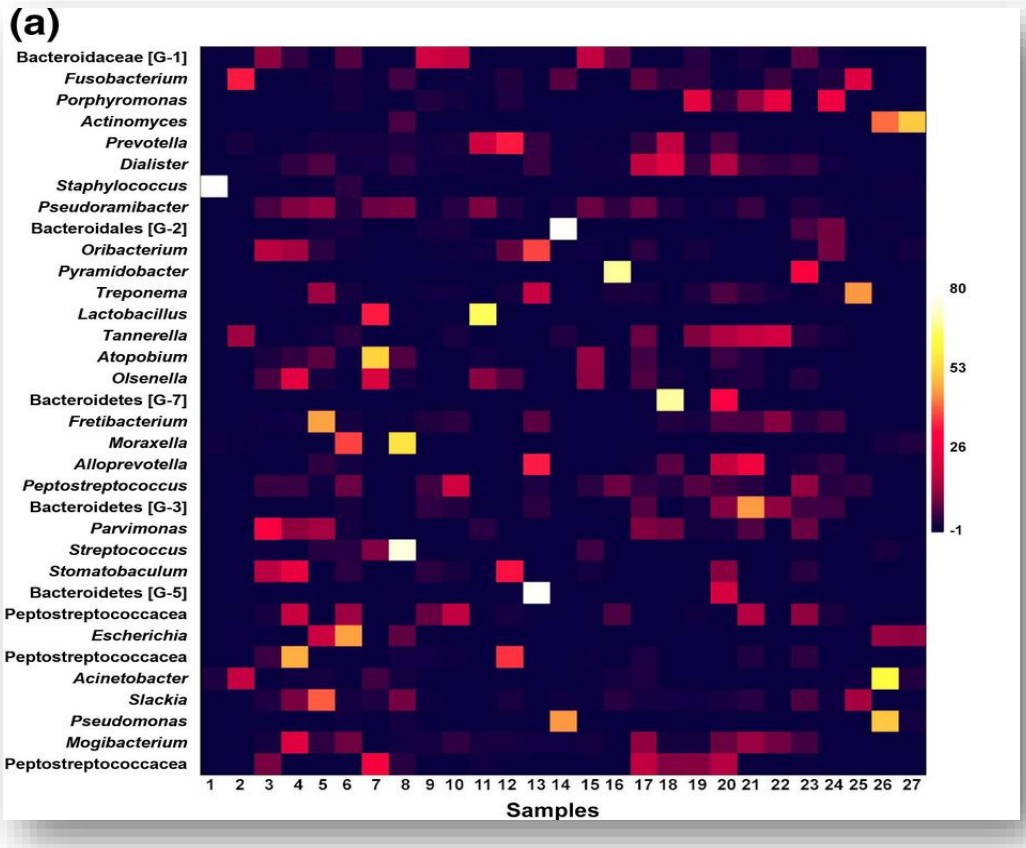

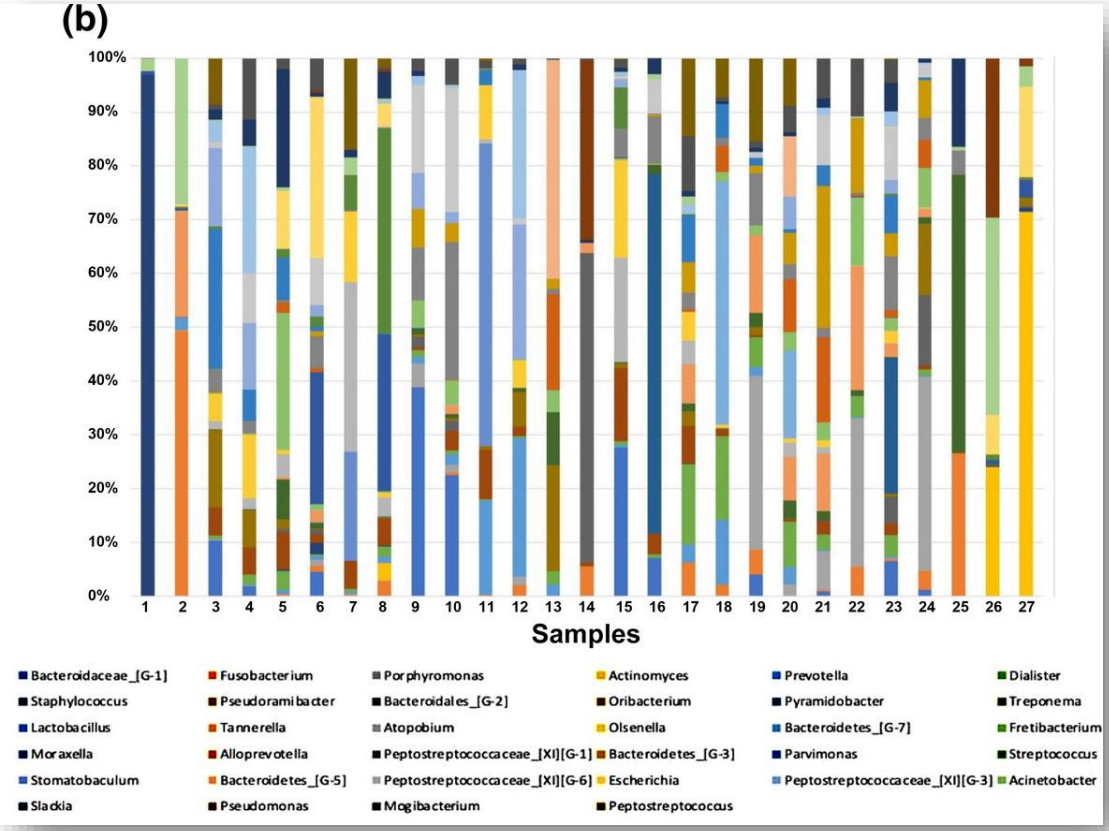


Figure 1.5: Unpublished data by Siqueira & Rocas (2022) showed interindividual variability in the root canal microbiome (richness and relative abundance) in teeth with asymptomatic primary apical periodontitis. It was noted that not two individual samples were the same, as seen in the heatmap (a) and stacked bar chart (b).

Persistent/secondary infected root canals are associated with microorganisms which have survived the chemo-mechanical procedures or invaded the canal via coronal leakage. The microbiota is composed of a more restricted group of species as compared to primary infections. Facultative anaerobic and Gram-positive bacteria predominate in these canals. Some bacteria have exhibited the ability to survive in a quiescent phase with low metabolic activity during periods of nutrient scarcity, awaiting the opportunity to re-establish once nutritional conditions become favourable (Molander et al., 1998). *Enterococcus faecalis*, a

facultative and opportunistic Gram-positive bacterium, which has the abovementioned characteristics and can survive independently as a mono-species biofilm (Fisher et al., 2009; Molander et al., 1998). Other bacterial species, frequently found in cases of persistent disease include streptococcal species, *Parvimonas micra*, *Propionibacterium* species and *Pseudoramibacter alactolyticus*, which are commonly reported in persistent intraradicular infections. Candida species are also more frequently detected in these teeth (Munson et al., 2002; Pinheiro et al., 2003; Siqueira 2009) and they have been detected in brains of dementia patients (Carrasco et al., 2017).

In chronic apical abscesses caused by endodontic infection, a draining sinus may track through the periodontium, forming a deep, narrow and isolated periodontal pocket, adjacent to, or alongside, the gingival sulcus. Jansson et al. (1995) reported that periodontitis patients lost more attachment when root canal infection was present as compared to teeth with no periapical lesions. Untreated endodontic infection has also been shown to impair periodontal healing following non-surgical periodontal therapy (Ehnevid et al., 1993).

Extra radicular infections, although uncommon can also occur due to an inadvertent inoculation of intra-radicular microorganisms beyond the apical opening of the root canal during chemo-mechanical debridement. This is characterised by apical abscess. Apical actinomycoses can also occur as an independent lesion, caused by Actinomyces spp. and the opportunistic Propionibacterium spp., requiring periapical surgery for their resolution (Gomes & Pinheiro 2007; Narayanan et al., 2010).

The combined ‘endo-perio’ disease is characterised by the presence of both the pulp and periodontal infection in the same tooth (Abbott et al., 2009). The anatomic connections

between the dental pulp and the periodontium provide an explanation as to the overlap in microbiota. Molecular detection demonstrated a correlation between *T. forsythia*, *P. gingivalis*, *F. nucleatum* and *A. actinomycetemcomitans* at concurrent sites in endodontic-periodontal diseases (Lacevic et al., 2015, Das et al., 2020). This supports the notion that periodontal lesions can be a source of endodontic pathogens and in turn, apical periodontitis can sustain periodontal lesions (Kurihara et al., 1995), Figure 1.6. Elevated systemic cytokine levels have also been detected with both disease processes (Barkhordar et al., 1999, Gamonal et al., 2000).

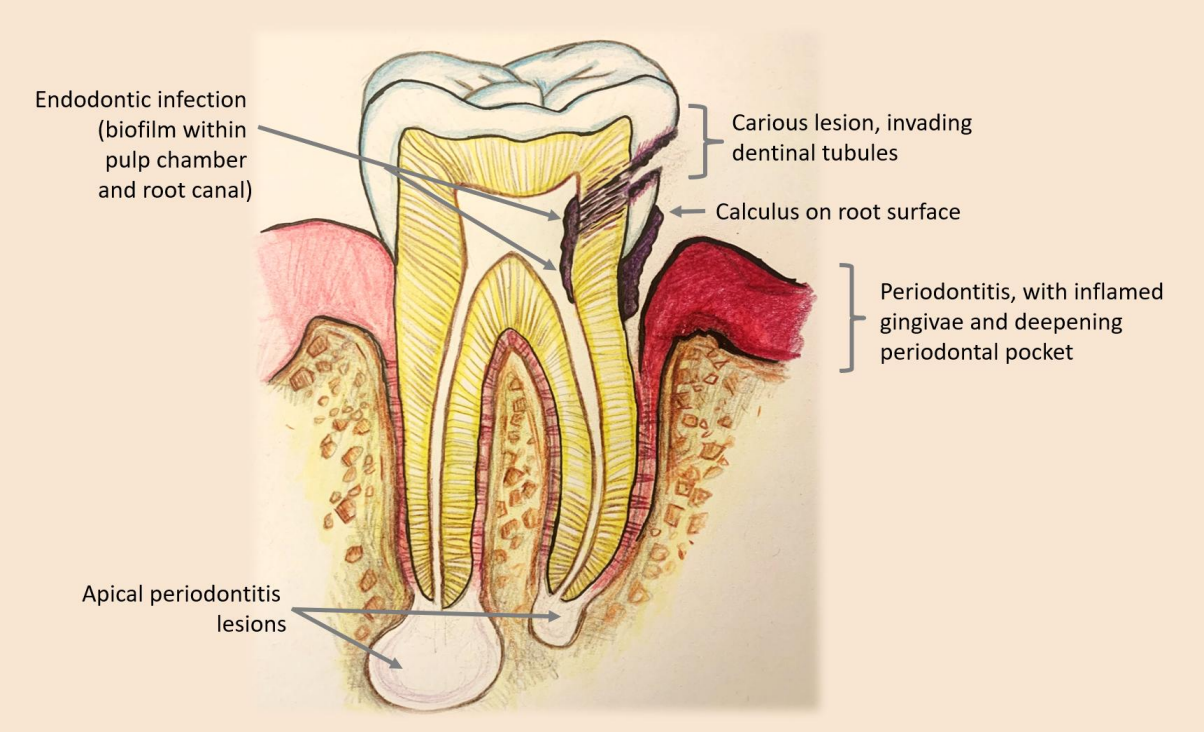


**Figure 1.6:** Endodontic-periodontal disease showing concurrent periodontal disease (with inflamed gingivae and deepening periodontal pockets, due to host response to the accumulation of calculus on the root surface (containing subgingival biofilm). Dental caries is typically the cause of endodontic infection as seen by the invasion of dentinal tubules, into the pulp chamber and infection of the root canals, leading to a pulpal necrosis. This triggers the subsequent inflammatory immune response, resulting in the development of periapical lesions representing apical periodontitis.

## 1.4 Periodontitis and AD

There is mounting evidence to show a positive link between periodontitis and AD. To date, there are arguments as to which disease comes first, as the causal relationship has not been established between the two disease entities (Harding & Singhrao, 2021). More studies are reporting that patients with periodontitis present a higher risk of developing AD (Stein et al. 2007, Sparks-Stein et al., 2012; Demmer et al., 2020, Ma et al.,2021), whereas patients with AD typically have difficulty maintaining optimal oral hygiene habits due to their cognitive decline, making them more likely to develop periodontitis (Ryder & Xenoudi, 2021).

### 1.4.1 Bacteraemia

Periodontal conditions (gingivitis and periodontitis) as well as endodontic infections have been reported to increase the risk of bacteraemia (Bender et al., 1960; Debelian et al., 1995; Parahitiyawa et al., 2009). Researchers have reported a risk of bacteraemia arising from daily dental hygiene activities or chewing as well as from invasive dental treatment (Selton-Suty et al., 2012; Tubiana et al., 2017). In fact, bacteraemia is well recorded in dentistry by researchers who have linked this to dental extractions, surgical flaps, periapical curettage, non-surgical root canal treatment and even dental scaling (Baumgartner et al., 1976, Heimdahl et al., 1990). While transient bacteraemia may not significantly impact healthy individuals, those who are immunocompromised may face life-threatening complications such as septic shock and organ failure (Nielsen, 2015). When ulceration occurs in non-keratinised periodontal pockets and junctional epithelium, this can create an entry portal for bacteria and their endotoxins to enter the systemic circulation (Tomas et al., 2012).

### 1.4.2 Inflammatory mechanisms and comorbidities in periodontitis and AD

Increased microbial load on the gingival epithelium (junctional complex) can initite and amplify the host innate immune inflammatory response (Graves, 2008). Neutrophils migrate into the area, secreting chemokines and proteases which facilitate epithelial disruption and attract more immune cells (Balta et al., 2017). This makes the periodontal pocket a gateway for inflammatory mediators and bacteria into the bloodstream and facilitates its ability to reach distant organs, aggravating chronic inflammatory conditions (Fine et al., 2020). The mouth–body link is driven by multiple microorganism-induced immunological mechanisms that converge to increase the susceptibility of patients with periodontitis to NCD chronic inflammatory diseases.

NCDs are associated with a constant low grade inflammation stimulus (silent risk factor), which may be provoked and sustained by ongoing periodontal disease (Moutsopoulos & Madianos, 2006). C-reactive protein (CRP), produced by the liver in response to inflammation, with values above 3 mg/L, but below 10 mg/L, can be considered as low grade inflammation (Loos, 2005; Cecoro et al., 2020). Many researchers have reported that patients with periodontitis exhibit increased neutrophils in the blood stream as well as elevated levels of inflammatory mediators such as IL-1, IL-6, CRP and fibrinogen as seen in patients with cardiovascular disease (Genco et al., 2010; Bokhari et al., 2012; D'Aiuto et al. 2013).

Pathogens challenge the innate and the adaptive immune response with the release of cytokines, which are responsible for the further amplification of the local inflammatory reaction (Bui et al., 2019; Konkel et al., 2019, Ramadan et al., 2020). Periodontitis, cardiovascular disease, diabetes and cognitive decline have been reported to have co-dependent risk. This is supported by the positive correlation between achieving good oral health (periodontal stability) to diabetic

control (Chapple et al., 2013). D'Aiuto et al. (2018) reported reduced plasma glucose concentrations and HbA1c and improved vascular and kidney functions in Type 2 Diabetes Mellitus patients who underwent effective periodontal therapy. Similar trends in improvements in various biomarkers were reported in patients with hyperlipidaemia and liver disease, (Yoneda et al., 2012, Bajaj et al., 2018, Orlandi et al., 2020). Refer Figures 1.7 and 1.8.

Goto et al. (2020), extracted molar teeth (to simulate tooth loss from periodontitis) in triple transgenic AD (3xTg-AD) mice and revealed a neurodegenerative pathway involving the trigeminal distribution within the periodontal ligament to the locus coeruleus. From this location, tau pathology subsequently spread to the hippocampus. Gingipains have similar APP-cleaving action as cathepsin B (of the host) can interact with the APP signalling pathways (amyloid cascade) to release Aβ (Wu et al., 2017). Together with LPS, gingipains can proteolytically activate kinases such as GSK-3β which can cause hyperphosphorylation of neuronal tau (Dominy et al., 2019, Haditch et al., 2020, Illievski et al., 2018).

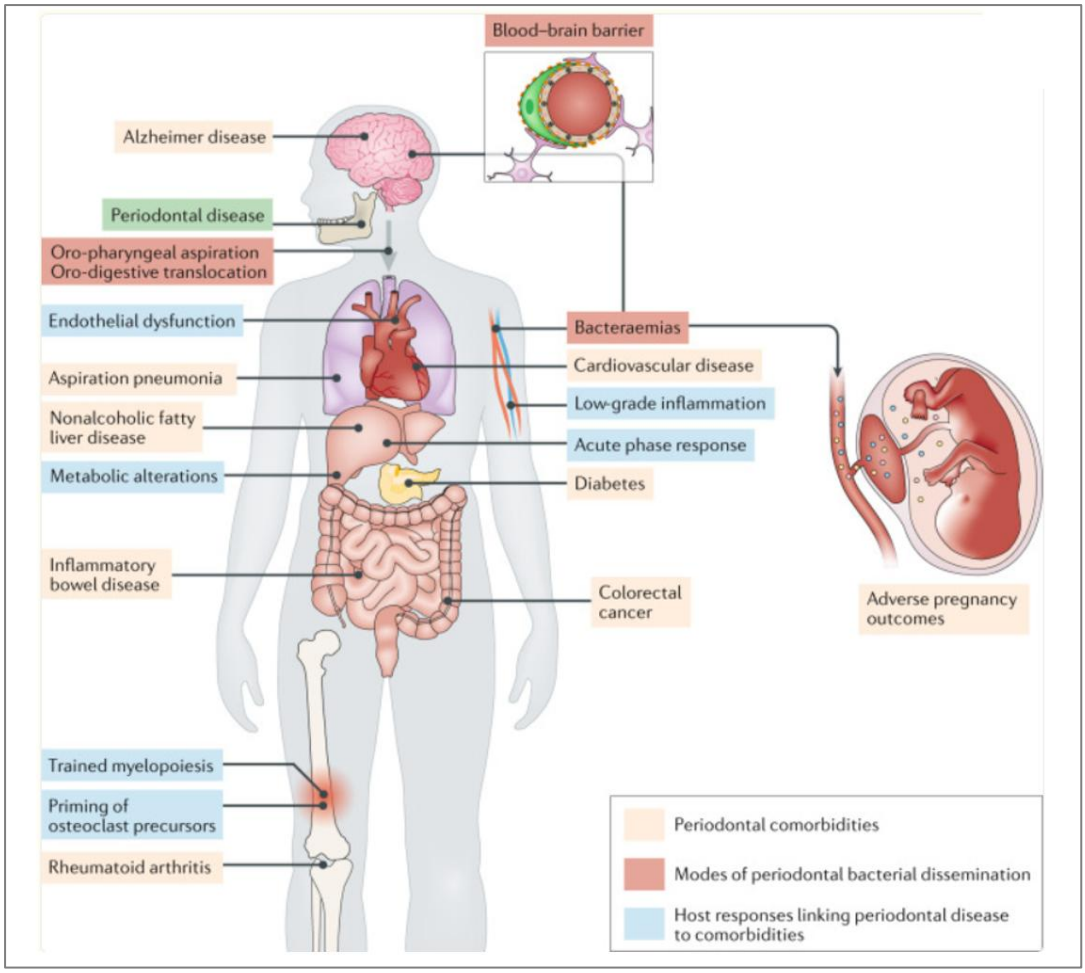


**Figure 1.7:** Periodontal bacteria such as P. gingivalis can spread via different routes e.g. haematogenous, oropharyngeal and orodigestive to get to extra-oral sites. Periodontitis share a number of comorbidities with a multitude of systemic diseases based on epidemiological evidence, clinical studies as well as animal model research. As a result of bacteraemia and systemic inflammation, metabolic and inflammatory alterations can occur in the liver and bone marrow, which impacts comorbid conditions (Image credit: Hajishengallis & Chavakis 2021).

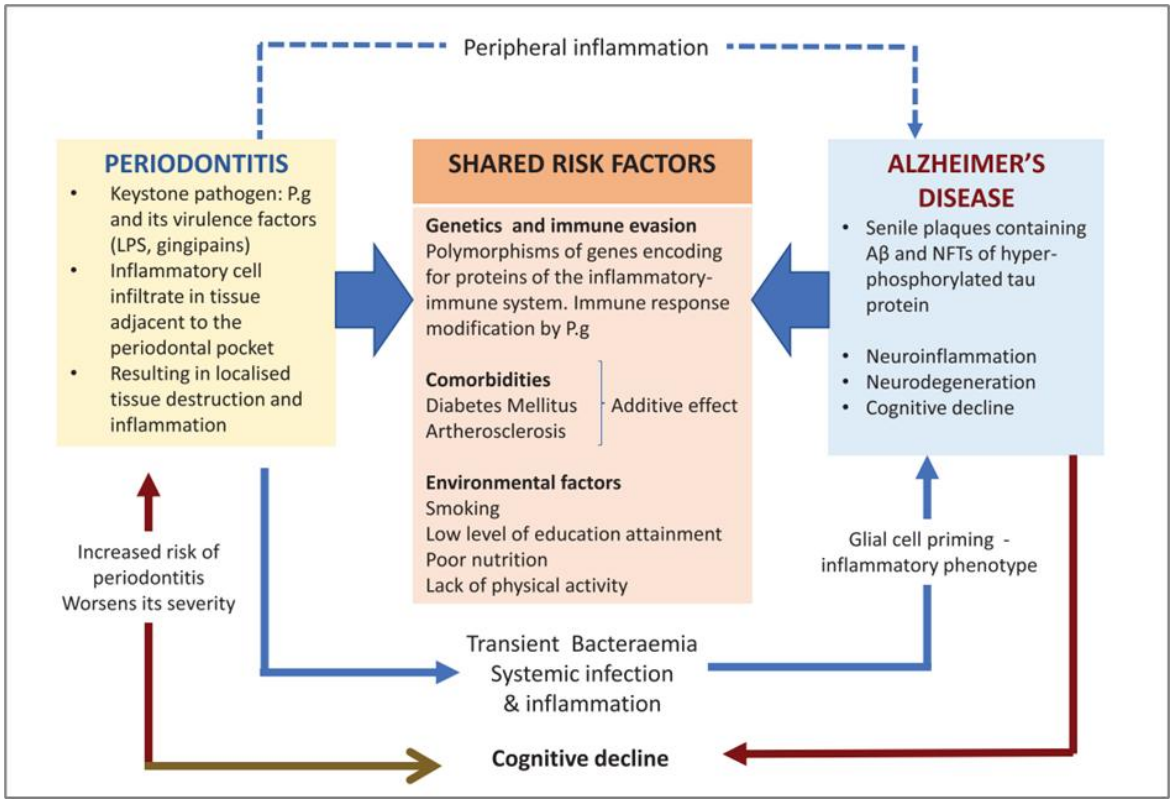


**Figure 1.8:** Transient bacteraemia facilitates the keystone periodontal pathogen, *P. gingivalis* (Pg) in invading the bloodstream and gaining access to the brain via multiple routes, including a leaky BBB. The cerebral immune response triggers neuroinflammation and the eventual formation of the two diagnostic lesions of AD (Aβ and NFTs). Periodontitis also has an indirect influence by sustaining peripheral inflammation via immune modulators e.g. IL-1, IL-6 and TNFα (blue dotted arrow). This can cause astrogliosis and microgliosis. Clearing of toxic neuropeptides from the central nervous system (CNS) can be impaired by the ongoing neuroinflammation. The plausibility of a causal relationship of periodontitis and AD is further supported by shared risk factors such as genetics, comorbidities and environmental factors (Image credit: Kanagasingam et al., 2020).

### 1.4.3 Epidemiological evidence linking periodontitis and AD

Multiple studies have reported improved cognitive function in dementia patients who received appropriate dental care (Rolim et al., 2014; Schwahn et al., 2021; Yoneyama et al., 2022). Conversely, poor oral hygiene and oral diseases have been associated with increased incidence and severity of AD (Hugo et al., 2007; Cicciu et al., 2013; Hatipoglu et al., 2011; Ribeiro et al.,

2012; Syrjala et al. 2012). The risk of developing AD doubled when periodontal disease persisted for ten years from initial diagnosis (Sparks Stein et al., 2012; Chen et al., 2017).

Longitudinal studies which have provided robust evidence to support the plausibility of a causal link between periodontitis and cognitive status have been summarised in Table 1.1. Poor dentition, a late surrogate marker of early-life oral diseases such as periodontitis, is linked to both cognitive impairment and incident dementia i.e. the first ever diagnosis of dementia for an individual (Gatz et al., 2006; Stein et al., 2007; Stewart et al., 2008, Nobel et al., 2008). Results from the longitudinal cohort studies carried out by Stein et al. (2010), Cicciu et al. (2013), Paganini-Hill et al. (2012) and Arrive et al. (2012) were in agreement that lower number of remaining dentition (with an average of less than 9 teeth) is associated with cognitive decline.

A number of large scale, population-based insurance medical database studies have utilised Cox Regression Models to predict dementia development after adjusting for other variables. Lee et al. (2017) analysed medical records of 187,747 Taiwanese subjects with periodontitis over 10 years. They found that subjects who did not receive periodontal treatment and those with severe periodontitis had a significantly higher risk of developing dementia. Similarly, Chen et al. (2017) concluded that a 10-year exposure to periodontal disease was linked to a 1.7 fold increase in the risk of AD. Kim et al. (2020) analysed retrospective medical records from 237,940 South Korean subjects and showed that 1 to 9 remaining natural teeth is considered a modifiable risk factor for development of AD, vascular dementia and mixed dementia.

In fact, a nationwide nested case-controlled study utilising the Taiwan National Health Insurance database were the first to link dementia and endodontic treatment. Over 200,000 AD

cases were matched to over 800,000 healthy controls to carry out conditional regression modelling. The authors reported that root canal treatment and limited numbers of extractions lowered dementia odds ratios (Lin et al., 2020). In line with previous studies, the number of teeth extracted had a temporal impact i.e. the extraction of more than 4 teeth over 10 years increased the odds ratio of dementia. Comorbidities such as cardiovascular disease, hypertension, stroke and diabetes were implicated in increasing the odds of developing AD (Lin et al.,2020). These results agreed with interventional studies which have reported potential benefits of optimal endodontic and periodontal therapy in reducing serum levels of inflammatory biomarkers associated with cardiovascular disease risk and metabolic disorders (Tonetti et al., 2007; Merchant et al., 2016; Al-Abdulla et al., 2023).

Insurance database studies are limited by reliance on diagnostic coding, lack of clinical detail, and potential misclassification of cases, as well as potentially inaccurate analytical algorithms. The generated data should still be considered as this is the only method to include large scale cohorts, with long-term data.

**Table 1: Summary of characteristics and critical findings of longitudinal studies on oral health and cognitive status**

| Author, location, study title | Sample and study details | Critical findings |
|---|---|---|
| **Kaye et al., 2010**<br><br>Tooth loss and periodontal disease predict poor cognitive function in older men.<br><br>Boston, MA, USA | N= 1231, males<br>Ages: 24-84<br>Convenience sample<br>Follow up: every 3 years, up to 32 years | Tooth loss, alveolar bone loss, deeper periodontal pocket, new carious lesions and restorations were all associated with lower MMSE and SCT scores |
| **Stein et al., 2010**<br><br>Tooth loss, apolipoprotein E, and decline in delayed word recall.<br><br>Milwaukee, WI, USA | N= 144 nuns, with known APOE ε4 status.<br>Ages: 75-98<br>n=32 dementia<br>n=112 without dementia<br>n=101 with adequate follow up<br>Follow-up: annual,12 years | Subjects with APOE ε 4 allele, ≤9teeth, or both had poorer delayed recall scores at baseline<br><br>Cognitive decline occurred faster than those with one or neither of the 2 risk factors |
| **Paganini-Hill et al., 2012**<br><br>Dentition, Dental Health Habits, and Dementia: The Leisure World Cohort Study<br><br>Laguna Hills, CA, USA | N=5468<br>Ages: 52-105 (median 81)<br>Male=1733<br>Female=3735<br><br>Number with dementia=1145<br>Follow-up: up to 18 years | Men with poor natural masticatory function and did not wear dentures had a 91% greater risk of dementia compared to those with adequate natural masticatory function (≥10 upper teeth and ≥6 lower teeth).<br><br>This risk was also greater in women but not statistically significantly.<br><br>Dentate individuals who reported not brushing their teeth daily had a 22-65% higher risk of dementia than those who brushed 3 times daily. |
| **Arrive et al., 2012**<br><br>Oral health condition of French elderly and risk of dementia: a longitudinal cohort study<br><br>Gironde, France | N=405<br>Ages: 66-80 (Median 70)<br>M=184, F=221<br>Follow-up: 10 years | Having ≥ 11 missing teeth seemed to be associated with a lower risk of dementia in subjects with lower education, possibly owing to the suppression of source of chronic inflammation. |

MMSE: Mini Mental State Examination
SCT: Spatial copying task

## 1.5 Originality, Hypothesis and Overall Aims and Objectives

To date, there is no conclusive evidence to prove the causative link between periodontitis and AD. This PhD project is original and builds on the existing research related to the infection model of AD, through *P. gingivalis* for the hallmark AD lesions, Aβ, phosphorylated tau and NFTs.

The first hypothesis was that periodontal, cariogenic and endodontic bacteria contribute to peripheral pools of Aβ with the potential for spreading into the brain.

The second hypothesis was that *P. gingivalis* virulence factors and pro-inflammatory cytokines can modulate the amyloidogenic processing in neuronal cells to increase peripheral pools of Aβ.

The third hypothesis assumed that *P. gingivalis* and *F. nucelatum* infection in a co-morbidity mouse model for obesity and diabetes would reproduce AD pathological hallmark proteins in the mouse brain tissues.

The fourth hypothesis was that tau fragments cleaved by gingipains would exhibit antibacterial effects against *P. gingivalis*.

The fifth hypothesis assumed that tau can form helical twists *in vitro*.

The final hypothesis was that tau-bound NFTs are birefringent.

The overall aim was to gain a better understanding about the relationship between periodontal infection and AD pathogenesis, including the development of AD hallmark lesions which are responsible for cognitive decline.

The objectives of this PhD research project were:

- To detect amyloid-β (Aβ) within microbial biofilms.
- To determine whether conditioned medium from *Porphyromonas gingivalis* can cleave APP to release $A\beta_{40}$ and $A\beta_{42}$.
- To investigate the effect of *P. gingivalis* and *F. nucleatum* oral infection on the development of AD pathophysiology in an obese, diabetic (db/db) mouse model.
- To assess whether gingipains-fragmented tau peptides display antimicrobial properties and the potential for paired helical/straight filament (PHF/SF) formation.

The methodologies chosen for this research project included the use of extracted infected teeth, light microscopy, scanning electron microscope (SEM) and transmission electron microscope (TEM). These techniques were to facilitate morphological examinations and immunolabelling.

An *in vitro* cell culture methodology involving SH-SY5Y cell line challenged with *P. gingivalis* conditioned medium in the presence and absence of cytokines was also employed to simulate the clinical situation in a controlled manner. The cells and their supernatants were assessed for APP cleavage fragments by immunoblotting and TEM.

An obese, diabetic (db/db) mouse model was used to investigate the potential for development of AD hallmark proteins (Aβ, tau and NFTs) when inoculated with *P. gingivalis* and *F. Nucleatum*. The methenamine silver impregnation technique and immunohistochemistry were employed to assess for signs of neuroinflammation.

*P. gingivalis* antibacterial assays were performed to assess if gingipains-fragmented tau peptides displayed antimicrobial properties. Circular dichroism (CD) was undertaken to determine tau peptide secondary structure. Paired helical/straight filament (PHF/SF) formation was evaluated using polarizing light microscopy and TEM.

At the time of developing the experimental protocols for this PhD research study, to the best of the candidate's knowledge, there were no studies which had been carried out with the abovementioned combination of research protocols.

# CHAPTER 2

## *EX VIVO* DETECTION OF AMYLOID-BETA IN ORAL BIOFILM OF EXTRACTED HUMAN TEETH WITH ENDODONTIC AND PERIODONTAL DISEASE

The work presented in this chapter is fully published by the author of this thesis, see reference below.

**Kanagasingam S**, von Ruhland C, Welbury R, Singhrao SK. Ex vivo Detection of Amyloid-β in Naturally Formed Oral Biofilm. J Alzheimers Dis Rep. 2022 Dec 16;6(1):757-773. doi: 10.3233/ADR-220076.

# *EX VIVO* DETECTION OF AMYLOID-BETA IN ORAL BIOFILM OF EXTRACTED HUMAN TEETH WITH ENDODONTIC AND PERIODONTAL DISEASE

## 2.1 INTRODUCTION

The two pathological hallmarks of AD, namely Aβ and NFTs define this disease and are strongly considered to contribute to intrathecal neuroinflammation (Miklossy 1993; Akiyama et al., 2000; McGreer et al., 2002; Bertram et al., 2010; Heneka et al., 2015; Moir et al., 2018). However, this hypothesis overlooks the contribution of peripheral inflammation that impacts the brain due to extraneous factors that reach the brain during life. To date, the sporadic form of AD (sAD) has no confirmed aetiology, although a multidomain risk factor model has recently been proposed (Akushevich et al., 2023). Amongst the various hypotheses, infection has been implicated as a potential pathway for peripheral and intrathecal neuroinflammation, with viruses, fungi and bacteria reported to be the potential causative agents (Miklossy, 1993; Balin et al., 2008; Poole et al., 2013; Zhan et al., 2016; Itzhaki et al. 2016; Alonso et al., 2017; Dominy et al., 2019). The discovery of significantly more bacterial DNA and the lipopolysaccharide, or LPS, component of bacterial outer membranes in AD brains compared to age-matched non-AD subjects lends support to the ‘infection hypothesis’ in recapitulating the hallmark proteins of AD following oral infections with P. gingivalis (Ilievski et al., 2018; Dominy et al., 2019). This explains the pervasive inflammation in AD and the involvement of innate immunity (Akiyama et al., 2000; McGreer et al., 2002; Poole et al., 2013; Heneka et al., 2015–15; Moir et al., 2018).

The role of the functional amyloid protein, Aβ is not fully understood in AD pathogenesis. Accumulation of these aggregated proteins can form insoluble fibrillar structures has been recognised to be neurotoxic and may lead to neuronal death. It has been further proposed that Aβ may also have an antimicrobial function which may confer potential neuroprotection (Moir et al., 2018). The "Antimicrobial Protection Hypothesis" of AD proposes that the formation of amyloid could be an early innate immunological reaction to actual or falsely perceived immune threats. Initially, Aβ captures and destroys invasive microorganisms, acting like conventional cytokines. Aβ fibrillization subsequently occurs to combat the infection and remove the amyloid-pathogenic deposits. This triggers and sustains neuroinflammatory pathways, resulting in neurodegeneration. This hypothesis explains how an increase in the quantity of bacteria in the brain may increase inflammation, amyloid build-up, and the progression of AD (Itzhaki et al., 2016; Moir et al.,2018). The role of Aβ in the dysregulation of the innate immune response is compatible with the well accepted 'Amyloid Cascade Hypothesis' which identifies β-amyloid deposition as the central event in AD pathogenesis. This has ultimately driven therapeutic strategies with mixed outcomes (Karran & De Strooper, 2022).

Both soluble and insoluble Aβ have been associated with AD. Soluble Aβ levels in the brain parenchyma increased threefold in AD and correlated significantly with markers of disease severity, whereas the overall Aβ load (mainly in the form of insoluble Aβ) is diagnostic of AD (McLean et al., 1999). Functional amyloids are characterised by highly organised fibrillar protein polymers that may self-assemble from their monomeric protein form and are defined by a cross-quaternary structure (Dueholm & Nielsen 2017; Fandrich 2007). These functional amyloids have been found to be common in both naturally occurring and artificially created microbial biofilms in histological investigations using amyloid-specific dyes (Congo red, Thioflavin T/S), or amyloid conformation-specific antibodies (Sunde et al., 1997; Chapman et

al., 2002,). These amyloids serve as 'functional' supports for the structure of biofilms; proteins from microbial appendages including curli, pili, and fimbriae are examples of functional amyloids. These appendage proteins are unique to each genus of bacteria, which may undergo conformational changes to form microbial Aβ fibrils under yet unknown physiological conditions (Sunde et al., 1997; Jimenez et al., 1999; Nelson et al., 2005; Friedland 2015).

Friedland (2015) suggests that microbial amyloids may have a sinister role in AD risk via the phenomenon known as 'cross-seeding'. This is the method by which amyloid deposits can aggregate and spread throughout a tissue, or transfer from one organ to another (Subedi et al., 2022). This could occur similarly to the mechanism of transmission of 'prions' in transmissible spongiform encephalopathies. Prions are abnormal, pathogenic proteins which can stimulate abnormal folding of specific normal cellular prion proteins, which are abundant in the brain, leading to progressive brain damage and eventual death (Eisenberg & Sawaya, 2017).

The possible translocation of Aβ generated peripherally (by platelets, skeletal muscle cells, skin fibroblasts, and monocyte/macrophages) to the brain has been demonstrated by Zeng et al. (2021) via the receptor for advanced glycation end (AGEs) products, which is up-regulated in cerebral endothelial cells upon *P. gingivalis* infection. Friedland (2015) continued to theorise that Aβ cross-seeding was a risk for cognitive deterioration. This appears to be corroborated by the Human Microbiome Project, whereby pathogens implicated in gastrointestinal tract dysbiosis were linked to AD pathogenesis (Minter et al. 2016). Indeed, Aβ plaques have been detected in non-neural tissues (skin, subcutaneous and intestinal tissues) and blood vessels of the AD patients. This alludes to the possibility that these plaques may be produced locally in numerous organs (Joachim et al, 1989).

A large-scale study utilizing a Taiwanese national insurance database included more than 200,000 cases of AD, retrospectively observed over a 10-year period. Dental procedures which removed the source of infection (e.g. root canal treatment and restricted extractions) were shown to reduce the risk of dementia. On the other hand, patients who frequently experienced periodontal problems and those who had more than four teeth removed had a higher risk of developing AD (Lin et al., 2020).

Periodontal disease may play a role in sAD hallmark formation, as seen in experimental laboratory investigations involving oral infections with *P. gingivalis* in a mouse model (Ilievski et al., 2018). This investigation hypothesized that oral diseases associated with root canal (endodontic) and periodontal infection may also be a risk of developing sAD. Endodontic infection primarily involves intra-radicular biofilm formation (Siqueira & Rocas, 2009). Without adequate endodontic intervention, this may lead to persisting or secondary infection (Siqueira, 2001). Periodontal disease involves chronic inflammation and infection of the tooth supporting tissues, caused by a microbial biofilm on the external root surface (Socransky et al., 1998; Hajishengallis et al., 2019). As the pulp and the periodontium are connected via multiple anatomical pathways, endodontic lesions can worsen the severity of periodontitis and conversely, a periodontal lesion may initiate pulpal inflammation. If both endodontic and periodontal disease are left untreated, this can result in pain, spreading infection and ultimately tooth loss (Simon et al., 1972; Herrera et al., 2018). Microorganisms common to root canal infections are also found in periodontal disease lesions, including *Porphyromonas gingivalis*, *Prevotella intermedia, Eubacterium* and *Fusobacterium* species, *Peptostreptococcus*, *Capnocytophaga*, *Actinomyces* and *Streptococcus* genera of bacteria (Caton et al., 2018).

All human cells express the Aβ protein precursor (APP) gene, and research has shown that the gingival tissue was rich in soluble Aβ (Dominy et al., 2019). It is possible to hypothesise that oral biofilms constantly release upregulated APP and/or soluble Aβ as an antimicrobial peptide. Some bacterial species such as *Enterococcus* and *Streptococcus* have been reported to express curli fibres which are proteinaceous filaments, which are essential for adhesion in biofilm formation and host colonization (Chapman et al., 2022). It is reasonable to assume that natural endodontic biofilm in the human host could demonstrate Aβ or Aβ-like deposits in the extracellular polymeric substance (EPS), which may be visible via transmission electron microscopy (TEM). This is because human Aβ-fibrils are known to be the equivalent of bacterial curli fibres (Sleutel et al., 2023). The premise for this investigation was the discovery that bacteria carry different proteins, such as curli on their surface membranes, which, under the correct pathophysiological conditions, transform into functional amyloid fibres within biofilm EPS (Chapman et al., 2002). In a 'human model' with infected teeth and periodontium, Aβ could potentially be secreted in response to the immune challenge, as an antimicrobial peptide. It was anticipated that there would be a potential for finding both human and microbial amyloid. The implication is that the human and microbial Aβ protein from infected oral tissues may be transported to the brain by the receptor for AGE products (Zeng et al., 2021) and could potentially cross-seed Aβ into the brain, thereby increasing the risk of developing AD.

### 2.1.1 Hypothesis:

Periodontal, cariogenic and endodontic bacteria contribute to peripheral pools of Aβ with potential for carriage to the brain via defects in the blood-brain barrier because of aging and AD.

### 2.1.2 Aims and Objectives

Aim: To investigate the oral pathogens' contribution to the hallmark proteins Aβ in the pathophysiology of AD.

Objectives:

(i) To examine the interaction of oral bacteria sourced from human teeth with periodontal and endodontic disease, with AD Aβ and tau-neurofibrillary tangles.

(ii) To establish if the naturally formed periodontal and endodontic biofilm secretes Aβ as part of its extracellular polymeric substance.

### 2.1.3 Ethical approval

This project was approved by the Health Research Authority (HRA), the Research Ethics Committee (local REC), the UCLan Ethics Committee (STEMH) and the UCLan Biological Safety Officers (BSO) committee:

- IRAS approved project ID: 249743: Short project title: Oral biofilms and dementia version 1.
- REC reference: 19/NI/0019
- STEM (UCLan ethics) approval reference: 1001
- BSO (UCLan) approval reference: 0219-01
- The project was adopted by the NIHR, who provided help with CPMS: 40822 IRAS: 249743 - Oral Biofilms and Dementia - Performance Monitoring

### 2.1.4 Funding award:

This project was awarded the 2018 Oral and Dental Research Trust Oral Health Innovations (PreViser) grant which covered the cost of consumables for part of this study, M.Phil stage (2018-2021) worth £5000.00.

## 2.2 MATERIALS & METHODS

All general purpose laboratory reagents used for the preparation of standard solutions and buffers for the work presented in this chapter are listed here: 10% neutral buffered formalin (Sigma-Aldrich, Merck Ltd Dorset, UK) , absolute alcohol (AnalaR grade, 100%) and 95% ethanol of were purchased from Fisher Scientific UK Ltd (Leicestershire, UK), and graded ethanol at 70, 80 and 100% were prepared with distilled water (in house supply), phosphate buffered saline (PBS, 0.01M pH 7.4) was prepared in house with components purchased from (Sigma-Aldrich, Merck Ltd (Dorset, UK), 10% ethylenediaminetetraacetic acid or EDTA (pH 7.4) with 0.07% glycerol was prepared in house. Analar-grade xylene was purchased from (Sigma-Aldrich, Merck Ltd, Dorset, UK); paraffin wax pellets and embedding molds were obtained from (Fisher Scientific UK Ltd, Leicestershire, UK). Ready to use Gram stain components crystal violet (PL7000) solution Lugol's iodine (PL7052) solution, Gram differentiator (PL7006/25), Safranin O (PL7012) were all obtained from (Fisher Scientific, Leicestershire, UK), Giemsa, and Mayer's haem alum and Eosin for H&E staining components were ready made and purchased from Raymond A. Lamb (Durham, North Carolina, USA). Grocotts silver impregnation reagents chromic acid, sodium metabisulphite ($Na_2S_2O_5$), methenamine, silver nitrate, gold chloride, sodium thiosulphate, acetic acid and Light green dye powder (CI 42095) were obtained from Fisher Scientific (Leicestershire, UK). Gurr's DPX, mounting medium was obtained from Fisher Scientific (Leicestershire, UK). 25% glutaraldehyde and 2% aqueous osmium tetroxide solution, propylene oxide and Epoxy resin Araldite CY212, kit containing all components (hardner, accelatior and plasticisor), and polypropylene Beem® capsules, pin stubs, carbon tabs (or adhesisive discs) were all purchased from Agar Scientific Ltd. (Stanstead, UK). 98-100% formic acid (Fisher Scientific, Leicestershire, UK). The primary antibodies: anti-Aβ antibody (clone 6e10) was from

BioLegend Inc. (San Diego, CA, USA), and the mouse anti-*E. coli* LPS (ab35654) was from Abcam PLC, Cambridge UK). The secondary detection antibody from Vectastain mouse peroxidase IgG kit (PK 400, Vector Laboratories, UK). Normal horse serum was included in the Vectastain mouse peroxidase IgG kit (see above). The DAB peroxidase Kit (SK 4100 Vector Laboratories, UK). Rabbit anti-tau (phosphorylated S202-205) clone AT8 was purchased from Abcam UK. The secondary detection antibody kit for the rabbit antibodies was the Vectastain peroxidase IgG kit (PK 4002) and the detection kit was the DAB Peroxidase Kit (SK 4100). (Vector Laboratories, UK). The methodologies have been described in detail by Kanagasingam et al. (2022).

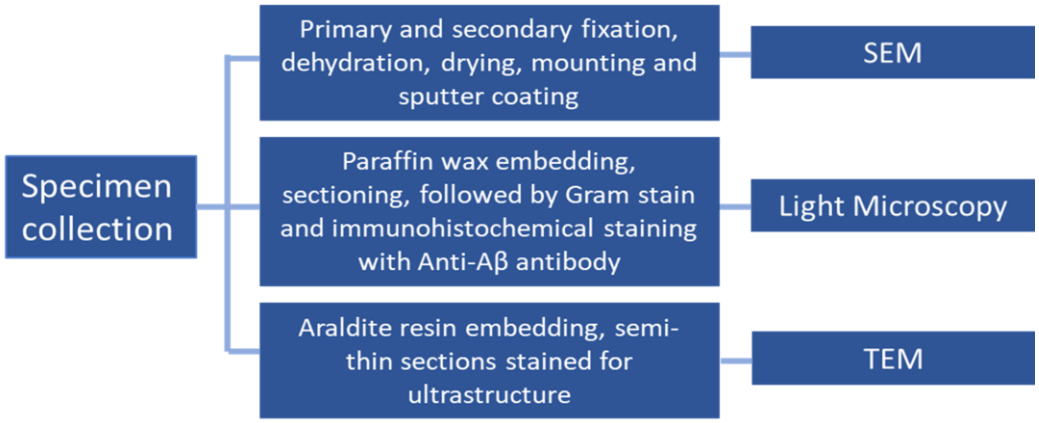


Figure 2.1: Flowchart of methods used for specimen preparation and imaging techniques used.

### 2.2.1 Specimen collection

HRA and HCRW approval IRAS Project ID: 249743, REC ref: 19/NI/0019) was received on 11th March 2019. Researchers then proceeded to recruit NHS general dental practices in the Northwest region to collect freshly extracted teeth. A pragmatic decision was made to choose dental practices which were located less than an hour's drive from UCLan in order to facilitate collection of the extracted teeth. The following dental practices confirmed their participation:

- Thomas & Thomas Dental Associates, The Surgery, 129 Whitegate Drive, Blackpool FY3 9BU
- Great Eccleston Dental Surgery, 4 The Square, Great Eccleston, Preston PR3 0ZB
- Lotus Dental Practice, 169 Towngate, Leyland, PR25 2TE

Training was provided to dental staff on selection of teeth including the inclusion/exclusion criteria for the required teeth (cognitive healthy adults between the age of 50-90 undergoing dental extraction, who voluntarily consented), and consent taking, and information packs were given to all dental practice staff members in accordance with the ethical approval. Inclusion criteria were teeth which required extraction due to periodontal and endodontic disease and healthy teeth which required extraction for orthodontic reasons. The diseased teeth included teeth which were diagnosed with apical periodontitis in patients with periodontal disease. The indication for extraction can be due periodontal and/or endodontic reasons. Both teeth which were had not been previously root treated as well as root treated teeth were both included in this study. Teeth which had vertical root fractures or were extensively damaged were not included.

Extracted teeth were collected in 70% ethanol (Sigma-Aldrich, Merck Ltd, Dorset, UK) in individual Duran bottles. Researchers collected the bottles from each practice and matched the number of consent forms to the number of extracted teeth collected. The teeth were then fixed in 10% neutral buffered formalin (Sigma-Aldrich, Merck Ltd Dorset, UK) for 24 hours at 4°C. All specimens were stored in the designated room (room 330, Darwin Building, UCLan) as per the Human Tissue Act of 2004 UK regulations. Consent forms were scanned as e-copy on a

USB stick together with hard copies kept in a locked cabinet stored in HA132 (Harrington Building, University of Central Lancashire). Figure 2.1 shows an overview of the method used.

### 2.2.2 Preparation of specimens

The tooth specimens examined with dental loupes at 4.0X magnification (SurgiTel, Ann Arbor, MI, USA) and grouped into the following categories: Group A (vital, healthy teeth), Group B (teeth with primary endodontic or root canal infection and periodontitis) and Group C (teeth with secondary root canal infection i.e. failed root treatment, and periodontitis). Teeth which were not intact e.g. root fractures, grossly carious affecting a significant part of the root, were discarded.

(i) Root calculus

Calculus was either directly viewed on intact teeth or scraped from selected teeth (with major deposition of calculus) using a sterile scalpel with the operator using 4.0X loupes magnification (SurgiTel, Ann Arbor, MI, USA). The calculus samples from each tooth were placed into 0.01M PBS (Fisher Scientific, Leicestershire, UK) in separate containers.

(ii) Demineralization of teeth

Following fixation in formalin solution, neutral buffered, 10% (Sigma-Aldrich, Merck Ltd, Dorset, UK), all teeth were demineralised in 10% ethylenediaminetetraacetic acid or EDTA (pH 7.4) with 0.07% glycerol for variable times (3 to 4 months) depending on the type of tooth (incisor, premolar or molar). Upon demineralisation (cut easily with a scalpel blade or not), the tooth was cut longitudinally in half, and then washed in PBS for processing and embedding in paraffin wax.

(iii) Paraffin wax embedding

All specimens were dehydrated in graded ethanol at 70, 80 and 100% (Sigma-Aldrich, Merck Ltd, Dorset, UK). This was followed by clearing in 3 changes of histological-grade xylene. The tissues were infiltrated in molten paraffin wax (3 times, overnight) in a tissue processor (Leica TP1020, Leica Microsystems UK Ltd, Sheffield, UK) as per routine histology laboratory procedure and embedded in moulds with freshly melted paraffin wax (Fisher Scientific UK Ltd, Leicestershire, UK).

(iv) Sectioning and slide preparation

Paraffin sections were cut into 4 µm thickness using the Leitz 1512 rotary microtome (Marshall Scientific, Hampton, New Hampshire, USA) and collected on 0.1% gelatine coated glass microscope slides. The slides were dried in an incubator at 37°C and stored in a slide box, at room temperature.

### 2.2.3 Tissue Morphology and Biofilm Detection under Light Microscopy

Dewaxed and rehydrated paraffin wax tissue sections were subjected to a variety of staining techniques including Gram-staining to observe characteristics of infecting microbes, the silver impregnation methods to detect the presence of fungi and immunohistochemistry to determine the presence of LPS and Aβ. The tissue sections were examined for infecting microbes using neutral light microscopy staining (Gram and Grocott-Gomori) methods and where possible, under the scanning electron microscope (SEM), refer section 2.2.5.

(i) Gram stain

The Gram stain is one of the most commonly used methods to distinguish bacteria from host cells in clinical specimens and differentiated into two classifications based on their cell wall

characteristics; Gram-positive (appearing either purple or blue in colour) and Gram-negative (turns pink or red in colour). Gram staining can reveal most presumptive bacteria (Vijayakumar et al. 2023). The published method of Gerhardt *et al*., (1994) was adapted for use with tissue sections. Paraffin sections were dewaxed in 2 changes of absolute xylene for 5 minutes each, and then rehydrated through a graded alcohol series which included 2 changes of absolute alcohol for 3 minutes each, followed by 90% and 70% alcohol for 3 minutes each (both the xylene and alcohol were obtained from Genta Medical, York, UK). Sections were subsequently washed briefly in PBS and then tap water. The rehydrated paraffin wax tissue sections were then exposed to crystal violet (PL7000) solution (Fisher Scientific, Leicestershire, UK) for 1 minute and flooded with Lugol's iodine (PL7052) solution for another minute and then allowed to drain. The Gram differentiator (PL7006/25) was applied to the slide drop wise, observing until no more colour was released. After multiple thorough washings in distilled water, the slides were then counter-stained with Safranin O (PL7012) for 30 to 60 seconds and washed prior to air drying and mounting under a glass coverslip using Gurr's DPX mounting medium (Fisher Scientific, Leicestershire, UK) and left to dry overnight. The slides were examined under a light microscope (Nikon Eclipse Ci Microscope, Nikon, UK) and images were captured using DS-L4 Software (Nikon, UK). The abovementioned methodology has been described in detail in Kanagasingam et al. (2022).

(ii) Grocott-Gomori's methenamine silver impregnation (GMS)

Grocott-Gomori's Methenamine Silver (GMS) stain is a histological stain with a high sensitivity for detecting fungi and other polysaccharide-rich microorganisms in paraffin embedded rehydrated tissue sections (Grocott, 1995; Alturkistani et al., 2015). The tissue sections were oxidised with 4% aqueous chromic acid at room temperature for 1 hour in the fume hood. Following a brief wash in distilled water (1 x 30 seconds), they were treated with 1% sodium

metabisulphite ($Na_2S_2O_5$) for 1 minute. A further wash was performed in running tap water followed by a distilled water rinse. Pre-heated working silver solution was prepared in clean glassware using 3% methenamine (23 ml), 5% silver nitrate (1.25 ml), 5% borax (3 ml) in distilled water (25 ml) and placed in an incubator at 60 °C. Test sections on slides were placed into the prewarmed silver solution for 30 mins or so until section turned yellowish-brown. The sections were then rinsed in distilled water and toned with 0.2% gold chloride (1 x 2 minutes). Following further washes in distilled water, the sections were treated with 2% sodium thiosulphate (1 x 2 minutes). Following another wash with running tap water (1 x 5 minutes), the sections were counter stained in 0.01% light green (CI 42095) in 1% acetic acid for 10 seconds. Any excess light green was rinsed with 95% ethanol before mounting in Gurr's DPX mounting medium and left to dry overnight. The slides were examined under a light microscope as described above (Gram stain section). The abovementioned methodology has been described in detail in Kanagasingam et al. (2022).

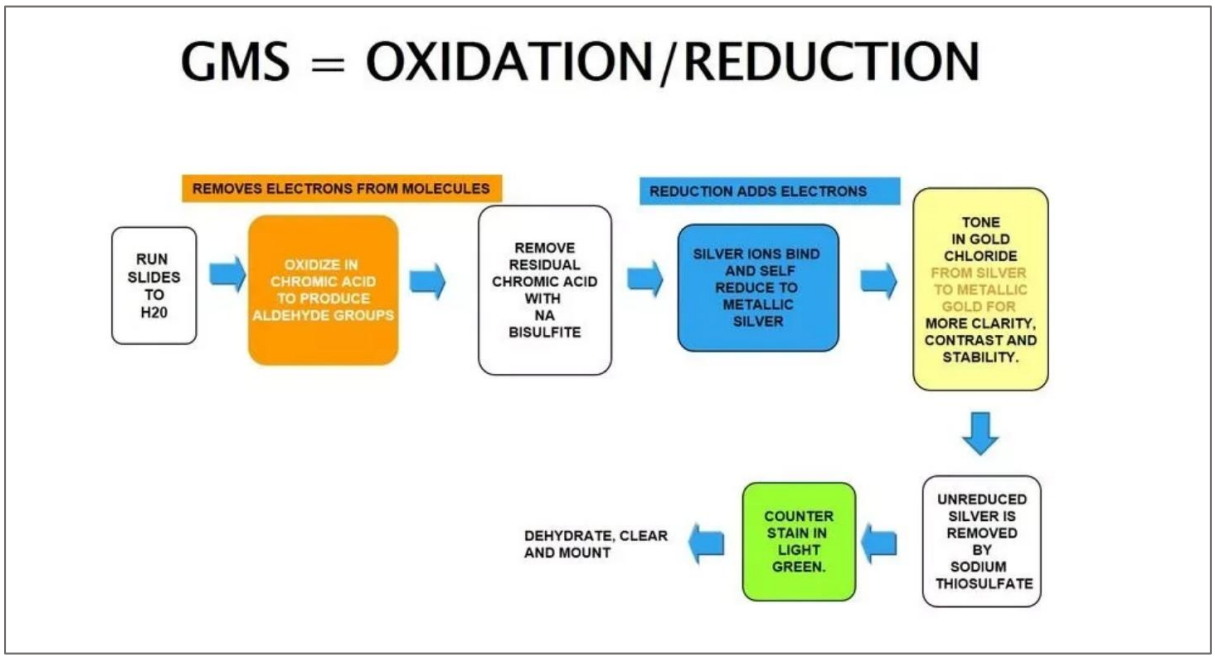


Figure 2.2: Workflow of Grocott's Gomori Methenamine Silver (GMS) Staining.

This diagram illustrates the step-by-step oxidation–reduction process used in the GMS stain for identifying fungal microorganisms. Tissue sections were first hydrated and then oxidised in chromic acid, which removed electrons from cell components and converted polysaccharides into aldehyde groups. Residual chromic acid was cleared with sodium bisulfite before the slides were exposed to a methenamine silver solution, where silver ions bind to aldehyde-rich fungal cell walls and were reduced to visible metallic silver. The sections were then toned in gold chloride to enhance clarity, contrast, and stability of the silver deposits. Unreduced silver was removed with sodium thiosulfate, and the slides were counterstained lightly (commonly with light green), dehydrated, cleared, and mounted (Image credit: www.leicabiosystems.com).

### 2.2.4 Immunohistochemical microscopy

(i) Anti-β-Amyloid antibody, Mouse monoclonal

Anti-β-Amyloid antibody, Mouse monoclonal, clone (6e10) BAM-10, purified from hybridoma cell culture (Sigma-Aldrich Merck UK Ltd, Dorset, UK) was used in immunohistochemistry to detect Aβ peptide in human tooth tissue sections. Sections were dewaxed and rehydrated by standard procedures as described in the earlier section (2.2.2) and their endogenous peroxidase activity was quenched using 0.3% hydrogen peroxide in methanol for 20 minutes and the sections were then rehydrated in running tap water for 20 minutes.

*Antigen retrieval procedure*

An antigen retrieval was performed by placing tissue sections in neat (98-100%) formic acid for the anti-β-Amyloid antibody (Fisher Scientific, Leicestershire, UK) for 10 minutes at room temperature followed by thorough washing with distilled water (2x2 washes for 5 minutes). A variety of antigen retrieval procedures were tested with the rabbit anti-tau (phosphorylated S202-205) clone AT8 on the paraffin wax embedded calculus biofilm sections.

*Immuno-histochemistry procedure*

Following washing with distilled water, sections were equilibrated, for 5 minutes, in phosphate buffered saline (PBS) (0.1M PBS, pH 7.2). Non-specific antibody binding was controlled for by 30-minute incubation in block solution (containing 0.1% normal horse serum from Vectastain kit, (VectorLabs, Newark, California, U.S.) PK 4002, in PBS). The primary antibody was mouse anti-Aβ (clone 6E10, BioLegend) diluted 1:200 in block solution. The negative control sections were incubated in the block buffering solution whereby the primary antibody was omitted. All sections were incubated overnight at 4°C in a humidity chamber. On the next day, slides were washed (3 x 5 minutes) each in PBS before incubating the sections in the secondary detection antibody from Vectastain mouse peroxidase IgG kit (PK 400, Vector Laboratories, UK), according to the supplier's instructions. The detection was completed using the DAB peroxidase Kit (SK 4100Vector Laboratories, UK), again according to the supplier's instructions. The sections were lightly counterstained in 0.001% light green before mounting under a coverslip in Gurr's DPX (Fisher Scientific, Leicestershire, UK) and examined under a light microscope as described above (section 2.2.3).

(ii) Rabbit anti-tau (phosphorylated S202-205) clone AT8

Rabbit anti-tau (phosphorylated S202-205) was used to identify the presence of endogenous tau peptides. Rehydrated paraffin wax calculus sections were exposed to PBS, and the non-specific antibody binding was controlled by 30 minute incubation in blocking buffer solution containing 0.1% normal goat serum (Vectastain kit, PK 4002) in 1x PBS containing 0.02% tween 20 for both the negative control slides (omission of the primary antibody) and the test slides (anti-tau), which were diluted in the blocking buffer solution 1:50. These were incubated overnight at 4ºC in a humidity chamber. On the next day, the slides were thoroughly washed in PBS (3x5minutes) and then subjected to the secondary detection antibody from

the Vectastain kit for rabbit peroxidase IgG kit (PK 4002) (Vector Laboratories, UK), according to the suppliers' instructions. The detection was completed using the DAB Peroxidase Kit (SK 4100). A light green counterstain was carried out before mounting with glass coverslips. Antigen retrieval was carried out as described previously.

(iii) Anti-Escherichia coli lipopolysaccharide (LPS)

This method was adapted for immunostaining from Zhan et al., (2016). Sections were deparaffinised and their endogenous peroxidase activity was quenched using 0.3% hydrogen peroxide in methanol for 20 minutes at room temperature and then rehydrated in running tap water (1 x 10 minutes). Following this, the rehydrated sections were incubated in PBS (0.01M PBS, pH 7.4) at room temperature. To prevent non-specific protein binding, sections were neutralised by 30 minutes of incubation in block solution (containing 0.1% normal horse serum, Vectastain kit, PK 4002, in PBS). The primary antibody was mouse anti-*E. coli* LPS (ab35654 from AbCam PLC, Cambridge UK) diluted 1:100 in block solution. The negative control sections were incubated in the blocking buffer solution whereby the primary antibody was omitted. The rest of the procedure is as described for mouse anti-Aβ above (section 2.2.4).

### 2.2.5 Biofilm morphology and characteristics under electron microscopy

(i) Scanning Electron Microscopy (SEM)

The scanning electron microscope scans surfaces of microorganisms, using a beam of electrons moving at low energy to focus and scan specimens. SEM utilise very short wavelengths in comparison to the wavelength of visible light in light microscope. This allows SEM to provide better resolution power and improved appreciation of finer details, as well as significantly higher magnification. The beam of electrons interacts with the specimen to produce signals, detailing surface topography and composition of the specimen. Examining microbial

specimens would require fixation, dehydration, and drying to maintain their cellular structural features and to prevent collapsing of the cells when exposed to the high vacuum of the SEM (Arana-Chavez & Castro-Filice, 2019).

Calculus on selected teeth and hemisected teeth (to expose the internal root canal walls) was fixed in 2.5% glutaraldehyde diluted in PBS for up to 3 hours at 4 °C followed by 1 prolonged wash in PBS overnight at 4 °C. On the next day, the specimen was post-fixed in 2% aqueous osmium tetroxide solution for 2 hours at room temperature, this was carried out in a fume hood. Subsequently, the specimens were washed thoroughly in distilled water and dehydrated in graded alcohols from 70% ethanol to absolute alcohol 3 times for 15 minutes each with absolute ethanol washes extended for a further 30 minutes each. Following this, the fully dehydrated specimens were placed onto pin stubs adhered with carbon tabs and placed into a bench top glass vacuum desiccator for a duration of 12 hours.

In addition, calculus (scraped off the tooth surface) were initially stabilized in 10% formalin washed in absolute ethanol, and subsequently, adhered to carbon tabs on pin stubs, sputter coated with gold (Emitech K550X, Richmond Scientific, Lancashire, UK) prior to examination under the JCM6000 Plus Scanning Electron Microscope (JEOL UK Ltd, Hertfordshire, UK). Images were recorded using the 6000 plus software (JEOL UK Ltd, Hertfordshire, UK). The abovementioned methodology has been described in detail in Kanagasingam et al. (2022).

(ii) Morphological visualisation and immunochemistry investigations under Transmission Electron Microscopy (TEM)

This aspect of the laboratory investigation was outsourced due to the lack of TEM facilities at the University of Central Lancashire (Dr Christopher Von Ruhland, Central Biotechnology

Services (CBS), Cardiff University). Transmission Electron Microscope (TEM) imaging is used to analyse the ultra-structural morphology of materials with high resolution and reliability. TEM imaging can achieve spatial resolutions of less than 50pm (Arana-Chavez & Castro-Filice 2009). In this study, TEM was used to observe the microorganisms in infected dental tissues and remnant root filling material. Specimens were fixed and embedded in resin before being sectioned with an ultramicrotome. LR White (Agar Scientific Ltd, Calibre Scientific Rotherham, UK) and Araldite (Agar Scientific Ltd, Calibre Scientific Rotherham, UK) resin were chosen due to low viscosity and relatively rapid infiltration. Ultrastructural immunochemistry was carried out with LR White and immunocolloidal gold, which is a technique utilising colloidal gold as a tracer marker applied to antigen and antibody. Further histological staining with Toluidine blue and immunohistochemical staining with Anti-β-Amyloid antibody were carried out to detect the presence of amyloid proteins. Correlative light and electron microscopy of semi-thin Araldite sections allowed initial analysis of a larger field of view via light microscopy which then facilitated more targeted TEM investigations. As TEM is more time-consuming and complex, using light microscopy first helped to avoid unnecessary analysis of irrelevant areas.

*Specimen fixation, dehydration, infiltration, polymerisation in Araldite resin*

To observe the morphology of the amyloid fibres within the EPS or within the infected tissue, selected specimens were processed for TEM. They were fixed in primary fixative (2.5% glutaraldehyde), which was followed on with secondary fixation in 2% aqueous osmium tetroxide as for SEM (see above, SEM section). The next steps involved specimen dehydration in graded alcohols from 70%, 80% ethanol to absolute alcohol (3x15 minutes each). Washing times in absolute ethanol were extended to 3x 30 minutes each. Subsequently, the fully dehydrated specimens were placed in propylene oxide (3x10 minutes each). A mixture of

propylene oxide and Araldite CY212 at a ratio of 1:1 was used for 2 hours to facilitate initial infiltration of resin into the specimen tissue at room temperature followed by 3 changes in fresh resin over 24 hours while on a rotary device, MX-T6-S Classic Roller Mixer (Camlab, Cambridge, UK). Specimens were then embedded in fresh Araldite using polypropylene Beem® capsules held in a metal rack, which contained specimen identity labels. After the tissue had sunk to the bottom of the capsule (within the Beem® of the capsule), the capsule was filled with more resin and the lids were sealed. The capsules were placed into an oven to polymerise the resin at 65 ºC for 48 hours. The abovementioned methodology has been described in detail in Kanagasingam et al. (2022).

*Specimen fixation, dehydration, infiltration, polymerisation in LR White resin*

Specimens were fixed, for up to 3hours at 4 °C, in 2.0% glutaraldehyde (Agar Scientific UK) diluted in PBS and washed overnight in PBS. The specimens were partially dehydrated in 70% ethanol (3 x 30 minutes each). The tissue was infiltrated in LR White resin (4 changes of 4 hours each). They were subsequently embedded in fresh cold LR White (Agar Scientific UK) to which manufacturer's accelerator was added at a concentration of 1.5µL/mL in prelabelled polypropylene Beem® capsules using the cold catalytic method (Newman and Hobot, 1987). All the resin blocks were sectioned to produce semi-thin and ultrathin sections. Morphological stains and heavy metal impregnation of the sections for electron microscopy visualisation was outsourced to Dr Chris von Rhuland (Facility Lead, Electron and Light Microscopy, Central Biotechnology Services, School of Medicine, Cardiff University, Cardiff, UK).

*Staining-semi-thin (Araldite and LR White) sections*

All sections were cut using glass knives on the Leica Ultracut E microtome (Leica Microsystems, Chesterton, UK). The semi-thin sections (below 1µM thickness) were collected

on glass slides, while the ultra-thin (80-100 nm thickness) sections were collected onto 300 mesh naked nickel grids. A drop of filtered toluidine blue (0.5%) in 0.5% borax was placed for about 30 seconds onto the semi-thin sections on the slide whilst placed on the hot plate. All excess stain was washed off thoroughly under tap water. Following this, the sections were air dried and mounted in Gurr's DPX (Fisher Scientific UK Ltd, Leicestershire UK) and examined under TEM.

To increase the overall contrast of the ultrathin sections, solutions of electron opaque heavy metal salts were used. The grids were fully immersed for 20 minutes in filtered, 2% aqueous uranyl acetate solution (Taab Laboratory Equipment Ltd, Padworth, UK) on a sheet of dental wax and washed in distilled water (3 x 2 minutes each). The grids were then treated for 5 minutes in Reynolds (1963) lead citrate solution followed by further washings in distilled water (3 x 2 minutes each) and finally air dried. The grids were stored in a grid box and their position was recorded for TEM analysis. Staining-grids for Araldite embedded tissue sections for electron microscopy visualisation was outsourced to Dr Chris von Rhuland (Facility Lead, Electron and Light Microscopy, Central Biotechnology Services, School of Medicine, Cardiff University, Cardiff, UK). The abovementioned methodology has been described in detail in Kanagasingam et al. (2022).

*Examination and image capture of Araldite embedded tissue sections*

Outsourced to Cardiff University, Dr Chris von Rhuland (as above).

*Immunocolloidal gold silver staining (IGSS)* of LR White embedded semi-thin tissue sections

Outsourced to Cardiff University, Dr Chris von Rhuland (as above).

A common sensitive and targeted immunohistochemical visualisation method is the immunogold silver staining method (IGSS). IGSS allows for low magnification visualisation using light or electron microscopy by selectively depositing metallic silver at the immunogold labelling location (Lackie et al., 1996). The methodology involved LR White resin embedded Tg2576 mouse brain (as a positive control for Anti-β-Amyloid antibody) and gutta percha biofilm.

*Anti-Aβ antibody, Mouse (clone 6e10) on LR White semi-thin sections*

Outsourced to Cardiff University, C/O Dr Chris von Rhuland (as above).

Positive control mouse brain sections were equilibrated for 10 minutes in 20mM PBS pH 7.4 containing 0.6% bovine serum albumin (PBS/BSA) followed by 1 hour in anti-Aβ antibody (clone 6e10) diluted in PBS/BSA to a range of dilutions (1/100 to 1/10,000). This step helped to determine the appropriate antibody titre for subsequent immunohistochemical staining of the biofilm specimens. PBS/BSA alone was included as primary antibody omission controls in each experiment. Sections were washed for 2 x 1 minute in PBS/BSA and 1 minute in 20 mM tris buffer pH 7.4 containing 0.6% bovine serum albumin (TB/BSA) followed by 1 hour in anti-mouse IgG 10 nm colloidal gold conjugate (Sigma-Aldrich, Massachusetts, US). Sections were washed in distilled water and photochemical intensification solutions prepared in-house were applied for 20 minutes to sections (Newman & Jasani, 1998) to reveal immunolabelling. Following thorough washings in distilled water, sections were lightly counterstained with 0.1% Light Green (as was carried out for immunochemistry of paraffin wax sections above, section 2.2.4). fully air dried and mounted under a coverslip in Gurr's neutral mounting medium. A dilution of 1/2000 anti-Aβ antibody (clone 6e10) was chosen and applied to Tg2576 brain tissue sections (positive controls) alongside of the test gutta percha biofilm sections as described above. This methodology was described in detail in Kanagasingam et al. (2022).

*Toluidine blue staining for morphology*

Toluidine blue is a thiazine cationic dye widely used as a biological stain, with an affinity for nucleic acids, and therefore binds to nuclear material of tissues with a high DNA and RNA content. This histological stain is well recognised for its use in analysing oral tissues, including identification of dysplasia and carcinoma, certain bacterial species (e.g. *Cornebacterium* and *Helicobacter* species) as well as for staining amyloid (stains blue, but under polarized light would give a bright red birefringence) (Sridharan & Shankar, 2012). All semi-thin sections were treated with a drop of filtered 0.5% Toluidine blue in 0.5% borax, which was placed for a duration of 20 seconds onto semi-thin sections on microscope glass slides placed on a hotplate, which was set to 65°C. All of the excess stain was washed off under tap water and the section was fully dried before mounting under a glass coverslip in Gurr's DPX mounting medium (Fisher Scientific UK Ltd, Leicestershire, UK) and examined under the light microscope as described previously. Outsourced to Cardiff University, Dr Chris von Rhuland.

*Araldite embedded biofilm sections*

The grids were fully immersed for 20 minutes in filtered, 2% aqueous uranyl acetate solution (Taab Laboratory Equipment Ltd, Padworth, UK) on a sheet of dental wax and thoroughly washed in distilled water (3 x 2 minutes each). Based on the method described by Reynolds (1963), the grids were treated for 5 minutes in lead citrate solution, then further washings were carried out in distilled water (3 x 2 minutes each), followed by air drying. Following this, the grids were observed using a Hitachi HT7800 TEM (Hitachi High Tech Ltd., UK) at 100kV, and images were captured with Radius software (EMSIS GmbH, Germany). Outsourced to Cardiff University, Dr Chris von Rhuland (as above). The abovementioned methodology has been described in detail in Kanagasingam et al. (2022).

## 2.3 RESULTS

The process of collecting the tooth specimens (healthy and diseased teeth) was carried out over a period of about 4 months. Twice weekly trips were made to each practice to collect the teeth in order for the processing to be done within less than a week of the extraction. A total of 87 patients consented to donate their extracted teeth, with 41 females and 46 males. The donors had an average age range of 62-66 years.

### 2.3.1 Collection of extracted teeth

Eighty-seven teeth were collected prior to 1st October 2019 (n = 87). Figure 2.3 shows the total number of teeth collected, including unsuitable teeth which were discarded as they were grossly carious or had root fractures. Some teeth were lost due to extensive damage after demineralisation, as well as some teeth which were kept for too long due to limited access to the laboratory during the pandemic. The teeth were separated into vital (uninfected) teeth and diseased teeth. All periodontally diseased teeth were divided into groups of teeth with primary endodontic infection and secondary endodontic infection or failed root treated teeth (Figure 2.1). Example of the tooth specimens are shown in Figure 2.4 (a-e).

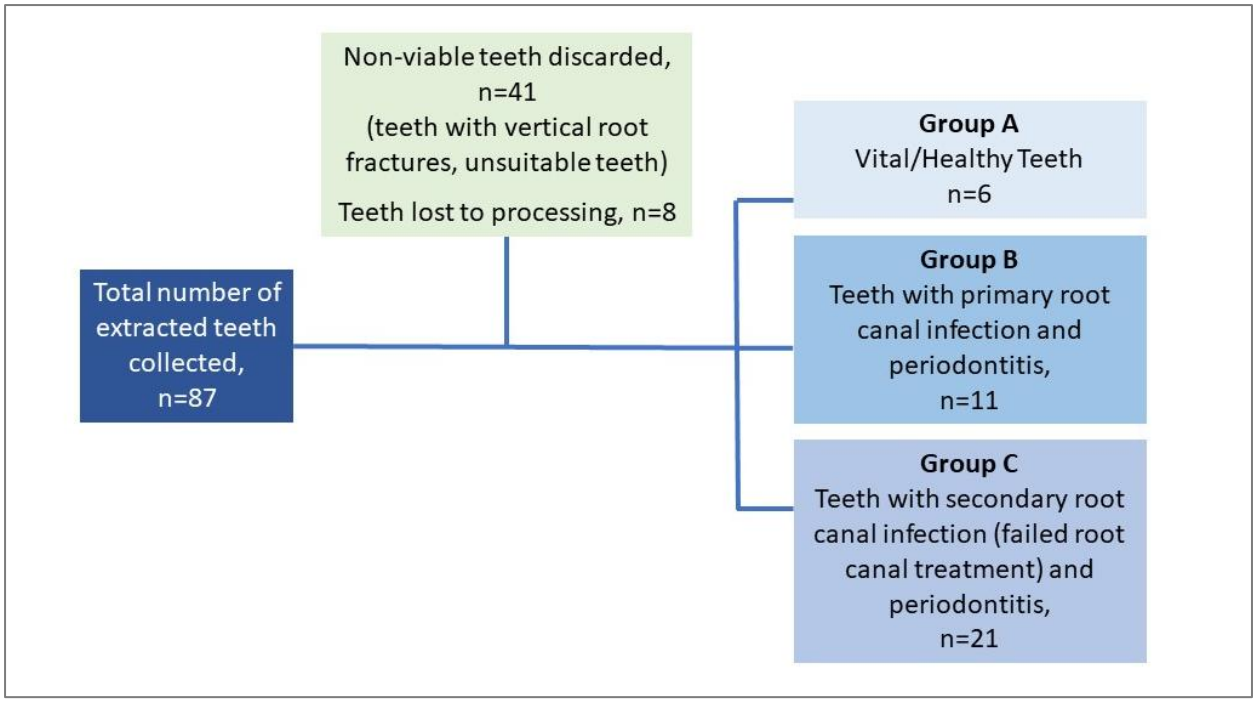


**Figure 2.3 Flowchart showing the numbers and grouping of the extracted teeth**

Teeth specimens were divided into 3 categories based on their clinical status. Group A consisted of 6 vital or healthy teeth. Group B had 11 teeth with primary root canal infection and periodontal disease, whereas 21 teeth which had secondary root canal infection (teeth with failed root canal treatment) and periodontal disease were placed in Group C.

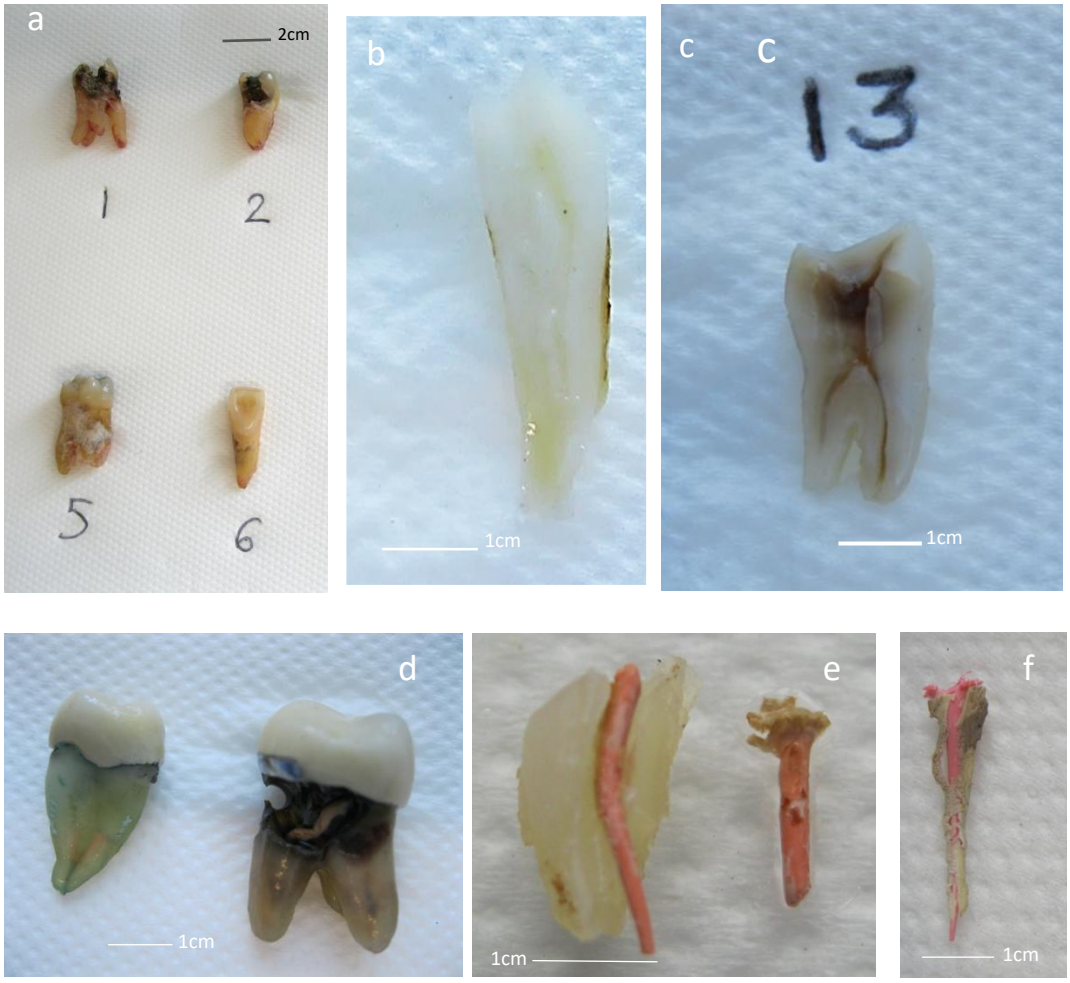


**Figure 2.4: Photographs showing a selection of the freshly extracted human teeth collected for the study.**

Examples of the freshly extracted human teeth (a) which were collected and subsequently categorised into 3 experimental groups. Teeth with vital pulps (uninfected teeth) were categorised as Group A (b). Teeth with primary endodontic disease were placed in Group B, a cross section of the molar tooth showed discolouration of the pulp chamber and root canal space due to deep caries and endodontic infection (c). Group C consisted of teeth with secondary endodontic disease as seen by evidence of existing root filling material known as gutta percha which can be visualised in the tooth roots (d). Gutta percha samples, with a layer of root canal sealer cement were removed for further analysis (e,f). Magnification as per scale bar.

### 2.3.2 Collection of calculus on the root surfaces

Most of the extracted teeth collected had visible supragingival and subgingival calculus, which was expected considering that Group B and C were teeth with periodontal disease. This allowed researchers to scrape off the biofilm layer to be used for further investigations (Figure 2.5)

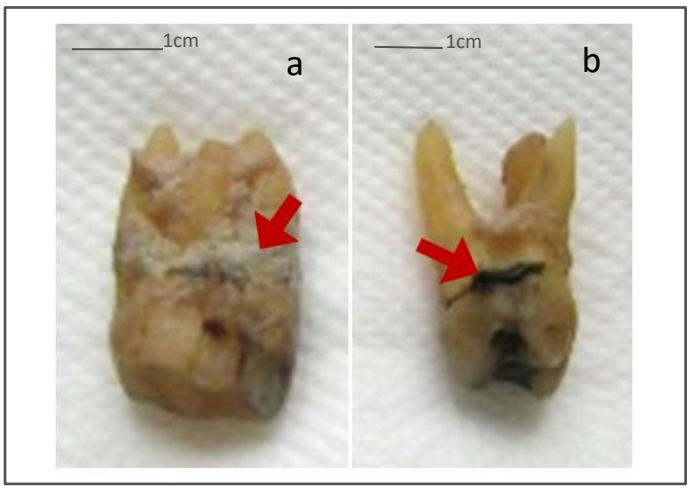


**Figure 2.5: Calculus deposits visualised on the root surfaces of extracted teeth**

Deposits of dental calculus were noted on the root surfaces of the extracted teeth (red arrows, a and b) which had been extracted due to periodontal disease. The calculus deposits were either kept intact or were removed using a sterile scalpel for experimental work. Magnification as per scale bar.

### 2.3.3 Light microscopy investigation of extracted teeth and calculus

The dehydrated and paraffin wax-embedded teeth and calculus sections underwent sectioning for slide preparation (Figure 2.6). The tissue sections histological staining with the Gram stain which differentiates bacteria based on their cell wall structure. Gram positive bacteria retain a purple dye due to their thick peptidoglycan layer whereas Gram negative bacteria lose the dye, hence appearing pink or red, due to their thinner peptidoglycan layer (Figures 2.7). Staining was also carried out with Grocott-Gomori's methenamine silver impregnation (GMS) to screen

for fungal microorganisms, whereby the reduction of the silver ions renders fungal cell walls black. All tooth groups did not demonstrate any positive result with GMS staining, however, the calculus specimens exhibited the black stain which was picked up by fungal hyphae (Figure 2.8). Aggregates of coccoid and filamentous bacteria were observed on the internal and external root specimens, including within the calculus, in the form of biofilm.

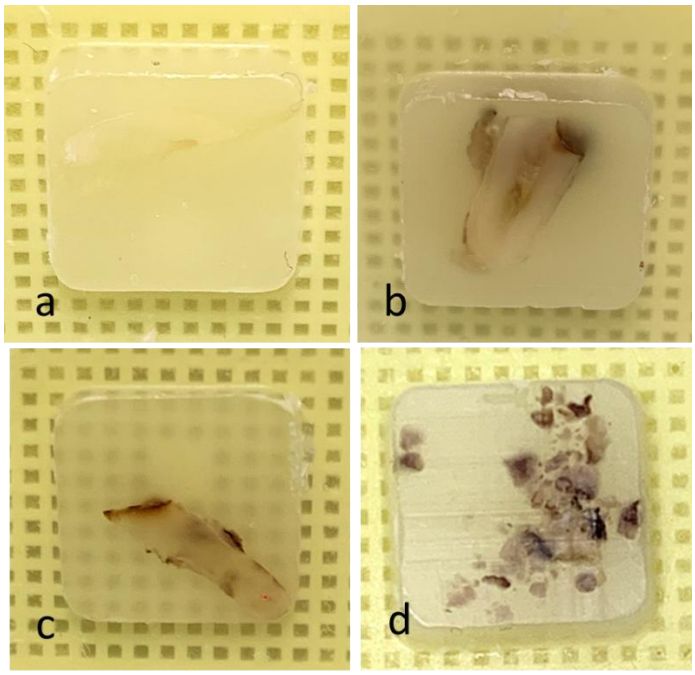


**Figure 2.6: Tooth sections and calculus specimens embedded in paraffin wax which were set in moulds**

The tooth sections from Group A, healthy tooth (a), Group B, primary endodontic infection and periodontitis (b) and Group C, failed root canal treatment and periodontitis, with visible remnant gutta percha at the root apex (c) were prepared and embedded in paraffin wax, prior to sectioning and slide preparation. Calculus from the tooth root surface were also prepared with the same technique for histological examination (d).

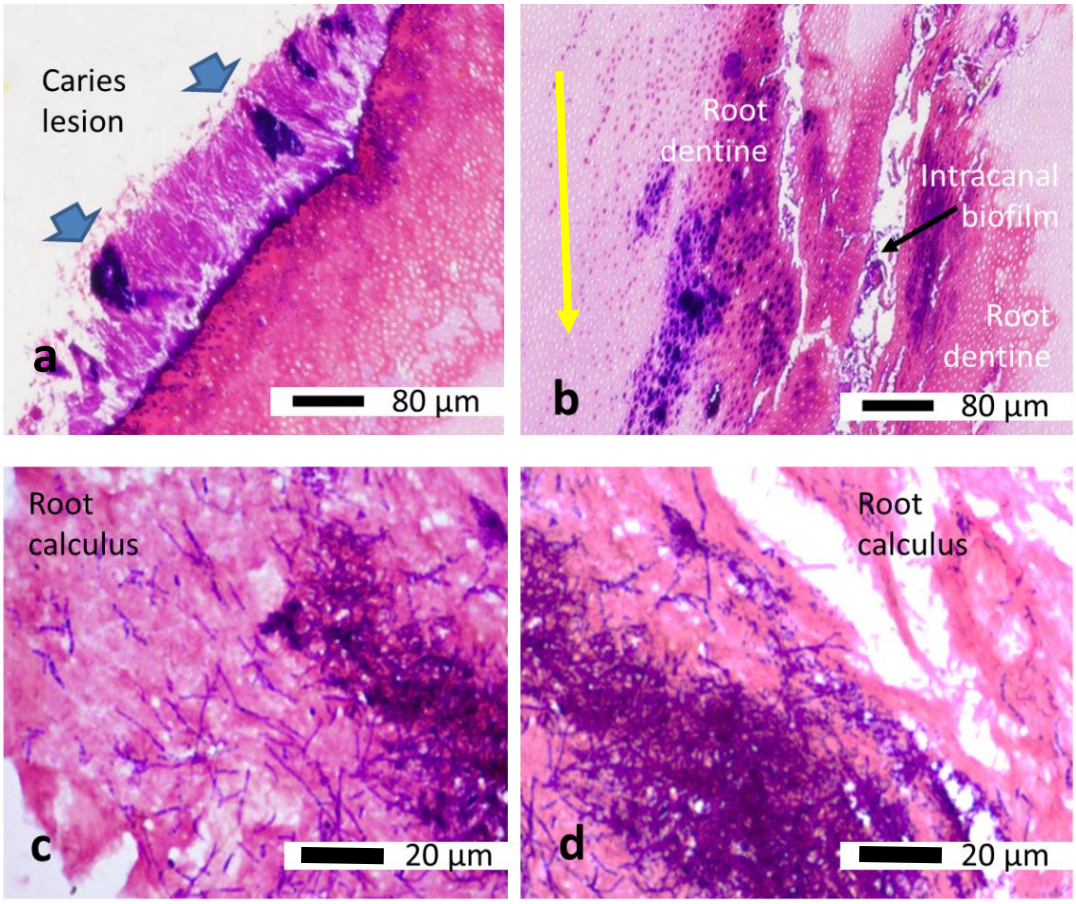


**Figure 2.7: Gram stain of tooth sections from Group B and root calculus**

Demineralised, paraffin wax embedded, rehydrated sections of a tooth from the primary root canal infection (Group B) showing a carious lesion with clusters of Gram-positive (purple) bacteria (blue arrows) and on the external surface, Gram-variable bacteria were noted (a). The same tissue section shows the bacterial infection had invaded deeper within the dentinal tubules to reach the root canal of the tooth. The yellow arrow indicates the coronal to apical orientation of the tooth root (b). Rehydrated paraffin wax embedded sections of scraped root calculus showed both Gram-positive (purple) bacteria aggregating with filamentous and coccoid Gram-negative (pink and red) bacteria. Bacteria on the internal and external surface of the root, including within the calculus layer appear to be a biofilm (c and d). Magnification as per scale bars (Kanagasingam et al. 2022).

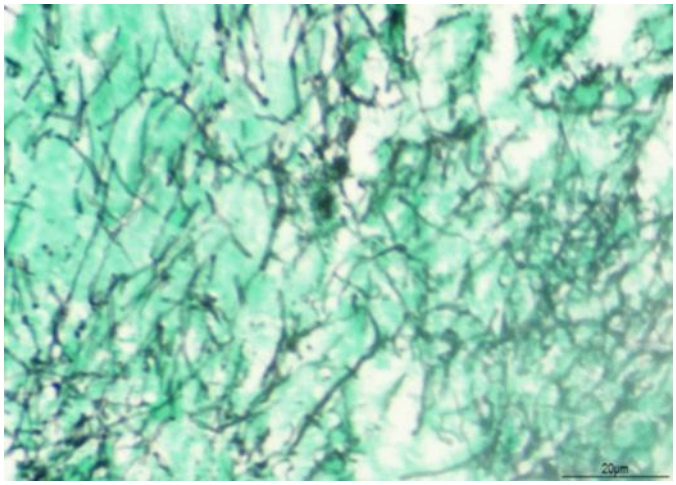

**Figure 2.8: Grocott-Gomori's methenamine silver impregnation of root calculus**

Demineralised, paraffin wax embedded, rehydrated sections of the root calculus from Group B, exhibited a positive response to Grocott-Gomori's stain, highlighting the presence of fungal hyphae (seen as black staining of multiple filamentous structures, against a light green background). Magnification as per scale bar.

### 2.3.4 Immunohistochemical light microscopy investigation of extracted teeth and calculus

Immunohistochemical microscopy was carried out with detect Aβ peptide in human tooth tissue sections and calculus using Anti-β-Amyloid antibody, Mouse monoclonal, clone (6e10) BAM-10 (Figure 2.9 and 2.10). Rabbit anti-tau (phosphorylated S202-205) AT8 and Anti-Escherichia coli lipopolysaccharide (LPS) were used to detect endogenous tau protein and bacterial LPS respectively in tooth tissue as well as calculus. Extracellular patches of brown/black staining may represent Aβ were evident, suggestive of soluble form rather than insoluble Aβ (Figure 2.8). After immunostaining with mouse Anti-*Escherichia coli* LPS antibody, clusters of what appeared as bacteria were immune-positive. Light green counter stain allowed the differential contrast between brown/black immunostaining and background staining (Figure 2.10). Immuno-staining with Rabbit anti-tau (phosphorylated S202-205) clone AT8 failed to detect tau protein in the paraffin wax embedded tooth and calculus sections. This was similarly noted

in the negative controls, which were completely devoid of any immunostaining. These results suggest that tau protein was not detected within calculus and (infected and non-infected) root dentine. The positive control from brain tissue of the transgenic mouse model for Alzheimer's disease supplied by Dr Nazira Albargothy (courtesy of Professor Roxana O Carare, University of Southampton, UK) was positive for amyloid plaques.

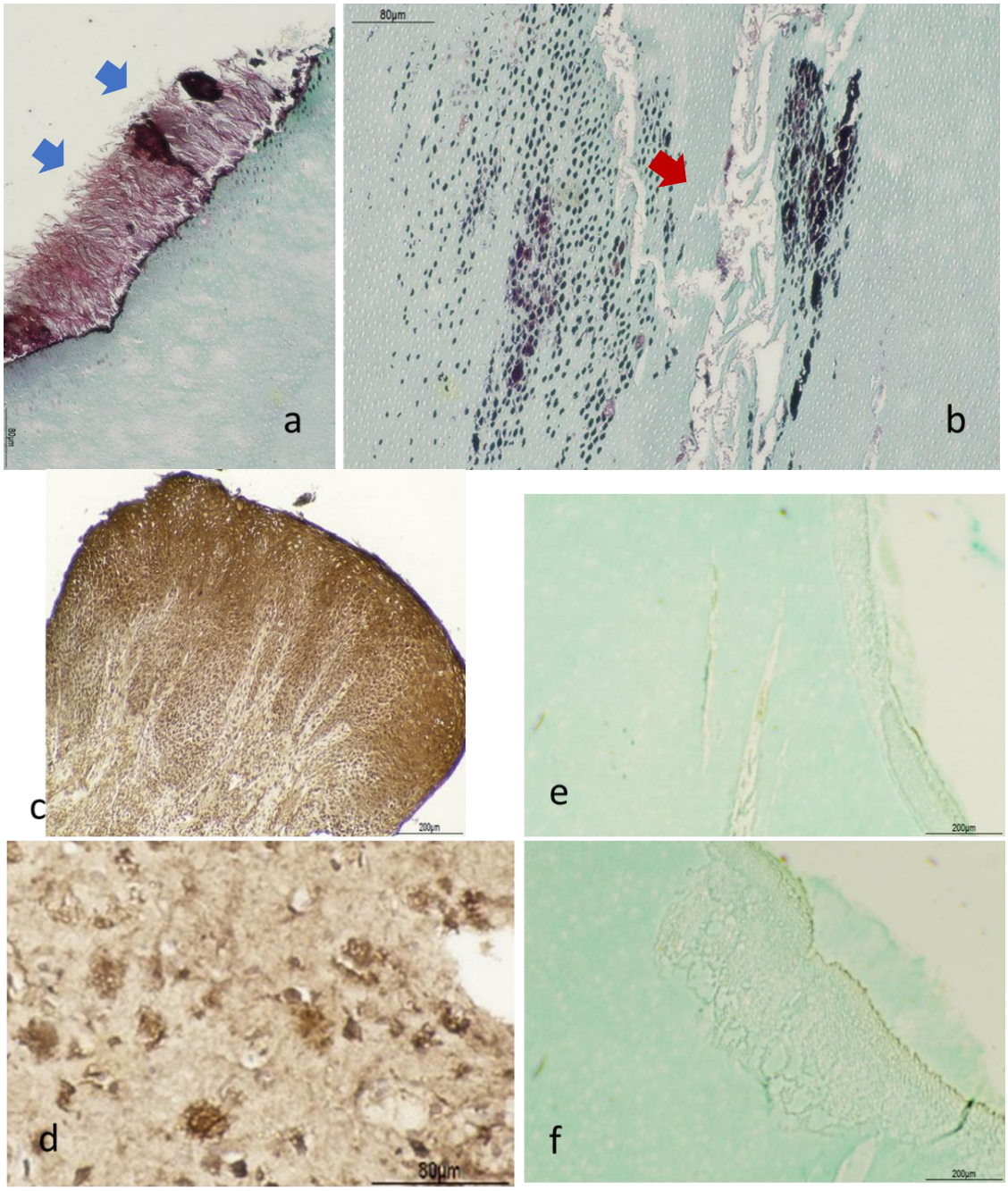


**Figure 2.9: Immunohistochemical staining of tooth sections with Anti-β-Amyloid antibody**

Serial sections of the same tooth from Group B (primary root canal infection associated with a carious lesion) as shown in Figure 2.5 underwent immunohistochemical staining with Anti-β-Amyloid antibody 1:200. The region of the tooth which showed a positive response to the immunostaining suggests the detection of β-Amyloid peptide (a). The colocalization of intracanal bacteria as seen in the serial section from Figure 2.5 are seen in the same region in this figure (red arrow), as well as previously seen intra-tubular bacteria (within root dentine) previously observed in Figure 2.5, have also demonstrated immunostaining with Anti-β-Amyloid antibody (b). A section of gingival tissue with periodontitis picked up the stain from Anti- β-Amyloid antibody 1:200 (c). A section of a transgenic AD mouse brain served as positive control using Anti- β-Amyloid antibody 1:200 (d). A no primary antibody control

showed that the staining observed was not caused by non-specific binding of the secondary antibody (negative controls) on tooth tissue from the serial sections - these were flipped as they were picked up in this manner during specimen preparation (e,f). Magnification as per scale bar.

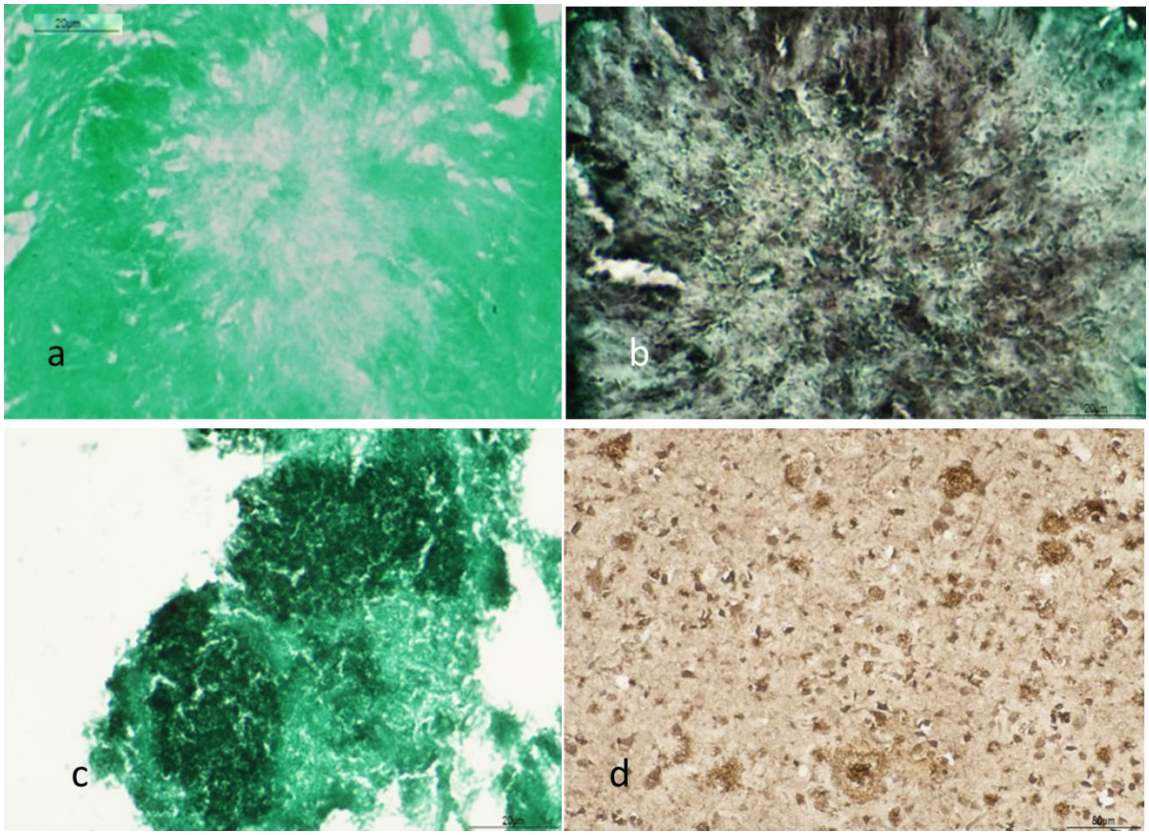


**Figure 2.10: Immunohistochemical staining of calculus sections with Anti-β-Amyloid antibody and Anti-Escherichia coli lipopolysaccharide (LPS)**

Immunostaining of the calculus section without the primary antibody served as the negative control showed that there was no non-specific antibody binding of the secondary antibody (a). The calculus section immune-stained with Anti-β-Amyloid antibody 1:200 showed a positive reaction which confirmed the presence of β-Amyloid peptide (b). The serial section of root calculus previously exhibited a positive result with Gram and Grocotts-Gomori's staining (as seen in Figures 2.10 and 2.11). A positive result was seen in calculus sections stained with Anti-Escherichia coli lipopolysaccharide (LPS) 1:50 (c). A section of a transgenic AD mouse brain served as positive control using Anti- β-Amyloid antibody 1:200 (d). Magnification as per scale bar.

### 2.3.5 Correlative light and electron microscopy of semi-thin Araldite sections

The biofilm on the root filling material or gutta percha was well preserved as seen in the SEM images (Figure 2.11). A variety of microbes were observed by light microscopy, however, their shapes and sizes were better confirmed by high resolution electron microscope imaging. The specimens were prepared and stained with Toluidine blue to undergo light microscopy prior to electron microscopy as this allowed for quick and easy identification of the areas of interest. This facilitated more targeted TEM analysis.

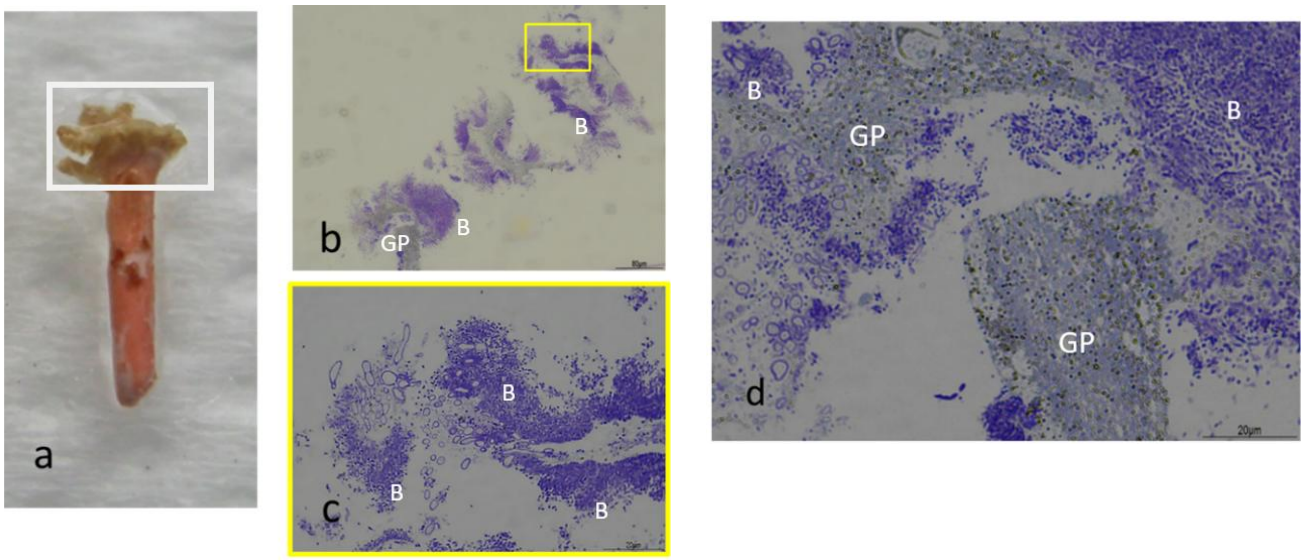


**Figure 2.11: Light microscopy of gutta percha from a failed root treatment with periodontal disease (Group C) stained with Toluidine Blue.**

Light microscopy was carried out (a) shows gutta percha removed from a failed root treatment (secondary endodontic infection) with the region of interest within the white box, which was subsequently processed for correlative light microscopy with Toluidine blue staining prior to dedicated ultrastructure analysis in Araldite resin. Image b shows a semi-thin histology section with the morphology stain Toluidine blue, likely showing clusters of bacteria and biofilm (B) which appears dark bluish purple. The gutta percha remnants (GP) has picked up a more 'greyish' stain due to the presence of mineral ions. Toluidine does not typically stain inorganic compounds, however, gutta percha is considered an organic material as it is primarily derived form natural rubber, a polymer of isoprene. However, the presence of inorganic fillers such as zinc oxide may impact its reaction to the stain. Image c is a magnification of the yellow boxed section of image b (x4). Image d showed a variety of microbes (B) at a higher magnification (x60). Magnification as per scale bar.

### 2.3.6 Light microscopy of immunocolloidal gold silver staining (IGSS) of LR White resin embedded gutta percha biofilm sections.

Immunohistochemical staining with Anti-β-Amyloid antibody was carried out on specimens of GP and adherent root canal sealer cement from Group C. The specimens were embedded in LR White resin. Tg2576 mouse brain sections were used as positive and negative controls.

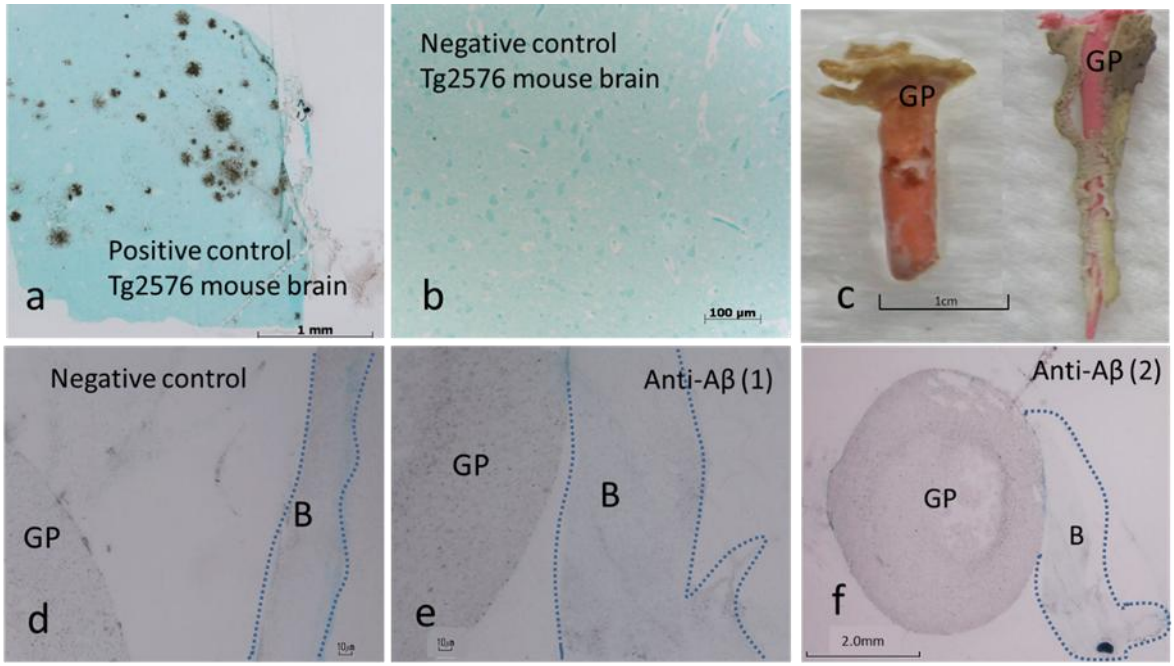


**Figure 2.12: Light microscopy of immunocolloidal gold silver staining (IGSS) for Anti-Aβ antibody, Mouse (clone 6e10) of LR White resin embedded gutta percha biofilm sections.**

Tg2576 mouse brain sections served as a positive control demonstrated insoluble Aβ plaques with the IGSS and Anti-Aβ antibody, Mouse (clone 6e10) (a). The negative control utilised the same immunohistochemical stain without the primary antibody on tissue sections taken from Tg2576 brain. The tissue sections remained free of any non-specific binding of the secondary antibody (b). For the experimental group, sections of gutta percha (GP) points with residual sealer cement (c) were prepared for embedding in LR White resin. The GP and its associated biofilm are demarcated by dotted lines. The negative control section remained free of specific immunostaining (d). The semi-serial sections of the gutta percha (GP) and its associated biofilm (B) showed an absence of staining for Aβ in gutta percha biofilm, as shown in the images labelled anti-Aβ(1) and anti-Aβ(2), e-f. Kanagasingam et al. (2022)

### 2.3.7 SEM imaging of extracted teeth

SEM produced high resolution images for direct morphological examination of the internal surface of the root canal of selected teeth from Groups A to C (Figure 2.13). SEM analysis showed the presence of bacterial infection in root canal cross-sections and bacterial penetration within the dentinal tubules (Figures 2.14 and 2.15).

**Figure 2.13: Selection of teeth from Groups A-C prepared for SEM imaging**

The sectioned tooth specimens had been prepared and mounted onto carbon tabs on pin stubs and sputter coated with gold, ready for observation and image processing.

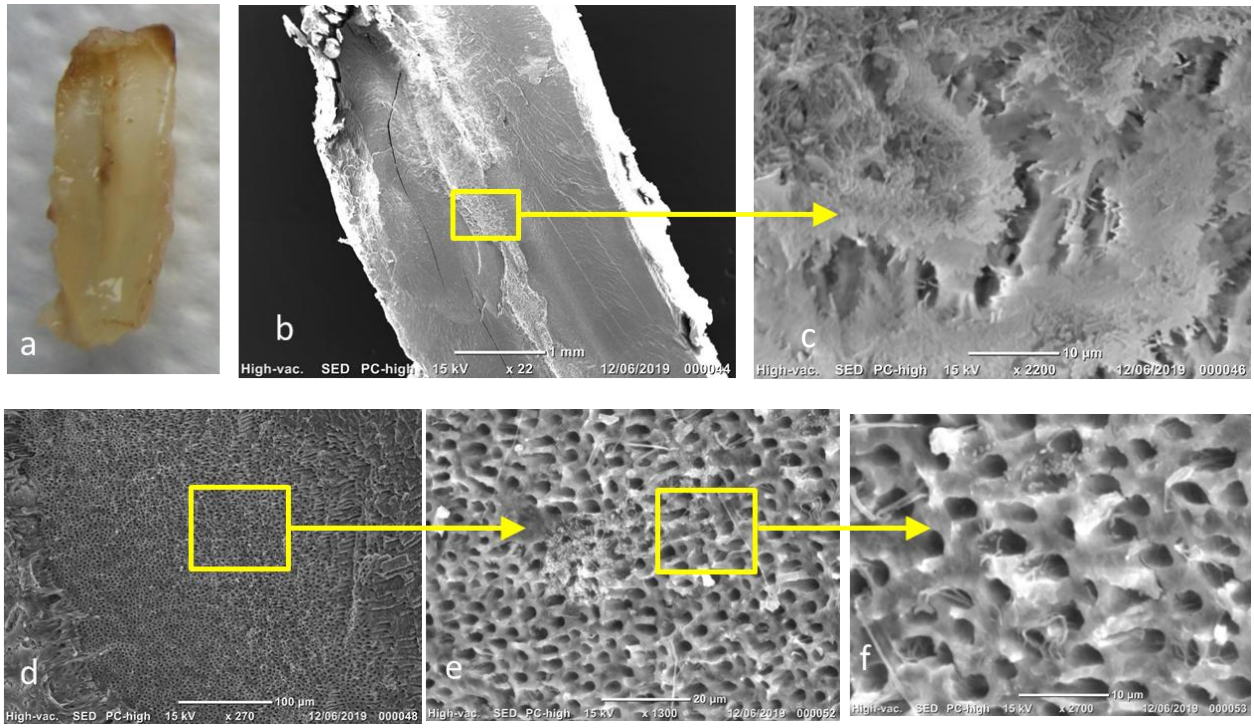


**Figure 2.14: SEM images of the extracted tooth with primary root canal infection and periodontal disease.**

The longitudinal cross section of a tooth from Group B with primary root canal infection, underwent SEM analysis. The infected root canal (b) showed a layer of biofilm on the surface of the root canal walls, with the yellow box which was examined at higher magnification as seen in image (c). Upon higher magnification, the section of the root canal with exposed dentinal tubules (d) showed filamentous and cocci shaped microorganisms on the dentine surface (e) as well as within the dentinal tubules. Magnification as per scale bar.

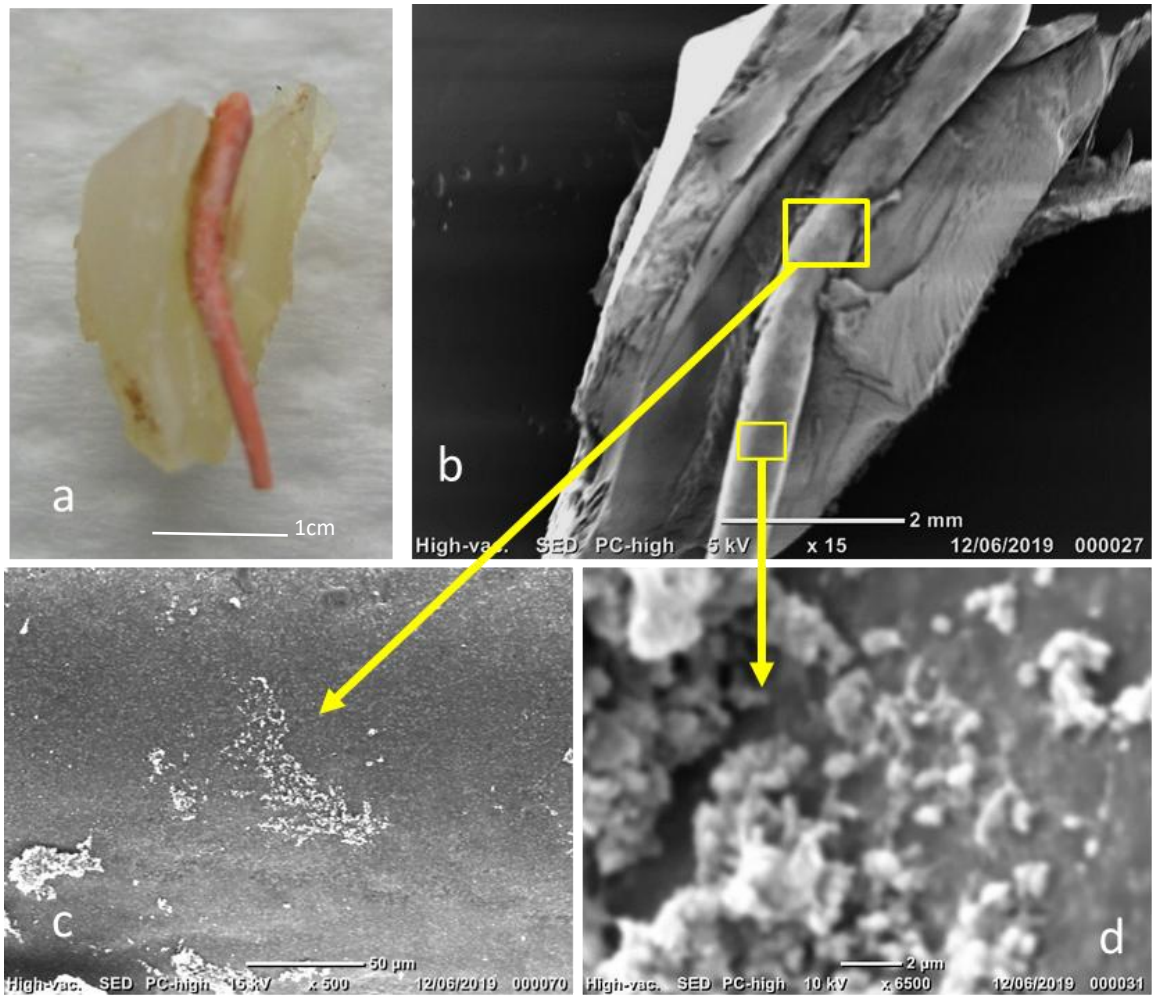


**Figure 2.15: SEM images of extracted tooth with secondary root canal infection and periodontal disease**

The longitudinal cross section of a tooth from Group C, with gutta percha in situ underwent SEM analysis (a). SEM images confirm the presence of microorganisms in planktonic and biofilm form adhering to the gutta percha (b-d) within the root canal. Higher magnifications of the yellow squares in image b, demarcated by yellow arrows extending to images c and d, confirm the presence of an early biofilm formation on the gutta percha. Magnifications as per scale bar.

### 2.3.8 SEM imaging of calculus

SEM was used to produce high resolution images for direct morphological examination of the calculus on the root surface as well as the calculus which had been removed. The extracellular polymeric substance (EPS) had microscopic channels, which were identified as biofilm water channels. Several well-preserved cocci (Co) and some filamentous microbes including rods (Ro) were present (Figure 2.16 and 2.17). The rod-like appearance may be representative morphologies oral microflora such as *P. gingivalis*, *T. Denticola, T. Forsythia* and *Aggregatibacter Actinomyetemcomitans.* Oral bacteria which appear as 'cocci' (spherical or oval shaped), growing in chains or clusters, are typical of *Streptococcus mutans, Streptococcus gordonii* and *Streptococcus salivarius*. The Eubacterium species would appear in the filamentous form.

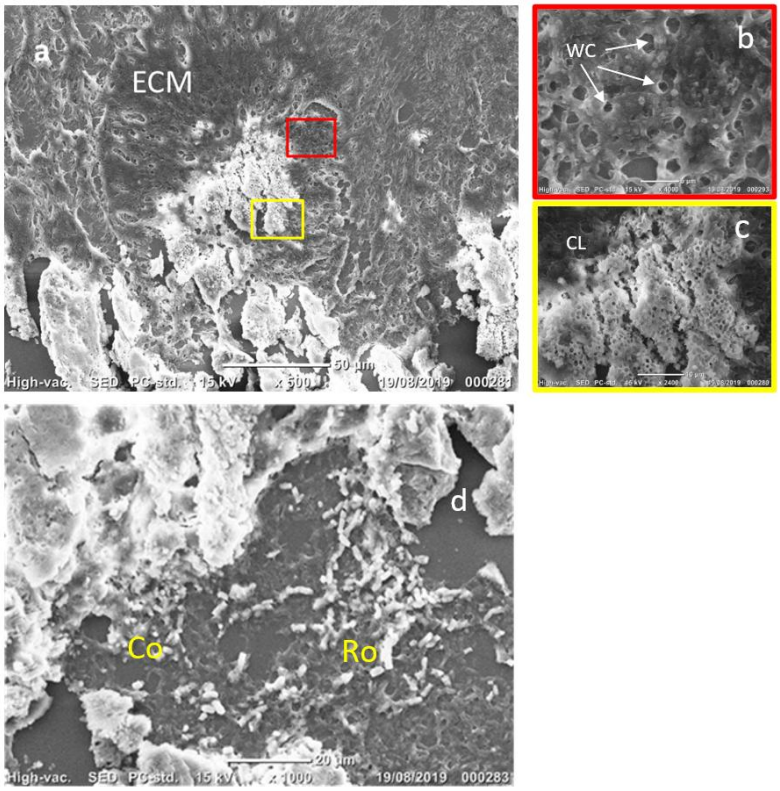


**Figure 2.16: SEM imaging of the calculus deposits from the external tooth root surface** SEM analysis revealed a polymicrobial biofilm consisting of extracellular matrix (ECM) (Magnification x500). Multiple water channels (WC, white arrows) can be seen throughout the biofilm (Magnification

of x4000). Calcific layers (CL) show a honeycomb appearance (Magnification x2400). Cocci (C) and rods (R) shaped microorganisms were seen within the biofilm (Magnification x1000).

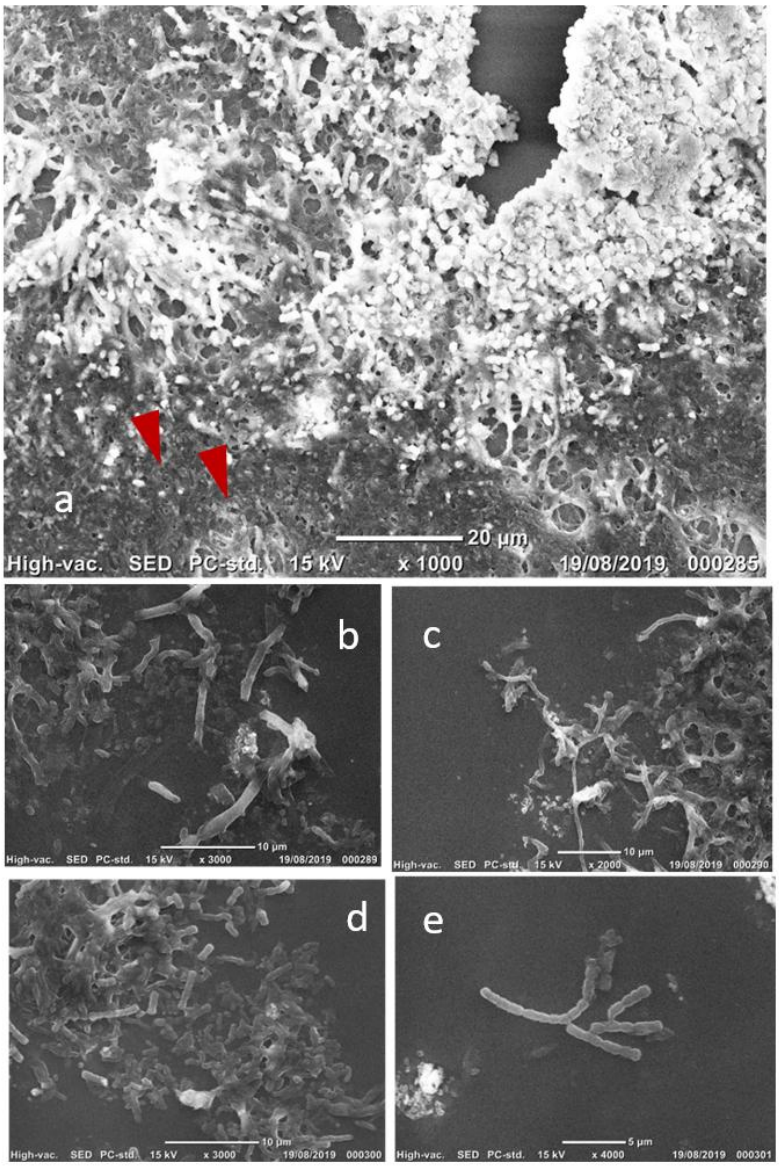


**Figure 2.17: SEM imaging of root calculus microorganisms**

SEM analysis shows sections with diverse microorganisms, including cocci (a, examples arrowed in red) rods, curved rods (b-d) and filaments (e).

### 2.3.9 Morphological visualisation a immunochemistry investigations under Transmission Electron Microscopy (TEM)

The carious tooth sections with primary root canal infection observed under TEM identified a variety of rounded and elongated shaped bacteria on the root canal and dentinal tubules (Figure 2.17). Freshly infected dentinal tubules (Figure 2.17a) exhibited an abundance of collagen surrounding the dentinal tubules. The infected dentinal tubules appeared to contain degraded bacteria within them. Root dentine also appeared to be degraded (Figure 2.17a, rectangular box). Closer examination at higher magnification of the degraded tissue is seen in the boxed area, revealing the presence of fibrils resembling insoluble Aβ (Figure 2.17b, black arrows).

The ultrastructure of the biofilm showed the diverse morphotypes of the biofilm bacteria that were seen in the earlier light microscopy Toluidine blue preparations (Figure 2.10). As seen in the specimens which underwent Gram staining (Figure 2.6), both Gram-positive and Gram-negative bacteria were also observed in the TEM micrographs, based on the thickness of their electron dense walls (Figure 2.18). The average range of thickness of Gram-positive bacterial cell walls is 20-80 nm, whereas Gram-negative bacterial cell walls had an average range of thickness of about 1-10nm (Silhavy et al., 2010). Gram positive bacterial cell walls are thicker due to its significant layer of peptidoglycan.

Higher magnification images clearly demonstrated EPS (Figure 2.18) in between bacterial cells. The internal content of a bacterium appeared to contain “virus-like” particles (Figure 2.18b-c). Examination of the EPS at greater magnification from 2.18d-f, areas within the boxes demonstrated some short electron dense fibrils within the electron lucent amorphous matrix. Further examination of the gutta percha biofilm (Figure 2.19a) showed more fibrils (area demarcated with a line and two arrows to show few fibrils) were clearly different in

morphology (longer) to those seen in 2.18e-f. Continued analysis of the specimen under the TEM demonstrated more very fine long fibrils (Figure 2.19b, black arrows) which appeared very similar to the fibrils observed in Figure 2.17b, presumed to be host Aβ. It is accepted that the process of dehydration during specimen preparation for the TEM is known to introduce artefacts, which have to be taken into consideration when interpreting these results.

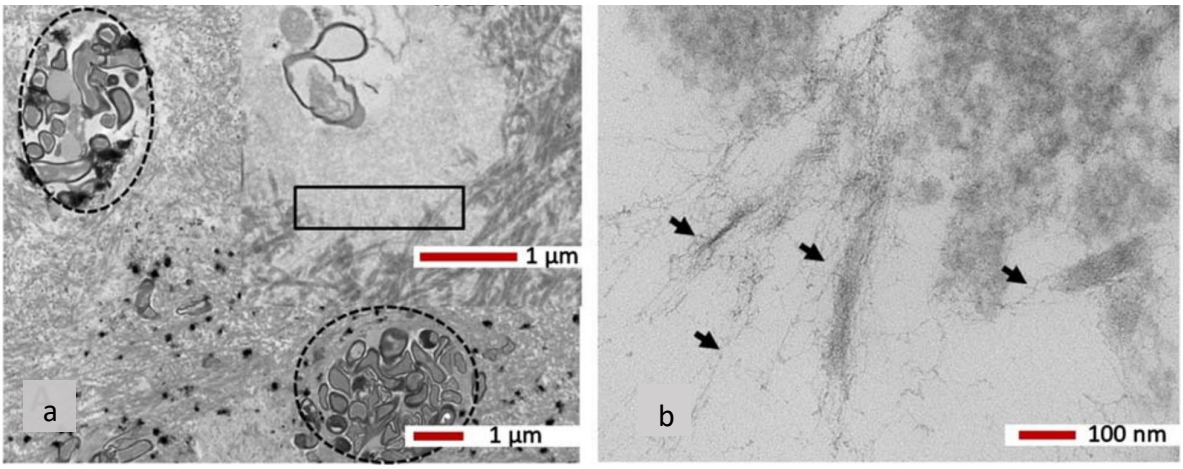


**Figure 2.18: TEM High resolution ultrastructure images from teeth in Group B (primary root canal infection with periodontitis) in araldite resin.**

TEM micrographs of a tooth section from a primary root canal infection associated with caries and primary root canal infection from Group B (a) shows dentinal tubules laden with bacteria (circled with dotted lines). Image (b) shows a higher magnification of the dentinal tubules with degraded bacteria and degraded collagen (within the black rectangle), some insoluble fibrils were observed. The fine fibrils appeared to be very similar to the host Aβ (black arrows) Magnification as per scale bar (Kanagasingam et al., 2022).

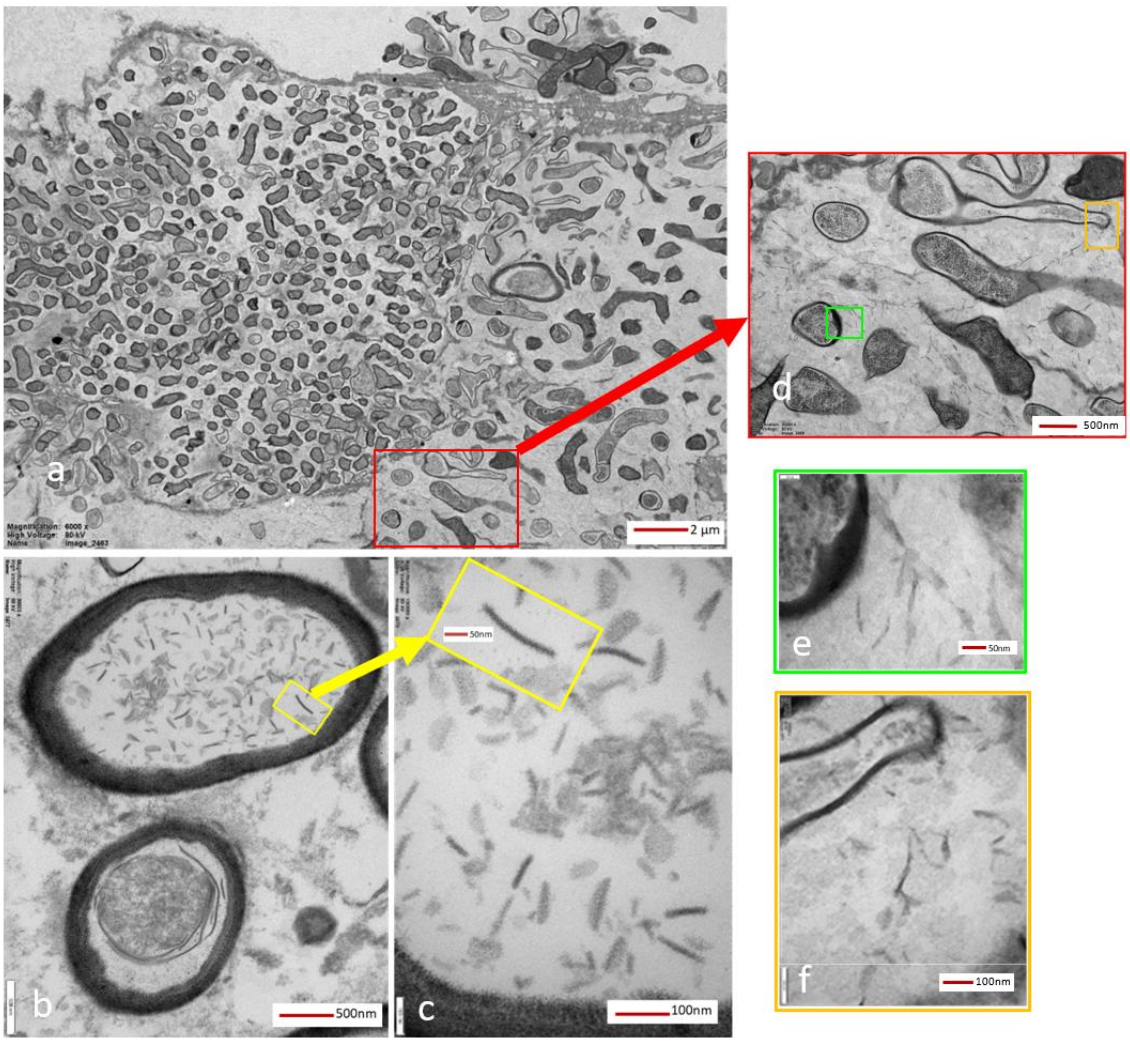


**Figure 2.19: TEM ultrastructure of a specimen of gutta percha and biofilm from failed root canal treatment and periodontal disease, Group C which were embedded in Araldite resin.**

TEM micrograph (a) shows a variety of morphotypes of the biofilm bacteria. Examination under higher magnification shows cross sections of bacteria, showing internal content contain short electron-dense fibrils or degraded extracellular matrix (yellow box in b, which is magnified in the insert in c). A higher magnification of the bacteria seen in (a) has been shown in (d). Based on the thickness of the cell walls, both Gram-positive and Gram-negative bacteria were observed alongside the extracellular polymeric substance (EPS) as seen in the regions demarcated by the green and orange boxes (e and f respectively). Multiple short electron dense fibrils within the EPS are obvious in images e and f. These fibrils appear different to host Aβ fibrils as seen in Figure 2.15b. Magnification as per scale bar.

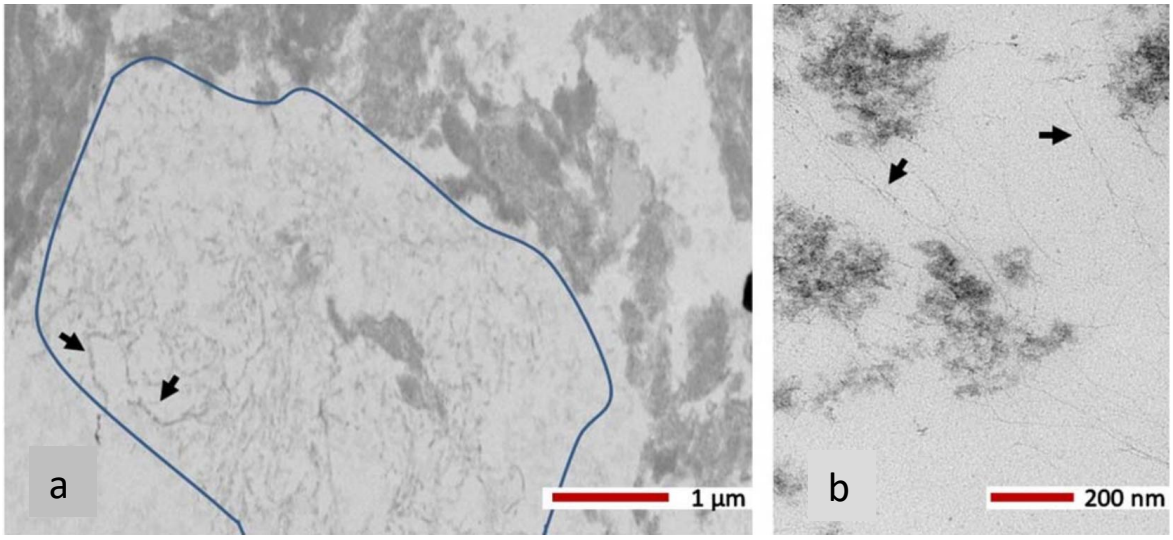


**Figure 2.20: Ultrastructure of a specimen of gutta percha and biofilm from failed root canal treatment, Group C which were embedded in Araldite resin.**

TEM micrographs further examined specimens with gutta percha biofilm in (a), showing more fibrils (area demarcated with the blue line and two black arrows pointing to the fibrils) which were clearly different in morphology to those seen in Figure 2.17a-b. More very fine fibrils (black arrows) were observed which appeared very similar to host Aβ fibrils as seen in Figure 2.18e-f. Magnification as per scale bar. (Kanagasingam et al., 2022).

### 2.3.10 Combinations of morphological and immunochemical investigative images for comparison across the various experimental techniques utilised

For an overview, Figure 2.20 demonstrates the various imaging techniques used for morphological and immunochemical imaging including Gram staining (2.20a-b) and Anti-Aβ antibody, Mouse monoclonal (6e10) (2.20c-d) as well as the matching SEM images (2.20e-f). Serial sections were matched for meaningful comparison and to highlight the presence of bacteria as seen in the Gram-stained histological slides and SEM images, coincided with the positive immunostaining with Anti-Aβ antibody, Mouse monoclonal (6e10). This showed that the immunostained regions were limited to the areas within the root dentine which were infected with what appeared to be filamentous and coccoid bacteria.

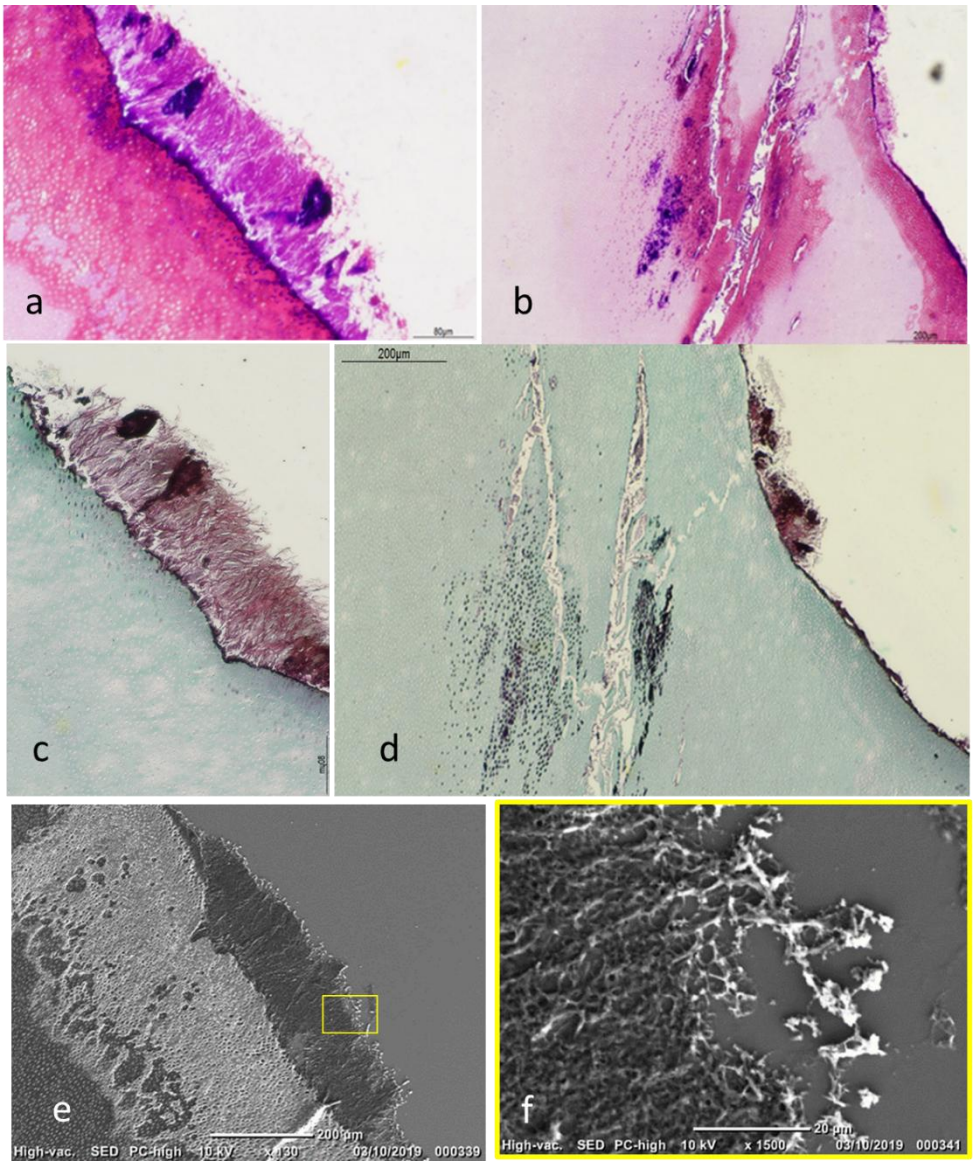


**Figure 2.21: Morphological and immuno-staining investigations with light microscopy and SEM imaging**

Gram staining revealed Gram positive and Gram negative bacteria in biofilm (a) on serial sections of tooth tissue, which coincide with similar regions which reacted positively to the Anti-Aβ antibody, Mouse monoclonal (6e10). The stained Aβ protein were observed within the dentinal tubules whereny bacteria and biofilm were identified in (a) as well as via SEM imaging (e), where higher magnification showed aggregates of filamentous and coccoid bacteria (f). Magnification as per scale bar.

## 2.4 DISCUSSION

Epidemiological studies have reported an association between chronic periodontal disease and AD (Sparks Stein et al., 2012; Chen et al., 2017). More recently, endodontic disease has been implicated as a potential risk factor. Lin et al. (2020) identified the impact of root canal treatment and limited numbers of extractions which appeared to be protective, lowering dementia odds ratios. Large numbers of extractions (more than 4 teeth extracted) and periodontal emergencies were associated with higher odds ratios. This relatively new link to endodontic disease is not surprising as the tooth pulp and periodontium are closely connected via anatomical as well as pathological pathways (as discussed in Chapter 1). In fact, untreated endodontic disease can be considered a local modifying risk factor for the progression of periodontal disease (Abbott & Salgado 2009; Herrera et al., 2017). This inspired the present study as the question arose as to the existence of host or microbial amyloid in naturally formed oral biofilm from patients with both periodontal and endodontic diseases. As such, it was clear that the freshly extracted human teeth and calculus samples were the most appropriate specimens.

As there were no existing studies which had attempted to detect Aβ within oral tissues, the methodology was predicated on the University of Central Lancashire's previous research output utilising immunohistochemical techniques in postmortem AD human and apolipoprotein E gene knockout (ApoE−/−) mouse brains (Poole et al., 2013; Singhrao et al., 2017). The closest comparable laboratory study was carried out by Kubota et al. (2014), whereby periodontitis-affected gingival tissue underwent colocalization of Aβ Precursor Protein (APP). While APP, a type I membrane glycoprotein plays a role in the physiological function of neurons, it can also be processed by β- and γ-secretases, leading to accumulation of Aβ peptide in tissues In the Kubota study, paraffin sections of the gingival tissues were

subjected to immune-staining with mouse monoclonal anti-APP antibody (clone 1B11F3, IgG2a) from LifeSpan BioScience (Seattle, WA, USA). The gingival tissue samples exhibited macrophages which expressed APP in the connective tissues of the subepithelial area, and this finding was confirmed with morphological observation.

The present study employed morphological and immunohistochemical analytical techniques to detect the presence of Aβ in freshly extracted human teeth. Three categories of specimens were studied, healthy teeth (Group A) and diseased teeth (teeth with primary root canal infection and periodontal disease, Group B and secondary root canal infection and periodontal disease, Group C). Morphological imaging with the Gram stain revealed a diverse group of bacteria which could be representative of Gram-positive bacteria such as *Streptococcus, Parvimonas, Filifactor* and *Actinomyces species*, and Gram-negative bacteria including *Prophyromonas*, *Treponema, Dialister, Propionibacterium* and *Fusobacterium* species (Fouad et al. 2002, Rôças & Siqueira 2018, Siqueira et al. 2007, Niazi et al. 2010, Li et al. 2014, Rosen et al. 2017). Similarity between the microbiota of both endodontic and periodontal disease supports the pathways of infection between the pulp and periodontium (Gomes et al., 2015).

Gram and Grocott-Gomori's silver impregnation stains confirmed the presence of a variety of bacteria and fungi within calculus samples. Although the tooth specimens did not produce a positive reaction to the Groctott-Gomori's stain, chemoorganotroph eukaryotic microorganisms such as *Candida albicans* have been identified as an endodontic and periodontal pathogen (Gomes et al., 2017).

Serial sections allowed the examination of the same regions in the tooth specimens which had been infiltrated by bacteria. The histological slides showed a positive reaction to the

immunohistochemical staining with Anti-Aβ antibody, Mouse clone (6e10), thereby confirming the presence of Aβ proteins in the regions of the tooth where bacteria and biofilm were detected using light microscopy and electron-microscopy techniques. These images were collated in Figure 2.20 for ease of comparison. This pattern was observed across specimens from Groups B and C. All calculus specimens which were laden with bacterial biofilm had significant uptake of the Anti-Aβ antibody, Mouse clone (6e10). As there was no uptake of the immunostaining in Group A (healthy teeth) and bacteria-free sites, each slide acted as its own experimental control.

SEM and TEM are well established methodologies for investigating tooth tissues and oral microbes (Beniash et al., 2000; Xu et al., 2022). The initial morphological investigations with SEM revealed biofilm on the root canal walls, within dentinal tubules as well as on the gutta percha surface. Immunohistochemical staining with Toluidine blue and Immunocolloidal gold silver staining (IGSS) with anti- Aβ antibody showed clusters of bacteria and biofilm, however, did not detect Aβ. In the absence of antibodies to microbial functional amyloid such as anti-curli antibodies, TEM ultrastructure was employed to visualise insoluble Aβ as shown by Chapman et al. (2002). Anti-curli antibodies specifically target and bind to bacterial amyloid protein called ‘curli’, produced by certain bacteria such as *Escherichia coli* and *Salmonella*. Curli forms a key component of bacterial biofilm structure and forms an amyloid-like structure, not unlike Aβ in AD (Sleutel et al., 2023, Sleutel & Remaut, 2025).

The rabbit anti-tau (clone AT8) remained negative for the biofilm sections. It was effective when initially tested on mouse and human cells from cell culture to detect endogenous tau protein. This suggested that either the biofilm organisms are not stimulating tau release by the host or the mechanism for their contribution (if any) to AD tau may be different. This was

subsequently tested with alternative methodologies which form Chapter 5. Further discussion on tau protein was not considered feasible for this chapter.

### 2.4.1 Challenges, strengths and limitations of study

Freshly extracted tooth specimens were collected for this study and immediate processing was carried out to minimise the risk of specimen degradation. However, the need for demineralization to facilitate sectioning of the dental hard tissue posed certain challenges. The teeth had to be soaked in EDTA for an average of 8-12 weeks to produce tissue sections at a thickness of 4-5 μm for optimal histological staining and immunohistochemistry. This also resulted in the loss of the membrane integrity and damage to the microbial biofilm. Moreover, the mineralised dental tissue was a barrier to penetration of dyes and antibodies, which tended to be more effective on soft tissues.

Processing and sectioning artefacts were also noted on some specimens, including tissue folds, shrinkage and scoring (caused by invariable remnant of minerals in the specimen). The methodology was optimised to decrease occurrence of these avoidable artefacts. Where calculus was kept intact on teeth or scrapped off prior to demineralisation for SEM, there was a better preservation of the microbes. The calculus biofilm demonstrated EPS that also contained channels to support the biofilm community. Light microscopy of the calculus specimens yielded adequate information regarding neutral stains to detect and localise microbes with better preservation. However, the limitation was insufficient magnification to distinguish the morphology of the microbes within the biofilm. With SEM images together with light microscopy neutral staining methods, it was evident that both Gram positive and negative bacteria were present, with shapes ranging from filamentous, cocci to rods. *P. gingivalis* and *Aggregatibacter Actinomycetecomitans* are Gram negative, rod-shaped

bacterium. *T. forsythia* and *T. denticola* are both Gram negative, bacteria, which are filamentous-shaped and spiral shaped respectively. S. mutans is a Gram-positive spherical coccus which can appear in pairs or chains. F, nucleatum are long, thin, Gram-negative rod-shaped bacteria. Actinomyces are Gram positive bacteria, appearing rod-shaped and branch out into filaments (Wan & Fan, 2023). These abovementioned oral bacteria have been detected in post-mortem AD brains (Poole et al., 2013; Emery et al., 2017; Siddiqui et al., 2019, Wan & Fan 2023).

The key for successful TEM imaging of dentine structure is to prepare a thin section of dentine specimens. As dentine is made up of up to 30% collagen, there can be a risk of degradation, resulting in pore formation during the Focused Ion Beam milling process. The resultant artefacts may cause inaccuracies image interpretation. They may also cause curtaining issues whereby large electron transparent areas may not be obtained. Careful implementation of the metal staining process plays an important role in eliminating the creation of artefacts (Xu et al., 2022). Although this part of the research was outsourced due to the lack of facilities on site, there was frequent and consistent communication with Dr Chris von Rhuland (Facility Lead, Electron and Light Microscopy, Central Biotechnology Services, School of Medicine, Cardiff University, Cardiff, UK) for targeting the TEM imaging.

As this study involved collecting extracted human teeth, progress was limited by regulations governing research ethics associated with the Human Tissue Act. This was compounded by difficulties faced during recruitment, training and sample collection. The experimental challenges included the prolonged duration taken for demineralization of the teeth for histology and limitations in penetration of the antibody to its antigen in the dental tissue. Furthermore, the delays due to outsourcing of TEM examination of grids was also a factor in the timely

completion of this investigation. The lack of functional equipment required for sectioning resin tissue blocks had also caused some delays. The researcher together with the supervisory team's support, had to apply to the UCLan Research Centre for Brain and Behaviour Application for additional funding to replace the necessary equipment.

Limitations of this study also include the small sample size and the lack of traceability of the extracted tooth to the donor subject. Therefore, it was not possible to correlate the results with the donor's medical history.

The study would have benefitted the use of a 'pan antibody'. Theoretically, a 'pan amyloid antibody' would allow detection of multiple variants or isoforms of the microbial amyloid protein, including the curli protein, monomers, oligomers, and fibrils. Recognizing a broad spectrum of amyloid structures, regardless of their specific conformation would be beneficial to research and diagnostics. At the time of this experimental work, this was not available.

An animal and cell culture study carried out by Nie et al. 2019 reported that Aβ was released following *P. gingivalis* infection in macrophages *in vitro*. Macrophages follow on from the inflammatory response generated by bacterial infection underneath the gums. The new finding in the present study is that Aβ may be peripherally generated in extracted teeth which have been infected under natural oral biofilm forming conditions in teeth afflicted by endodontic and periodontal disease. The Aβ deposition may be an immune response to pathogens or foreign antigens (Miklossy 1993; Balin et al., 2008, Poole et al., 2013; Kanagasingam et al., 2020).

### 2.4.2 Clinical relevance

The implication for Aβ is that the human and microbial Aβ protein in the oral cavity may be transported to the brain by the receptor for advanced glycation end products (Zeng et al., 2021). In addition, the tau protein aggregation following its release by the host, due to microbial infection, was explored because tau is also hypothesized to be taken up by neurons and has the potential for cross seeding via connecting neurons into adjacent anatomical parts of the brain contributing to spread and severity of AD. Therefore, in order to explain the link of microbial agents to AD, it is essential to find out if they contribute to the hallmark lesions of the brain. Dominy et al. (2019) showed that gingival tissue with periodontal disease stained positively with RgpB-specific monoclonal antibody 18E6 which identifies one of *P. gingivalis'* virulence factors- gingipains. In the present study, where an extracted tooth had attached gingivae, it stained positively for Aβ (Figure 2.7). Immunostaining of root calculus detected bacteria, Aβ and bacterial LPS, which corroborates the findings of Dominy et al. (2019). These results confirm that there is a potential for host and microbial Aβ to contribute to the existing pool of amyloid proteins in AD brains, potentially instigated by chronic inflammation associated with periodontitis and root canal infection Kamer et al., 2015).

In this study, we used an *ex vivo* model to confirm the immunolocalization of Aβ to the site of naturally occurring biofilm in infected extracted human teeth. To the best of our knowledge, this methodology is unique as the infected regions of the teeth included both intracanal (endodontic) as well as extra-radicular (periodontal) naturally formed biofilm. The results support Moir's 'Antimicrobial Protection Hypothesis' (Moir,2018), whereby infected regions of the tooth mirrored Aβ deposition in the semi-serial sections, following Gram staining and immunostaining (as seen in Figure 2.20).

There is evidence to suggest that amyloid-forming proteins such as tau and Aβ, while yet to be proven infectious in the classical sense, share certain essential properties with prions. This could explain the similar patterns of spread within the nervous system (Frost & Diamond, 2009). To date, the pathological form of prion proteins has not been detected in dental pulp tissue. However, there is a theoretical risk of cross infection in individuals with Creutzfeldt-Jakob disease via endodontic instruments which contact pulpal neurovascular tissue during root canal treatment. Previous studies have shown that the prion-protein resists conventional sterilization methods, and the transfer of these proteins can occur from infectious Creutzfeldt-Jakob disease patients (Walker et al., 2007; Sonntag et al., 2007). The pathogenic isoform of prions has a three-dimensional conformation with a higher content of β-sheet structure and aggregates to form medium and large size polymers, leading to the deposition of insoluble fibrils in Aβ plaques (Soto & Satani, 2011). When cross-seeding of prions occurs, involving the central nervous system, they can cause spongiform degeneration. This could theoretically be spread from human to human via infected brain or nerve tissue. This led national organizations, including the Disease Control and Prevention and World Health Organization to restrict endodontic instruments to single use as a precautionary measure (WHO/CDS/CSR/APH/2000, Centers for Disease Control and Prevention (2003) Guidelines for Infection Control in Dental Health-Care Settings. MMWR Morb Mortal Wky Rep 52, 2003, WHO consultation (1999) WHO Infection Control Guidelines for Transmissible Spongiform Encephalopathies. World Health Organization Communicable Disease Surveillance and Control, Geneva, Switzerland 74–76).

This study is the first to report that potentially pathogenic insoluble Aβ have been detected within root canals of endodontically and periodontally infected teeth. The clinical significance of these findings raises concerns over the extent of translocation of the Aβ from oral sites to

the central nervous system. Questions arise regarding the potential for the 'Aβ infection' spreading between humans through medical or surgical instruments contaminated with Aβ proteins, in the same way prions are thought to spread. At this time, there is no evidence to suggest that AD is in any way contagious, however, patients should be reassured that existing cross infection protocols are effective in minimizing infection risk from dental procedures. In the UK, root canal instruments such as endodontic files and reamers are strictly single use. The findings of this study do not support the notion that dental procedures pose a risk of AD. In fact, patients should be aware that infected teeth which have root canal infection and periodontal disease may harbour the Aβ protein. The key message to patients is that root canal infection and periodontal disease should not be left untreated.

### 2.4.3 Future studies

Ideally, it would have been beneficial to have the opportunity to collect extracted teeth and calculus (from teeth which were already planned for extractions) from subjects with dementia, with similar aged healthy subjects, with and without periodontal disease. It would be interesting to identify the pathogenic bacteria present as well as conduct immunohistochemical staining for Aβ proteins amongst the various groups. If each tooth specimen could also be traced back to the donor, their medical history could also be analysed. As with most studies, it would have been ideal to have a larger sample size.

While light microscopy and electron-microscopy are useful for observing microbial morphology, for future studies, the methodology could be supplemented by PCR-based techniques based on 16S rRNA gene (or 16S rDNA), DNA-DNA hybridization (macroarray) or DNA microarray (Siqueira & Rôças, 2022) for more accurate identification of microorganisms associated with oral disease.

By examining dentine structure in an unstained, frozen-hydrated state, it may be possible to prevent artefacts which are usually associated with the staining and dehydration processes that are required for conventional TEM. Hence, a future study may also include cryo-TEM analysis (Beniash 2000, Quan and Sone 2013).

The use of a pan antibody could improve the detection of all conformations of amyloid protein. At the time of writing, an online search revealed that as of 21.12.2024, a pan antibody Anti-amyloid beta peptide (MOAB-2), pan, clone 6C3 (mouse monoclonal) was available from Merck Life Science (Dorset, UK). Based on manufacturer's information, this pan antibody detects multiple amyloid-beta 40 and amyloid-beta 42 conformations including unaggregated, oligomeric and fibrillar, reportedly showing greater specificity to Aβ compared to Anti-Aβ antibody (6E10).

As curli forms a key component of bacterial biofilm structure and forms an amyloid-like structure and are potent inducers of the host inflammatory response, it would be interesting to identify endodontic and periodontal pathogens which have the curli gene.

## 2.5 CONCLUSION

The present study serves as pilot study to gain a better understanding of the potential for Aβ formation potentially induced by a heterogenous consortium of oral bacteria. The host appears to have responded to the infection by releasing Aβ as an innate response in Groups B and C, including endodontic and periodontal bacteria and biofilm. The immunolocalization of the insoluble Aβ coincided with infected regions of the tooth tissue. The microbes can give rise to insoluble Aβ experimentally, not dissimilar to the mechanism with which prions deposit insoluble fibrils in Aβ plaques. Like prions, insoluble Aβ can be at risk of being cross seeded to the brain and may contribute to the development of AD later in life. Further research is required to clarify the extent of such a risk and the mechanism by which Aβ could translocate from oral tissues to the brain.

# CHAPTER 3

## *PORPHYROMONAS GINGIVALIS* CONDITIONED MEDIUM *IN VITRO* CHALLENGE OF SH-SY5Y CELLS INDUCES AMYLOIDOGENIC PROCESSING OF THE AMYLOID-β PRECURSOR PROTEIN

The work presented in this chapter is fully published by the author of this thesis

**Kanagasingam S**, von Ruhland C, Welbury R, Chukkapalli SS, Singhrao SK (2022) *Porphyromonas gingivalis* conditioned medium induces amyloidogenic processing of the amyloid precursor protein upon in vitro infection of SH-SY5Y cells. J. Alzheimers Dis Rep. 6(1):577-587.

# *PORPHYROMONAS GINGIVALIS* CONDITIONED MEDIUM *IN VITRO* CHALLENGE OF SH-SY5Y CELLS INDUCES AMYLOIDOGENIC PROCESSING OF THE AMYLOID-B PRECURSOR PROTEIN

## 3.1 INTRODUCTION

*P. gingivalis*, through its virulence factors can induce the local release of inflammatory cytokines, which are key signalling molecules which could enter the systemic circulation (Vernal et al., 2009; Díaz-Zúñiga et al., 2020). This highlights the critical role that *P. gingivalis* plays in initiating various chronic diseases, besides periodontitis, through pro-inflammatory cytokines (IL-1β, IL-6, and others), including atherosclerosis, insulin resistance and hyperglycemia (Makiura et al., 2008, Chiu et al., 2016; Bale et al., 2017; Sansores-España et al., 2021). The above mentioned vascular and metabolic related conditions become increasingly common with advancing age, posing a significant health, societal and economic burden (Olsen et al., 2016; Chen et al., 2017; Lin et al., 2020). Prior research has indicated that oral infections caused solely by *P. gingivalis* or by the introduction of its virulence factors e.g. its endotoxin, lipopolysaccharide (LPS), fimbriae and gingipains can result in the development of critical lesions that are hallmarks of AD neuropathology (Watts et al., 2008; Wu et al., 2017; Ishida et al., 2017; Ding et al., 2018; Zhang et al., 2018).

In longitudinal studies involving periodontitis-AD infection mouse models, long-term exposure to *P. gingivalis* and its LPS triggered an increase in inflammatory biomarkers, resulting in neuroinflammation and neurodegeneration. Increased Aβ accumulation were observed within neurons as well as higher amyloid load in the hippocampus and cortex regions

of the brain (Wu et al., 2017; Ishida et al., 2017; Zhou et al., 2017, Illievski et al., 2018; Zhang et al., 2018).

The ‘Amyloid Hypothesis’ also known as the ‘Amyloid Cascade Hypothesis’ suggests that a build-up and deposition of oligomeric and fibrillar Aβ is the primary cause of AD. In healthy individuals, Aβ is excised from APP by β- and γ-secretase, subsequently released outside the cell and degraded. Elderly subjects may not be able to eliminate Aβ as efficiently, thus Aβ peptides such as $A\beta_{40}$ and $A\beta_{42}$ (Hardy & Selkoe, 2002, Kametani & Hasegawa, 2018). Increased levels of $A\beta_{42}$ instigates Aβ amyloid fibril formation, which develop into senile plaques, found in abundance in the brains of AD patients (Karran & DeStrooper 2022).

The Amyloid precursor protein (APP) is proteolyzed to produce Aβ peptides. This transmembrane glycoprotein has diverse physiological functions, including intracellular signalling, synaptic and neuroplasticity and cell adhesion. APP also mediates the attachment of Aβ to the neuronal cell surface and induces intracellular signalling, contributing to Aβ toxicity. Dysfunction of APP or mutations in the APP gene can increase the production of the more toxic Aβ42 (O'Brien & Wong, 2011; Pfundstein et al., 2022). Figure 3.1 illustrates the APP processing and cleavage via the non-amyloidogenic and amyloidogenic pathways. While the amyloid hypothesis has mainstream acceptance, placing APP and Aβ at the centre of AD aetiology, there is still a gap in knowledge with regards to the regulation of APP’s processing, and the mechanisms of Aβ-induced toxicity. Moreover, the influence of *P. gingivalis* on the processing of APP has not been clearly elucidated in current literature. A recent murine model (utilising C57BL/6J mice) of periodontitis induced by oral administration of *P. gingivalis*, investigated the change of APP processing and Aβ metabolites in peripheral tissues and the

brain. Researchers concluded that the expression of APP variants in the brain were modulated by *P. gingivalis* infection (Shen et al., 2023).

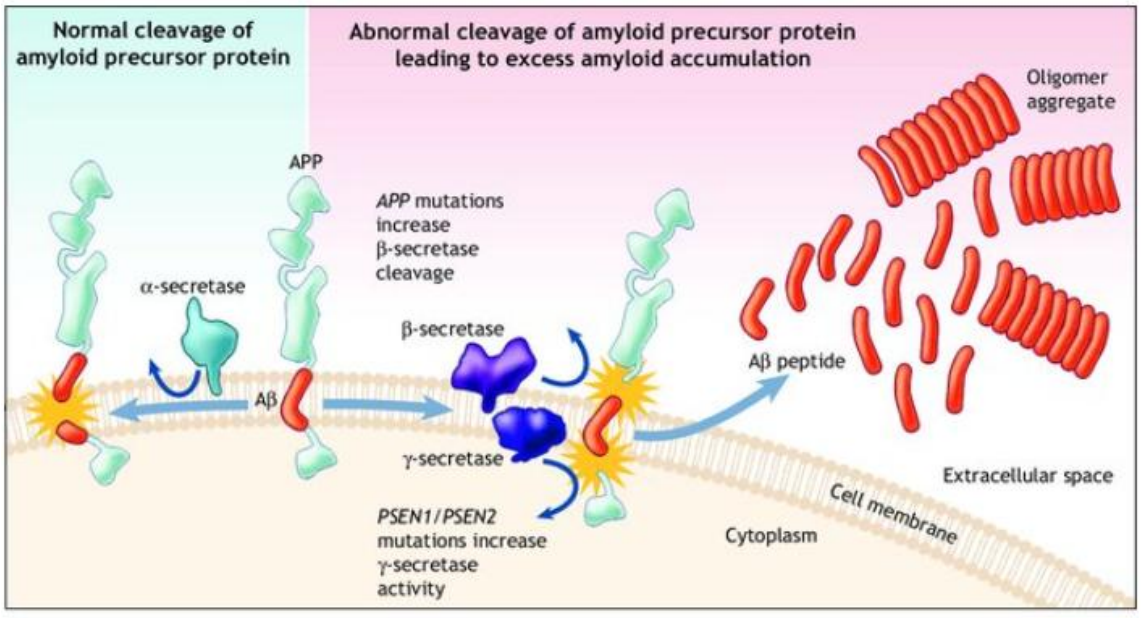


**Figure 3.1: APP processing and cleavage to produce Aβ proteins via the non-amyloidogenic and amyloidogenic pathways**

APP (a transmembrane protein) undergoes proteolytic cleavage by β-and γ-secretase enzymes. The non-amyloidogenic pathway involves APP cleavage by α-secretase of the Aβ domain. The amyloidogenic pathway produces neurotoxic Aβ peptides when APP is cleaved by β-and γ-secretase enzymes. The accumulation of the releases Aβ, aggregates, forming Aβ plaques. Mutations in the APP gene favours preferential cleavage by β-secretase, as cleavage by α-secretase is inhibited. Presenilin-1 and presenilin-2 genes (PSEN1 and PSEN2), which form subunits of the γ-secretase complex, can undergo mutation which result in increased cleavage by γ-secretase at this site. This ultimately leads to excess Aβ peptide production. As described by the Amyloid Hypothesis, the soluble Aβ oligomers can cause neurodegeneration. The oligomers have a propensity to aggregate into insoluble β-sheet amyloid fibrils, triggering a local inflammatory response. Subsequent oxidative stress and biochemical changes, can lead to neuronal death and the development of neuritic plaques pathognomonic of AD (Image credit: Patterson et al., 2008)

The present *in vitro* study aimed to investigate the effect of *P. gingivalis* supernatant (ATCC strain FDC 381) crude virulence factors on the amyloidogenic processing of APP

in the wild type (SH-SY5Y). The *P. gingivalis* strain FD381 supernatant is commonly used in laboratory studies as it is well characterised and relatively less virulent compared to other strains (e.g. W83, ATCC 33277), thereby causing less tissue destruction in animal models. This feature allows researchers to analyse immune pathways without an overwhelming inflammatory reaction. FDC 381 readily invades various cell types. Its well-documented genetic profile facilitates the analysis of specific mechanisms involved in its pathogenicity (Sandros et al., 1994; Igboin et al., 2009).

*In vitro* cell models simulate the characteristics of the disease in question by using appropriate bacterial supernatants as used here are essential for the investigation of biochemical and molecular processes involved in neurodegeneration. As AD is characterised by neurodegeneration and eventual neuronal death throughout the brain, a cell model which closely mimics this would involve exposure of neuronal cells (either postmortem human primary neuronal cells, animal-derived neuronal cells or neuron-like immortal cell lines) to a compound that induce neuroinflammation and neurotoxicity (Cetin et al., 2022). As for the choice of cell line, the wild-type SH-SY5Y cell line is an unmodified human neuroblastoma cell line, thrice cloned subline of the neuroblastoma cell line SK-N-SH (ATCC HTB-11), from a metastatic bone tumour from a 4-year-old cancer patient (https://www.atcc.org/products/crl-2266). This cell line is regularly used as an *in vitro* AD model to investigate molecular mechanisms of AD, especially facilitating investigations on the behaviour of APP (Balyaev et al., 2010; Wan et al., 2012; Kulatunga et al., 2024)

In this study, SH-SY5Y cells were selected as this cell line has been used in *in vitro* models of neuronal function and differentiation. Mature SH-SY5Y cells naturally express APP

along with including α-secretase, β-secretase (BACE1), and γ-secretase complex, allowing for the generation of various APP cleavage products, which means researchers may study its processing without the need to artificially overexpress these features (Shipley et al., 2016).

In general, conditioned medium is useful for studying virulence factors and investigating host cell interactions as they contain various proteins, including growth factors, cytokines, and chemokines. The virulent factors such as gingipains (proteases), lipopolysaccharides, and toxins, which are expressed in *P. gingivalis* conditioned medium are key contributors to its pathogenic potential (Holt et al., 1999). This allows the investigation of secreted gingipains-mediated effects on APP processing in SH-SY5Y cell lines, without the influence of direct cell-to-cell contact. (Singhrao et al., 2024). An additional variable which could impact the experimental conditions and better represent clinical settings is the presence or absence of pro-inflammatory cytokines. Elevated levels of IL-1β, IL-6, and TNF-α have been detected in AD patients as compared to healthy controls. Higher serum levels of IL-6 have been associated with steeper cognitive decline as well as worsening psychomotor speed (Ng et al. 2018). Similarly, the abovementioned cytokines are considered key inflammatory markers for periodontal disease progression as they promote periodontal bone loss and soft tissue inflammation (Neurath & Kesting, 2024). As such, this study endeavoured to create an *in vitro* cell culture model which could simulate as closely as possible the *in vivo* conditions of active periodontal disease with neuroinflammation, and its impact on amyloidogenic processing.

### 3.1.1 Hypothesis

*P. gingivalis* virulence factors and pro-inflammatory cytokines can modulate amyloidogenic processing in neuronal cells to increase peripheral pools of Aβ.

### 3.1.2 Aims and Objectives

Aim: To investigate the *in vitro* effects of *P. gingivalis* (FDC 381) conditioned medium on the amyloidogenic processing of Aβ-Precursor Protein (AβPP) in the SH-SY5Y cell line.

Objectives:

**(i)** To determine the effects of *P. gingivalis* conditioned medium containing virulence factors in the presence and absence of cytokines on SH-SY5Y cells

**(ii)** To assess the SH-SY5Y cells and their supernatants for the presence of AβPP cleavage fragments by immunoblotting and transmission electron microscopy (TEM).

### 3.1.3 University Approvals

This project received approval from BSO (UCLan) approval ref: 0219-01

## 3.2 MATERIALS AND METHODS

This study involved cell culture techniques utilising SH-SY5Y cells with *P. gingivalis* conditioned medium containing virulence factors to establish an *in vitro* model of AD to assess cellular responses and molecular changes in these cells with regards to amyloidogenic processing. The added variable of the presence or absence of pro-inflammatory cytokines, IL-6, IL-1β and TNF-α allowed observation of how inflammation would impact AβPP cleavage. Western blotting was used to separate and identify proteins based on their molecular weight, which facilitated the detection of the Aβ variants. TEM was beneficial in this study to identify insoluble Aβ fibrils in the Pg381 treated supernatant from the SH-SY5Y in conditioned medium. As with previous studies (Gu et al., 2013) and results from Chapter 2, TEM imaging can provide ultra-structural morphological visualisation of Aβ fibrils.

The *P. gingivalis* conditioned medium containing crude virulence factors and sterile control medium was kindly provided by our collaborator Dr Sasanka Chukkapalli (University of Florida, USA). The methodology has been described in detail in Kanagasingam et al. (2022) and Singhrao et al. (2024). Similar methodological protocols were employed in UCLan student projects which were supervised by Dr Sim Singhrao and the author of this thesis (JL Fernandes Inacio, MSc dissertation and Zaid Patel, BSc research projects).

### 3.2.1 Source of reagents

All general purpose laboratory reagents used for the preparation of standard solutions and buffers for the work presented in this chapter were: *P. gingivalis* (ATCC strain FDC 381) conditioned medium and sterile growth medium tryptone soya broth or TSB (as control), were a gift from Dr Sasanka Chukkapalli from the University of Florida, USA, now relocated to the

University of Texas A & M University, USA. The human neuroblastoma SH-SY5Y, CRL-2266™ cell line was obtained from the American Type Culture Collection (ATCC) (https://www.atcc.org/products/ SH-SY5Y CRL-2266™). Dulbecco's modified Eagle's medium (DMEM,), Foetal bovine serum (FBS). Cytokine(s) IL-1β (Life Technologies, Thermo Fisher Scientific, UK); TNF-α (Gibco, Thermo Fisher Scientific, UK). Phosphate buffered saline (PBS) from tablets, Radioimmunoprecipitation assay (RIPA) buffer, pH 8.0: Tris, NaCl, EDTA, Sodium deoxycholate, NP-40, sodium dodecyl sulphate. phenylmethanesulphonyl or PMSF and 5mM dithiothreitol, protease inhibitor cocktails 2 and 3, and Coomassie Blue Protein Assay were purchased from Sigma-Aldrich, Precast 12% mini-protean TGX stain-free linear gels (BioRad Laboratories, USA). Protein ladder, (Pageruler Plus, Lot.00498336 from Thermo Fisher). Mercaptoethanol (Alfa Aesar, Thermo Fisher Scientific), Polyvinylidine difluoride (PVDF) membranes (Thermo Fisher Scientific). Rabbit anti-APP C-terminal (cat no A8717) antibody and rabbit anti-APP N-terminal (cat no A8967) both from Sigma Aldrich (Dorset, UK) and mouse anti-Aβ (clone 6e10) from BioLegend (London, UK) and Chemiluminescent substrate (SuperSignal® West Pico, ThermoFisher Scientific, UK).

### 3.2.2 *P. gingivalis* conditioned medium as source of crude virulence factors

Briefly, our collaborator (Dr S. Chukkapalli, University of Florida, USA) cultured *P. gingivalis* (ATCC strain FDC 381) under anaerobic conditions to density of $5\times10^9$ per mL in mycoplasma broth (VWR) supplemented with hemin (5 µg/mL final concentration, Sigma-Aldrich, Dorset, UK), and menadione (1 µg/mL final concentration). The conditioned media which contained crude virulence factors and sterile control medium were received frozen, and were kept at -80°C.

### 3.2.3 *In vitro* cell culture

The human neuroblastoma SH-SY5Y, CRL-2266™ cell line (ATCC, Virginia, US) is a thrice cloned human neuroblastoma cell subline which was established in 1970 from a metastatic bone tumour from a 4-year-old cancer patient (https://www.atcc.org/products/crl-2266#product-references). The human neuroblastoma SH-SY5Y, CRL-2266™ cell line (ATCC) was cultured in Dulbecco's modified Eagle's medium (DMEM), which was supplemented with 5% foetal bovine serum (FBS). The SH-SY5Y, CRL-2266™ cells were grown at 80% confluence, and challenged for 48 hours, with and without *P. gingivalis* medium containing virulence factors. This was diluted at 1:5 in T-DMEM only as well as with recombinant cytokine(s) IL-1β at 10 ng/ml; TNF-α at 10 ng/ml and IL-6 at 5 ng/ml, alone and in combination with *P. gingivalis* virulence factors. The sterile microbiological growth (TSB) medium which was for *P. gingivalis* was diluted 1:5 in T-DMEM was used separately as a control. A preliminary cytotoxicity assay demonstrated *P. gingivalis* virulence factors diluted 1:5 was non-toxic to SH-SY5Y cells. The optimisation data was provided from a separate experimental study. The SH-SY5Y cells were grown in flasks and incubated at 37°C in a humidified atmosphere of 5% CO2, 95% air. The methodology for cell culture has been described in detail in Kanagasingam et al. (2022) and Singhrao et al. (2024).

**Table 3.1: The constituents of DMEM including relevant additives**

| Dulbecco's modified Eagle's medium (DMEM) | Manufacturer | For 500 mL |
|---|---|---|
| 10% foetal bovine serum (FBS) | Sigma-Aldrich, UK | 50 mL |
| 5mM Pen/strep | Gibco UK | 5 mL from stock |
| 5mM L glutamine | Gibco UK | 5 mL from stock |
| 5mM Sodium pyruvate | Gibco UK | 5 mL from stock |

T-DMEM was the treatment medium in which Pen/Strep were omitted. This was then used for the treatments carried out on SH-SY5Y, CRL-2266™ cell line (refer Table 3.2).

**Table 3.2: Summary of treatments carried out on SH-SY5Y, CRL-2266™ cell line**

| Treatment number | Cell Treatments on SH-SY5Y cells | Working Dilution | Prepared working dilution in treatment medium or T-DMEM |
|---|---|---|---|
| 1 | SH-SY5Y cells (control) | No treatment | Standard TC growth |
| 2 | *P. gingivalis* (Pg381) virulence factors | 1:5 in DMEM | 3 mL of Pg virulence factors + T-DMEM to 15 mL |
| 3 | IL-1β | 10 ng/ml | 1.5µL/mL IL-1β+ T-DMEM to 15mL |
| 4 | IL-6 | 5 ng/ml | 1.5µL/mL IL-6+ T-DMEM to 15mL |
| 5 | TNF-α | 10 ng/ml | 1.5µL/mL TNF-α + T-DMEM to 15mL |
| 6 | *P. gingivalis* (Pg381) virulence factors + IL-1β | 1:5 in DMEM + 10 ng/ml | 3mL of Pg381 virulence factors + 15µL/mL IL-1β+ T-DMEM to 15mL |
| 7 | *P. gingivalis* (Pg381) virulence factors + IL-6 | 1:5 in DMEM + 5 ng/ml | 3mL of Pg381 virulence factors + 15µL/mL IL-6+ T-DMEM to 15mL |
| 8 | *P. gingivalis* (Pg381) virulence factors + TNF-α | 1:5 in DMEM + 10 ng/ml | 3mL of Pg381 virulence factors + 15µL/mL TNF-α + T-DMEM to 15mL |

### 3.2.4 Cell lysate preparation

Following a 48-hour treatment, the supernatants from the undifferentiatedch SH-SY5Y cells were collected into sterile 15 mL Falcon tubes, centrifuged (Sigma3-16K, Sigma-Aldrich, UK) for 5 minutes at 3000 rpm to remove cell debris, and stored at -80°C. The remaining cells adhered to the flasks were washed twice with 5 mL phosphate buffered saline (PBS), detached, and suspended in PBS. Once detached, the cells were transferred into 15 mL sterile, Falcon tubes and centrifuged at 1000 rpm for 10 minutes. After draining off excess PBS, the cell pellet was lysed in 250 µL volume of lysis buffer (Radioimmunoprecipitation assay, RIPA buffer, pH 8.0: containing 50 mM Tris, 150 mM NaCl, 5 mM EDTA, 0.5% Sodium deoxycholate, 0.5% (v/v) NP-40, 1% sodium dodecyl sulphate (Table 3.3), 1:100 final of phenylmethanesulphonyl (PMSF) and 5mM dithiothreitol, 5% protease inhibitor cocktails 2 and 3 (Table 3.4). The cells were vortex mixed and incubated on ice for 10 minutes with further vortex mixing in between. At this stage, the cell homogenate was transferred into pre-labelled 1.5mL Eppendorf tubes and were centrifuged at 14,000 rpm for 20 minutes (Sigma 1-14 microfuge). The liquid phase was withdrawn, transferred into new pre-labelled 1.5mL Eppendorf tubes, and used to determine total protein following a protein assay (refer section 3.2.5). All cell lysates were stored at -80°C until needed for Western blotting (APP cleavage products).

**Table 3.3: List of lysis buffer components**

| RIPA buffer | RIPA supplementary buffer | Equal volumes of the RIPA buffer and RIPA supplementary buffer were mixed to acquire the final buffer concentration |
|---|---|---|
| 25mM Tris, pH 7.5<br>150mM NaCl<br>1% NP-40<br>1% sodium deoxycholate<br>0.1% SDS | 75mM Tris, pH 7.5<br>150mM NaCl<br>10mM EDTA<br>1.9% SDS | 50mM Tris, pH 7.5<br>150mM NaCl<br>5mM EDTA<br>0.5% NP-40<br>0.5% sodium deoxycholate<br>1% SDS |

**Table 3.4: Lysis buffer with protease inhibitors added to 48 mL of final buffer from Table 3.3, for the preparation of cell lysates (adapted from Zaid Patel, BSc research project)**

| **Phosphatase inhibitor cocktail (PIC 2 and 3) Sigma** | **Ref no. Sigma** |
|---|---|
| 0.5% Pic 2 = 240 µL/48 mL lysis buffer | P5726/ 1 mL |
| 0.5% Pic 3 = 240 µL/48 mL lysis buffer | P0044/ 1 mL |
| **Protease inhibitors (PI) from Sigma**<br>1/100 PI = 480 µL/48 mL lysis buffer | |
| Phenylmethanesulphonyl fluoride (PMSF) from Sigma<br>1/100 PMSF = 480 µL/48 mL buffer | Sigma **Ref no.** PMSF 93482/ 50 mL |
| 5 mM DTT → 109.44 µL/48 mL from Sigma | |

### 3.2.5 Protein assay

The Coomassie dye in assay reagent is a protein analysis tool utilised to ascertain the concentration of total protein. When the Coomassie dye in the Bradford reagent binds to protein in the sample, the absorption shifts instantly, and the solution's colour changes from red to blue. The amount of protein in a solution is ascertained by measuring the intensity of the ensuing blue colour using spectrophotometry. The Coomassie Blue Bradford Assay was performed to determine total protein concentration. The protein concentration was obtained from a standard

curve which was prepared using 100-400 mg/mL Bovine Serum Albumin (BSA) diluted in lysis buffer. After adding Coomassie Blue reagent to all standard and test samples, the absorbance was measured at a wavelength of 595 nm, using a Jenway™ Model 7315 UV/Visible Single Beam Spectrophotometer (Fisher Scientific, Leicestershire, UK). The calculation for the unknown protein concentration was calculated by comparing the absorbance values with the standard curve (Table 3.5 and Figure 3.2). The lysates were stored at -80°C until needed for Western blotting with Rabbit anti-APP C-terminal (cat no A8717) antibody and rabbit anti-APP N-terminal (cat no A8967) both from Sigma Aldrich (UK), and mouse anti-Aβ (clone 6e10) antibodies.

**Table 3.5: Protein assay data**

| BSA Standards and SHSY5Y Cell Lysates | Absorption 1 | Absorption 2 | Absorption 3 | Average Absorption |
|---|---|---|---|---|
| 100 µg/mL | 0.300 | 0.295 | 0.296 | 0.297 |
| 200 µg/mL | 0.340 | 0.339 | 0.340 | 0.339 |
| 300 µg/mL | 0.420 | 0.422 | 0.421 | 0.421 |
| 400 µg/mL | 0.561 | 0.560 | 0.562 | 0.561 |

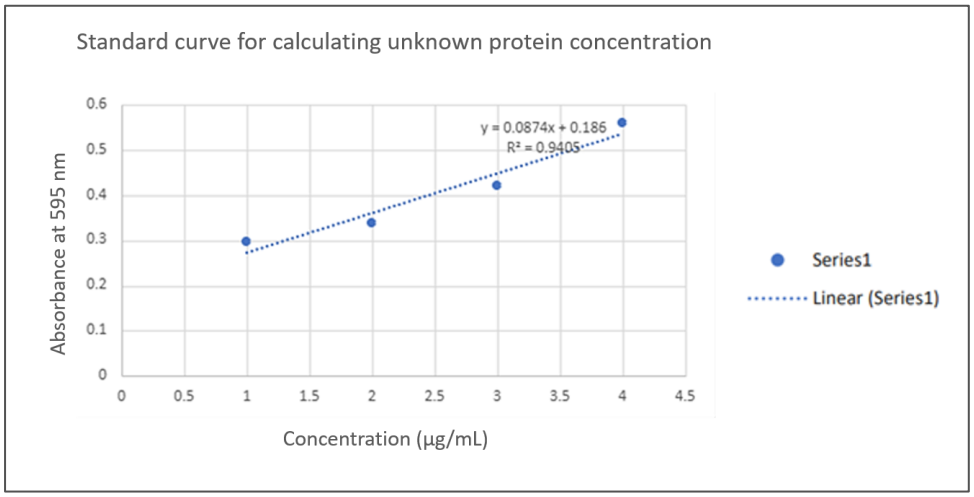


**Figure 3.2: Graph of protein assay data**

Protein assay data to determine the concentration of the unknown protein based on known protein concentrations plotted against their absorbance readings.

### 3.2.6 Western blot of cell lysates

This work was carried out by Dr Sim Singhrao with assistance from Shalini Kanagasingam, at the University of Central Lancashire. Similar methodological protocols were employed in UCLan student projects which were supervised by Dr Sim Singhrao and the author of this thesis (JL Fernandes Inacio, MSc dissertation and Zaid Patel, BSc research project).

Precast 12% SDS-PAGE gels, purchased from BIO-RAD (Mini-protean, Precast gels) were attached to the cell and the assembly was placed into the tank containing 1x electrophoresis buffer diluted from stock (10x buffer containing 144g glycine, 30g Tris base, 10g SDS /L distilled water, pH 8.3). Lysates from the SH-SY5Y cell line, with *P. gingivalis* virulence factors, cytokines, and a combination of *P. gingivalis* virulence factors with cytokines, were separated by SDS-PAGE on precast 12% mini-protean TGX stain-free linear gels. The protein ladder (Pageruler Plus, Lot.00498336 from Thermo Fisher, Massachusetts, USA) was loaded in the first well of each gel. The prestained Protein Ladder was a mixture of nine blue-, orange-, and green-stained proteins (10-250 kDa). The protein ladder is supplied in a ready-to-use format for direct loading onto gels; no need to heat, reduce, or add sample buffer prior to use. This was followed by the addition of test samples (10 µg) of total protein in Laemmli reducing sample buffer (0.3% mercaptoethanol). The experimental samples were heated at 95°C for 5 minutes using a heat block. The standard volume of 20 µL were delivered into each well per gel. Subsequently, electrophoresis was carried out at 100 V until the dye front (0.01% bromophenol blue in the Laemmli buffer) was observed approximately 1 cm from the bottom of the gel. The next stage involved the use of membranes (Immobilon-P, Merck Millipore, UK), which were cut according to the gel size. They were washed in methanol for 60 seconds, followed by immersion in 1x transfer buffer (from stock = 10x transfer buffer containing 144g glycine, 30g Tris base, 1L distilled water, pH 8.3) containing 10% methanol to equilibrate. The

arrangement of a “sandwich” layer in a specific order inside the plastic cassette was carried out as described. A sponge was placed on the clear side of the cassette, together with a filter paper, PVDF membrane, the gel, filter paper, and lastly the sponge layer (all moistened using 1x transfer buffer). Subsequently, the cassettes were closed and placed in the tank, which was filled with 1x transfer buffer containing 10% methanol to the appropriate level and connected to the electrodes. The setting for the power pack was at 180 mA for 2 hours, this allowed the transfer of the proteins from the gel (cathode +) to the membrane (Anode -). Following successful electro-transfer of proteins to the PVDF membrane, the non-specific antibody binding was quenched in 5% w/v skimmed milk/PBS for 30 minutes at room temperature, while shaking. Subsequently, the membranes were incubated overnight at 4°C (cold room) in goat anti-rabbit horseradish peroxidase (HRP) conjugated IgG diluted (refer table 3.6) in 5% w/v skimmed milk/PBS. The following day, the membranes were washed (3 x15 minutes) in PBS containing 0.25% tween 20, which were then incubated in the detection antibody diluted in 5% w/v skimmed milk/PBS for 2 hours, at room temperature. Upon completion of the incubation stage, the membranes were thoroughly washed (3 x 15 minutes) in PBS containing 0.25% tween 20. After that, the enhanced super signal west Pico Plus® chemiluminescent substrate reagent (Thermo Scientific, Massachusetts, USA), were used as per manufacturer’s instructions to allow detection of positive bands. The ChemicDoc® (Bio-Rad, UK) was used to visualise specific signal from the protein on the membranes. All relevant images were captured using Image Lab® Software Version 6.0.1.

The membranes were incubated overnight in rabbit anti-APP C-terminal (cat no A8717) antibody diluted 1:4000 and rabbit anti-APP N-terminal (cat no A8967) diluted 1:1000, and mouse anti-Aβ (clone 6e10) was diluted 1:1000 in PBS/5% milk on a rotary device at 4°C. After 24 hours, the membranes were washed in PBS tween 0.01 % (3x15 minutes), carried out

on the Rotamix. They were then washed again in PBS/5% milk for 30 minutes, and the secondary antibody (anti rabbit peroxidase conjugated diluted 1:10,000 in PBS/5% milk (Sigma Aldrich) for 1 hour at room temperature on the Rotamix. A further wash with PBS tween (3x15 minutes) was carried out. Chemiluminescent substrate (SuperSignal®) West Pico was prepared and applied to the membranes according to manufacturer's instructions. Specific protein signal from the membranes was visualized using a ChemiDoc® (Bio-Rad, UK) and images captured with Image Lab® Software Version 3.0.1. The membrane was stained with India ink to determine the amount of protein transferred onto the membrane(s) as a loading control. Densitometry was carried out on the bands (in triplicate blots) using the Image J software, and the resulting data was normalised to the loading control.

**Table 3.6: Antibodies used in the experimental work, including their sources and relevant working dilutions**

| Antibody | Source | Working dilution |
|---|---|---|
| Rabbit anti-APP C-terminal (cat no A8717) | Sigma Aldrich, Dorset, UK | 1:5000 |
| Rabbit anti-APP N-terminal (cat no A8967) | Sigma Aldrich, Dorset, UK | 1:4000 |
| Mouse anti-Aβ (clone 6e10) | BioLegend, London, UK | 1:5000 |
| Secondary antibody HRP conjugated IgG goat anti-rabbit | Abcam, Cambridge, UK | 1:10,000 |
| Secondary antibody HRP conjugated anti-mouse | Abcam, Cambridge, UK | 1:5000 |

### 3.2.7 Transmission Electron Microscopy (TEM) detection of Aβ fibrils

This aspect of the laboratory investigation was outsourced to Dr Christopher Von Ruhland, Central Biotechnology Services, Cardiff University. The TEM techniques have been described in detail in Chapter 2. Only the appropriate collected test supernatants were supplied. The

contribution was appropriately acknowledged by including the researcher as a co-author. Briefly, the negative staining involved all the supernatants being dispensed as 50 µL droplets onto Nescofilm (Bando Chemical Industries Ltd. Kobe, Japan) in a humidified chamber. Formvar/carbon coated nickel grids (400 mesh) were floated, film side down, on droplets of each supernatant for 20 minutes, transferred to 1% glutaraldehyde in PBS for 10 minutes, and washed by placing on droplets of PBS (3 x 1 minute) and reverse osmosis-purified water for 6 x 1 minute. Grids were then transferred to 2% uranium acetate for 10 minutes, lifted off with fine forceps, excess stain solution was drained with Whatman 50 filter paper and grids allowed to air dry before examination in a Philips CM12 TEM (FEI UK Ltd) at 80 kV. Images were captured with a Megaview III camera and AnalySIS software (Soft Imaging System GmbH, Germany). Aβ fibrils, prepared from a commercial peptide $A\beta_{1-42}$ (Severn Biotech, Worcestershire, UK) that was reconstituted to 1mg/mL in Ringer's buffer acted as a positive control (Kanagasingam et al., 2022; Singhrao et al., 2024).

### 3.2.8 Statistical analysis

The data was evaluated using the Statistical Package for the Social Sciences (SPSS). The data was determined to be non-parametric, and the Mann-Whitney U test was used to analyse the differences between various combinations of the two independent groups including: SH-SY5Y untreated (TSB) versus Pg381; TNF-α versus Pg381+TNF-α; IL-1β versus Pg381+IL-1β; and IL-6) versus Pg381+IL-6 treated groups. The detected levels of $A\beta_{1-40/42}$ were analysed statistically for each of the abovementioned groups as well as the relative $A\beta_{1-40/42}$ levels across all test conditions as compared to the TSB control. A statistical probability (p value) of less than or equal to $\leq 0.05$ was considered significant.

## 3.3 RESULTS

Western blotting was carried out to investigate whether pro-inflammatory cytokines, alone or in combination with P. *gingivalis* virulence factors contributed to APP processing in a human neuroblastoma cell line expressing APP processing. SH-SY5Y cells were treated with pro-inflammatory cytokines (IL-1β, IL-6 and TNF-α) in the presence and absence of *P. gingivalis* virulence factors (Pg381) for 48 hours, and then cell lysates were collected and subjected to western blotting to determine the expression of APP C-terminal and APP N-terminal. The results were reported in Kanagasingam et al. (2022).

### 3.3.1 Western blot: Rabbit anti-APP C-terminal antibody

After immunoblotting of the SH-SY5Y cell lysates, several high molecular bands in the region of 100-80 kDa corresponding to APP695, APP751 and APP770 (not quantified) were observed (Figure 3.3) in lanes; TSB (control), *P. gingivalis* only (Pg381), IL-6 only (IL-6), combination of *P. gingivalis,* Pg381 with IL-1β (Pg381+ IL-1β), and the combination of *P. gingivalis*, Pg381 with TNF-α (Pg381 + TNF-α). The low molecular bands corresponding to the APP C99 dimerised fragment were observed in the *P. gingivalis*, Pg381 only and IL-6 only treated SH-SY5Y groups. It was noted that significantly more intense bands (indicating a higher concentration of the proteins) coincided with the *P. gingivalis* in combination with cytokine groups i.e. Pg381+IL-1β and Pg381+TNF-α. The band corresponding to the APP C83 fragment was observed in groups with cells treated with TNF-α alone as well as in groups combining *P. gingivalis* with each cytokine, which included Pg381+IL-1β, Pg381+IL-6 and Pg381+TNF-α. Although the C83 band appeared less bright band, signifying a lower concentration of the C83 dimer fragments.

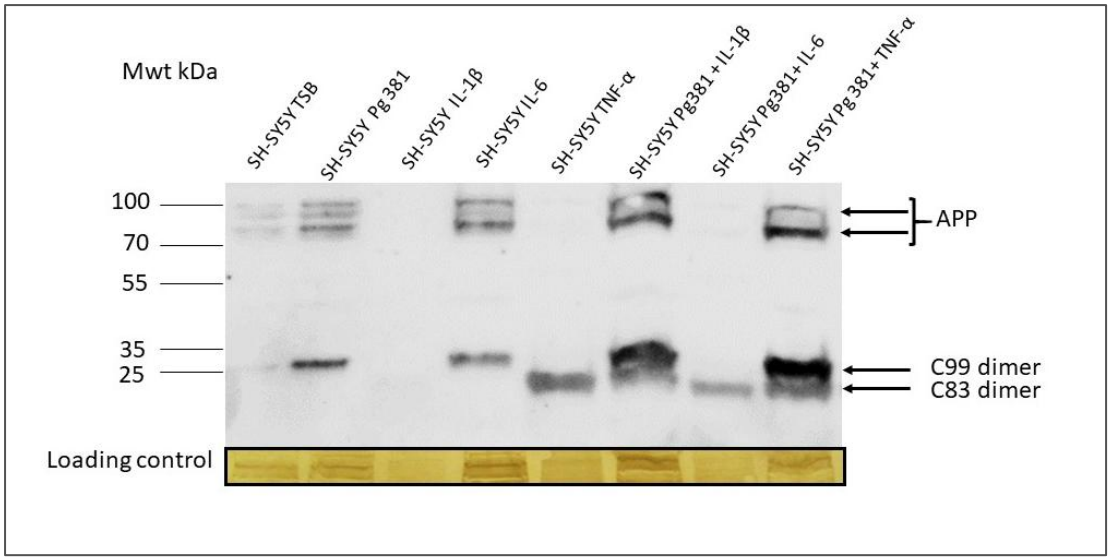


**Figure 3.3: Immunoblot of the cell lysate with Rabbit anti-APP C-terminal antibody.**

The signal density of the bands of around the 100 kDa molecular weight size corresponded to APP in lanes with the SH-SY5Y with TSB as well as combinations of *P. gingivalis* conditioned medium only and with various cytokines; the Pg381 group, IL-6 group, Pg381+IL-1β group and Pg381+ TNF-α group. The low molecular bands corresponded to the APP C99 fragment in the Pg381 treated group, IL-6 which were of lower relatively lower density compared to significantly more intense bands with SH-SY5Y groups treated with *P. gingivalis* and cytokines; Pg381+IL-1β and Pg381+TNF-α. The APP C83 dimer band were less intense compared to C99, corresponding to the lanes with SH-SY5Y cells treated with TNF-α only and in combination with P. gingivalis and cytokines; Pg381+IL-1β, Pg381+IL-6 and Pg381+TNF-α (Kanagasingam et al., 2022).

### 3.3.2 C99 bands densitometry analysis

Statistical analysis revealed that the visualised C99 dimer band intensity (Figure 3.4), were highly significant across the groups; TSB versus Pg381 ($p=0.0001$); TNF-α only versus the combination of Pg381+TNF-α ($p=0.00003$); IL-1β only vs Pg381+IL-1β ($p=0.0000001$); and IL-6 only versus Pg381+IL-6 ($p=0.00003$). Among the treatment groups, the highest differences were seen with the detection of C99 dimer in the Pg382+TNF-α (more than 2.3-fold) and Pg381+IL-1β (more than1.6-fold), compared to the respective cytokines alone.

### 3.3.3 C83 bands densitometry analysis

Statistical analysis showed that the signal intensity for the APP C83 fragment (Figure 3.5), were not significant across the following groups; TSB versus Pg381 (p=0.3); TNF-α only versus the combination of P. gingivalis and TNF- α, Pg381+TNF-α (p=0.2). The differences between the groups were deemed to be highly significant for the following groups; IL-1β versus Pg381+IL-1β (p=0.003); IL-6 versus Pg381+IL-6 (p=0.00002). The C83 dimer detection showed a consistent trend across the treatment groups, showing consistently higher values of densitometry in all combinations of Pg381+TNF-α, Pg381+IL-1β and Pg381+IL-6.

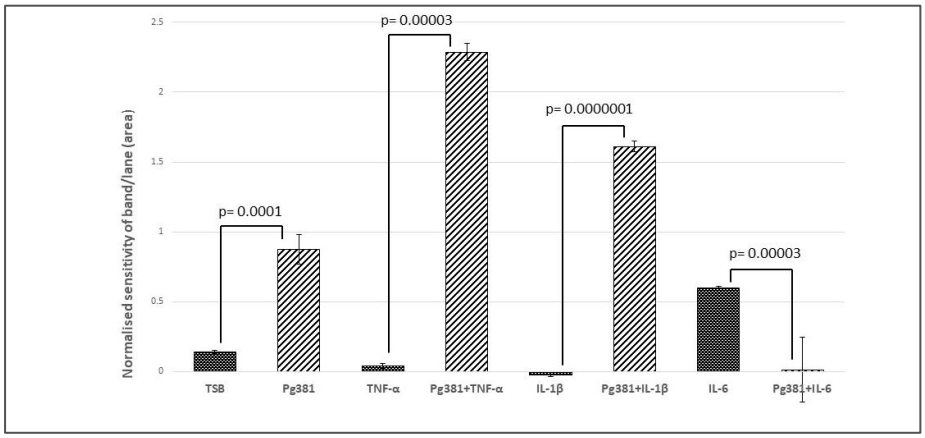


**Figure 3.4: Densitometric analysis of the cell lysate immunoblotted with anti-APP C-terminal antibody C99.** Statistical analysis of the results for the C99 bands revealed p values were highly significant across (TSB) versus Pg381 (p=0.0001); TNF-α versus Pg381+TNF-α (p=0.00003); IL-1β versus Pg381+IL-1β (p=0.0000001); and IL-6 vs Pg381+IL-6 (p=0.00003). All error bars represent standard error of mean. Among the treatment groups, the highest differences were seen with the detection of C99 dimer in the Pg382+TNF-α (more than 2.3-fold) and Pg381+IL-1β (more than1.6-fold), compared to the respective cytokines alone. It was noted the margin of error was very high for the group treated with Pg381+IL-6 (Kanagasingam et al., 2022).

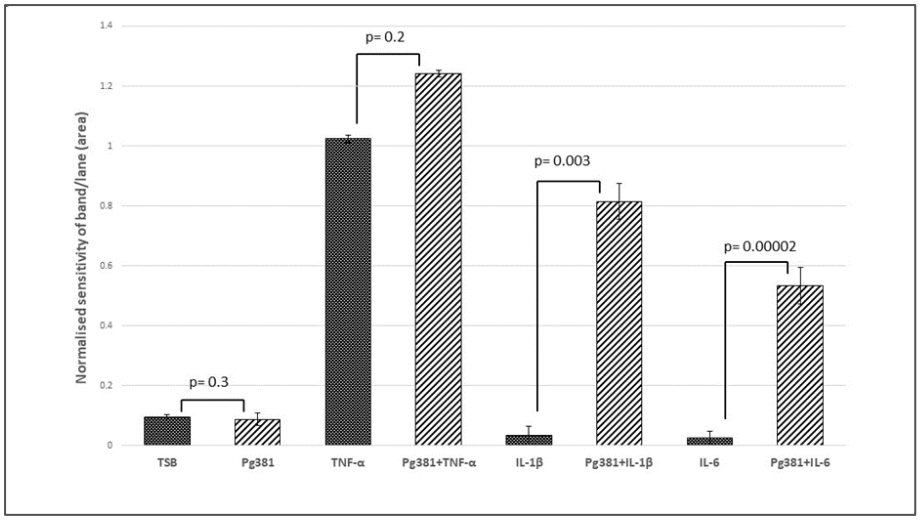


**Figure 3.5: Densitometrical analysis of the cell lysate immunoblotted with anti-APP C-terminal antibody C83.** Statistical analysis of the results for the APP C83 fragment showed that p values were not significant across (TSB) versus Pg381 (p=0.3); TNF-α versus Pg381+TNF-α (p=0.2); but were statistically significant for IL-1β versus Pg381+IL-1β (p=0.003); and statistically significant for IL-6 vs Pg381+IL-6 (p=0.00002). The C83 dimer detection showed a consistent trend across the treatment groups, showing consistently higher values of densitometry in all combinations of Pg381+TNF-α, Pg381+IL-1β and Pg381+IL-6 (Kanagasingam et al., 2022).

### 3.3.4 Western blot: Rabbit anti-APP N-terminal antibody

The full APP bands at the 1:4000 dilution were detected along with other non-specific bands.

The cell lysates immunoblotted with the anti-APP N-terminal antibody (Figure 3.6) demonstrated some weak bands of the full-length APP and these were not quantified. There were more prominent bands, which appear to be the C99 dimerised fragment in the groups treated with Pg381 only, IL-6 only as well as combinations of Pg381+IL-1β and Pg381+TNF-α treated groups. The bands for the Pg381, IL-6 and Pg381+TNF-α treated groups appear to have a higher intensity compared to the weaker, less intense band seen with the Pg381+IL-1β treated group.

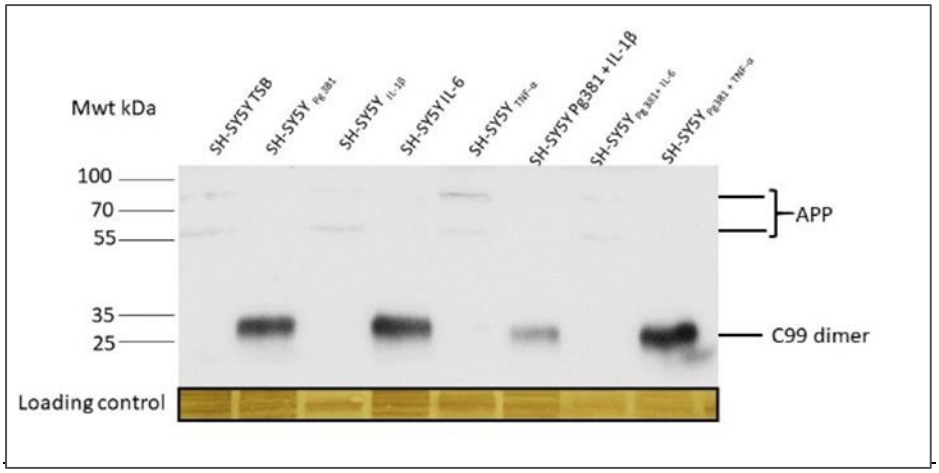


**Figure 3.6: Immunoblot of the cell lysate with Rabbit anti-APP N-terminal antibody**

SH-SY5Y cell lysate immunoblotted with anti-APP N-terminal antibody showed distinct bands around 25 kDa, which corresponded to APP C99 dimer in lanes prefixed SH-SY5Y followed by treatment identity. The cell lysates which were immunoblotted with the anti-APP N-terminal antibody exhibited intense bands coinciding with the C99 fragment in lanes of the SH-SY5Y groups treated with only *P. gingivalis*, Pg381, IL-6 alone and the combinations of P. gingivalis and cytokines; Pg381+IL-1β and Pg381+TNF-α. The band associated with the Pg381+IL-1β treated group was observed to be weaker and less intense (Kanagasingam et al., 2022).

### 3.3.5 C99 bands densitometry analysis

Analysis of the results for the C99 dimerised protein bands (Figure 3.7) demonstrated statistically significant differences across the treated groups compared; TSB versus Pg381 ($p=0.00003$); TNF-α versus Pg381+TNF-α ($p=0.00003$); IL-1β versus Pg381+IL-1β ($p=0.0002$). Although SH-SY5Y cells treated with IL-6 was found to have a highly significant difference compared to the Pg381+IL-6 treated group ($p=0.000001$), a large error margin was noted in the Pg381+IL-6 treated group. A highly significant difference was also observed amongst in the Pg381+TNF-α which showed the highest detection of C99 dimer (more than 13-fold) compared to TNF-α alone.

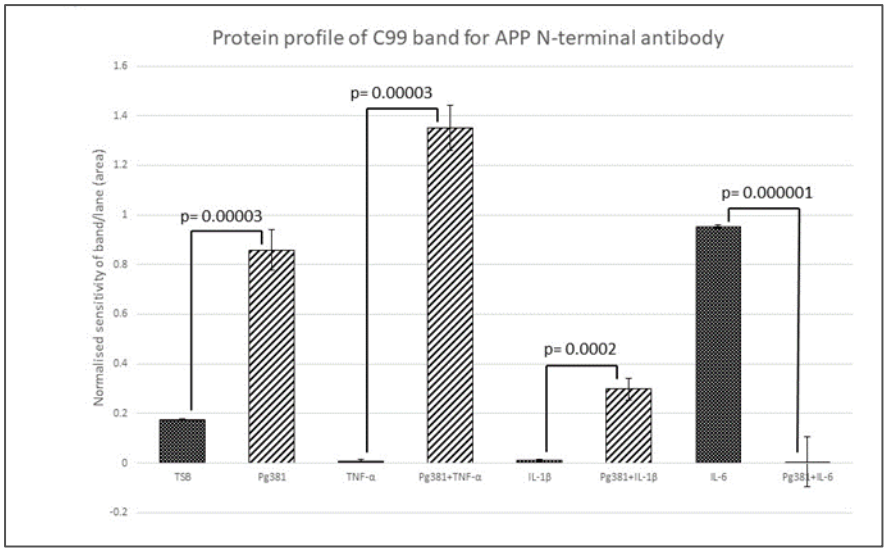


**Figure 3.7: Densitometric analysis of the cell lysate immunoblotted with anti-APP N-terminal antibody C**

Statistically, the results for the C99 bands, are highly significant across the groups treated; TSB versus Pg381 (p=0.00003); TNF-α versus Pg381+TNF-α (p=0.00003); IL-1β vs Pg381+IL-1β (p=0.0002). The groups treated with only IL-6 showed a highly statistically significant difference when compared to Pg381+IL-6 (p=0.000001), however the Pg381+IL-6 group had a very large margin of error. The most significant result amongst the treatment groups was noted with the Pg381+TNF-α treatment which showed the highest detection of C99 dimer (more than 13-fold) compared to TNF-α alone. Error bars represent standard error of mean (Kanagasingam et al., 2022).

### 3.3.6 Western blot: Mouse anti-Aβ (clone 6e10) antibody

The anti-Aβ antibody apart from detecting the high molecular weight APP, it also detected the C99 and C83 bands (not quantified) and above all detected the $A\beta_{1\text{-}40/42}$ bands as compared with the positive control reconstituted $A\beta_{1\text{-}42}$ peptide (Figure 3.6). The $A\beta_{1\text{-}40/42}$ bands were determined to be statistically significant when the detected quantities of $A\beta_{1\text{-}40/42}$ were pooled across all experimental groups and compared to the untreated SH-SY5Y cells with TSB group. This allowed comparison of both Aβ isoforms.

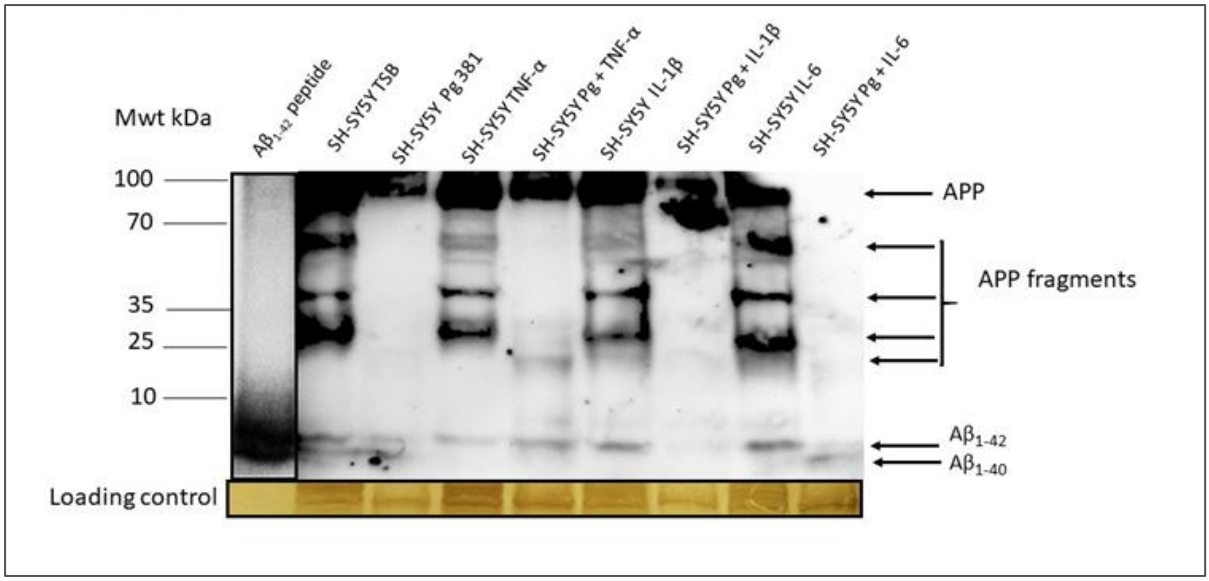


**Figure 3.8: Immunoblot of the cell lysate with mouse anti-Aβ antibody**

Western blot image from and related densitometric analysis of $A\beta_{1\text{-}40/42}$ bands and when data was pooled for the relative abundance of Aβ isoforms to facilitate densitometry analyses. The anti-Aβ antibody detected full APP, its associated cleavage fragments with variable lengths as well as detection of $A\beta_{1\text{-}40/42}$ (Kanagasingam et al., 2022).

### 3.3.7 $A\beta_{1\text{-}40}$ densitometry analysis

Statistical analysis of the results for the $A\beta_{1\text{-}40}$ band (Figure 3.7), were confirmed to be statistically significantly different across the comparison groups of TSB versus Pg381 ($p=0.013$) as well as the cytokines on their own compared to treated with *P. gingivalis*; TNF-α versus Pg381+TNF-α ($p=0.0007$). The SH-SY5Y cells treated with IL-1β produced a significantly higher quantity versus Pg381+IL-1β ($p=0.0006$); and IL-6 versus Pg381+IL-6 ($p=0.006$). Amongst the combined treatment groups, only the combinations of Pg381+TNF-α and Pg381+IL-6 showed an increase in detection of $A\beta_{1\text{-}40}$.

### 3.3.8 $A\beta_{1-42}$ densitometry analysis

The densitometric analysis for the $A\beta_{1-42}$ band (Figure 3.8), were highly significant across control (TSB), which was statistically higher than the *P. gingivalis*, Pg381 conditioned medium treated group (p=0.0006). Among all the treatment groups, the highest density of Aβ1-42 was noted with TSB. When analysing the cytokines alone compared to the combination of cytokines with *P. gingivalis* conditioned medium groups, only the TNF-α group showed a statistically significant increase in $A\beta_{1-42}$ when combined with *P. gingivalis*. (p=0.0001). SH-SY5Y cells treated with IL-1β alone and IL-6 alone stimulated significantly more Aβ1-42 compared to the combinations of Pg381+IL-6 and Pg381+IL-1β, p=0.03 and p=0.001, respectively.

### 3.3.9 $A\beta_{1-40/42}$ relative abundance densitometry analysis

Statistical evaluation of the relative abundance of both species $A\beta_{1-40/42}$ showed a significantly higher quantity of both Aβ isoforms across the 'all treatment' groups which combined the effects of *P. gingivalis* conditioned medium and various cytokines for $A\beta_{1-40}$ (p=0.0007) and for $A\beta_{1-42}$ (p=0.00008) (Figure 3.9). The ratio of the pooled $A\beta_{1-40/42}$ from the densitometry values from intracellular stores was around 1:2 for both isoforms. The Aβ1-40 was detected almost 2-fold more in the treatment groups compared to the TSB control, whereas Aβ1-42 had a 2.4-fold increase in the treatment groups.

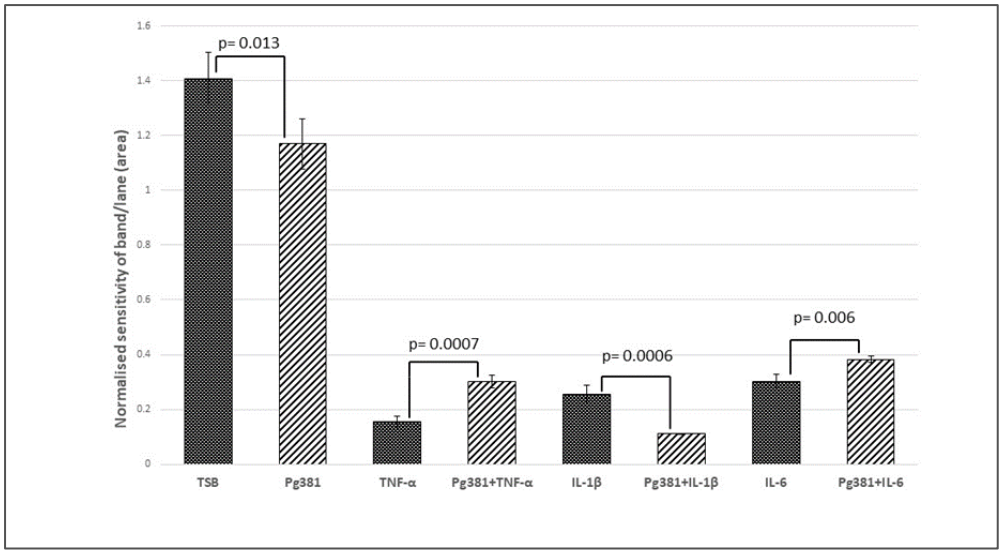


**Figure 3.9: $A\beta_{1-40}$ densitometry.**

The densitometric results for the $A\beta_{1-40}$ band, were significant across TSB versus Pg381 (p=0.013) as well as across all groups treated with only cytokines compared to cytokines in combination with *P. gingivalis*; TNF-α vs Pg381+TNF-α (p=0.0007), IL-1β instigated a significantly higher quantity of Aβ1-40 compared to Pg381+IL-1β (p=0.0006); and IL-6 was significant versus Pg381+IL-6 (p=0.006). Among the *P. gingivalis* treated groups, the combinations of Pg381+TNF-α and Pg381+IL-6 showed a significant increase in detection of $A\beta_{1-40}$. All error bars represent standard error of mean (Kanagasingam et al., 2022).

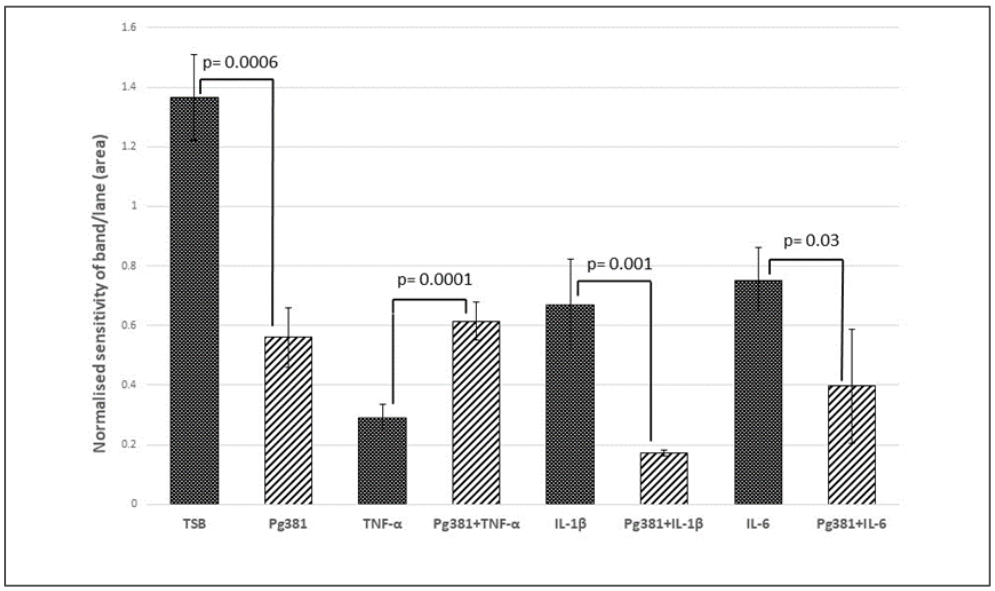


**Figure 3.10: $A\beta_{1-42}$ densitometry.**

The results for densitometric analysis for $A\beta_{1-42}$ bands, were found to be statistically significant across all compared groups; control TSB versus Pg381 (p=0.0006); TNF-α versus Pg381+TNF-α (p=0.0001), IL-1β versus Pg381+ IL-1β (p=0.001) and IL-6 versus Pg381+IL-6 (p=0.03). All the combinations of

Pg381+IL-1β and Pg381+IL-6 showed a significantly reduced quantity of stimulated $A\beta_{1-42}$. In the treatment groups, the detection of Aβ1-42 was detected in abundance in the Pg381 + TNF-α compared to TNF-α alone. All error bars represent standard error of mean (Kanagasingam et al., 2022).

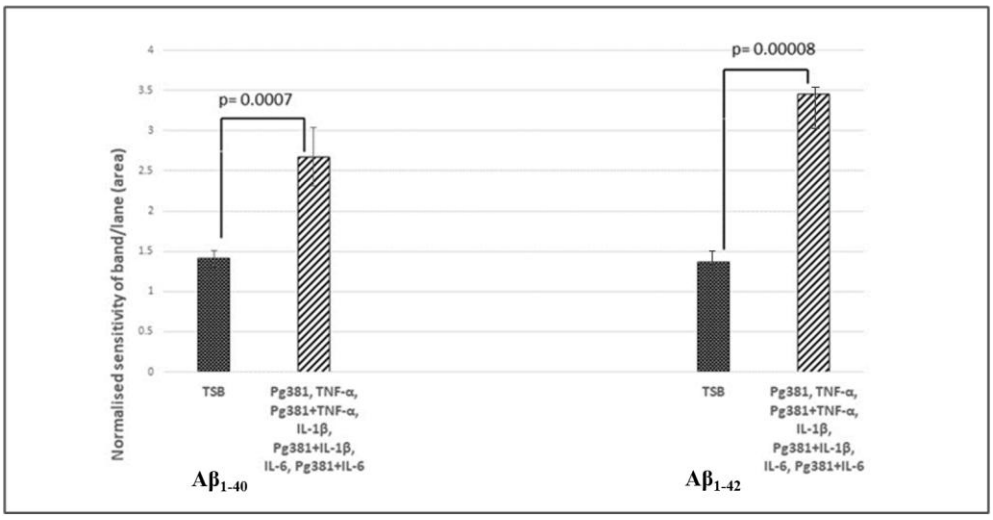


**Figure 3.11: $A\beta_{1-40/42}$ relative abundance densitometry.**

The relative abundance of both isoforms $A\beta_{1-40/42}$ were statistically evaluated, for SH-SY5Y treated control group (TSB) compared to the combination of all treatment groups including *P. gingivalis* and various cytokines. A statistically significant difference was noted whereby 'all treatment' groups stimulated a higher density of both $A\beta_{1-40}$ (p=0.0007) as well as $A\beta_{1-42}$ T(p=0.00008) compared to the TSB groups. The $A\beta_{1-40}$ was detected almost 2-fold more in the treatment groups compared to the TSB control, whereas $A\beta_{1-42}$ had a 2.4-fold increase in the treatment groups. All error bars represent standard error of mean (Kanagasingam et al., 2022).

### 3.3.10 TEM detection of Aβ fibril formation in supernatants

These results were provided by Dr Christopher Von Ruhland (Central Biotechnology Services, Cardiff University). Test supernatants were collected from the treatment of cells with *P. gingivalis* FDC381 conditioned medium, with and without cytokines exhibited the presence of fibrils. Insoluble fibrils were consistently visualised when the supernatant from SH-SY5Y cells were treated with *P. gingivalis* FDC381 virulence factors (Figure 3.10 a, boxed area, shown in b, black arrows). These fibrils appeared very similar to Aβ fibrils by using the $A\beta_{1-42}$ peptide

included as a positive control reference standard (Figure 3.10c). The microtubule fragments from collected test supernatants were labelled 'MT' (Figure 3.10a).

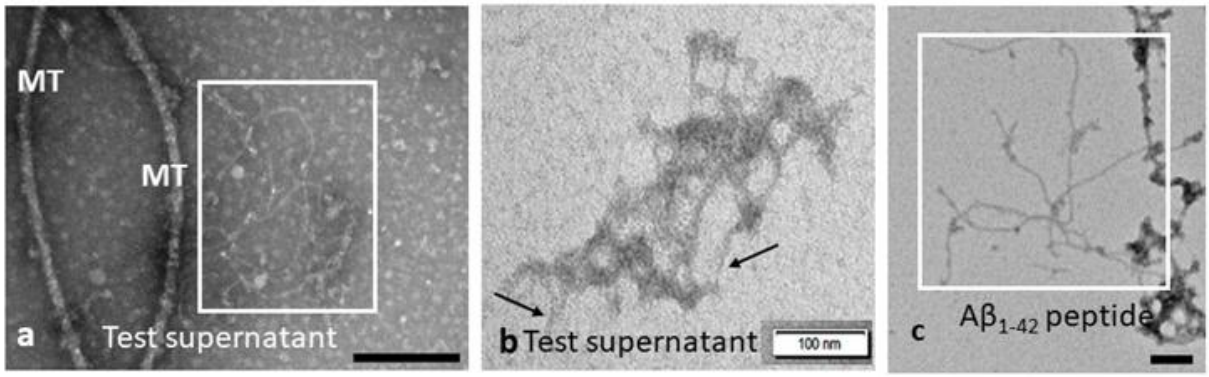


**Figure 3.12: TEM ultrastructural morphological analysis of the supernatant from SH-SY5Y**

TEM ultrastructural morphological examination appeared to confirm the presence of insoluble Aβ in the supernatant from SH-SY5Y treated with *P. gingivalis* crude conditioned medium (3.10a, white rectangle, magnified and shown in b, black arrows). The Aβ fibrils were observed consistently and appeared similar to the positive control for Aβ fibrils, utilising a commercial peptide $A\beta_{1-42}$ as seen in Figure 3.10c (boxed area) as examined under TEM. Microtubule fragments (labelled 'MT') were also visualised. Micron bars represent 100 nm size (Kanagasingam et al., 2022).

## 3.4 DISCUSSION

*In vivo* experimental models have suggested LPS from oral, Gram negative bacteria does have a role in chronic local inflammation (DiCarlo et al., 2001); Aβ release (Sheng et al., 2003; Wu et al., 2017); declining cognition (Wu et al., 2017) and tau protein cleavage from its bound state on microtubules and phosphorylation (Lee et al., 2010; Ilievski et al., 2018; Dominy et al., 2019; Haditch et al., 2020; Kanagasingam et al., 2020). The present study aimed to understand how the virulence factors from *P. gingivalis* may contribute to the amyloidogenic processing of APP and Aβ release, as periodontitis is prevalent in individuals with poor oral hygiene and high dental plaque index, which represents a risk factor for developing AD later in life

(Armitage et al., 1982; Poole et al., 2013). The virulence factors of *P. gingivalis* and its functions are presented in Table 3.7. Researchers have reported that *P. gingivalis* DNA or its virulence factors, including lipopolysaccharide (LPS) and gingipains, have been detected in AD patients' brain tissues and has been closely associated with AD pathological changes (Poole et al., 2013; Dominy et al., 2019). It has been surmised that these virulence factors can reach the brain via the circulatory system, during episodes of transient bacteraemia associated with periodontal disease. Although the blood-brain barrier (BBB) is a structural and functional barrier with low permeability to prevent the ingress of toxic substances, it can be compromised because of the virulence factors in increasing permeability (Sweeney et al., 2018; Kanagasingam et al., 2020).

**Table 3.7: *P. gingivalis* virulence factors and its function**

| Virulence factors | Function |
|---|---|
| Fimbriae | Fimbriae are considered the main virulence factor. It helps the bacteria with adhesion to oral surfaces, promote biofilm, bacterial motility, invasion of host cells and co-aggregation with other bacteria e.g. *Streptococci* and *Actinomyces* species. Fimbriae can also trigger the production of pro-inflammatory cytokines e.g. IL-1, IL-6, TNF- $\alpha$ (Lin *et al.* 2006, Jia *et al.* 2019, Hasegawa *et al.* 2021). |
| Hemolysin and Hemaglutinin | These are pore forming toxins which cause lysis of red blood cells to supply heme (Smalley *et al.* 2017) |
| Capsule | The encapsulated *P. gingivalis* helps the bacteria to evade the immune system, survive in host cells and avoid phagocytosis (How *et al.* 2016). |
| Outer membrane vesicles | OMVs play a role in host cell invasion, decrease macrophage responsiveness to LPS, induces production of IL-8, causes cell detachment and contributes to antibiotic resistance (Zhang et al. 2021) |
| Lipopolysaccharides (LPS) | LPS triggers pro-inflammatory factors such as TNF-α, IL-1βand IL-6, which leads to platelet proliferation and thrombosis (Poole et al. 2013, Xu *et al.* 2020) |
| Gingipains | Gingipains accounts for 85% of bacterial proteolytic activity, breaking down host proteins and tissues. Italso triggers adhesion and initiates protease-activated receptors which leads to platelet aggregation (Li & Collyer 2011) |

Blasko et al. (2000) used a human astrocyte cell line as well as primary astrocytes isolated from postmortem brains tissues or healthy and AD patients. Upon exposure to cytokines (IFNγ, TNFα, IL-6, IL-1β and TGF-β1), immunoblotting was carried out with antibodies to detect APP and Aβ. The researchers reported that astrocytes, which play an important role in maintaining and supporting the function of neurons, were a source of Aβ in the presence of certain combinations of inflammatory cytokines (i.e. IFNγ in combination with TNFα or IL-1β). Interestingly, Aβ was not detected following exposure to TNF-α , IL-6, IL-1β and TGF-β1 when each were used alone. In contrast, the present study utilising SH-SY5Y neuroblast-like cells, all cytokine exposure groups detected the presence of $A\beta_{1-40}$ and $A\beta_{1-42}$, however, the $A\beta_{1-40/42}$ relative abundance densitometry which included *P. gingivalis* virulence factors, showed a significant increase in the detection of both Aβ isomers compared to the TSB controls. Table 3.8 describes the effect of the cytokines used in this study, as well as its association with periodontitis and AD. The gingival crevicular fluid (GCF) of patients with periodontitis contains noticeably more IL-1β, IL-6, and TNF-α than that of healthy patients. These cytokines cause connective tissue to break down, causing bone loss by activating different cells in the periodontal tissues, such as osteoclasts, fibroblasts, and macrophages (Neurath & Kesting, 2024). The influence of cytokines on periodontitis and AD are summarised in Table 3.8.

**Table 3.8: Cytokines used in this study (IL-1β, IL-6 and TNF-α) and their potential influence on periodontitis and AD**

| Cytokine | Periodontitis | AD |
|---|---|---|
| **IL-1β** | Considered an important biomarker in periodontitis, it stimulates bone resorption by activating osteoclasts, promotes inflammation, and recruits immune cells to the site of (Relvas *et al.* 2024) | IL-1β is a key driver of neuroinflammation, overexpression is associated with β-amyloid plaque progression and tau phosphorylation neuronal apoptosis and the formation of fibrous plaques (Shaftel *et al.* 2007) |
| **IL-6** | While less studied than IL-1β and TNF-α, IL-6 is still considered a significant pro-inflammatory | Elevated plasma IL-6 levels are correlated with cognitive impairment and brain atrophy. IL-6 may reduce the |

| | | |
|---|---|---|
| | cytokine in periodontitis, involved in the recruitment of immune cells, stimulating inflammatory responses, and potentially contributing to systemic inflammation. IL-6 levels in GCF and saliva were higher in more aggressive periodontal disease (Relvas *et al.* 2024) | release and metabolism of dopamine and serotonin, which can impact brain volume and cognition. IL-6 has also been reported to contribute to Aβ and Tau deposits in AD. Dysfunction to the BBB is also has also been linked to IL-6 (Emmons *et al.*2023, Zhao *et al.* 2024) |
| **TNF-α** | Contributes to bone destruction by activating osteoclasts, indirectly triggers leukocyte recruitment and vascular permeability, and plays a role in tissue breakdown.TNF- $\alpha$ mediates macrophage induced angiogenesis which impacts periodontal granulation tissue formation. However, evidence is inconclusive as to the link between TNF- $\alpha$ and severity of disease (Varghese *et al.* 2015) | Elevated TNF-α levels were reported in biological fluids in aging, mild cognitive impairment and in AD patients. TNF-α levels were noted to be elevated in the cerebrospinal fluid of AD patients compared to healthy patients (Brosseron et al. 2014). However, a meta-analysis did not find a significant difference between the two populations of patients (Swardfager et al. 2010). |

The suitability of the SH-SY5Y cells has been discussed previously, and researchers have frequently used this cell line in both its undifferentiated and differentiated states. In their undifferentiated state, SH-SY5Y rapidly proliferate and appear to be non-polarized, with very few, short processes, as compared to differentiated cells which extend long, branched processes, decrease in proliferation, and in some cases polarize (Shipley et al., 2016). SH-SY5Y cells are frequently used in investigating Parkinson's disease and AD (Agholme et al., 2010). SH-SY5Y cells naturally express endogenous β-secretase and γ-secretase enzymes to cleave APP, resulting in the production of Aβ (Riegerová et al., 2021).

As discussed, and illustrated previously (Introduction section and Figure 1), APP processing can occur via two pathways: the non-amyloidogenic pathway and the pro-amyloidogenic

pathway. In the amyloidogenic pathway, the synthesis of Aβ begins with the cleavage at the N-terminal of the protein by β-site APP cleaving enzyme 1 (BACE1). This produces the secreted APPsβ fragment and Aβ, of which the 42-amino acid fragment ($A\beta_{1-42}$) is considered the most neurotoxic (Shen et al., 2023), refer Figure 3.11.

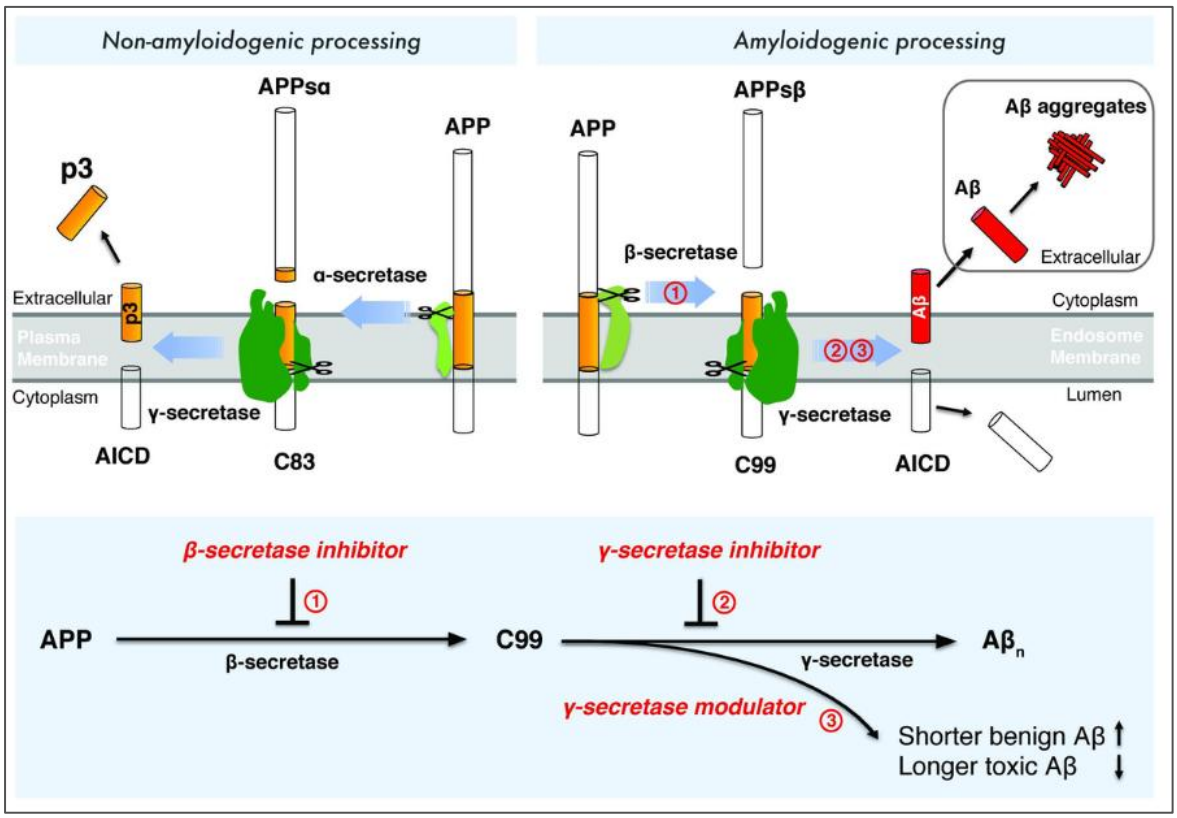


**Figure 3.13: Cleavage of APP by two proteases (β- and γ-secretases) liberate Ab from APP.**

The BACE1(β-secretase 1) **(1)** cleaves APP first to generate the N terminus of the Aβ domain, thus producing a membrane bound C-terminal fragment called C99, along with a soluble form of APP, sAPPβ. Then, γ-secretase cleaves C99 to release the mature Aβ peptide **(2)**. A third protease, α-secretase, cuts APP within the Aβ domain to produce sAPPα and C83, thus preventing Aβ formation. The γ-secretase processing produces several Aβ peptides with heterogeneous C termini ranging from 38 to 43 residues in length **(3)**. BACE1 cleavage occurs precisely at Asp+1 and Glu+11 of Aβ (Shen et al., 2023).

In this study, the putative C99 fragment was detected when the cell lines were exposed to *P. gingivalis* virulence factors, with added TNF-α and similarly with IL-1β, respectively. The C83 fragment of APP were detected when the cell lines were exposed to cytokines TNF-α, IL-1β and IL-6. The 4 and 3 kDa Aβ bands detected by immunoblotting which alluded to further cleavage of APP as confirmed by the positive control for the APP metabolites. The combination of Pg381+TNF-α and Pg381+IL-6 produced a statistically significant amount of released $A\beta_{1-40}$. The release of $A\beta_{1-42}$ appeared to be associated to the specific combination of Pg381+TNF-α treatment only. It has been suggested that the mechanism of Aβ cleavage in the wild type APP (not mutated) is mediated by cathepsin B (a lysosomal cysteine protease which breaks down protein within the cell) and gingipains, which is a cysteine protease produced by *P. gingivalis* (Kanagasingam et al., 2020).

The primary virulence factor produced by *P. gingivalis* that is associated with inducing Aβ is thought to be gingipains. The 3 types of gingipains are lysine-specific gingipain (Kgp), arginine-specific gingipain A (RgpA), and arginine-specific gingipain B (RgpB) can directly cleave APP to generate Aβ peptides due to their proteolytic activity which is similar to host proteases involved in APP processing (Lei et al., 2023). They have been implicated in Aβ production due to their proteolytic activity, which is similar to host proteases involved in APP processing. (Dominy et al., 2019).

While Dominy et al. (2019) managed to characterise the gingipain cleave sites within tau via mass spectrometry, the specific cleavage sites of the APP protein caused by gingipains has yet to be confirmed. Although, it is reasonable to expect this to be near the β and γ secretase sites for the release of $A\beta_{40/42}$. While not directly involved in Aβ formation, LPS, which is another virulence factor of *P. gingivalis*, can contribute to neuroinflammation and allow the entry of

bacterial components into the brain, thereby heightening the detrimental effects of Aβ (Sheng et al., 2003). Having said this, literature suggests that low levels of endogenous Aβ present in a healthy brain, is essential to enhance hippocampal long-term potentiation and synaptic plasticity, ultimately boosting memory function (Puzzo et al., 2011). This sheds light as to why antibody-based therapies developed to mop up Aβ in AD patients have not resulted in improved memory (Panza et al., 2019).

On the other hand, after microbial infection, insoluble Aβ fibrils have been observed, which has been linked to its antimicrobial peptide function. This means fibrillar Aβ plays a role in the host innate immunity (Ennerfelt & Lukens, 2020). In the present study, the Aβ fibre formation had a similar morphological ultrastructure appearance to those reported by Kumar et al. (2017). The significant upregulation of APP following interaction of neuronal cells with *P. gingivalis* virulence factors combined with cytokines suggests it may also involve the innate immune protein. This study results proposes that the presence of virulence factors or the live *P. gingivalis* bacterium itself can contribute to APP processing, culminating in the release of Aβ40 in combination with IL-6 and $A\beta_{42}$ release with TNF-α. Parallel to this, is the detection of *P. gingivalis* and its virulence factors in AD autopsy brains. This periodontal pathogen and its associated toxins have been identified as antigens of the host immune system, which can trigger the release of Aβ that eventually deposits as the extracellular plaques (Poole *et al.* 2013, Siddiqui *et al.* 2019).

Emerging research indicates that *P. gingivalis* possesses an extensive glycosylation system and expresses multiple glycosidases, including mannosidases and sialidases, which enable it to modify both its own surface proteins and host glycoconjugates. These enzymatic activities may contribute to nutrient acquisition, immune evasion, and enhanced virulence within periodontal

tissues. In parallel, APP is known to be heavily glycosylated in mammalian cells, with both N- and O-linked glycans influencing protein folding, intracellular trafficking, and proteolytic processing into amyloidogenic or non-amyloidogenic fragments. Alterations in APP glycosylation have been associated with increased amyloid-β generation and Alzheimer's disease (AD) pathology (Rangarajan et al., 2013, Schedin-Weiss et al., 2014). Theoretically, *P. gingivalis*-derived glycosidases could influence host glycoprotein by directly or indirectly modifying glycan structures, raising the possibility that bacterial exposure may disturb APP processing and contribute to downstream neurodegenerative mechanisms. OMVs carry gingipains and glycosidases across the blood brain barrier, whilst suppressing and redirecting host immune responses patient (Zhang et al., 2021). However, despite biological plausibility and growing interest in periodontal-neurodegenerative interactions, there is currently no direct experimental evidence demonstrating that *P. gingivalis* glycosidases modify APP glycosylation *in vivo* or *in vitro*. Further mechanistic studies are required to determine causality, substrate specificity, and disease relevance.

### 3.4.1 Challenges, strengths and limitations

As far as the researchers were aware, at the time of developing the methodology for this was the first laboratory study to investigate the effect of inflammatory mediators on amyloid processing in neuronal cells, with or without bacterial factors on undifferentiated neuroblastoma cells. The closest methodology was from Blasko et al. (2000), however, this particular laboratory study evaluated the influence of only cytokines on human neuronal cells and astrocytes. Interestingly, they subsequently carried out a similar study with the addition of cyclooxygenase inhibitor, Ibuprofen, which decreased the secretion of total Aβ (Blasko et al., 2001). The authors concluded that the immune system played a key role in AD, which was supported by retrospective clinical studies, reporting an inverse relationship between the

prevalence of AD and the use of nonsteroidal anti-inflammatory drug (NSAID) therapy (Breitner et al., 1995; Anthony et al., 2000). This reinforces the present study's focus on the AD aetiology of infection-triggered inflammation and immune involvement.

Questions arose about the virulence factors present in the *P. gingivalis* conditioned medium. This information was provided by co-researcher, Dr S. Chukapalli (University of Florida, USA), however, the present study could have been improved by determining the specific virulence factors and their quantification within the conditioned medium. Gingipains although well recognised as the major constituent virulence factor could have been detected using fluorogenic peptide substrate for fluorescence measurement assays (Park et al., 2024). LPS can be detected using molecular techniques (PCR) or immunoassays (e.g. Enzyme-linked immunosorbent assay, ELISA or SDS-PAGE). Ideally, it would have been good to modulate the gingipains in the conditioned medium to investigate their exact role in APP metabolism and Aβ production. Although, this was beyond the scope of the present study.

Normalisation is a critical step in western blot analysis to ensure that differences in band intensity accurately reflect true biological variation rather than experimental artefacts such as unequal sample loading, inconsistent transfer efficiency, or variations in membrane exposure and antibody binding. This study applied the densitometric method of normalisation, which involved quantification of the optical intensity of the target protein band using image analysis software relative to controls, thereby correcting for loading differences and allowing expression of the target protein relative to the internal reference (Aldridge et al., 2008).

We have used the SH-SY5Y in this study. This cell line is a neuroblastoma derived, non-differentiated immortalised cell line representing a mixed phenotype with predominantly

cancer cells. Therefore, the translational value of the results presented here may vary and not fully simulate the results of other fully differentiated cell types. Although undifferentiated SH-SY5Y cells have certain benefits, including ease of culture and reproducibility, experiments conducted using undifferentiated neuronal cell lines are sometimes disputed. This is due to the undifferentiated SH0-SY5Y cell lines may not accurately reflect the complexity of mature neurons and their stimuli-response mechanisms (Kulatunga et al., 2024). The SH-SY5Y cells can be easily differentiated with the addition of all-trans-retinoic acid (ATRA). ATRA induces neural maturation as well as axon and dendrite development during neuronal differentiation (Jacobs et al., 2006). Having said this, Riegerova et al. (2021) noted that in 2019, only 2% of published works used fully differentiated SH-SY5Y cells, with the majority of researchers chose to use undifferentiated cells. With hindsight, it is clear that the use of sufficiently differentiated SH-SY5Y could decrease the risk of APP mislocalisation.

### 3.4.1 Clinical relevance

It appears that neuroinflammation plays a significant part in the aetiology of AD. *P. gingivalis* may have a significant role in triggering neuroinflammation since it produces gingipains and LPS, two inflammogens that have been found in the brains of AD patients. *P. gingivalis* specifically impacts microglia, Aβ, tau, Cathepsin B, and potentially Protein Kinase R (PKR). It is likely that multiple agents engage in a complex and poorly understood vicious cycle of inflammation (Singhrao et al., 2015, Kanagasingam et al., 2020).

By studying the functions of cytokines, researchers have been able to identify them as potential therapeutic targets, leading to the development of drugs designed to specifically block the production or activity of these cytokines, potentially treating diseases associated with their dysregulation (Yi et al., 2024). One important tactic to control the generation of Aβ has been

to interfere with the amyloidogenic processing of APP. The most common targets for AD medication discovery have been β-secretase and γ-secretase, two essential enzymes that catalyse the intramembrane proteolysis of APP. Several β-secretase inhibitors and γ-secretase inhibitors/modulators have been found in the last 20 years to either diminish the generation of total Aβn or shift the formation of Aβ to shorter and more benign Aβ species by inhibiting or modulating the amyloidogenic processing of APP.

Interference with the amyloidogenic processing of APP has been a major strategy to modulate Aβ production. As two crucial enzymes catalyzing the intramembrane proteolysis of APP, β-secretase and γ-secretase have been the most prominent targets for AD drug discovery. In the past two decades, numerous β-secretase inhibitors and γ-secretase inhibitors/modulators were discovered to inhibit or modulate the amyloidogenic processing of APP, either causing the reduced production of total Aβn or shifting the production of Aβ to shorter and more benign Aβ species.

Pharmacological approaches to the clinical management of AD are still dominated by the prevalent "amyloid cascade hypothesis," whereby the aetiopathology of the disease is primarily caused by the aberrant proteolysis of Aβ precursor protein (βAPP) into neurotoxic Aβ peptides. The pharmaceutical approaches include Aβ immunization-, anti-acetylcholinesterase-, β-secretase-, chelation-, γ-secretase-, N-methyl D-aspartate (NMDA) receptor antagonist-, statin-based amongst other strategies to modulate APP processing. Outcomes of treatment have been varied and some clinical trials have failed to achieve satisfactory outcomes (Dunn et al., 2021, Zhang et al., 2023).

### 3.4.2 Future work

(i) Identification of specific virulence factors in *P. gingivalis* conditioned medium utilising molecular techniques, immunoassays, xray crytalography, purify and crystalise a structure

(ii) Use of differentiated, mature SH-SY5Y cells

(iii) Increase complexity and diversity of cells in the experimental groups by adding microglial cells, astrocytes, oligodendrocytes, and pericytes to better mimic the structural and molecular complexity of the central nervous system environment. This would produce more suitable disease models (Ormel et al., 2018; Song et al., 2019; Speicher et al., 2019).

(iv) The inclusion of relevant controls, pre-incubate with gingipains inhibitor

## 3.5 CONCLUSION

When the SH-SY5Y cell line was exposed to *P. gingivalis* virulence factors or the cytokines TNF-α and IL-1β, the APP breakdown was accelerated. *P. gingivalis* virulence factors seem to have an impact on the C99 fragment, which is further amplified when combined with cytokines (TNF-α and IL-1β). It seems that the three cytokines (TNF-α, IL-1β, and IL-6) had a significant impact on the C83 fragment. Inflammation and infection have been documented in the AD brain, despite the fact that the release of $A\beta_{40}$ and $A\beta_{42}$ may be considered a typical metabolite of the SH-SY5Y cell line. Consequently, it is reasonable to conclude that the current study demonstrates that infection and inflammation can both lead to an excessive accumulation of $A\beta_{1\text{-}40/42}$.

# CHAPTER 4

## *P. GINGIVALIS* (W83) AND *F. NUCLEATUM* (ATCC 49256) INFECTION INDUCES ALZHEIMER'S DISEASE-LIKE PATHOPHYSIOLOGY IN OBESE AND DIABETIC MICE

The work presented in this chapter is fully published by the author of this thesis:

Bahar B, **Kanagasingam S,** Tambuwala MM, Aljabali AAA, Dillon SA, Doaei S, Welbury R, Chukkapalli SS, Singhrao SK (2021) *Porphyromonas gingivalis* (W83) infection induces Alzheimer's disease like pathophysiology in obese and diabetic mice. J Alzheimers Dis. 82 (2021) 1259–1275

# *P. GINGIVALIS* (W83) AND *F. NUCLEATUM* (ATCC 49256) INFECTION INDUCES ALZHEIMER'S DISEASE-LIKE PATHOPHYSIOLOGY IN OBESE AND DIABETIC MICE

## 4.1 INTRODUCTION

Experimental procedures in Chapter 2 and Chapter 3 focussed on an *ex vivo* and *in vitro* models to investigate if Aβ was actually being produced as an antimicrobial peptide to combat the oral biofilm microbes as suggested by Kumar et al. (2016). Researchers from Harvard Medical School utilised *in vivo* mouse and worm models, observing that Aβ expression protects against both fungal and bacterial infections. The mechanism is thought to involve decreasing microbial adhesion to host cells, and subsequent agglutination and entrapment of the microbes by Aβ fibrils (Kumar et al., 2016). This led well into the present chapter which introduces an *in vivo* infected mouse model. As it would have been impossible to carry out the investigations in the human brain, the animal model is crucial for capturing key features of AD pathology such as amyloid plaques and neuroinflammation (Zhong et al., 2024).

With mounting evidence showcasing 'cross talk' between AD and obesity, diabetes and periodontitis. Combined with aging, the common comorbidities can increase the risk of developing AD involving the overlapping pathways of oxidative stress/mitochondrial dysfunction, and inflammation (Ebrahimpour et al., 2018), seen in Figure 4.1. Metabolic syndrome or MetS is a cluster of medical conditions that increase the risk of cardiovascular disease and type 2 diabetes. The key features of MetS are listed in Table 4.1. The components of MetS most strongly associated with periodontitis are dysglycemia and obesity. A

bidirectional relationship has been reported between diabetes and periodontal disease (Grossi & Genco 1998, Preshaw et al., 2012). The persistent, low-grade inflammation associated with obesity, may induce oxidative stress which can trigger tissue damage and alveolar bone resorption as seen in periodontal disease. Excess visceral fat, releases inflammatory cytokines that interfere with insulin signalling, leading to insulin resistance. A vicious cycle links the 3 conditions whereby periodontitis can exacerbate insulin resistance, and obesity may increase the severity and progression of periodontitis (Song et al., 2016).

**Table 4.1: Key features of Metabolic Syndrome, MetS, including dysglyceamia and at least 2 other factors (adapted from Lamster & Pagan, 2020; WHO 1999)**

| Required Criteria for MetS | |
|---|---|
| **Central obesity** | W/H > 0.90 (male) or W/H > 0.85 (female) and/or BMI>30 kg/m$^2$ |
| **Triglycerides, TG** | TG ≥ 150 mg/dL and/or HDLc < 35 mg/dL (male) or <39 mg/dL (female) |
| **High density lipoprotein cholesterol, HDLc** | Hypertriglyceridemia and reduced HDLc fulfil the same criteria. |
| **Hypertension** | ≥140/90 mmHg |
| **Dysglycemia** | Glucose intolerance, impaired glucose tolerance or type 2 Diabetes Mellitus and/or Insulin Resistance |
| **Other** | Microalbuminuria (urinary albumin excretion rate ≥20 µg/min, or albumin:creatinine ratio ≥30 mg/g) |

Studies have linked type-2 diabetes and obesity to periodontal disease. Impaired glycaemic regulation may be impacted can be caused by active periodontal disease, leading to type 2 diabetes. Patients living with type 2 diabetes and periodontitis typically have fewer teeth and more severe clinical attachment loss (Campus et al., 2005, Chafee &Weston, 2010). The 2 primary virulence factors of *P. gingivalis* are gingipains and LPS. Increased pro-inflammatory cytokine expression (IL-1β, IL-6, and IL-8) can be induced by LPS, which in turn contribute to insulin resistance and hyperglycaemia (Chiu et al., 2016). Systematic reviews with meta-

analyses have reported a positive correlation between obesity and an increased risk of developing periodontal disease (Chaffee &Weston, 2010; Suvna et al., 2011). Having said that, the lack of good quality longitudinal studies makes it difficult to prove causality between these two conditions.

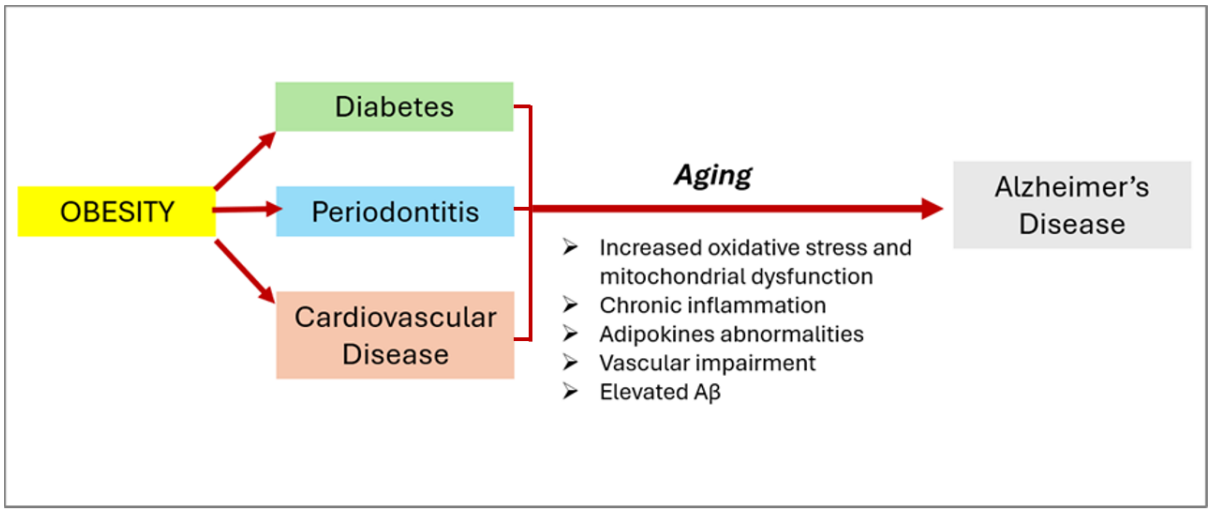


**Figure 4.1:** Common pathways of aging-associated disorders highlight the increased risk of AD by the combination of obesity, diabetes, cardiovascular disease and aging (Ebrahimpour et al., 2020).

Several mouse models have been developed for research on obesity and diabetes, including those induced by genetic mutations, dietary changes and/or selective breeding (Kleinert et al., 2018). Some of the commonly used models are included in Table 4.1. In contrast, some researchers may opt for Wild Type (WT) mice, which refer to laboratory mice that have not undergone genetic modification. They are used as a control group as they have normal genetic makeup with typical phenotype expected of the species.

The mouse model has also been used extensively in AD research, including the transgenic (Tg) mouse through over-expression of genetic mutations associated with familial AD and newer

generations utilising knock-in/knock-out or CRISPR (Clustered Regularly Interspaced Short Palindromic Repeats) gene editing technologies for AD (familial and sporadic types) risk genes (Zhong et al., 2024). A previous in vivo study by Poole et al. (2015) did not reproduce the AD defining hallmarks of fibrillary Aβ following an oral mono-*P. gingivalis* (strain FDC 381) infection in the apolipoprotein knockout (ApoE–/–) mice brains. However, the researchers detected the presence of *P. gingivalis* in the ApoE–/– mice brains, and confirmed the activation of the complement cascade, in response to the direct infection of P. *gingivalis* directly in the brain. The findings reiterate the significance of chronic local inflammation which constitutes a component of AD pathogenesis (Miklossy 2008; Poole et al., 2015).

**Table 4.2: Transgenic mouse models for investigations into obesity and diabetes**

**(Kleinart et al., 2018, Lutz & Woods, 2012)**

| **Mouse model** | **Characteristics** |
|---|---|
| *Genetic models* | |
| ob/ob | Mutation to ob gene which codes for leptin, a hormone which regulates appetite and metabolism. The mice become obese and develop Type 1 diabetes due to insulin resistance. |
| db/db | Mutation in the leptin receptor gene (Leprdb), leading to leptin resistance. Obesity and hyperglycaemia are manifested similar to ob/ob mice. |
| TALLYHO/Jng | Inbred polygenic model of type 2 diabetes with moderate obesity, exhibiting reduced insulin-stimulated glucose uptake and pancreatic dysfunction, resembling human type 2 diabetes. |
| NONcNZO10/LtJ | Polygenic model of type 2 diabetes with obesity, hyperglycemia and insulin resistance. |
| NZO | Polygenic model of obesity with type 2 diabetes primarily in males. Mice develop obesity dur to increased food intake and reduced enery expenditure. |
| TSOD | Polygenic model of obesity and diabetes, developed through selective breeding from the ddY strain (outbred mouse strain). |
| *Diet induced models* | |
| High Fat Diet (HFD) | Feeding mice a high fat diet leading to obesity, insulin resistance and type 2 diabetes. |
| High Sucrose Diet (HSD) | Similar to HFD, the high sugar diet leads to obesity, insulin resistance and type 2 diabetes. |

| *Other models* | |
|---|---|
| CRISPR-Cas9 induced Lep and Lepr knockout(KO) mice | Created by gene editing techniques to knockout the Lep and Lepr genes, producing phenotypes similar to ob/ob and db/db mice, respectively. |
| Streptozotocin (STZ)-induced diabetes | STZ is a drug that destroys pancreatic beta cells, leading to type 1 diabetes-like symptoms. |

**Table 4.3: Transgenic mouse models commonly used for investigations into AD (adapted from Zhong et al., 2024)**

| Mouse model | Characteristics |
|---|---|
| **Tg2576** | hAPP695 mutation, dense plaque (7-8 months), major plaque deposition (11-13 months) on parenchyma and vascular structures. |
| **TgCRND8** | Double mutant: hAPP 695 (KM670/671 NL and V717F), amyloid deposition in the cerebral cortex, neuritic pathology in hippocampus, midbrain, brainstem and cerebellum (4-5 months). |
| **PS19** | hMAPT (P301S) mutation, tau seeding (1.5 months), NFTs (6 months), no amyloid pathology, shortened life span. |
| **APP/PS1** | Double mutant: hAPP695 (KM670/671 NL) and PS1 (delEx9), Aβ deposits, microglial and astrocytic activation (4 months). Amyloid plaques in hippocampus and cortex (9 months). Increase in Aβ40 and Aβ42 in hippocampal regions and microglial activation. Lack of tau pathology |
| **5xFAD (C57BL6)** | Amyloid plaques (16 days), intraneuronal plaques (6 weeks). Plaques in cortex, hippocampus, thalamus (2 months) and spinal cord (3 months). Lack of tau pathology. Aggressive onset of amyloid pathology. |
| **3xTg-AD** | Extracellular amyloid deposits in frontal cortex (6 months), plaques in hippocampus (12 months). Aggregates of hyperphosphorylated tau in hippocampus (12–15 months). Intraneuronal Aβ immunoreactivity (3–4 months). |

The present study was heavily inspired by the work of Ilievski et al. (2018) who were the first to demonstrate the formation of extracellular $A\beta_{42}$ in young adult WT mice after repeated oral exposure to *P. gingivalis* (strain W38). Neurodegeneration was noted in the experimental group based on the observed reduction in intact neuronal cells, along with the detection of phosphorylated tau and NFTs. These findings were not observed in the brain tissues of the

control group. The University of Central Lancashire's longstanding collaborator Dr Sasanka Chukkapalli (University of Florida, USA) provided the optimal mouse model (db/db) incorporating the comorbidities common to periodontitis and AD i.e. obesity and diabetes. The obesity/type-2 diabetes (db/db) was chosen as they are able to develop obesity as early as 3-4 weeks of age, with elevated plasma insulin levels starting at 10–14 days. Similar to Illievski et al. (2018), the present study utilised *P. gingivalis* (strain W38), which is a well characterised strain and widely used to study the complex interactions between the bacteria and host immunity. This strain also expresses a majority of the virulence factors including gingipains and LPS (Boyer et al. 2020). While it is prudent to focus on *P. gingivalis*, there is also an argument to consider a secondary pathogen not from the 'red complex' of major periodontal pathogens. *Fusobacterium nuceatum* is a Gram negative, anaerobic bacterium is found in subgingival biofilm, which is from the 'orange complex'. It has been reported to act a 'bridging organism' within the biofilm, connecting early and late colonizing bacteria, helping to promote the growth and aggregation of other periodontal bacteria. *F. nucleatum* is not considered to be as virulent as *P. gingivalis*, however it can suppress the host immune response and contribute to activation of inflammasomes (Kendlbacher et al. 2024).

As such, the present study modified the approach by Illievski et al. (2018), by producing a disease co-morbidity model for periodontitis with the potential to produce AD pathological hallmarks. The inclusion of *P. gingivalis* and *F. nucleatum* would add interest as to the extent of the host response to the chronic oral infection comparing the more virulent versus less virulent species.

### 4.1.1 Hypothesis

*P. gingivalis* (W83) and *F. nucleatum* (ATCC49256) mediated oral infection can instigate Aβ plaque deposition and NFT formation in the comorbidity db/db mouse model.

### 4.1.2 Aims and Objectives

Aim: To investigate the effect of *P. gingivalis* (W83) and *F. nucleatum* (ATCC49256) oral infection on the development of AD pathophysiology in the db/db mouse model.

Objectives:

To detect the presence of Aβ and NFTs in db/db mice which were either orally infected with *P. gingivalis*, *F. nucleatum* or sham infected for 16 weeks.

### 4.1.3 University Approvals

University of Central Lancashire (UCLan) (MTA ref no. UCLan 4525, UF MTA-19-0157). Ethical approval was obtained from the animal projects committee of the University of Central Lancashire (UK academic institute) for research on animal tissues as secondary users (ref numbers: RE/21/09 and RE/17/18), as well as in accordance with the approved protocol guidelines (Protocol # 201004367). University of Florida Institutional Animal Care and Use Committee (IACUC, protocol #201304539).

## 4.3 MATERIALS AND METHODS

This investigation was a collaboration with Dr Sasanka S. Chukkapalli, Department of Oral Biology, University of Florida with an agreed project for material transfer agreement, MTA (UF MTA-19-0157) and the University of Central Lancashire (UCLan) (MTA reference number: UCLan 4525). Ethical approval was obtained from the animal projects committee of the University of Central Lancashire for research on animal tissues as secondary users (reference numbers: RE/21/09 and RE/17/18), as well as in accordance with the approved protocol guidelines (Protocol # 201004367) set forth by the Institutional Animal Care and Use Committee (IACUC) of the University of Florida. The University of Florida has an Assurance with OLAW and follows PHS policy, the Animal Welfare Act and Animal Welfare Regulations, and the Guide for the Care and Use of Laboratory Animals. The University of Florida is also AAALAC (Association for Assessment and Accreditation of Laboratory Animal Care International) accredited. Only the brains excised from the skull were sent to UCLan for the agreed ©nvestigations as per the MTA. Approval of their Animal Welfare and Ethical Review Board (AWERB) approval reference number: RE1718 (to receive tissue at UCLan). All db/db mice brains were examined at the University of Central Lancashire (UCLan), UK following approval by AWERB (approval reference number: RE19/02). Brain samples from AD transgenic Tg2576 mice with the Swedish mutation (n = 3) were obtained from Professor Roxane O. Carare, Faculty of Medicine, University of Southampton, UK, as secondary users of tissue, to act as positive controls for Aβ insoluble plaques and for immunohistochemistry. All experimental procedures were conducted strictly in accordance with the abovementioned regulations. This study involved oral inoculation of db/db mice with the periodontal bacteria, followed by detection of Aβ and NFTs via silver impregnation as well as immunohistochemistry for tau and neuroinflammation. The methodological techniques

employed in this chapter have been described in detail by Bahar et al. (2021) and Kanagasingam et al. (2022a).

### 4.3.1 Source of Reagents

PCR Master Mix consisted of 4 µl 5x HF buffer (Thermo Fisher Scientific, UK), 0.5 µl dNTPs (Thermo Fisher Scientific, UK), 0.5 µl each primer (10 µM forward and reverse) and 0.2 µl Phusion High-Fidelity Hot start II DNA Taq Polymerase (Thermo Fisher Scientific, UK). Microarrays were purchased from Thermo Fisher Scientific, UK. Agarose gel for electrophoresis and the RNA isolation kit were from Sigma-Aldrich, UK. The AD transgenic mouse brains (n = 3) were a gift (left over from a completed previous project) from Professor Roxane O. Carare, Faculty of Medicine, University of Southampton. Rabbit anti-Iba1 (Invitrogen®, cat no 13269248) and glial fibrillary acidic protein (GFAP) (ab7260, AbCam, UK). Paraffin wax pellets, absolute alcohol and xylene solvents were from Fisher Scientific, UK. Superfrost+® glass microscope slides (Leica, UK). Mouse anti-tau (clone AT8) was purchased from Invitrogen®. 0.2% citric acid (Sigma Aldrich Ltd., UK). The biotin labelled anti-rabbit IgG secondary detection antibody (kit PK-4001), the mouse peroxidase kit (PK-4002), and the DAB kit (SK-4100) were all purchased from Vector laboratories, Peterborough, UK. These kits are now only available via Bee Scientific Ltd., UK. DPX mounting medium was obtained from Fisher Scientific UK.

### 4.3.2 db/db mice and infection regime

Transgenic male mice were obtained from Jackson Laboratories, Bar Harbor, MA, USA. At 6 weeks of age, the mice became obese and type-2 diabetic due to the db/db mouse model exhibiting these disease related traits due to a spontaneous mutation in the leptin receptor gene (Lepr). The mice were randomly assigned to mono-infected (*P. gingivalis* W83 or *F. nucleatum*

ATCC49256) or sham-infected (control) groups. Antibiotic treatment (penicillin 1000 U/mL, streptomycin 1000 µg/mL) was administered for 3 days to reduce existing oral flora before initiating oral infection with the periodontal bacteria. Mice at 6 weeks were randomly assigned to any of the three groups, and periodontal disease was induced by orally infecting with $10^9$ colony-forming unit (CFU/ml) *P. gingivalis* W83 (n=9), and *F. nucleatum* ATCC 49256 (n =3) and uninfected (sham mice n=6 as carrier control). *P. gingivalis* and *F. nucleatum* cultures were with an equal volume of 4% (w/v) sterile carboxymethylcellulose (CMC; Sigma-Aldrich, St. Louis, MO) in phosphate buffered saline (PBS), this mixture was then used for oral infection ($5\times10^9$ bacteria *per* mL) in db/db mice as described previously (Rivera et al., 2013). All mice brain specimens had been separated into two whereby one cerebral hemisphere was fixed in 10% neutral buffered formalin for immunohistochemistry and microscopy while the other cerebral hemisphere was placed into RNA-later and stored at –80ºC for gene expression analysis, as described by Bahar et al. (2021).

### 4.3.3 Formalin fixed tissue processing

All mice brains were thoroughly washed in PBS pH 7.3 (at least 3 changes over 24 hours). The intact hemisphere was divided into the frontal cortex and temporal lobe inclusive of the hippocampus. Also, the brain stem and cerebellum were kept together where possible. The specimens were processed in cassettes through a series of alcohol and xylene washes using an automated tissue processor (Shandon Citadel 2000, Thermo Scientific, Masachusetts, USA) and embedded in molten paraffin wax. The protocol employed by the tissue processor was; 70% ethanol for 1 hour, 80% ethanol for 3 hours, 90% ethanol for 3 hours, 3 x 100% ethanol for 4 hours, 2 x 100% xylene for 4 hours, 100% xylene for 5 hours, 2x paraffin wax for 7 hours, then held in paraffin wax for a minimum of 1 hour. The tissue was then embedded in paraffin

wax in appropriately labelled embedding moulds using an embedding station (Raymond A. Lamb Ltd London, England). Standard procedures as described in Bahar et al. (2021).

### 4.3.4 Tissue Sectioning

The paraffin wax embedded tissue blocks containing the temporal lobe (including the hippocampus) were trimmed to expose the tissue specimen. They were subsequently pre-cooled on ice for 1 hour prior to sectioning with the Leica RM2235 microtome. A temperature regulated water bath was maintained at 50 °C to float sections and to collect them onto Superfrost+® glass microscope slides (Leica, UK). The pre-cooled block was held in a chuck to have the tissue facing the vertical plane of a microtome blade. The section thickness was set to 5 µm and ribbons of the sections were picked up with the aid of forceps and a paint brush and floated onto the surface of the water bath. More than 3 serial sections per slide and multiple slides per blocks were collected. All slides were allowed to dry at 37 °C in an incubator overnight. The tissue sections were allowed to achieve further bonding to the glass slides by placement of the slides at 65 °C for an extended duration of 2 hours. The slides were subsequently removed and stored at room temperature. The experimental groups included sham (non-infected), *F. nucleatum*, *P. gingivalis* infected and AD transgenic Tg2576 mouse tissue sections (positive control) were then prepared for immunohistochemistry. The standard procedures were as described in Bahar et al. (2021).

### 4.3.5 Methenamine silver impregnation

Methenamine silver solution was used to detect amyloid plaques and NFT. This was prepared by mixing three solutions; silver nitrate 0.0625 g (in 5 ml distilled water), 3% hexamine solution (in 25 ml distilled water) and 3% borax (disodium tetraborate, in 5 ml distilled water).

Rehydrated paraffin wax sections were initially oxidised in 0.5 % periodic acid for a duration of 10 minutes. Upon repeated washings in water, the sections were then transferred into pre-heated methenamine silver solution at 60 °C for about 40 to 60 minutes and monitored until the desired degree of silver impregnation was achieved. All sections were then rinsed in deionized water and fixed in 2.5 % aqueous sodium thiosulphate for 2 minutes. Subsequently, further washes in water were carried out and the sections were counterstained in haematoxylin (3 minutes), then blotted dry. The were then cleared using a series of xylene washes (2 x 5 minutes) and then mounted with DPX mounting medium. The standard procedures were as described by Bahar et al. (2021) and Kanagasingam et al. (2022a).

### 4.3.6 Immunohistochemistry

Upon dewaxing and undergoing alcohol dehydration, the mouse brain tissue sections from the db/db mice and Tg2576 were treated with 0.003% $H_2O_2$ in methanol for 20 minutes at room temperature to 164liminate endogenous peroxidase activity. All sections were washed thoroughly in running tap water. Antigen retrieval step was carried out for optimal antigen-binding. The rehydrated paraffin wax sections were prepared for antigen-antibody binding for the calcium-binding protein anti-Iba1 (Invitrogen®, cat no 13269248), which is specifically expressed by microglia, and the glial fibrillary acidic protein (GFAP) expressed by astrocytes (ab7260, AbCam, UK) using 10mM citric acid buffer (pH 6.1) for 15 minutes at 750W power. After multiple washes, sections were equilibrated, for 5 minutes, in PBS (0.1M PBS, pH 7.2), and the non-specific antibody binding was controlled by incubating tissue sections for 30 minutes in blocking solution containing 0.1% normal horse serum (Vectastain kit, PK 4002) in PBS. The Tg2576 mice tissue sections were used as positive controls, representing the neuroinflammation group. The negative antibody control sections were incubated in the block

solution, with omission of the primary antibody. All other tissue sections were incubated in a humidity chamber, overnight, at 4ºC in the primary antibodies (rabbit anti-GFAP, ab7260, 1/2000) and (rabbit anti-Iba1, 1/150) diluted in blocking solution. On the next day, the sections were washed in PBS (3x for 5 minutes each) and incubated for 60 minutes at room temperature in the biotin labelled anti-rabbit IgG (from kit PK-4001) diluted 1/200 in block solution. Following this, the rabbit peroxidase kit (Vector laboratories, Peterborough, UK) and the DAB kit (SK-4100) were used based on manufacturers' instructions. The sections were lightly counterstained in Mayer's haemalum (LAMB/170D) before dehydration in graded alcohols and clearing in xylene. The sections were mounted under a coverslip and examined using the Nikon Eclipse E200 Microscope (Nikon, Tokyo, Japan). Images were captured using the DS-L2 v.441 Software (Nikon, Tokyo, Japan). The method for mouse anti-tau (clone AT8, Invitrogen®) immunohistochemical assay was carried out as described previously, except that the antigen retrieval stage was omitted. The block solution consisted of PBS 0.1% (triton X-100, horse serum 0.01%) and the mouse anti-tau antibody was diluted 1/20. The secondary detection antibody employed was the biotin labelled anti-mouse IgG (from kit PK-4002) diluted 1/200 in block solution. The standard protocols were carried out as described by Bahar et al. (2021) and Kanagasingam et al. (2022a).

## 4.4 RESULTS

### 4.4.1 Preserved histology of the temporal lobe in infected db/db mice and a mouse model of AD

Haematoxylin and Eosin staining of the formalin fixed, paraffin wax embedded and rehydrated temporal lobe tissue sections from Tg2576, *P. gingivalis* W83, *F. nucleatum* ATCC49256 infected and sham mice were observed well preserved (not shown). The tissue sections from

the mouse brains from the T256 group demonstrated numerous Aβ plaques upon silver impregnation. The plaques were present if variable sizes and randomly distributed within the fronto-temporal cortices, including the hippocampus region (Figure 4.2a). In the sham mice group, the argyrophilic Aβ plaques and NFTs were not observed in the hippocampus or in the fronto-temporal cortices of db/db brain tissue sections (Figure 4.2b). Similarly, there was an absence of Aβ plaques or NFTs in the groups of *F. nucleatum* ATCC49256 infected (Figure 4.2c) and *P. gingiv*alis W83 (Figure 4.2d).

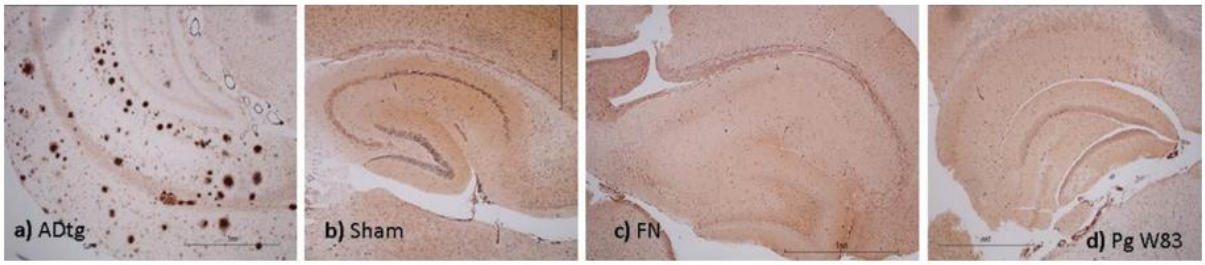


**Figure 4.2:** The obese, diabetic db/db mice rehydrated paraffin wax embedded brain tissue sections (from the reion of the hippocampus) were stained with methenamine silver to demonstrate insoluble Aβ plaques. In the slide with the AD transgenic mouse (positive control for Aβ plaques), methenamine silver impregnation showed a multitude of argyrophilic plaques of variable sizes in the hippocampus, which were in close proximity to the neurons within the cornu ammonis (CA). Some blood vessels were also observed following silver impregnation (a). The sham infected obese diabetic db/db mice, Sham (b), *F. nucleatum* ATCC49256 infected brain tissue, FN (c) and *P. gingivalis*, Pg W83 (d). The histological slides shown in b-d from the obese diabetic mice brain tissue showed no discernible presence of Aβ plaques. Scale bars as shown (Bahar et al. 2021)

### 4.4.2 Immunohistochemistry

(i) Neuroinflammation - Microgliosis

The negative control groups, with the omission of primary antibody showed no reaction (Figure 4.3, a-d). In the AD transgenic Tg2576 mice (Figure 4.3e black arrows), the sham infected mice (Figure 4.3f, black ni arrows) and the *F. nucleatum* ATCC49256 infected mice (Figure 4.3g, black arrows) exhibited only resting microglia, which appear small, ramified

appearance, with fine branches. Very few activated microglia were observed in the *P. gingivalis* W83 infected mice brain tissue sections (Figure 4.3 h and i, black arrows), appearing larger, amoeboid-like and with less branching.

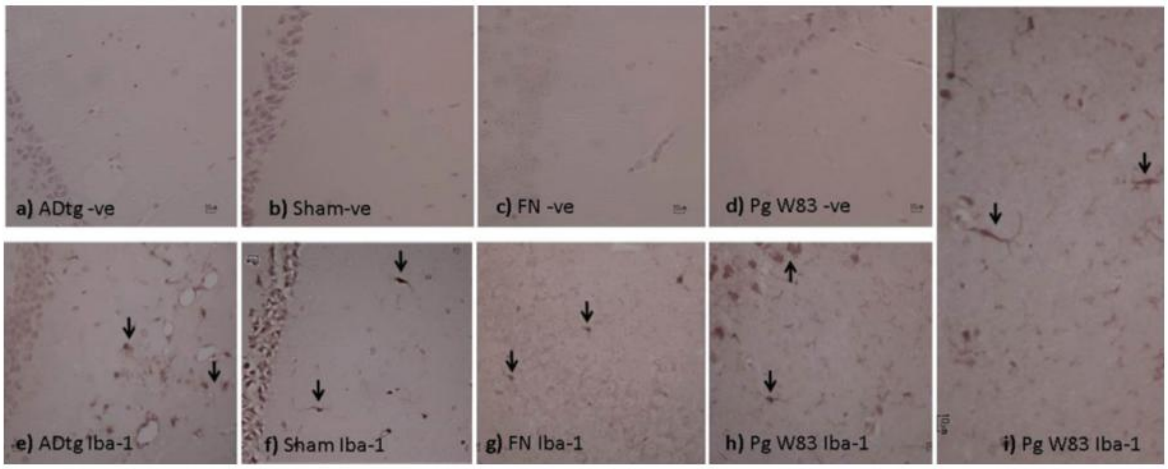


**Figure 4.3:** Rehydrated paraffin wax tissue sections underwent immunostaining with rabbit anti-Iba-1 antibody to detect activated microglia. The order of the images follow the order of the experimental groups as per Figure 4.2. Histological slides a-d exhibited minimal staining as a negative control when the primary antibody was omitted in all the mouse group categories. Variable degrees of activated microglia scattered within the hippocampus as shown by the black arrows in images e-i. Only a few resting microglia were seen in the sham-infected mice group (f) and the *F. nucleatum* ATCC49256 infected mice group (g) mice. The brain tissues of the mouse group inoculated with *P. gingivalis* W83 exhibited more reactive microglial cell distribution with branched processes within the hippocampus (h, i), black arrows. Scale bars as shown (Bahar et al., 2021).

(ii) Neuroinflammation - Astrogliosis

Upon immunostaining with Anti-GFAP of the AD transgenic Tg2576 mice brain sections, the presence of abundant, reactive astrocytes in close vicinity to the Aβ plaques were noted, Figure 4.4a. The area within the inset box (b) shows 'p' representing the $A\beta_{1-42}$ plaque core. The sham-infected mice brain tissue sections (c), whereby the area within the inset box (d) exhibited resting astrocytes, appearing as 'star-shaped' or 'bushy' morphology, with a small cell body

and radial branches. In the *F. nucleatum* ATCC49256, group, the infected mouse hippocampus demonstrated considerable numbers of activated astrocytes (e), with the inset box content (f). The *P. gingivalis* W83 infected mice brain tissue sections (g), with area within the smaller box showing reactive astrocytes (h). The larger inset box (g) is seen in (i), whereby an abundance of reactive astrocytes were noted, similar to the density of astrocytes observed in *F. nucleatum* ATCC49256 infected mice tissue sections (e-f).

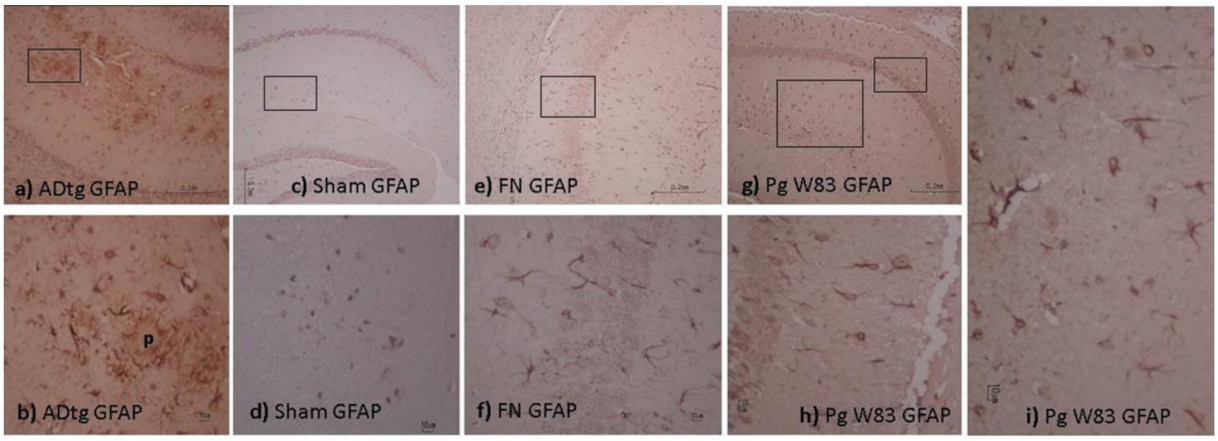


**Figure 4.4:** The rehydrated paraffin wax tissue sections underwent immunostaining with Anti-GFAP immunostaining to identify astrocytes. The order of the images follows the order of the experimental groups as per Figure 4.2. The AD transgenic Tg2576 mice brain sections (a-b) demonstrated numerous reactive astrocytes in close vicinity to the amyloid plaques. The inset box from slide (a), is seen under higher magnification in slide (b), whereby 'p' represents the amyloid plaque core. The sham brain sections (inset box, d, with the area within the box shown under higher magnification in c) showed resting astrocytes. The hippocampus region of the *F. nucleatum* ATCC49256 infected mice (e-f) exhibited substantial numbers of activated astrocytes, the inset box in (e) is seen under higher magnification in image (f). The *P. gingivalis* W83 brain tissue sections, the inset boxes in slide g are shown in h and i. These slides (g-i) also demonstrated abundant reactive astrocytes. Scale bars as shown (Bahar et al., 2021).

(iii) Mouse anti-tau (AT8) immunostaining for detecting neurofibrillary tangles

The AD transgenic Tg2576 mice exhibited an intense positive reaction for tau within numerous cornu ammonis (CA) neuronal cell bodies. The axon hillock of some neurons took up the

immunostaining (Figure 4.5a, black arrows). In general, the tau staining in the sham (non-infected) group of mice was very faint (b, single black arrow). In the group of the *F. nucleatum* ATCC49256 infected mice, a weak tau immunostaining was observed within the CA neurons, however, the axon hillocks did not pick up the immunostaining (c). The *P. gingivalis* W83 infected mice demonstrated tau immunostaining within the CA neurons (d) as well as strong tau positivity within thickened bundles of axonal hillocks in the hippocampal CA neurons (e, with inset boxed area shown in f, black arrows point to the thickened axonal hillocks).

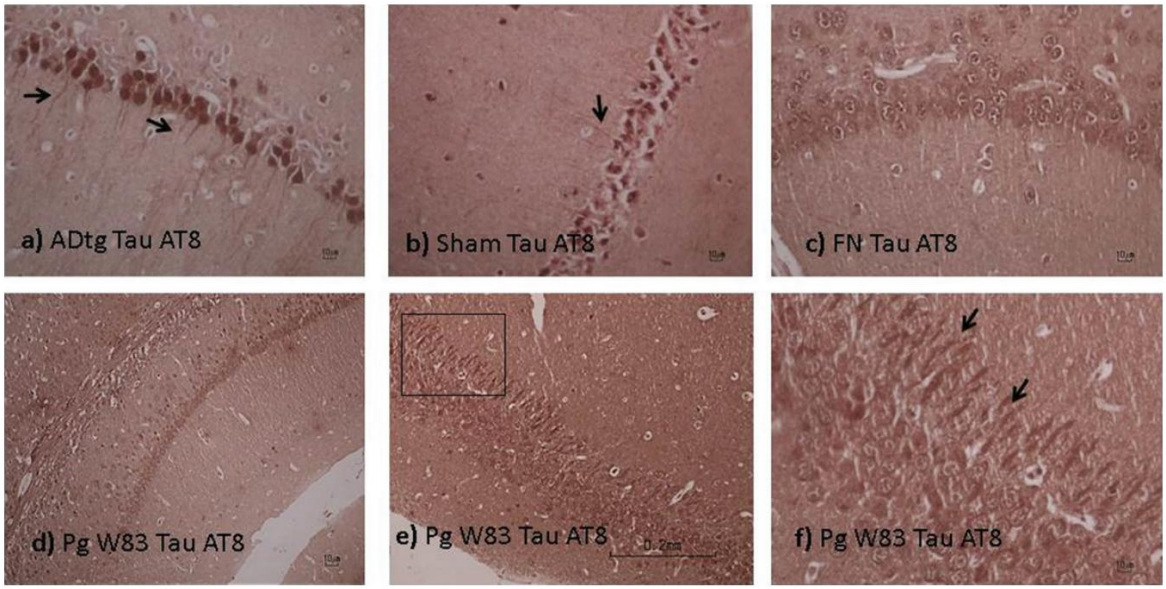


**Figure 4.5.** The rehydrated paraffin wax tissue sections were immunostained with Mouse anti-tau (AT8) to detect NFTs. The Tg2576 mice group exhibited an intense immunopositive staining within numerous CA neuronal cell bodies within the hippocampus. The axon hillock of some neurons displayed apparent immunostaining (a, black arrows). The sham infected mice group showed indistinct staining in the neuronal axon hillocks (b, black arrow). In the *F. nucleatum* ATCC49256 mice group, a weak, diffuse tau immunostaining was exhibited within the CA neurons, without obvious staining within the axon hillock (c). The tissue sections from *P. gingivalis* W83 infected mice exhibited positive immunostaining for tau within the CA neurons and much stronger immunostaining for tau and thickened bundles of axon hillocks in the hippocampus region (d-f, with the inset box in e shown in higher magnification f, black arrows). Scale bars as shown (Bahar et al., 2021).

## 4.5 DISCUSSION

This study highlights the shared inflammatory pathways between periodontitis, MetS (including obesity and diabetes) and AD. To investigate this complex inter-relationship, the mouse model is seen to be the most appropriate methodology as it facilitates controlled experimental settings and genetic manipulation (Illievski et al., 2018; Zhong et al., 2024). The research team were privileged to benefit from Dr Sim Singhrao's collaborative partnership with Dr Sasanka S. Chukkapalli from the Department of Oral Biology, University of Florida and Professor Roxane O. Carare, Faculty of Medicine, University of Southampton. The cost and logistics involved with producing the mouse model in-house at the University of Central Lancashire would have been prohibitive. The sample size numbers in this were not equal for experimental groups (*P. gingivalis* W83 and *F. nucleatum*), negative control group (sham) and positive control group (Tg2576) as some samples were degraded during storage and transportation from the University of Florida.

The specific db/db mouse model chosen for this study has a mutation involving dysfunction of leptin receptors, thereby impairing the leptin signalling pathway which is regulates satiety and energy balance. As a result, these mice experience hyperphagia, leading to severe obesity, which induces insulin resistance and pancreatic beta-cell dysfunction, leading to type 2 diabetes. This mouse model has been reported to exhibit impairments in cognitive function, which offers insights into how metabolic conditions or MetS may contribute to neurodegeneration. (Sharma et al., 2010). Previous research using db/db mice have also shown that diabetes is a significant risk factor for periodontitis as these mice have demonstrated more severe gingival inflammation and increased bone loss compared to non-diabetic mice (Wang et al., 2021). The Tg2576 mice were used as a positive control as they overexpress the human amyloid precursor protein (APP), which is key to the development of amyloid plaques.

Researchers have previously reported experimental mouse models of periodontitis with *P. gingivalis* which have produced early hallmark AD lesions (Illievski et al., 2018, D´ıaz-Zu´niga et al., 2020, Ciccotosto et al., 2024). The present study was unique in that a co-morbid disease model was used as opposed to the AD-prone C57BL/6 mice used by Ilievski et al. (2018) and Ciccotosto et al. (2024) as well as the more 'generic' Sprague-Dawley rats used by D´ıaz-Zu´niga et al. (2020). After 16 weeks of chronic infection of the db/db mice, the present study did not detect the presence of Aβ plaques or NFTs in the hippocampus or other anatomical brain regions, following methanamine silver impregnation.

As for the anti-tau immunostaining, the observations from the present study were similar to D´ıaz-Zu´niga et al. (2020). They also observed thickened axons in the hippocampal neurons of the *P. gingivalis* infected rat brains which were postulated to be equivalent to human AD NFT lesion (D´ıaz-Zu´niga et al. 2020). Along the same lines, the present study's results for anti-tau immunostaining showed thickened axon hillocks of cortical hippocampal neurons. An interesting finding was noted with the mice infected with *F. nucleatum* ATCC49256, whereby the hippocampi demonstrated significant numbers of reactive astrocytes but not microglia. This showed that even a less virulent, bridging bacterium such as *F. nucleatum* ATCC49256 can trigger inflammatory changes to astrocytes, however a much stronger immune stimulation was instigated by *P. gingivalis* (W83) which led to activation of both astrocytes and microglia. These results concur with human studies cognitive deficit after a period of infection (Holmes et al., 2003. Ide et al., 2016). Astrogliosis and microgliosis are responses to injury in the brain, usually as a result of trauma, stroke and neurodegeneration (Zhang et al., 2013). Microglia are the brain's resident immune cells and are first responders, releasing pro-inflammatory cytokines, removing harmful stimuli, clearing of cell debris and releasing neurotrophic factors

(Sarlus & Heneka, 2017). Astrocytes maintain the blood-brain barrier and play a role in repair and glial scar formation to help guide axon regrowth (Linnerbauer & Rothhammer, 2020). The astrogliosis-microgliosis axis (d'Errico et al., 2022) are key contributors to AD pathogenesis due to persistent inflammation leading to accumulation of TNF, IFNs and IL-6, lymphocytes, apoptotic cells and debris, thus disrupting functional haemostasis (Onyango et al., 2021).

Further collaborative work was carried out in relation to this study, which was outside of the scope of this PhD, however, the results will be discussed briefly here as they add to the current findings. Gene expression analysis was carried out using quantitative real-time PCR (qPCR) array (by Dr Sim Singhrao). Gene ontology and pathway analysis was performed using the database for annotation, visualisation and integrated discovery (DAVID), a web-based bioinformatics tool (by Dr Bojlul Bahar). The detailed results have been reported in the article (Bahar et al. 2021). To elucidate the inflammatory activity resulting from *P. gingivalis* W83 infection, gene expression analysis of a panel of 184 genes which were modified as a result of oral infection showed that the pathways of insulin signalling and neuroinflammatory immune response mediated by PI3K/AKT1 were hyperactivated in the brain. Hyperactivation of AKT1/GSK-3B may elevate a pro-inflammatory state through phosphorylation of STAT3, a transcription factor essential for induction of pro-inflammatory cytokines (Jope et al., 2017). Elevated levels of the mRNA abundance of the STAT3 gene and several pro-inflammatory cytokines (IL1A and IL1B) genes in relation to the present study agree with existing evidence for *P. gingivalis* infection mediated cytokine release (Vernal et al., 2009). The stimulation of insulin secretion together with insulin receptor signalling and IGF-1 signalling pathways were mediated by *P. gingivalis* infection. Multiple signalling routes were showed to potentially contribute to AD pathophysiology as seen in Figure 4.6. As for the gene expression pathway analysis, 11 genes (GLP1R, PIK3R1, PIK3R2, PRKACA, PRKAR1A, PRKCA, PRKCB,

PRKCD, INSR, JAK2, and STAT3) were identified, whereby mRNA abundance pointed to stimulation of a localized insulin secretion mechanism in the hippocampal region. A potential pathway for insulin secretion in the brain is through the glucagon-like peptide 1 (GLP-1), which can cross the blood brain barrier during a hyperglycaemic episode (Meloni et al., 2013; Fu et al., 2020), acting to inhibit glucose utilization and cause insulin secretion (Knauf et al., 2005; Sandoval et al., 2015). *P. gingivalis* infection resulted in an increased mRNA abundance of GLP1R and several kinases and their receptors. The AD-MetS association is characterised by insulin resistance, oxidative stress and neuroinflammation (Bedse et al., 2015; Li et al., 2015; de la Monte, 2019), Figure 4.6.

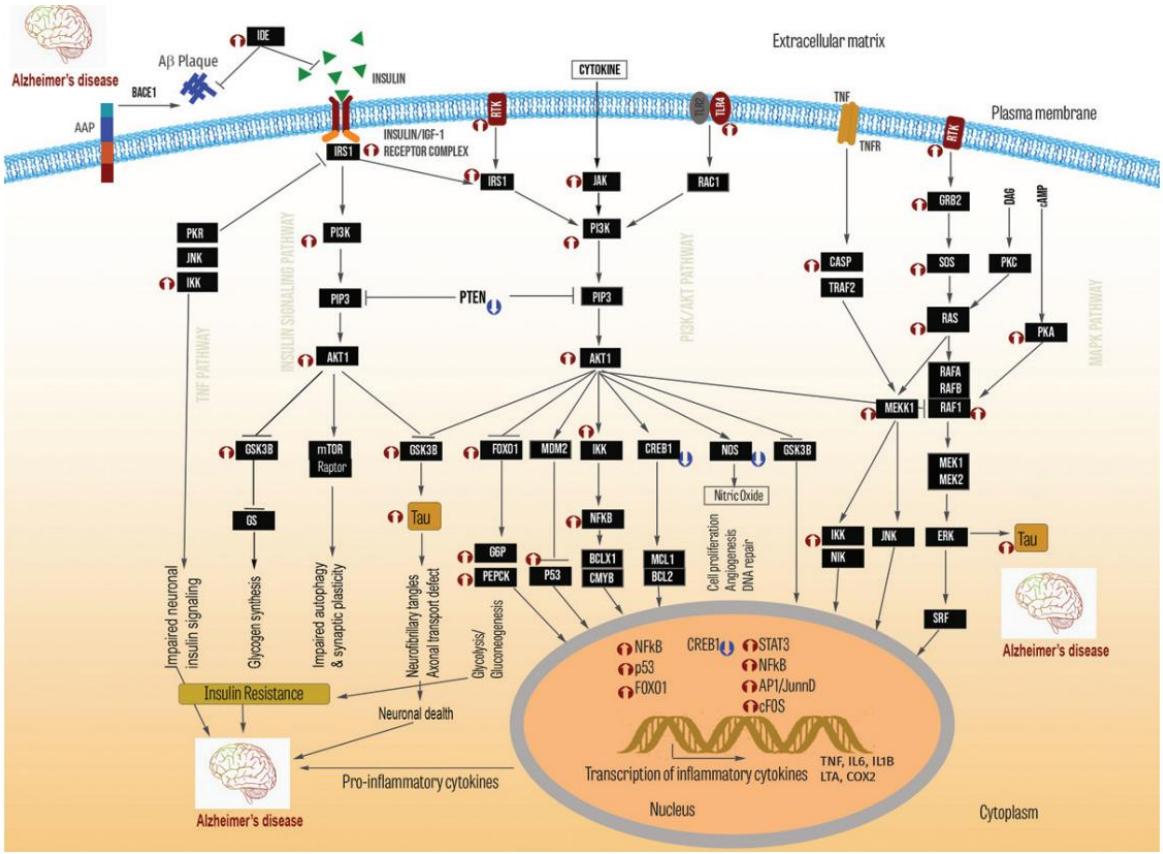


**Figure 4.6:** A schematic outline of 4 major pathways including PI3K/AKT, MAPK, TNF and insulin signalling impacted by *P. gingivalis* W83 infection in the db/db mice. The interconnected pathways led

to modified kinase activities (PI3K/AKT1, RAS/MEKK1), altered oxidative stress (NOS2), impacted insulin signalling (IRS1) and nutrient metabolism (AKT1) as well as transcriptional activation of pro-inflammatory genes (NFKB, AP1, cFOS). This can contribute to the development of AD pathophysiology, Aβ plaque and NFTs. Various mRNA markers are shown to increase (up arrows) or decrease (down arrows) following inoculation with the more pathogenic *P. gingivalis* W83, as compared to inoculation with the bridging species, *F. nucleatum* ATCC49256 (the figure was published in Bahar et al. 2021).

### 4.5.1 Challenges, strengths and limitations

With mounting evidence pointing to periodontitis and MetS potentially exacerbating the onset of AD (Holmes & Cotterell, 2009, Marques et al., 2013), this study was the first to use the db/db mouse model to investigate the co-morbidities. The experimental model could have been improved by inoculating a combination of bacteria to reflect the biofilm in the clinical presentation of periodontitis. *P. gingivalis* and *F. nucleatum* are known to participate in adhesion and co-aggregation, commonly cultivated from subgingival plaque of inflamed gingivitis and periodontal pockets (Weiss et al., 2000). Previously, Polak et al. (2009) reported that a mixed infection mouse model using *P. gingivalis* (ATCC 33277) and *F. nucleatum* (strain PK1594) aggravated alveolar bone loss and induced a stronger inflammatory response compared to mono-infections of either bacterium. When *P. gingivalis* and *F. nucleatum* were co-cultured, they induced significant augmentation of the expressions of IL-1β, IL-8, and TNF-α and a synergistic increase in the IL-6 expression (Yanez et al., 2024). This synergistic effect can enhance the modulation of the host immune response to promote *P. gingivalis* survival through cellular colonization and spreading, resulting in systemic effects (Mulhall et al., 2020). The effect of the interface between bacteria in a polymicrobial infection on host response warrants further research in the context of AD development.

The immunohistochemical investigations were performed by including a no primary antibody control to rule out non-specific binding (false positives) of the secondary antibody and detection reagents. This process entailed the incubation of the brain tissue sample with only the antibody diluent and omitting the primary antibody, followed by the standard secondary antibody and detection reagent. This would confirm that any staining would be due to the primary antibody binding to its target antigen (Hewitt et al., 2014). When utilising monoclonal antibodies, the inclusion of an isotype (i.e. an antibody of the same isotype; IgG2, IgY, IgM and host species as the primary antibody, which targets a protein which absent from the sample controls) would validate the staining was specific to the protein of interest as opposed to a positive immunostaining due to non-specific interactions of the antibody with the other components of the tissue samples. This would act as a convincing negative control (This was well explained and discussed via https://www.bosterbio.com/blog/post/6-ihc-controls-you-should-know).

Densitometric studies of microglial cells in AD provide accurate information on microglial response to physiological and pathological challenges. Several parameters can be employed for quantification including the density of cells per target area, Nearest Neighbour Distance, NND (i.e. the average distance of each microglial cell to its nearest neighbouring cell), the spacing index (calculated by multiplying the squared average of NND by density of the region of interest (Khakpour et al., 2022). Manual analysis can be carried out using ImageJ software (NIH, v.1.50b), however, it is time-consuming with inter-operator variability (Paris et al. 2018). Automated analysis has been described by Khakpour et al. (2022) using a specific script to implement automatic analysis of microglial density and distribution, which includes sequential steps developed for ImageJ software (NIH, v.1.50b). Counting was not carried out in this study, however, the histological slides were assessed by multiple examiners who were blind to the

experimental conditions. A more favoured approach for morphometrical imaging stained/labelled microglia would be to use confocal laser scanning microscopy. This technique ensures accurate assessment of intact microglial architecture, while avoiding sectioning artefacts, which can be superior to microscopy imaging (Vulders et al., 2021). This equipment was not available at the University of Central Lancashire.

### 4.5.2 Clinical relevance

This study results add to the current evidence-base which suggests that periodontitis can instigate infiltration of the brain with bacterial products, resulting in induction of AD-like biomarkers, neurodegeneration, and increased inflammation. While the exact complex pathways (especially involving insulin signalling and secretion in the brain) are not fully understood, the presence of comorbidities can increase the risk of neuroinflammation. It is important to increase awareness in relation to the impact of metabolic syndromes related conditions including obesity and diabetes which are modifiable risk factors. Preventive benefits of life-style changes including the maintenance of good oral health, nutritious diet, adequate exercise, sufficient sleep as well as optimal management of other systemic conditions can decrease the risk of AD.

### 4.5.3 Future work

(i) Inoculation of a combination of bacteria from the 'red complex' (*P. gingivalis, T. forsythia, T. denticola*) or consider a combination with synergistic bacteria such as *F. nucleatum.* The effect of co-culture models on how bacterial interactions can potentially modify virulence and the ensuing cellular responses of the host would merit further investigations, using a comorbidity animal model for AD.

(ii) Use of appropriate positive and negative controls. While it is important to have a control group with the primary antibody omitted, a proper negative control is to substitute the serum or isotype-specific immunoglobulins at the same protein concentration as the primary antibody.

(iii) Employing more accurate morphometric imaging and densitometric analysis of microglia. Confocal laser scanning microscopy can be considered for imaging small field images of microglia in tissue sections. The use of automated slide scanners (e.g. ZEISS Axioscan 7 and Olympus VS120) facilitate accurate imaging of entire brain regions or whole sections. This would allow numerous microglial images to be acquired, with reduced sampling bias. In line with this, light-sheet microscopy can be used in conjunction with other methods to clear brains containing fluorescently labeled microglia, thereby allowing the acquisition of large microglial image datasets.

## 4.6 CONCLUSION

The hypothesis was partially accepted as even though Aβ and NFTs were not detected, the study results demonstrating neuroinflammation suggest that chronic oral infection with *P. gingivalis* can initiate the development of neuropathology leading to AD, in subjects with comorbidities of obesity and Type 2 diabetes. Patients who have significant risk factors for AD including aging and apolipoprotein E gene allele 4 inheritance, as well as comorbidities of obesity and diabetes, would have a higher susceptibility to infection. Preventive measures

which include maintenance of periodontal health should be considered for susceptible individuals to decrease their risk of developing AD.

# CHAPTER 5

## ANTIMICROBIAL PROPERTIES, AND PAIRED HELICAL FILAMENT STRUCTURES OF SELECTED TAU PEPTIDES FRAGMENTED BY GINGIPAINS

The work presented in this chapter is fully published by the author of this thesis:

**Kanagasingam S**, von Ruhland C, Welbury R, Singhrao SK (2022) Antimicrobial, polarising light and paired helical filament properties of fragmented tau peptides of selected putative gingipains. J Alzheimers Dis. 89(4):1279-1291.

# ANTIMICROBIAL PROPERTIES, AND PAIRED HELICAL FILAMENT STRUCTURES OF SELECTED TAU PEPTIDES FRAGMENTED BY GINGIPAINS

## 5.1 INTRODUCTION

The diagnosis of AD depends on clinical symptoms and two pathological lesions namely the Aβ plaques and NFTs in post-mortem brain tissue sections (Hyman et al., 2012). The Amyloid Hypothesis has been the mainstream concept underlying AD research over the almost 30 years. This points to the accumulation and deposition of oligomeric or fibrillar peptide plaques as the main cause of AD. Having said that, the modest or uncertain therapeutic effects of anti- amyloid drugs have prompted researchers to explore other factors and mechanisms (Kametani & Hasegawa, 2018). A recent systematic review of the efficacy of monoclonal anti-amyloid therapeutic medications such as Lecanemab (Leqembi®), Aducanumab (Aduhelm®) and Gantenerumab (Roche®) revealed limited or mixed results in reducing cognitive decline (Chhabra et al., 2024).

At the time of this investigation, a Californian-based biotech company, was in the midst of trialling Atuzaginstat (also known as COR388) which is an oral therapeutic agent developed to inhibit *gingipains*, a group of toxic enzymes released by *P. gingivalis* which has been shown to contribute to neuronal damage in AD patients. The initial results appeared to slow cognitive decline in participants with AD and *Porphyromonas gingivalis* infection in the phase II/III GAIN trial, which supported the theory that this oral pathogen may be involved with the initiation or in the progression of AD or both [https://www.alzheimer-europe.org/news/cortexyme-begins-european-screening-phase-ii/iii-clinical-trial-cor388-mild-moderate-ad?language_content_entity=en, accessed on 26/09/2019]. Tau protein is a key

component of NFTs in AD and can undergo fragmentation by gingipains (Dominy et al., 2019; Haditsch et al., 2020)

When exposed to microbial pathogens, the brain relies on its innate immune inflammatory responses, although other clearance pathways have been suggested (Olsen & Singhrao 2015; Singhrao & Olsen 2019; Olsen & Singhrao 2019). The ensuing inflammation may worsen neuronal damage associated with AD. Parallel to the Amyloid Hypothesis, this study builds on previous investigations by Kobayashi et al. (2008), suggesting that tau peptides may also have antimicrobial properties. Kobayashi et al. (2008), surmised that several motifs in tau protein exhibited antimicrobial properties. Two of the motifs ("VQIINK" and "VQIVYK") were identified in the gingipains-fragmented tau peptides (Figure 5.1). This has led to the interest in investigating the antimicrobial phenomenon associated with these two hexapeptide motifs on *P. gingivalis* planktonic cultures.

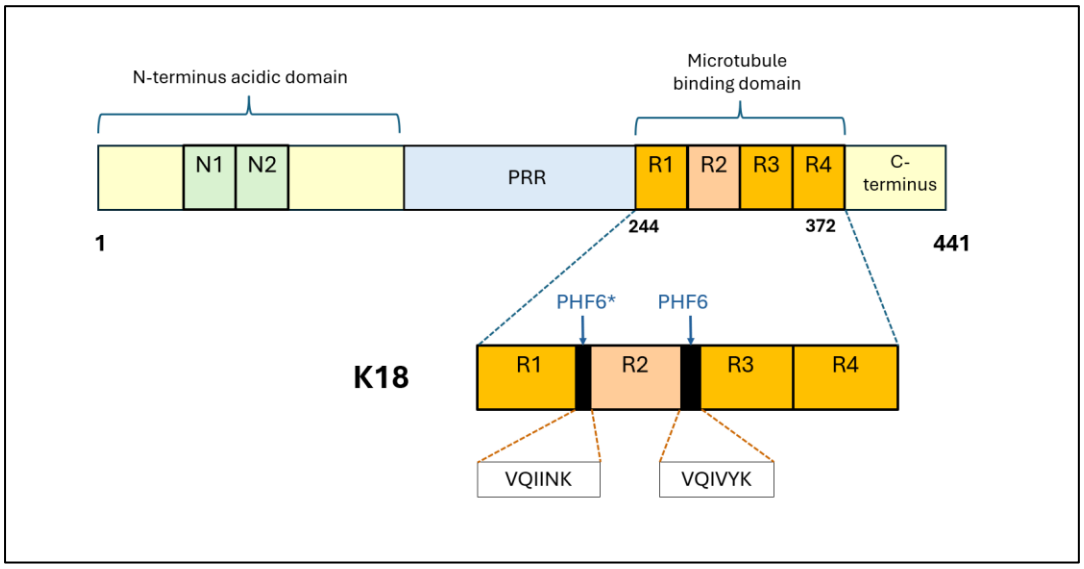


**Figure 5.1: Schematic diagram showing tau domain organization which including the N-terminal (N1, N2) the proline rich region (PRR), the microtubule binding region and the C-terminus extensions.** The microtubule-binding region contains three or four partially repeated sequences, R1 to R4, that are involved in direct binding to microtubules, which plays a key role in stabilizing these structures. Tau aggregation is associated with two nucleating 6-residue segments, namely PHF6

(VQIVYK) and PHF6* (VQIINK). These peptides are located in R2 and R3, respectively. The longest tau isoform corresponds to 441 amino-acid residues. The K18 Tau fragment is a key component in AD taupathy as it is involved in the process of aggregation-seeding, whereby preformed aggregates of K18 fibrils can promote the aggregation of other tau proteins. The proline-rich region (PRR) has many phosphorylation sites which are altered in AD, resulting in forming PHF that accumulate as NFTs within neurons (adapted from Fichou et al., 2019; Kanagasingam et al., 2020)

Tau's physiological role is binding to microtubules and supporting their cellular functions, which includes providing a structural backbone for axons and dendrites. Microtubules act as compression-bearing struts and are a major network for the active transport of proteins and organelles in both directions within axons and dendrites (Gendron & Petrucelli 2009). Tau is known to have 6 isoforms, with the presence of aggregation-promoting 'hotspots' found in all Tau isoforms, as described previously and shown in Figure 5.1: "VQIVYK" and "VQIINK". These hexapeptides underpin Tau aggregation and are essential for Tau-dependent toxicity (Perez et al., 1996; von Bergen et al., 2000).

Tau protein is susceptible to hyperphosphorylation by several kinase enzymes and one of these is glycogen synthase kinase 3-beta, GSK-3β (Figure 5.2). This enzyme is activated by *P. gingivalis* LPS (Bahar & Singhrao 2021; Singhrao et al., 2024; Kanagasingam et al., 2020). Studies have confirmed that GSK-3β activation by *P. gingivalis* can lead to phosphorylating tau at ser396 and thr231 amino acid residues (Perry et al., 1991; Quinn et al., 2018) firmly implicating this periodontal pathogen in tauopathy pathogenesis in AD. Tau binding to microtubules are released into the neuronal cytoplasm with neurotoxic fragments contributing to NFT formation (Kanagasingam et al, 2020).

The focus of this investigation is on NFT biosynthesis from microbial virulence factors binding to tau leading to its breakdown along the microtubule binding domains of tau, forming paired

helical and straight filaments (PHFs and SF). Phosphorylated tau features in NFTs and in PHFs, with dimensions of the helices being approximately 20 nm wide, 80 nm apart with the twist being 10 nm long (Terry 1963). Abnormal neurites or neuropil threads (denoting a dense substrate consisting of axons, dendrites, and glial cells typically observed in the grey matter of the central nervous system) are a widespread and characteristic lesion associated with AD (Perry 1991). The spread of the NFTs, and neuropil thread pathology is considered in Braak staging (mild, moderate, and severe) as a measure of AD disease progression (Braak, 2006; Braak et al., 2011).

Periodontal pathogenic bacteria and its implications to AD development is supported by evidence derived from laboratory as well as epidemiological studies (Sparks Stein et al., 2012; Poole et al., 2013; Chen et al., 2017; Dominy et al., 2019). Tau pathology has been proposed to spread like an infectious process from neuron to neuron (Cope et al., 2018). Dominy et al. (2019) has reported that tau is a target of gingipain proteolysis, which supports the concept of trans-neuronal spread of *P. gingivalis*. Poole et al. (2013) first detected *P. gingivalis* lipopolysaccharides (LPS) in AD brains, some of which, appear like clusters of outer membrane vesicles (OMVs). The OMVs have a role in carrying gingipains and other less pathogenic virulence factors such as adhesins, hemolysins, and hemaglutinins (Nonaka et al., 2024). A review by Zhan et al. (2018) highlighted studies which detected more bacterial LPS in postmortem AD brains compared to the control brain samples. Similarly, Dominy et al. (2019) identified the presence of *P. gingivalis* DNA and gingipain antigens in AD brains. Bacterial LPS are potent immune modulators and can induce immune signalling cascades that produce NFT biogenesis, which contribute to AD pathogenesis (Mazgaeen & Gurung, 2020). In addition, Tau which undergoes excessive phosphorylation becomes toxic and insoluble. This

prompted the investigation into the function of gingipains' fragmented tau peptides in order to better understand their functional properties.

The following motifs within the tau protein sequences were recognised for their potential antimicrobial peptide functions; VQIVYK, VQIINK, KVQIINKKL, KKVAVVR, KVQIINKK, KKVAVVRT, SVQIVYKPN and KVQIINKKLDLSN (Kobayashi et al., 2008) This is in line with the effects of the $A\beta_{1\text{-}40/42}$ peptides, which have been shown to possess similar antimicrobial peptide properties, thought to be mediated by their ability to disrupt the cell membranes of pathogens by triggering the formation of pores or channels in the membrane, leading to cell death (Spitzer et al., 2016). The resultant antimicrobial immune responses give rise to neuroinflammation and subsequent neuronal death.

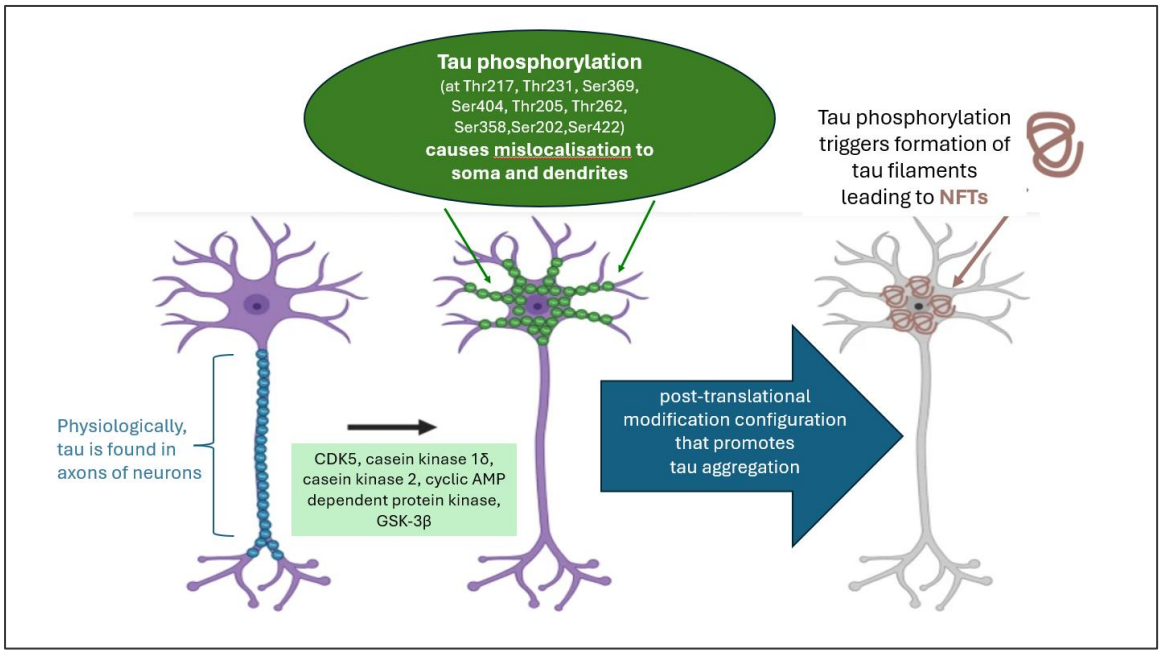


**Figure 5.2: Tau phosphorylation and formation of NFTs within neurons**

Phosphorylation triggered by host enzymes (CDK5, casein kinase 1δ, casein kinase 2, cyclic AMP dependent protein kinase, GSK-3β) and others promote tau mislocalisation and aggregation, which results in the formation of NFTs. Under physiological conditions, most tau protein is found within neuronal axons. Tau phosphorylation leads to tau mislocalisation to the region of the soma and dendrites. As a result of tau

phosphorylation, the formation of tau filaments is enhanced, thereby leading to the production of NFTs (Xia et al., 2020, Plattner et al., 2006).

A number of host enzymes have been implicated in tau phosphorylation including CDK5, casein kinase 1δ, casein kinase 2, cyclic AMP dependent protein kinase, GSK-3β (Plattner et al. 2006, Wang et al. 2007, Haditch et al. 2020). The process by which *P. gingivalis* causes tau to become hyperphosphorylated implies that either the infection or its virulence factors (LPS, gingipains) can trigger signalling pathways which may indirectly activate GSK-3β, as reported in both *in vivo* and *in vitro* conditions (Kanagasingam et al. 2020, Haditch et al. 2020, Bahar et al. 2021) As has been previously reported, this can in turn lead to phosphorylation of *de novo* tau at ser396 and thr231 residues (Davila-Bouziguet et al, 2019, Bahar et al. 2021).

### 5.1.1 Hypothesis:

Hypothesis 1: Tau fragments cleaved by gingipains have antimicrobial or cytotoxic activities against *P. gingivalis.*

Hypothesis 2: Tau can form helical twists *in vitro,* displaying their paired helical filaments (PHFs) and/or straight filamets (SFs) features which are the main components of NFTs.

### 5.1.2 Aims and Objectives

Aims:

To investigate possible causal links of fragmented tau peptides containing putative gingipains binding hexapeptide motifs with periodontal disease with AD in the biogenesis of the NFT lesion.

Objectives:

(i) To evaluate the if gingipains fragmented tau peptides have antimicrobial and cytotoxic properties on *P. gingivalis*

(ii) To assess if the tau containing "VQIINK" and **"**VQIVYK" hexapeptide motifs, which form helical twists *in vivo*, are also able to form helical twists *in vitro* to confirm their PHF and/or SF features that link them to NFTs.

### 5.1.3 Ethical approval

This project was approved by the UCLan Biological Safety Officers (BSO) committee.

### 5.1.4 Funding award:

TC White Young Researcher Award (2018-2021), RCPS Glasgow, £10,000.00

## 5.2 MATERIALS AND METHODS

This study involved culturing of *P. gingivalis* for antibacterial assays when exposed to a variety of tau peptides. To further examine the mechanism of action of tau peptides, Circular Dichroism Spectra was used to investigate the secondary structure of proteins, with the small amounts of sample of tau peptide A in its non-phosphorylated and phosphorylated forms. The tau peptides were also prepared for TEM imaging, which provided ultra-structural morphological visualisation of their fibrillar conformation. The standard methodological procedures have been described in Kanagasingam et al. (2022b) and was also employed in a student research project supervised by Dr Sim Singhrao and the author of this thesis (Iqra Amir and Katelan Newnham, Module BL3299).

An initial peptide toxicity prediction was requested from the manufacturers of the peptides, Severn Biotech Limited, UK (Table 5.1). The selected non-phosphorylated peptides were then synthesised, before undertaking further laboratory testing.

**Table 5.1 shows the initial non-phosphorylated peptide toxicity prediction carried out by Severn Biotech Ltd., UK**

| Region in Tau N-C termini | Peptides A-G | Predicted toxic status | Number of residues | Charge |
|---|---|---|---|---|
| **R211-R221** | **Peptide A** TPSLPTPPTR | No | 10 | +1 |
| **K259-K290** | **Peptide B** HQPGGGK**VQIINK**KLDLSNVQSK | Yes | 23 | +3 |
| **K28-K290** | **Peptide C** **VQIINK**KLDLSNVQSK | Yes | 16 | +2 |
| **K298-K317** | **Peptide D** HVPGGGS**VQIVYK**PVDLSK | Yes | 19 | +1.09 |
| **K298-K321** | **Peptide E** HVPGGGS**VQIVYK**PVDLSKVTSK | Yes | 23 | +2 |
| **K294-K317** | **Peptide F** DNIKHVPGGGS**VQIVYK**PVDLSK | Yes | 23 | +1.09 |
| **K294-K321** | **Peptide G** DNIKHVPGGGS**VQIVYK**PVDLSKVTSK | Yes | 27 | +2 |

### 5.2.1 Source of reagents

Tau peptides A-G were purchased from Severn Biotech Ltd., Kidderminster, UK. *P. gingivalis* strain ATCC 33277™ gifted by Professor Daniel Grenier, Faculté de Médecine Dentaire, Université Laval, Québec, Canada. This is a seronegative strain has been commonly used for characterisation of virulence factors (Naito et al., 2008). Hemin and menadione (Sigma Aldrich, Dorset, UK), tryptone soya broth (Thermo Scientific Oxoid, Hampshire, UK), yeast extract granulated (Thermo Fisher Scientific, Cambridge, UK), oxolated horse blood (Thermo Scientific Oxoid, Hampshire, UK), L-cysteine hydrochloride (Sigma-Aldrich, Dorset, UK) and agar powder (Thermo Fisher Scientific, Cambridge, UK). Ringer's buffer solution was made by dissolving 1 Ringer tablet (Sigma-Aldrich, Dorset, UK) in 500 mL neutral deionised water, then sterilised in the autoclave for 15 minutes at 121 °C (Sigma-Aldrich, Dorset, UK). Sodium hydroxide 98.5% pellets (Thermo Fisher Scientific, Cambridge, UK). Ethyl alcohol (Thermo Fisher Scientific, Cambridge, UK). Anaerobic sachet (Thermo Scientific™ Oxoid™ AnaeroGen™ 2.5L Sachet). Phosphate Buffered Saline, Tablets, High-Purity (Sigma-Aldrich, Dorset, UK) and 2, 2, 2-trifluoroethanol / phosphate buffered saline (TFE / PBS; 50% v/v), supplied by Dr Sarah Dennison, Research Fellow, School of Pharmacy & Biomedical Sciences.

### 5.2.2 *Porphyromonas gingivalis cultures*

Over 10 days, the freeze-dried bacteria were revived by careful rehydration of the pellet in degassed tryptone soya broth (TSB) medium. Hemin stock solution of 1 mg/mL Hemin soluble in 1M sodium hydroxide was made using 50 mg dissolved in 1 mL of 1M sodium hydroxide and addition of 49 ml of distilled water to make up a total 50 mL. Subsequently, Menadione 50mg, 50 mL of distilled water and ethanol 95% 50 mL was used to make up Menadione stock solution of 0.5 mg/mL. The Menadione stock solution was dissolved in ethyl alcohol, followed

by distilled water. This was then stored in the refrigerator in a dark bottle, which was wrapped in aluminium foil. The products and amounts used to make TSB are shown in Table 5.2.

**Table 5.2: Reagents and amounts used to produce TSB**

| Product | Supplier and catalogue number | Amount for 500mL |
|---|---|---|
| Tryptone Soya Broth | Oxoid CM0129 | 15g |
| Yeast extract | Fisher BP1322-500 | 2.5g |
| L-cysteine hydrochloride | Sigma Aldrich C7880 | 0.25g |
| Water (autoclaved) | - | 495 ml |
| When cool add Hemin 1mg/ml stock | Sigma Aldrich H5533 | 2.5ml |
| Add Menadione 5 mg/ml stock | Sigma Aldrich M9429 | 1ml |

Tryptone soya broth-blood agar plates (BAP) were made using the same method for producing TSB (as described above), except the broth was substituted with tryptone soya agar (Thermo Fisher Scientific, Cambridge, UK). Sterilization of the media was carried out in a bench-top autoclave for 15 minutes, at a temperature of 121°C, with pressure settings at 15lb/inch$^2$. Upon cooling of the medium to 55°C, 1mL of Menadione (5 mg/ml stock), 2.5 mL Hemin (1mg/mL stock) and 25 mL of defibrinated, oxalated horse blood (Thermo Scientific Oxoid, Hampshire, UK) were added and mixed well between each addition. Following sufficient cooling of the agar-containing medium, it was poured into sterile petri dishes.

Culturing of *P. gingivalis* ATCC 33277 was carried out for 25 hours in Tryptone soya broth (TSB) under anaerobic conditions at 37°C. The log phase growth was achieved at an optical density (OD) of 0.240 at 660 nm. This reading has been reported to be within the log phase period for *P. gingivalis* ATCC 33277™ (Grenier et al., 2001). The dilution of the planktonic cells carried out to $10^{-6}$ in sterile Ringer's buffer. This produced a countable range of colony-forming units per millilitre (cfu/mL) of 30-300. Fixed volume aliquots (20 µl) of *P. gingivalis*, of a $1x10^{-4}$ diluted cell suspension were pipetted (in triplicate), onto the surface of freshly poured, dried and pre-labelled Tryptone soya agar blood plates (BAP), based on the surface

drop method (Miles et al., 1938). Under anaerobic conditions, the BAP plates were incubated for 72 hours. Inoculation of a single colony of the 72-hour BAP culture of *P. gingivalis* was used to prepare a 25-hour anaerobic culture. The Jenway$^{TM}$ Model 7315 UV/Visible Single Beam Spectrophotometer (Thermo Fisher Scientific, Cambridge, UK) was used to obtain optical density was readings.

Serial dilution of the 25-hour broth cultures were carried out down to $1x10^{-10}$ in ¼ strength sterile Ringers solution (Figure 5.3). This produced initially acceptable countable number of colonies, within a range of 30-300 cfu/mL. The *P. gingivalis* cultures were prepared for antimicrobial activity of various Tau test peptides at various dilutions (Figure 5.4).

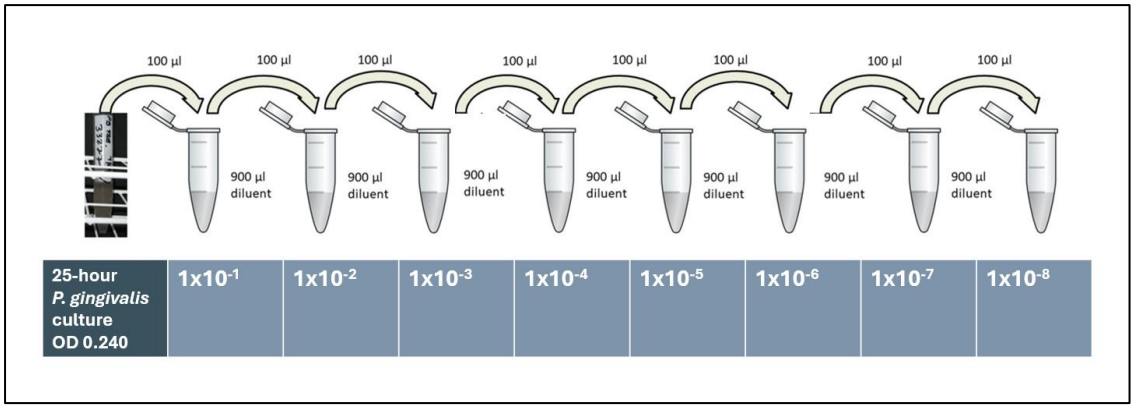


**Figure 5.3:** Diagram illustrating the serial dilution protocol used for *P. gingivalis*

### 5.2.3 Assessment of the putative gingipain binding tau hexapeptide motif antimicrobial activity on *Porphyromonas gingivalis*

The tau peptides were assigned labels A-G (non-phosphorylated) and $A^p$-$C^p$ (phosphorylated) (Table 5.3). Stock concentrations (1mM) of the tau peptides were freshly prepared in ¼ strength sterile Ringers on each day of the experiments. Working dilutions of each tau peptide were prepared at 100µL in sterile Eppendorf tubes. Each peptide was prepared at various

concentrations; 750µM, 500µM, 333µM, 150µM, 50µM and 10µM in equal volumes (20µL), in cell suspensions diluted to $1x10^{-4}$ and plated onto BAP media. Control plates consisted of 20µL of sterile ¼ strength sterile Ringers in a bacterial cell suspension of $1x10^{-4}$ plated out onto BAP media. After incubation, the plates were checked to confirm the formation of discrete colonies within the range of 30-300 cfu/mL. Calculations were carried out according to the appropriate dilution factor using the following formula:

$$\text{cfu/mL} = \frac{\text{Average number of colonies x 10 x 5}}{\text{dilution factor } (1x10^{-4})}$$

Based on Miles et al. (1938), the cfu/mL were calculated and adjusted for the dilution factor, by diluting 1 in 10 and again by 5 (1/5 of 100 µL volume).

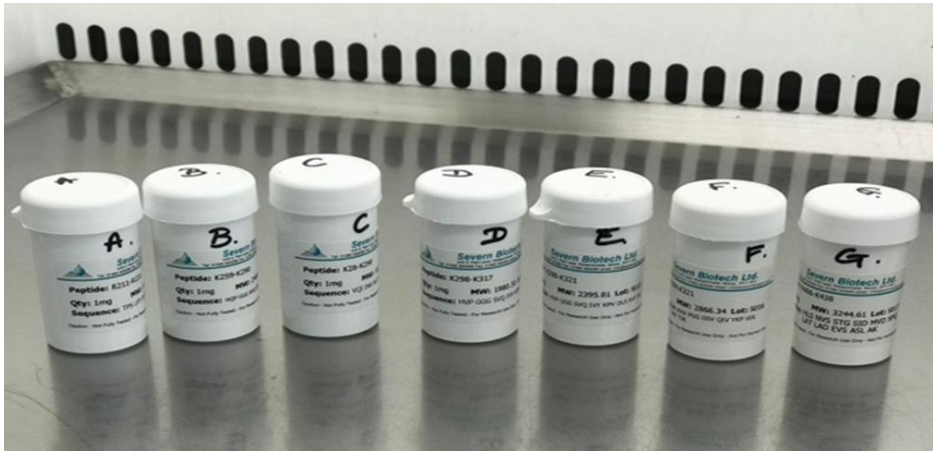


**Figure 5.4:** Tau peptides which were designated as A-G (non-phosphorylated) were commercially synthesized and supplied by Severn Biotech Limited (Kidderminster, UK) in their purified crystallised (powder) form with/without post-translational modification.

**Table 5.3: Tau peptides (A-G) of interest in this study**

| Tau Peptide (non-phosphorylated) | Region in Tau N-C termini | Peptide sequence identity in full length Tau* **Test concentration range = 500µM; 333µM; 150µM; 50µM and 10µM** (Amount 1mg powder/peptide reconstituted in Ringers solution for 1mM stock solution) |
|---|---|---|
| A | R211-R221 | TPSLPTPPTR |
| B | K259-K290 | HQPGGGK**VQIINK**KLDLSNVQSK |
| C | K28-K290 | **VQIINK**KLDLSNVQSK |
| D | K298-K317 | HVPGGGS**VQIVYK**PVDLSK |
| E | K298-K321 | HVPGGGS**VQIVYK**PVDLSKVTSK |
| F | K294-K321 | DNIKHVPGGGS**VQIVYK**PVDLSKVTSK |
| G | K406-K438 | HLSNVSSTGSIDMVDSPQLATLADEVSASLAK |
| **Phosphorylated Tau Peptide** | **Region in Tau N-C termini** | **Peptide sequence identity in full length Tau** **Test concentration range = 500µM; 333µM; 150µM; 50µM and 10µM** (Amount 1mg powder/peptide reconstituted in Ringers solution for 1mM stock solution) **Green** residues indicate phosphorylation |
| $A^{p}$ | R211-R221 | 211TPSLPTPPTR220 |
| $B^{p}$ | K259-K290 | 267HQPGGGKVQIINKKLDLSNVQS$^{184}$K287 |
| $C^{p}$ | K28-K290 | VQIINKKLDLSNVQS$^{184}$K |

* Tau peptides N = 7 (A-G) of interest in this study were based on those identified by Dominy et al. (2019) and the putative phosphorylated residues (green) as reported by Bahar et al. (2021). The VQIINK and VQIVYK motifs indicate PHF-containing regions of tau constituting NFTs that bind to the microtubule binding domains.

### 5.2.4 Circular dichroism spectroscopy for assessment of the secondary structure of tau peptide A (non-phosphorylated and phosphorylated)

Circular Dichroism (CD) spectroscopy was carried out in solution and in the presence of trifluoroethanol (TFE), which promotes peptide stability during the spectroscopy process. CD in this study was performed by Dr Sarah R. Dennison (Biomedical Research Facilities Manager and a Research Fellow, School of Pharmacy and Biomedical Sciences, University of Central Lancashire). CD is an optical spectroscopic method used to examine the structures and conformational changes of proteins. By harnessing the differential absorption of left- and right-circularly polarised light by chromophores, the structural information about protein conformations can be derived (Miles et al., 2021). Phosphorylated and non-phosphorylated tau peptide A were diluted in either neutral pH PBS or 50% 2,2,2-trifluoroethanol (TFE), followed by measurement of its absorbance a JASCO J-815 fluorescent spectrophotometer (JASCO UK Ltd, West Yorkshire, UK) using a 1-mm path-length, in a quartz cuvette to minimize any non-specific absorbance. Each sample was scanned 10 times and readings were averaged over a wavelength range of 180-260 nm at 0.5 nm intervals. A scan speed of 100 nm/minute with a bandwidth of 1 nm was employed. The average readings from the blank spectra from PBS alone were subtracted from the test peptides. CD spectra were deconvoluted using the SELCON 3 Algorithm (protein reference set 3) to achieve the secondary structure estimation (Sreerama & Woody, 1993; Sreerama et al., 1999) on the DichroWeb (Whitmore & Wallace 2004; Whitmore & Wallace 2008, Whitmore et al.,2010).

### 5.2.5 Transmission Electron Microscopy (TEM)

This TEM aspect of the laboratory investigation was outsourced to Dr Christopher Von Ruhland, Central Biotechnology Services, Cardiff University due to the lack of TEM facilities at the University of Central Lancashire. Reconstituted peptides in the ¼ strength sterile

Ringer's buffer were dispensed onto Nescofilm (Bando Chemical Industries Ltd. Kobe, Japan) in droplets of 50µL and then stored in a humidified incubation chamber. Formvar/carbon coated nickel grids (400 mesh) were floated with their film side down, on droplets of each supernatant for 20 minutes. This was subsequently transferred to 1% glutaraldehyde in PBS for 10 minutes, followed by thorough washing in PBS (3 x 1 minute). The samples were then washed in reverse osmosis-purified water for 6 x 1 minute. The grids were subsequently transferred to 2% uranium acetate for 10 minutes (Bils & Hall, 1962). After being gently lifted off with fine forceps, excess stain solution was drained with Whatman 50 filter paper. The grids were then allowed to air dry. The samples were examined using a Hitachi HT7800 TEM (Hitachi High Tech Ltd., UK) at 100 kV. All images were captured with Radius software (EMSIS GmbH, Germany). All protocols as described by Kanagasingam et al. (2022b).

### 5.2.6 Statistical analysis

The data was analysed using the Statistical Package for the Social Sciences (SPSS). A Shapiro-Wilk test confirmed the non-parametric nature of the data. A Mann Whitney U test was used to determine the differences between two independent groups of tau peptides and corresponding controls. The mean cfu/mL for all dilutions were calculated to determine antimicrobial activity (3 experimental readings were carried out for each group). A statistical probability $p \leq 0.05$ was considered significant.

## 5.3 RESULTS

### 5.3.1 Anaerobic growth of *P. gingivalis* ATCC 33277 from in TSB culture

The revival of *P. gingivalis* (ATCC 33277) from freeze-dried culture took about 11 days. After the initial revival, the *P. gingivalis* growth cycle returned to its natural cycle of 0-72 hours. All *P. gingivalis* cultures placed in the anaerobic jars demonstrated growth (as seen by the turbidity of the broth compared to control TSB). A pellet of cells were present at the bottom of the tube. No changes were seen in the control of TSB. Incubation of the blood agar plates (BAP) were carried out at 37ºC under anaerobic conditions. The streaked plates from the 72-hour culture are shown in Figure 5.5. *P. gingivalis* (ATCC 33277) entered its log phase after 20-hour initial inoculation period, based on Grenier et al. (2001).

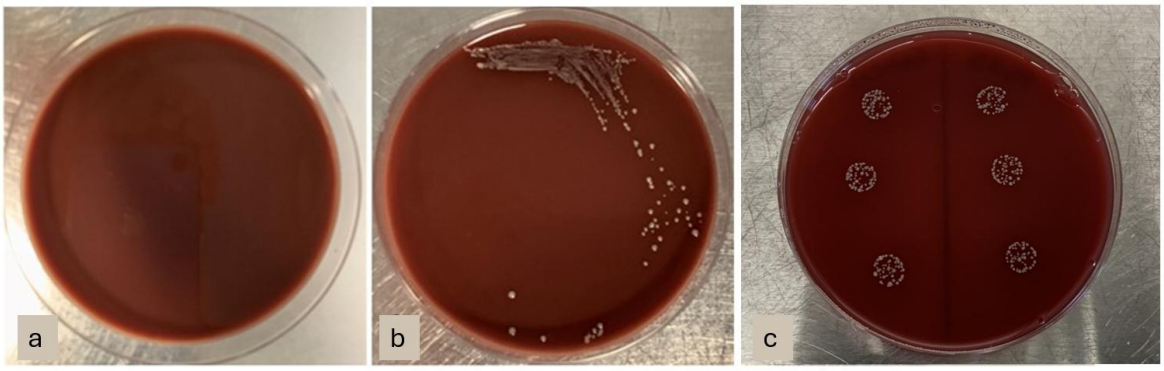


**Figure 5.5:** The blood agar plates showing the control plate which remained sterile (a), with the streaked plate from the 72-hour *P. gingivalis* ATCC 33277 culture showed circular, raised smooth colonies (b) and a plate showing the surface drop method whereby discrete colony forming units can be calculated (Miles et al. 1938).

Based on the 3 readings per experimental group, the cfu/mL the mean was calculated. This was then adjusted for the 1 in 10 dilution factors. Table 5.4 lists the enumeration for the 25-hour *P. gingivalis* ATCC 33277 cfu/mL counts with each dilution. This determined the optimal concentration for testing with the surface drop method first proposed by Miles et al. (1938).

**Table 5.4: Enumeration for the 25-hour broth P. gingivalis cfu/mL counts with each dilution to determine the optimal dilution for use with the surface drop method.**

| 25-hour culture dilutions | Number of colonies | CFU/mL |
|---|---|---|
| **$1x10^{-1}$** | Overlapping colonies, too many to count | - |
| **$1x10^{-2}$** | Overlapping colonies, too many to count | - |
| **$1x10^{-3}$** | Discrete colonies, too many to count | - |
| **$1x10^{-4}$** | Discrete colonies, too many to count | - |
| **$1x10^{-5}$** | 266 | $26.6 \times 10^{5}$ |
| **$1x10^{-6}$** | 63 | $6.3 \times 10^{-6}$ |
| **$1x10^{-7}$** | Less than 30 | - |
| **$1x10^{-8}$** | Less than 30 | - |

Based on the data above, the ideal dilution of the 25-hour broth culture range for the spread plate method was confirmed to be in the range of $1x10^{-5}$ to $1x10^{-6\ to}$ achieve a colony count of between 30-300 CFU/mL. With adjustment for the dilution factor, which was carried out with a dilution of 1 in 10 and then again again by 5 (1/5 of 100 µL volume), the CFU/mL were calculated as described previously. The predetermined dilution of $1x10^{-5}$ for *P. gingivalis* ATCC 33277 confirmed to produce discrete colonies in the range of 30-300 colonies per drop for 20µL, for testing with non-phosphorylated and phosphorylated tau peptides.

### 5.3.2 Assessment of the putative gingipain binding hexapeptide motif antimicrobial activity on *P. gingivalis* ATCC 33277

Non-phosphorylated tau peptides (A-G) which have putative regions which confer antimicrobial activity where exposed to *P. gingivalis* ATCC 33277 to determine the impact on bacterial growth. The Mann Whitney U test found no statistically significant differences between the control groups and non-phosphorylated tau peptide A solutions at concentrations of 500 µM (p=0.658), 333µM (p=0.827), 150µM (p=0.268), 50µM (p=0.077) and 10µM (p=0.825). Representative data can be seen for non-phosphorylated tau peptide A in Table 5.5 and Figure 5.7. Similar results were noted for non-phosphorylated tau peptides B-G. The

results indicated that the non-phosphorylated peptides had no growth enhancing nor toxicity effects on *P. gingivalis*.

**Table 5.5: Number of colonies for non-phosphorylated peptide A and control groups, with the average number of colonies and results of the Mann-Whitney U test.**

| Non-phosphorylated Peptide A | | | | | |
|---|---|---|---|---|---|
| **Concentration (µM)** | Number of colonies for control | Average no. of colonies for control (CFU/mL) x$10^6$ | Number of colonies for test peptide | Average number of colonies for test peptide (CFU/mL) x$10^6$ | P value using Mann-Whitney U test |
| **500** | 26,31,32 | 15 | 21,26,33 | 13 | 0.658 |
| **333** | 28,38,25 | 15 | 32,26,33 | 15 | 0.827 |
| **150** | 15,15,18 | 8 | 13,11,16 | 7 | 0.268 |
| **50** | 18,21,32 | 12 | 18,16,15 | 8 | 0.077 |
| **10** | 9,12,3 | 4 | 10,8,8 | 4 | 0.825 |

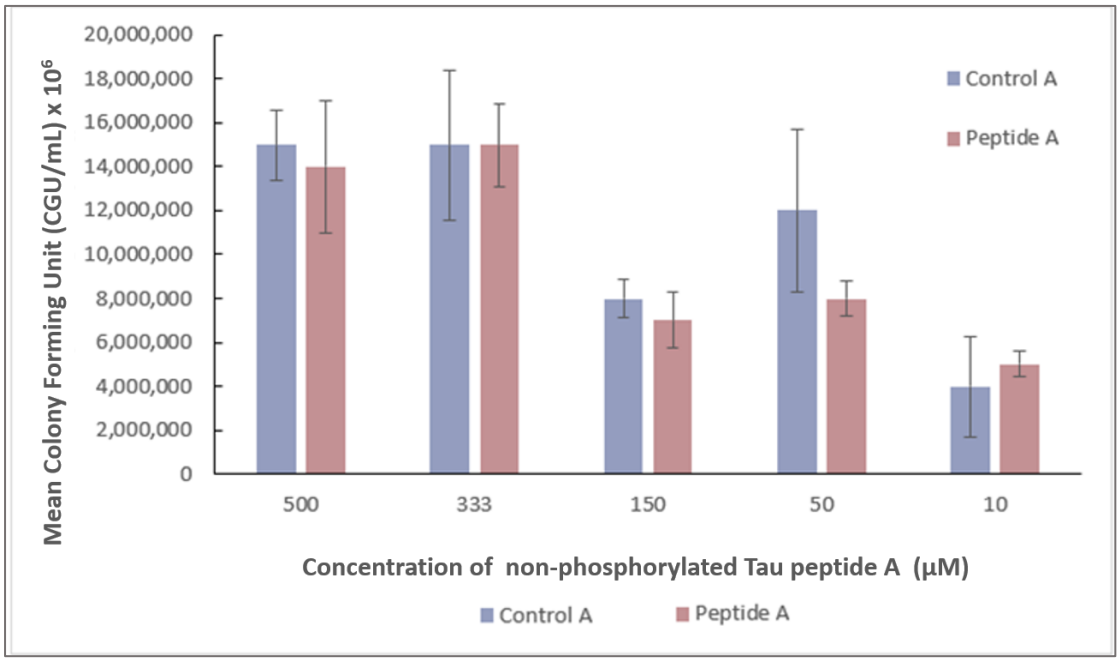


**Figure 5.6:** The bar chart shows the growth of viable *P. gingivalis* ATCC 33227 (CFU/mL) in concentrations of 500µM, 333µM, 150µM, 50µM and 10µM, which were inoculated with tau peptide A in it non-phosphorylated form (light red) and corresponding controls (light purple). Error bars represent mean ± standard deviation, n=3. At the level of significance of α=0.05, a Mann-Whitney U test showed no statistical significance between all non-phosphorylated tau peptide A concentrations and their controls.

Conversely, when growth of *P. gingivalis* ATCC 33277 was assessed following exposure to phosphorylated tau peptide A, a significant reduction in *P. gingivalis* mean colony forming units was observed at all concentrations of 750 µM, 500 µM, 333 µM, 150 µM and 50 µM of phosphorylated tau peptide A in a dose-dependent manner compared to the equivalent no peptide controls, except for the lowest phosphorylated tau peptide A concentration of 10 µM which showed no antibacterial activity (Figure 5.7, with representative data in Table 5.6). This suggests that phosphorylated tau peptide A may have growth supressing effects on *P. gingivalis*.

**Table 5.6: Number of colonies for phosphorylated peptide A and control groups, with the average number of colonies and results of the Mann-Whitney U test.**

| Phosphorylated Peptide A | | | | | |
|---|---|---|---|---|---|
| **Concentration (µM)** | Number of colonies for control | Average number of colonies for control (CFU/mL) $x10^6$ | Number of colonies for test peptide | Average number of colonies for test peptide (CFU/mL) $x10^6$ | P value using Mann-Whitney U test |
| **750** | 73,67,68 | 34 | 1,1,1 | 0.5 | 0.000 |
| **500** | 70,75,72 | 36 | 10,8,7 | 4 | 0.000 |
| **333** | 110,106,101 | 53 | 23,17,15 | 9 | 0.000 |
| **150** | 125,122,144 | 65 | 90,89,73 | 42 | 0.000 |
| **50** | 139,140,132 | 68 | 119,114,110 | 57 | 0.000 |
| **10** | 129,132,136 | 66 | 135,140,130 | 67 | 2.500 |

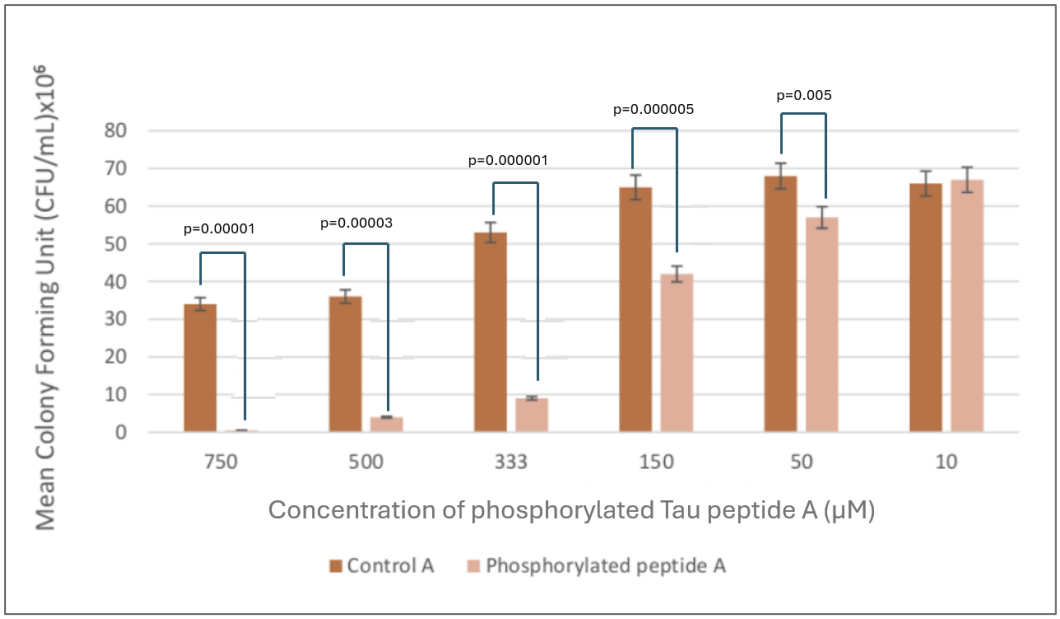


**Figure 5.7:** Bar chart showing mean colony forming units of *P. gingivalis* at varying concentrations of phosphorylated tau peptide A. With a level of significance of α=0.05, phosphorylated peptide A demonstrated statistically significant differences (p = 0.0000) antimicrobial action against *P. gingivalis* as compared to the control group, as determined by the non-parametric Mann Whitney U test across the range of dilutions tested at 50 µM, 150 µM, 333 µM, 500 µM and 750 µM. Only the lowest concentration of the phosphorylated tau peptide A at 10 µM did not show a significant difference compared to controls. Error bars represent mean ± standard deviation, n=3.

Exposure to phosphorylated Tau peptide B resulted in a reduction in the growth of *P. gingivalis* ATCC 33277 at concentrations of 333 µM, 500 µM and 750 µM, which was statistically different from the respective control groups. The lower concentrations of phosphorylated tau peptide B did not impact the growth of *P. gingivalis* compared to the control groups (Figure 5.8). Representative data of the number of colonies calculated for experimental and control groups are shown in Table 5.7.

**Table 5.7: Number of colonies for phosphorylated peptide B and control groups, with the average number of colonies and results of the Mann-Whitney U test.**

| Phosphorylated Peptide B | | | | | |
|---|---|---|---|---|---|
| **Concentration (µM)** | Number of colonies for control | Average number of colonies for control (CFU/mL) x$10^6$ | Number of colonies for test peptide | Average number of colonies for test peptide (CFU/mL) x$10^6$ | P value using Mann-Whitney U test |
| **750** | 67,64,72 | 34 | 36,46,27 | 18 | 0.000 |
| **500** | 91,90,75 | 42 | 55,63,55 | 29 | 0.000 |
| **333** | 73,79,69 | 37 | 59,51,50 | 36 | 0.000 |
| **150** | 100,78,87 | 44 | 85,71,79 | 39 | 2.000 |
| **50** | 108,100,113 | 53 | 100,110,99 | 51 | 2.500 |
| **10** | 107,103,93 | 50 | 89,97,94 | 46 | 2.000 |

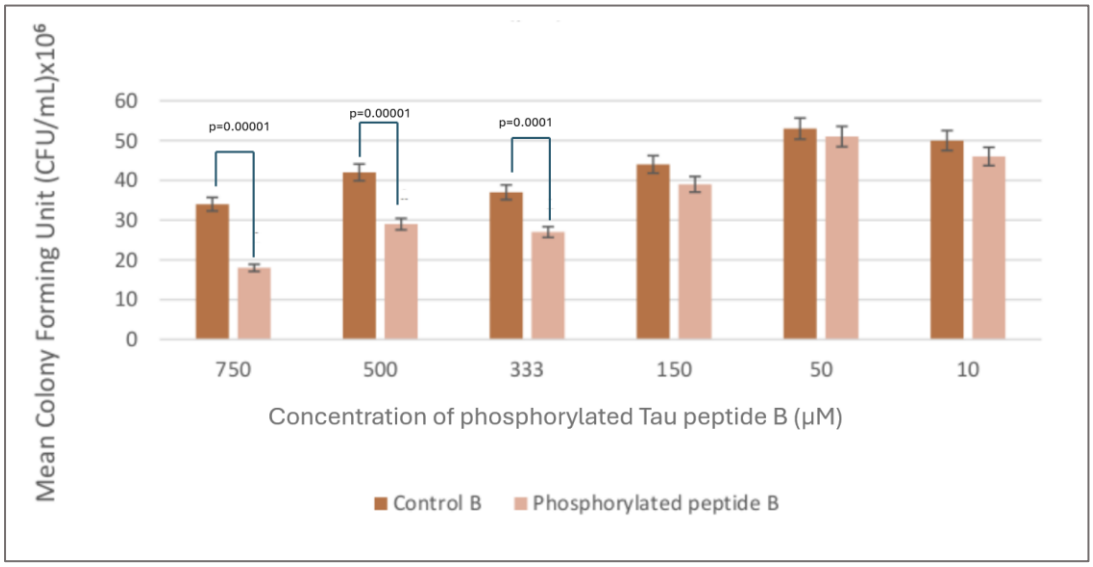


**Figure 5.8:** Bar chart showing phosphorylated peptide B demonstrated statistically significant differences (p= 0.00001) antimicrobial action against *P. gingivalis* as compared to the control group, as determined by the non-parametric Mann Whitney U test across the higher range of concentrations tested, from 333µM to 750 µM. Error bars represent mean ± standard deviation, n=3.

When the growth of *P. gingivalis* was assessed following exposure to phosphorylated tau peptide C, no significant differences were detected when compared to the non-peptide control group (Table 5.8 and Figure 5.9) indicating no cytotoxicity or growth-enhancing effects of the phosphorylated tau peptide. Similar results were demonstrated for all other phosphorylated tau peptides D, E, F and G as these peptides had neither antibacterial effects nor growth enhancing effects on *P. gingivalis* ATCC 33227 (not shown here).

**Table 5.8: Number of colonies for phosphorylated peptide C and control groups, with the average number of colonies and results of the Mann-Whitney U test.**

| Phosphorylated Peptide C | | | | | |
|---|---|---|---|---|---|
| **Concentration (µM)** | No. of colonies for control | Average no. of colonies for control (CFU/mL) $x10^6$ | No. of colonies for test peptide | Average no. of colonies for test peptide (CFU/mL) $x10^6$ | P value using Mann-Whitney U test |
| **750** | 66,73,70 | 35 | 53,57,62 | 28 | 0.000 |
| **500** | 93,100,95 | 48 | 107,103,90 | 50 | 3.000 |
| **333** | 122,125,130 | 63 | 107,100,105 | 52 | 0.000 |
| **150** | 103,112,120 | 56 | 129,122,125 | 62 | 0.000 |
| **50** | 111,114,116 | 57 | 120,119,115 | 59 | 1.000 |
| **10** | 128,120,121 | 61 | 117,115,110 | 57 | 0.000 |

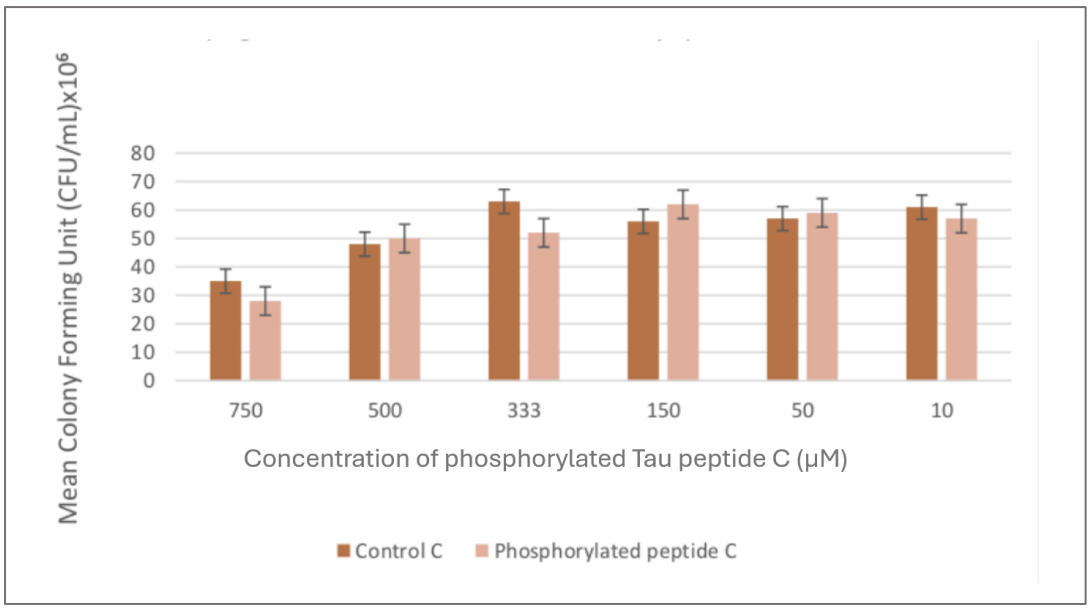


**Figure 5.9:** Bar chart showing mean colony forming units of *P. gingivalis* ATCC 33277 at varying concentrations of phosphorylated peptide C. With a level of significance of α=0.05, phosphorylated peptide C demonstrated no statistically significant differences for antimicrobial action against *P. gingivalis* as compared to the control group, as determined by the non-parametric Mann Whitney U test. Error bars as described previously. Error bars represent mean ± standard deviation, n=3.

A heat map was generated to facilitate visual comparison of the antimicrobial effect of tau peptides A-G and phosphorylated peptides Ap-Cp. The darker colours represent higher antimicrobial activity, which was noted in the groups tested with phosphorylated peptides A (Ap) and B (Bp). The heat map illustrates the mean antibacterial activity of peptides A–G across increasing concentrations (10–500 µM), enabling rapid visual comparison of dose–response patterns (Figure 5.10).

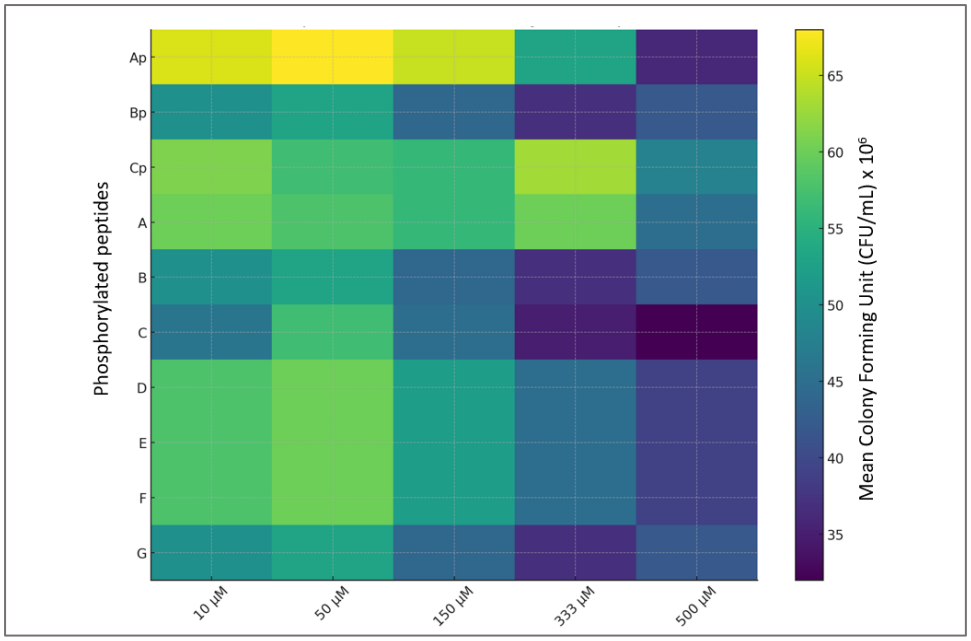


Figure 5.10: Heat map of mean antibacterial activity of tau peptides A-G and phosphorylated tau peptides Ap-Cp, across increasing concentrations, ranging from 10–500 µM. Colour intensity represents relative antibacterial activity, with lighter colours indicating higher values and darker colours indicating reduced activity. This visualisation highlights peptide-specific and dose-dependent trends in antimicrobial response.

### 5.3.3 Assessment of the secondary structure of the soluble peptide A in non-phosphorylated and phosphorylated forms using Circular Dichroism (CD)

Based on CD spectroscopy, phosphorylated tau peptide A in aqueous solution exhibited a conformation consisting of mainly β-type structures, with a maximum peak at 198 nm and a negative broad band (207 nm), which indicated partial antiparallel ß-sheet structures (Figure 5.10a). As for phosphorylated tau peptide, A an increase in β-sheet and decrease in α-helix secondary structure was noted based on the observed increase in the peak at 220nm and decrease at 200nm (5.10b). SELCON 3 provided further analysis of the spectra, confirmed the presence of mainly β-sheet type with unordered structures (Table 5.9). The presence of TFE, which stabilised the secondary structure, revealed a strong negative band at 198 nm and 203

nm, which is characteristic of a “turn” within the peptide representing an anti-parallel β-sheet structure. This has been reported by Kanagasingam et al. (2022b).

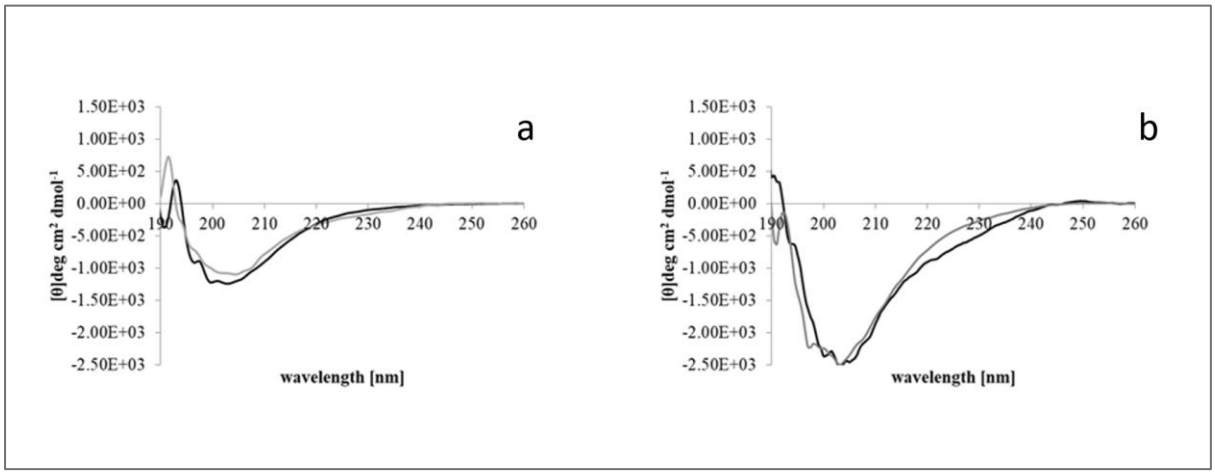


**Figure 5.11:** Circular dichroism spectroscopic analysis of non-phosphorylated tau peptide A (a) and phosphorylated peptide A (b) were plotted with wavelength (nm) against molar circular dichroism and ellipticity. Both forms of tau A peptides demonstrated circular dichroism spectra in the presence of PBS (black) and TFE (grey). The positive and negative CD bands indicate a β-sheet structure with the phosphorylated tau peptide A exhibiting an increase in β-sheet and decrease in α-helix (b). Image credit: Kanagasingam et al., 2022b.

**Table 5.9: Secondary structure determination using Circular Dichroism of tau peptide A in its non- phosphorylated and phosphorylated states**

| Peptide A | Conditions | Helix | Strand | Turns | Unordered |
|---|---|---|---|---|---|
| **Non- phosphorylated** | 1 x PBS | 15.2 | 32.2 | 22.2 | 34.9 |
| **Non- phosphorylated** | 50 % TFE | 13.7 | 32.4 | 21.5 | 34.5 |
| **Phosphorylated** | 1 x PBS | 13.4 | 31.7 | 21.2 | 34.1 |
| **Phosphorylated** | 50 % TFE | 13.5 | 32.7 | 21.5 | 34.3 |

### 5.3.4 Transmission Electron Microscopy (TEM) detection of helical twists to indicate pair helical filaments *in vitro*

For tau non-phosphorylated and phosphorylated peptides, A and G, there was no adsorption of the protein to the support film. Therefore, further analysis of these two peptides were not possible. Non-phosphorylated tau peptide B exhibited long (mean length 1164nm range 500-2000nm) fibrils, which were observed to form random aggregates. Several fibres displayed a clear and consistent distance along the twisted repeat morphology, although the measurements of the twists were not determined (Figure 5.12a, black arrows). Similarly, the phosphorylated version of peptide B also displayed long fibrils, however their helical repeats reduced significantly along the fibre length (Figure 5.12b) as compared to the non-phosphorylated form shown in Figure 5.12a).

The ultrastructure of non-phosphorylated tau peptide C exhibited short, with fibrils of a mean length of 439nm, within a range 143-725nm (Figure 5.12c). Having said this, a few longer fibrils were noted to be randomly aggregating with shorter fibrils. Phosphorylated tau peptide C mainly exhibited thickened fibrils (Figure 5.12d) versus its non-phosphorylated form as seen in Figure 5.12c. Phosphorylated tau peptide C fibrils appeared to display helical repeats along the fibre length (Figure 5.12d, black arrows) with regular and recurrent distances between each twist. Although, not measured, the twists in the phosphorylated tau peptide C were had a trend of being much tighter when compared to the periodicity of the twists observed in the non-phosphorylated tau peptide B.

The non-phosphorylated tau peptide D were observed as short, straight fibrils with a mean length 391nm, within a range 136-655nm (Figure 5.12e), suggesting a possible hydrophobic trait. Non-221229phosphorylated tau peptide E demonstrated medium length fibrils, with a

mean length of 658nm, within a range 200-1500nm. A pattern of random aggregation of fibrils were also observed with non-phosphorylated tau peptide E showed (Figure 5.12f). Non-phosphorylated tau peptide F were observed to form long fibrils, with a mean length of 1100nm, with a range 200-5097nm. A small number of aggregates revealed helical twists within the fibrils in this group (Figure 5.12g).

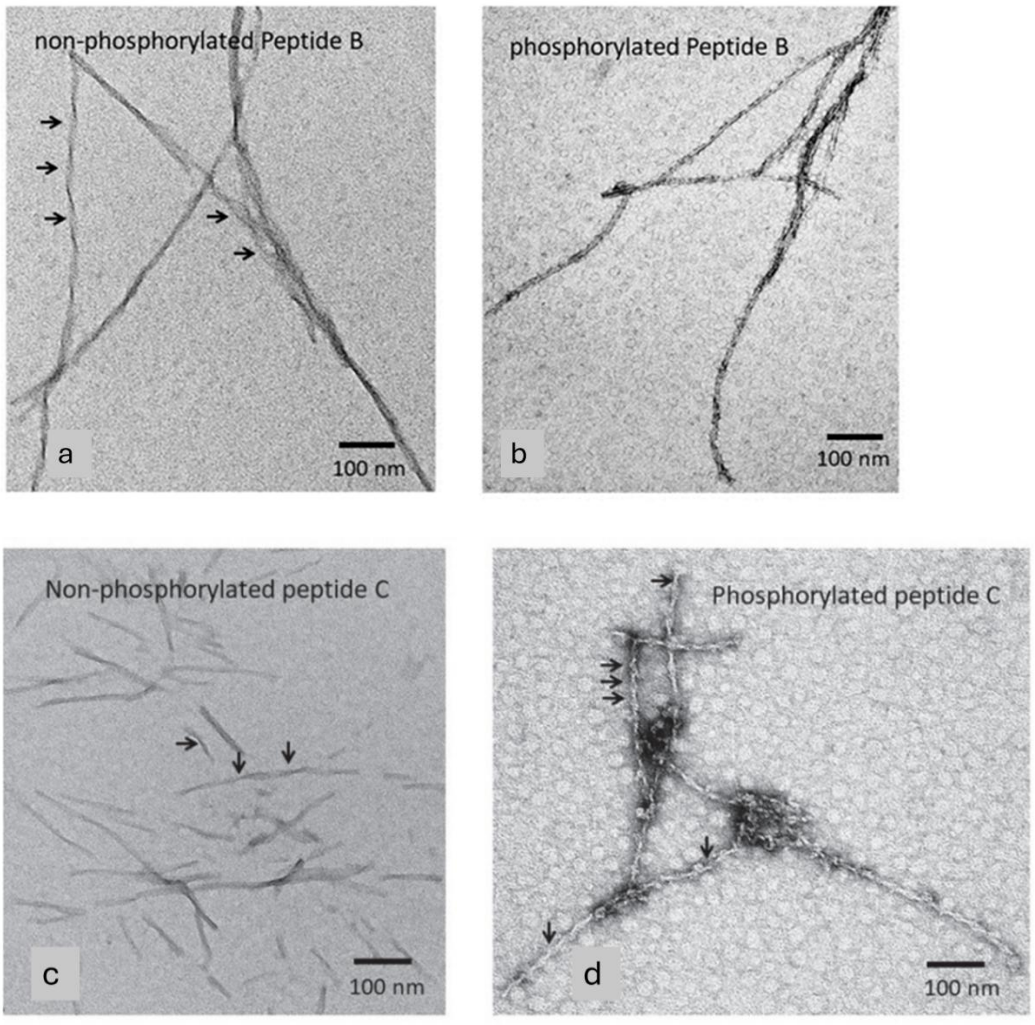

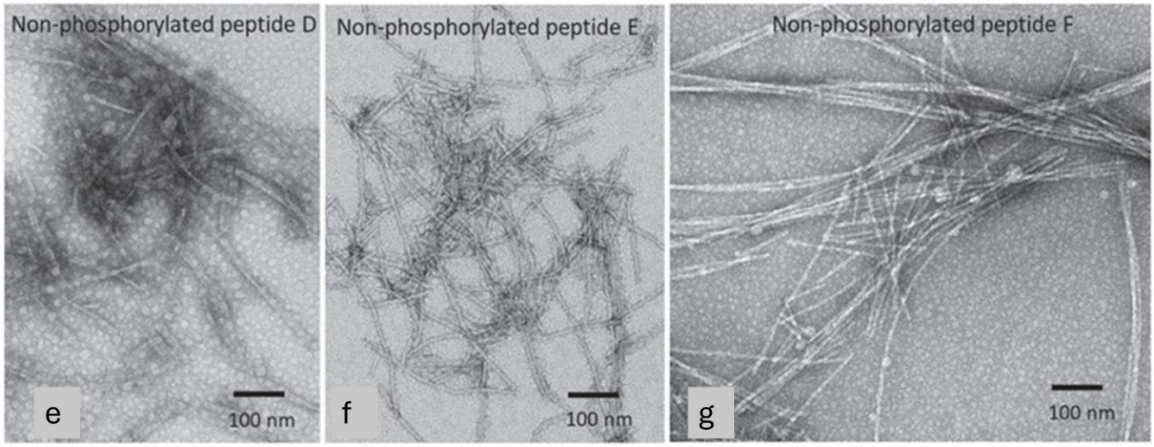


**Figures 5.12**: Non-phosphorylated tau peptide B displayed long fibrils with clear and regular periodicity of twists (a, black arrows). Phosphorylated tau peptide B showed a fibrillar pattern, with less well defined helical turns (b). Tau peptide C in its non-phosphorylated state were visualised as shorter fibrils. These appeared not to be fully assembled into fibers and displayed fewer twists (c, black arrows). Phosphorylated peptide C retained its fibrillar pattern, with many clear and consistent twists throughout all the fibers along their full lengths (d). These twists were noted to be 'tighter' or closer together compared to those seen at the same magnification for tau peptide B in its non-phosphorylated as seen in a (black arrows), to appear more paired helical-like in structure (d, black arrows). Non-phosphorylated peptide D had both short and long fibrils, which were randomly arranged without the presence of twists, instead clustering was noted (e). Random clusters were visualised in the images of non-phosphorylated peptide E appeared, suggestive of possible hydrophobic interaction with other fibrils. These were noted to be composed of short and some long fibrils without twists (f). Non-phosphorylated peptide E exhibited longer strands of fibrils, which could be the joining up of short fibrils, resulting in the appearance of longer fibers (g). Micron bar = 100 nm. This has been reported by Kanagasingam et al. (2022b).

## 5.4 DISCUSSION

It has been proposed that bacterial cysteine proteinases that digest host proteins to amino acids, as gingipains does, may provide nutrients for the bacterium (Imamura, 2003). In line with this, *P. gingivalis* is a keystone periodontal disease pathogen which produces gingipains, which are classified as collagenases and trypsin-like cysteine proteinases. Gingipains is thought to be capable of cleaving tau protein into several peptides (Dominy et al., 2019). As such, this study

sought to investigate the potential for enhanced bacterial survival and proliferation of *P. gingivalis* when exposed to various tau peptides in its non-phosphorylated and phosphorylated forms, across various concentrations. The activities of intra-neuronal gingipains may be a source of free tau peptides which could undergo phosphorylation and post-translational modification, giving rise to PHF and SF. Once cleaved from the microtubule binding domains, they can undergo self-aggregation and subsequently become incorporated into NFTs (Grundke-Iqbal et al., 1986; Maccioni et al., 1995; Plattner et al., 2006). NFTs can spread in a predictable pattern to involve connecting neurons that project between various regions of the brain, including individual cortical regions as well as hippocampus, amygdala, cortices of frontal, temporal and parietal lobes, and in a possible reverse order from the locus coeruleus (Braak & Braak 1991; Braak et al., 2011). NFTs are associated with Braak staging and progression of AD (Braak et al., 2011).

This study results allowed a better understanding of the impact of putative Tau fragments on *P. gingivalis*. Researchers had expected enhanced growth for the bacterium provided by the gingipains-fragmented tau peptides based on Imamura's paper (Imamura, 2003). Instead, the non-phosphorylated peptides (A-G) showed no positive or negative effect on the growth of *P. gingivalis*. This was surprising as it was presumed that exposure of the tau peptides to *P. gingivalis* would trigger tau phosphorylation due the presence of gingipains. As seen in Dominy's study (Dominy et al., 2019), recombinant tau-441 protein and higher molecular weight tau in SH-SY5Y cells were shown to be highly susceptible to gingipains protease fragmentation. In this study, SH-SY5Y cells showed a dose-dependant loss of soluble total tau within an hour of *P. gingivalis* infection compared to uninfected cells. When cells were *P. gingivalis* gingipain-defective mutant, soluble tau levels were similar to uninfected cells, thereby implicating gingipains for the loss of the tau peptides (Dominy et al., 2019). The same

study identified a mid-domain, RgpB-generated tau peptide fragment, TPSLPTPPTR (residues 212 to 221) after gingipains-cleavage. This tau peptide has been shown to be increased 1.7-fold in AD patients' cerebrospinal fluid as compared to healthy subjects (McAvoy et al., 2014). This was represented in the current study by Tau Peptide A. Unlike the present study, Dominy et al., (2019), utilised a different strain of *P. gingivalis* (ATCC BAA-308) at a higher CFU/mL i.e. $6x10^8$. Dominy et al., (2019) also utilised gingipains directly (lysine-gingipain, Kgp and arginine-gingipain B, RgpB), whereas the current study relied on the secretion of gingipains by the *P. gingivalis* strain ATCC 33277. The lower CFU/mL used and reliance on intrinsic gingipains secretion, may have impacted the results.

This study also involved the use of laboratory-made phosphorylated tau peptides. The results suggest that phosphorylated peptide A did have a detrimental effect on *P. gingivalis* numbers, at the higher range of concentrations of 50µM-750 µM, thereby rejecting Hypothesis 1: Tau fragments cleaved by gingipains have no antimicrobial or cytotoxic activities against *P. gingivalis*. This result goes against the predicted toxicity as carried out by Severn Biotech Limited, UK (Table 5.1) for phosphorylated Tau peptide A ($A^p$). As for phosphorylated tau peptide B ($B^p$), the prediction for toxicity was accurate for the higher concentrations of 333 µM to 750 µM, which significantly decreased the growth of *P. gingivalis*. Conversely, tau peptide C was predicted to be toxic, however, there was no difference between the phosphorylated tau peptide C ($C^p$) and control groups on the growth of *P. gingivalis*.

A number of computational tools are available for researchers to predict the toxicity of peptides based on deep learning models utilising independent datasets, half-life of peptides, sequence-based meta-prediction and motif-based recognition (Gupta et al., 2013). Although 'in silico' (or research or experiments conducted using computer modelling) can be more cost effective

and convenient, it is essential to validate the predictions of any toxicity prediction tool with experimental data, as experimental validation would be considered the reference standard for assessing peptide toxicity (Wang & Sung, 2024).

Based on the results of the TEM investigations, gingipains-fragmented tau peptides containing "VQIINK" and "VQIVYK" hexapeptide motifs, which form helical twists *in vivo*, appeared to retain their propensity to form tertiary structures *in vitro*. The tertiary structure seen in phosphorylated peptides B and C ($B^p$ and $C^p$), may form PHFs and SF *in vitro*. The role of soluble peptides A and G, under physiological conditions are believed to promote the development, elongation, maintenance, and stability of microtubule structure (Witman et al., 1976). On the other hand, insoluble peptides B, C, D and E can form PHF and SF, play a role in in forming cytoskeletal pathology leading to NFT formation in AD (Witman et al., 1976). In order to better understand the interactions between tau peptides and *P. gingivalis*, antimicrobial assays were undertaken. The proposed mechanism of eradicating bacteria or hampering bacterial growth is via outer membrane permeabilization. Antimicrobial peptides can disrupt both the outer and inner membranes of gram-negative bacteria, induce unregulated ion movement across the cell membrane and induce a form of apoptosis, leading to eventual cell death (Barreto-Santamaría et al., 2021). Kobayashi et al. (2008) tested tau peptides on bacterial and fungal strains including *Staphylococcus aureus* (Gram-positive), *Escherichia coli* (Gram-negative), and *Candida albicans.* The research Japanese research team were the one of the first to demonstrate the inherent antimicrobial function of tau peptides, which appeared to remain in the presence of salt, magnesium chloride, calcium chloride or horse serum. Multiple tau peptides were shown to have a heightened antimicrobial effect (Kobayashi et al., 2008).

*P. gingivalis* has been recognised as a microbial 'persister, which means it has adaptive mechanisms to improve survivability when exposed to lethal doses of antimicrobial agents by transitioning into a 'dormant' state. This bacterium can then revive itself at a time when the antimicrobial compound is no longer active (Hajishengalis et al., 2012; Li et al., 2018; Wang et al., 2020). The protective mechanism afforded *P. gingivalis* stems from its membrane phospholipid composition which is enhanced in phosphatidyglyerol over phosphatidylethanolamine (Nichols & Rojaanasomsith, 2006). In this study, the phosphorylation of tau peptide A ($A^p$) lowers the pH, which may have contributed to killing of *P.gingivalis* as its growth is inhibited by acidic conditions, preferring to grow within the narrow optimal pH range of 6.5-7.0 (Takahashi & Schachtele, 1990). Decker et al. (2021) have reported that AD is also associated with a lower pH of the brain and cerebrospinal fluid. This may strengthen the argument for tau as a substrate for phosphorylation by gingipains, resulting in the production of PHF and SF in NFT formation (Dominy et al., 2019). The phosphorylation of tau peptide by GSK-β activation is supported by gene array data from *in vitro* application of *P. gingivalis* LPS to the neuroblastoma IMR-32 cells (Bahar & Singhrao, 2021) as well as the *in vivo* periodontitis animal model for investigating AD (Bahar et al., 2021).

In the present study, peptides B, C, D, E and F were from the microtubule binding domains with VQIINK and VQIVYK motifs, which harbour PHFs and residues prone to phosphorylation. As for tau peptide G, with the C-terminal domain with at least 8 serine and threonine sites, which are known to be prone to phosphorylation. Excessive phosphorylation can result in normally soluble tau becoming insoluble (Decker et al., 2021). Consequently, the physicochemical properties of the peptides are impacted, leading to conformational changes. NFTs are considered toxic to nerve cells due to the associated spontaneous and uncontrolled aggregation of free and/or phosphorylated tau.

Tau peptides B and C (phosphorylated and non-phosphorylated), non-phosphorylated tau peptides D, E and F were observed to self-assemble and to form fibrillar structures based on the TEM ultrastructural investigations. Although tau peptides C, D, E and F contained either VQIVYK or VQIINK antimicrobial motifs, they did not exhibit antimicrobial activity against *P. gingivalis*. The functional groups that are contributing to the antimicrobial properties of the peptide may become inactive during the intermolecular hydrogen bonding and self-assembly into fibrillar structure.

The opportunity to use pure tau peptides allowed investigations into whether the helical twists occur *in vitro* as was considered by Terry (1963). NFTs are composed of twisted tubules or paired filaments arranged in a double helix with intermittent narrowing of a specific periodicity (Kidd, 1964). This study results agreed with both researchers (Terry, 1963; Kidd 1964), having shown that tau peptides form helical repeats or twists (although the dimensions were not able to be measured), however they appeared fibrillar rather than tubular *in vitro* under TEM observation. As the dimensions and periodicity of the twists were unable to be measured, as it was not possible to determine whether they represent the same ultrastructural properties of their periodicity or by twist width, as those previously reported (Terry, 1963). In this study, twists were observed in both non-phosphorylated and phosphorylated state, with variations in configuration, dependant on their post-translational status.

### 5.3.1 Challenges, strengths and limitations

The high cost of purchasing the tau peptides limited the ability to repeat experimental procedures. After the *P. gingivalis* antibacterial assays were carried out with the pure tau peptides (A-G), the decision had to be made to repeat the antibacterial assays using selected

phosphorylated peptides, specifically phosphorylated peptides A, B and C. It would have been ideal to repeat the investigations using all phosphorylated forms of tau peptides A-G. Similarly, it would have been ideal to submit all non-phosphorylated and phosphorylated peptides for the assessment of the secondary structure circular dichroism.

Similar to Dominy's study, the mixtures of the various peptides to *P. gingivalis* should have been tested for the presence of gingipains. This could have been carried out with fluorogenic peptide substrates, photoacoustic imaging, and solid-state nanopore sensors, which would have facilitated the detection and quantification of gingipains (Park et al., 2025). It would have been interesting to observe the association between the quantification of gingipains and the antibacterial effects of the tau peptides on *P. gingivalis*.

Kobayashi et al. (2008) did not report their secondary or tertiary structures for any of the short peptides as their focus as on the antimicrobial assays. As such, this study is unique in that the antibacterial assays were carried out in parallel with ultrastructural assessment via TEM imaging.

### 5.3.2 Clinical relevance

*P. gingivalis*, has been linked to AD through the bacteria's gingipains, which can damage tau proteins and exacerbate AD-related neurodegeneration. Gingipains are toxic proteases that can fragment tau, a protein crucial for neuronal function, leading to its hyperphosphorylation and accumulation in the brain, a hallmark of AD. This damage to tau, coupled with the inflammatory response induced by *P. gingivalis*, contributes to the development and progression of AD. Gingipains also promote neuroinflammation by triggering microglial migration and the release of proinflammatory mediators. Inhibition of gingipain activity may

have the potential as a therapeutic strategy for both periodontitis and AD (Olsen & Potempa, 2014).

Physiological concentrations of tau and phosphorylated tau in human plasma has been reported in the low pg/mL range. A meta-analysis reportex an average plasma total tau in healthy populations of 3.07 pg/mL, and slightly higher levels of phosphorylated isoforms and N-terminal fragments in neurodegenerative disease (Ding et al., 2021). There values are several orders of magnitude lower than micromolar concentrations of the synthetic tau-derived peptides used in the present study. This suggests that there any AMP-like effects observed *in vitro* would require significant local concentration, accumulation or compartmentalization to exert antibacterial effects *in vivo*.

### 5.3.3 Future work

Further research needs to be undertaken to investigate the structure of these peptides in the presence and absence of a membrane. By confirming the peptides structures the research needs to be expanded to investigate the binding of these peptides to bacterial membranes Jung et al. (2010). The liposome model can be used to estimate the efficacy of antimicrobial compound. Wall et al. (1995) devised a model for investigating the ability of a peptide to bind to a model membrane when the peptide lacks a tryptophan residue using a fluorescein-phosphatidylethanolamine (FPE) probe (O'Toole et al., 2000; Hawrani et al., 2010). Based on these studies the antimicrobial action of the peptides will give an insight into its ability to bind to the membranes of target organisms which may involve specific lipids or membrane receptors. For cytotoxicity of the hexapeptide and other motifs, further research should be carried out on differentiated neuronal cells *in vitro* for up to 72-hour time points with exposure

to the various concentrations of tau peptides in triplicate with a known toxic compound for meaningful comparison.

## 5.5 CONCLUSION

Phosphorylated tau peptides A and B were shown to have cytotoxic effects on *P. gingivalis*. The tertiary structure of tau peptides B and C (in both non-phosphorylated and phosphorylated forms) confirm physical changes caused by post-translational modification. TEM investigations of tau peptides B, C, D, E and F showed that PHF or SF ability to self-aggregate and become incorporated to form longer fibers. Phosphorylated tau peptide C were observed to have clear stacking and twisting of the fibers, which may suggest the potential for hydrophobicity on the external part of the fiber, which may contribute to further aggregation of PHF or SF to produce larger aggregates and bundles of filaments leading to NFT formation. Non-phosphorylated Tau Peptides B, C, D, E and F as well as phosphorylated tau peptides B and C exhibited mainly β-sheet type structures, which is a shared characteristic of tau with Aβ. A potential link with tau, as a substrate for gingipains, is strengthened via the *in vitro* formation of PHF and SF, which leads to NFT formation. The present study highlights the plausibility of free tau being released, by gingipains, from microtubules which can lead to neuronal death. Subsequently, the release of free tau into the cerebral parenchyma would activate the innate immune responses and contribute to neuroinflammation (Morales et al., 2010; Kovac et al., 2011). Free tau may spread to connecting neurons (Dioli et al., 2017). This study supports preventative measures by removing the potential causative agent (*P. gingivalis* or its gingipains) at the primary oral site, which could impact periodontitis and AD pathogenesis.

# CHAPTER 6

## BIREFRINGENCE OF GINGIPAINS FRAGMENTED TAU PEPTIDES

The work presented in this chapter is fully published by the author of this thesis:

**Kanagasingam S**, von Ruhland C, Welbury R, Singhrao SK (2022) Antimicrobial, polarising light and paired helical filament properties of fragmented tau peptides of selected putative gingipains. J Alzheimers Dis. 89(4):1279-1291.

# BIREFRINGENCE OF GINGIPAINS FRAGMENTED TAU PEPTIDES

## 6.1 INTRODUCTION

In AD, tau protein can form PHFs and SFs which are major protein subunits of NFT lesions (Dominy et al., 2019). The previous chapter (Chapter 5) confirmed that the tau peptides either in the non-phosphorylated or the phosphorylated states, formed helical repeats of twists in their fibrils *in vitro* as demonstrated by high resolution TEM. This has confirmed that the physicochemical properties of the selected peptides represented the tau containing "VQIINK" and **"**VQIVYK" hexapeptide because they were in the gingipains fragmented tau peptides and were mapped to their microtubule binding domains in PHFs and SFs, representing the NFT lesion (Kanagasingam et al., 2020). This in turn is related to Braak staging (Braak and Braak, 1995), which is a system used to classify the progression of NFT pathology, a key hallmar of AD. The 3 types of neurofibrillary changes include neuritic plaques, neuropil threads and NFTs. The accumulation of neuropil threads and NFTs in the cerebral cortex present a well-defined pattern of distribution, which Braak and Braak (1995) developed into a neuropathologic staging system. This framework comprised of 6 successive stages, which was subsequently updated in 2006 to incorporate contemporary immunohistochemical techniques to increase its accuracy and applicability (Braak et al., 2006), refer Figure 6.1. More recently, the use of PET (Positron Emission Tomography) imaging to detect tau PET ligands has been developed to map tau accumulation in the brain of live patients, allowing longitudinal investigations (Macedo et al., 2023).

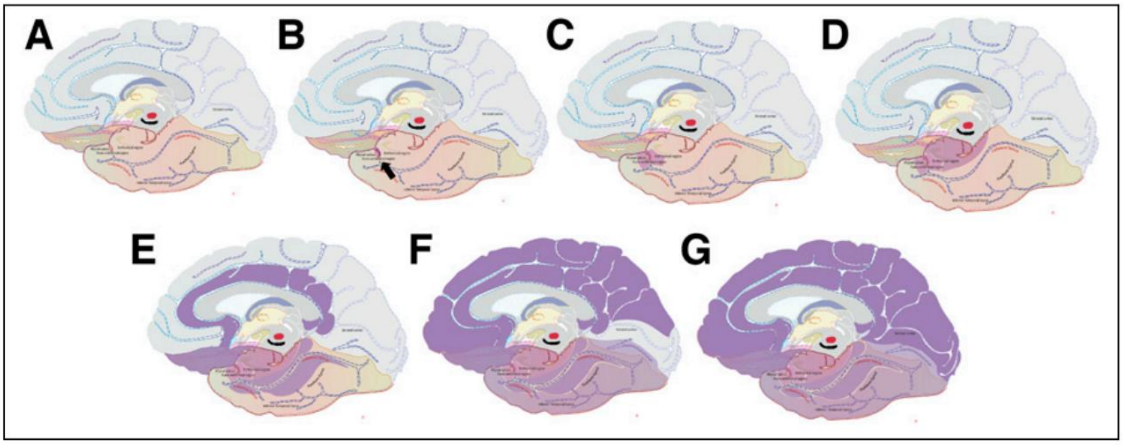


**Figure 6.1:** Images showing the topographic representation of Braak stages 0 (absence of tau accumulation) (A), I (B), II (C), III (D), IV (E), V (F), and VI (G) according to the original histopathologic descriptions, as observed on the sagittal section of the brain at the midline. The brain regions which have been affected have been coloured in different shades of purple (Image credit: Macedo et al., 2023).

Historically, the motif VQIINK seems to denote an area within the tau protein that causes the formation of fibrils and exhibiting Aβ-like properties. This is particularly interesting as the historian neuropathologist Divry proposed the occurrence of Aβ-like fibrils within NFT-bearing neurons but this was not widely accepted due to the confounding effect of the abundance of Aβ in AD brains (Beach, 2022). At the time, proving the Divry concept was difficult because of the lack of understand the pathophysiology of AD and the availability of modern research tools. However, Dominy et al. (2019) in their seminal study, identified colocalization of gingipain in tau tangles in human AD brains and their cell culture results confirmed that gingipains were indeed responsible for the cleaving tau. Furthermore, the researchers utilised mass spectrometry to identify specific sites of tau protein digestion by gingipains and the resultant sequence of the tau fragments. In parallel, they found that *P. gingivalis* infected mice exposed to gingipain-inhibitors significantly reduced both *P. gingivalis* load in the mouse brain as well as lower the host $A\beta_{1\text{-}42}$ response to the infection.

It is generally accepted that AD patients present with both extracellular Aβ plaques and intracellular tau within NFTs in the brain. Aβ has been implicated as the critical initiator of AD by triggering the cascade involving tau pathology and neurodegeneration, even though NFTs are more closely associated with neuronal loss and clinical symptoms (Arriagada et al., 1992). Although it has been presumed that Aβ and tau act independently, there is more evidence to suggest a possible synergistic effect (Bushe and Hyman, 2020). A number of clinical trials targeting Aβ reduction have failed to substantially improve clinical symptoms or slow down AD progression (Yiannopoulou et al., 2019). This has provoked questions regarding the inter-relationship between Aβ and tau, specifically is Aβ a component in the NFTs or is it tau-bound to NFTs?

Amyloid fibrils consist of polypeptide chains arranged in a twisted β-pleated sheet conformation. When amyloid is stained with Congo red and viewed under polarised light, they exhibit a typical apple-green birefringence (Howie et al., 2008). Historically, Congo red was used in the German synthetic dye industry, later gaining value as a histological stain and eventually, accepted as a diagnostic test in amyloidosis. Although it appears as red in ordinary illumination, it absorbs blue and green wavelengths, with a peak in the 'blue-green' (Howie et al., 2019). 'Birefringence' refers to a material that has 2 refractive indices, depending on its orientation in polarized light, thereby causing a colour shift. Divry and Florkin (1972) were the first to establish the principal diagnostic criteria of amyloidosis, which can be observed under the polarizing optical microscope for the apple-green birefringence from Congo red-staining (Cohen, 1967; Rosenblum, 2002). The birefringent characteristic of Aβ plaques is due to the parallel arrangement of the amyloid fibrils (Baumann et al. 2017). This formed the rationale for this study because it was

important to determine if the birefringence in NFT that Divry observed was due to intracellular Aβ and/ or tau.

### 6.1.1 Hypothesis:

Tau bound neurofibrillary tangles are birefringent due to their β-pleated sheet configuration.

### 6.1.2 Aims and Objectives

Aim:

To investigate if NFTs demonstrate birefringence and to confirm if this is due to intracellular amyloid-β or to tau binding to NFTs.

Objectives:

To assess the presence or absence of birefringence within the tau peptides via polarising microscopy

### 6.1.3 Ethical approval

This project was approved by the UCLan Biological Safety Officers (BSO) committee.

### 6.1.4 Funding award

TC White Young Researcher Award (2018-2021), RCPSGlasgow, £10,000.00

## 6.2 MATERIALS AND METHODS

This aspect of the laboratory investigation was outsourced to Dr Christopher Von Ruhland, Central Biotechnology Services, Cardiff University, due to the lack of a polarizing microscope at the University of Central Lancashire. However, the planning and the instructions were entirely those of the author of this thesis. The Congo Red birefringence assay is a histochemical technique employed to detect and visualise amyloid fibrils *in vitro*. Birefringence observation using polarised light microscopy allows detection of amyloid fibrils which would appear bright, apple-green. The technique used for dye preparation and the method of its uptake was based on the neuropathology laboratory method that applies to detecting Aβ in postmortem AD brain tissue sections (Jin et al., 2003). The methodology has been described in detail by Kanagasingam et al. (2022b).

### 6.2.1 Source of reagents

The laboratory reagents used in this chapter were provided by the outsourcing company. This included Congo Red solution, Amyloid Stain Kit (Merck Life Science, Dorest, UK Ltd), 50% ethyl alcohol in water (Thermo Fisher Scientific, Cambridge, UK), sodium chloride (Thermo Fisher Scientific, Cambridge, UK), mounting medium (Merck Life Science, Dorset, UK Ltd), xylene (Sigma-Aldrich, Dorset, UK).

### 6.2.2 Congo Red Staining and Polarising Light Microscopy

Droplets (25µL) of non-phosphorylated and phosphorylated-tau reconstituted peptides were placed onto Vectabond™-treated glass slides and allowed to air dry. Peptides firmly bonded to glass slides were dipped for 10 mins in a Coplin jar containing the filtered alkaline Congo Red

stain (50% Alcohol saturated with sodium chloride). The excess dye was washed off in water. The slides were allowed to briefly air dry and then dehydrated in absolute alcohol, cleared in xylene (3x for 1 min) and mounted in Gurr's neutral mounting medium under a coverslip. Samples were then examined for the presence of green birefringence (using the same wavelength range of 455 to 600 nm, as is typically used for Congo Red stained Aβ within AD brain tissue sections) through crossed polarisers on an Olympus BX51 light microscope (Olympus Optical Co. UK Ltd, England, UK). Photomicrographs were captured with a Zeiss Axiocam and Axiovision software (Carl Zeiss Vision GmbH, Hallbergmoos, Germany).

## 6.3 RESULTS

Both tau peptides A and G, in their unphosphorylated and phosphorylated states failed to bond permanently to the glass slides due to their solubility. During the procedure, the peptides washed off completely. Of the remaining tau peptides, B, C, D, E and F in their non-phosphorylated and phosphorylated forms produced the apple green birefringence through crossed polarisers over a wavelength range of 455 to 600 nm.

Non-phosphorylated peptide B exhibited a random fibrillar appearance with blue-green birefringence which is typical of amyloid deposits (Figure 6.2a). While the phosphorylated form of tau peptide B remained birefringent, observed as a darker green shade, a lattice-like crystal structure which was quite distinct from the non-phosphorylated peptide B was noted (Figure 6.2b). Non-phosphorylated tau peptide C also displayed a lattice crystal structure, with an apple green hue (Figure 6.2c) which appeared close to the apple green birefringence seen in Aβ fibrils. The phosphorylated tau peptide C (Figure 6.2d) presented with a blue-green birefringence with random aggregating short fibrils. Under polarising light, red and orange colours were noted across phosphorylated peptide B, non-phosphorylated peptide C and

phosphorylated peptide C (Figure 6.2b-d). Tau peptide D in its non-phosphorylated form (Figure 6.2e) displayed greenish birefringence with lattice structures, including some overlapping red and orange lattices. This may be the result of overlapping wavelengths due to Congo Red dye retention in between the fibrils. A greenish birefringence which appear as aggregated clumps, devoid of lattice structures were observed with the non-phosphorylated peptides E and F (Figure 6.2f and g)

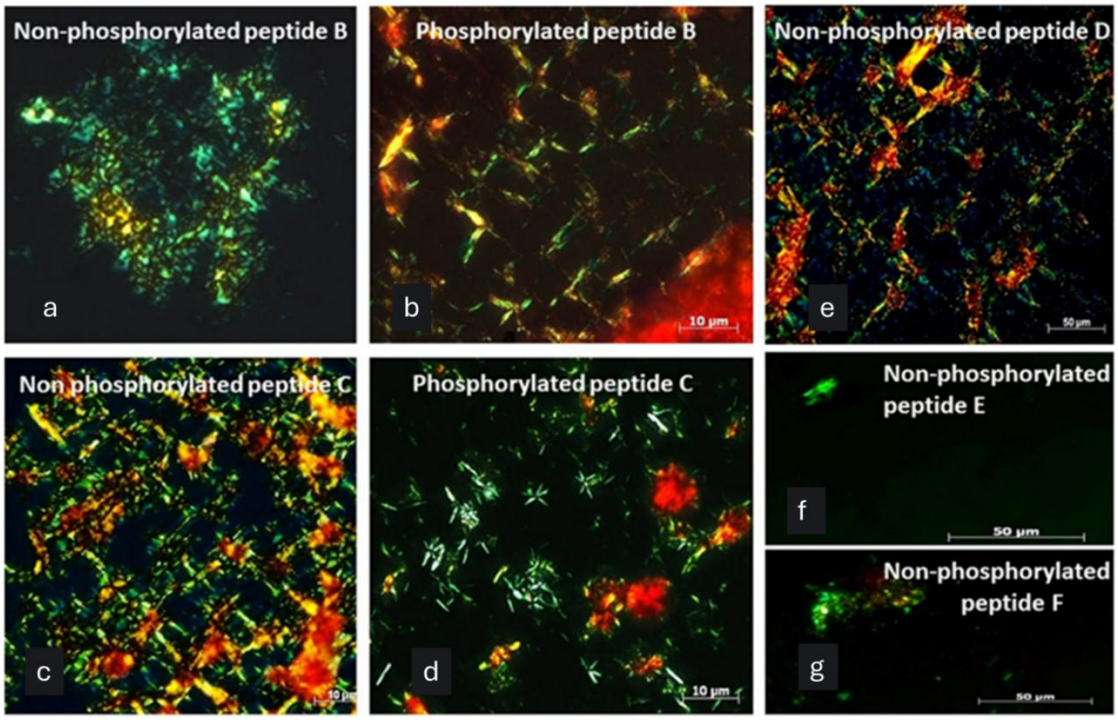


**Figure 6.2**: Congo Red staining and polarizing light microscopy showed an apple-green birefringence in tau peptides B and C in their non-phosphorylated and phosphorylated forms (a-d), as well as peptides D, E and F in their non-phosphorylated form (e-g). Tau peptide B in its non-phosphorylated form (a) underwent aggregation to produce a blue-green birefringence. The phosphorylated tau peptide B remained birefringent with deeper green shade (b). Tau peptide C (non-phosphorylated) displayed a lattice crystal structure, with an apple green birefringence (c). Phosphorylated peptide C (d) produced a blue-greenish birefringence, however, the lattice structure appeared to have been disrupted. Tau peptide D in its non-phosphorylated form (e) produced greenish birefringence, including visualisation of the lattice structure. Non-phosphorylated peptides E and F (f and g) exhibited a greenish birefringence which appeared as aggregated clumps, which were devoid of lattice-like structures (Kanagasingam et al., 2022b).

## 6.4 DISCUSSION

The specificity of the Congo Red methodology to be successful relies upon the β-pleated sheet structure configuration of Aβ and the alignment of the dye molecules to it. Since the tau peptides containing "VQIINK" and **"**VQIVYK" hexapeptide motifs, which formed helical twists *in vivo* (see Chapter 5), had retained their propensity to form helical twists *ex vivo* provided the extra confidence that the Congo Red dye would bind to the selected tau peptides and thereby show birefringence. The results clearly demonstrate that pure tau is a reason for the previously observed phenomena that NFTs too can show birefringence under polarising light which is clearly similar to that of the Aβ (plaques) in AD brains.

The monomeric Aβ peptides are typically degraded by the by proteolytic mechanisms in keeping with the dynamic balance of sustaining cell metabolism (Forman et al., 2004). Upon aging, however, this process may be inhibited and instead, the monomeric peptides can aggregate to form oligomers, eventually leading to the accumulation of amyloid fibrils. At a molecular level, these fibrils are characterized by their β-pleated sheet configuration, which are found in the pathognomonic plaques in AD. As for tau, the originally unfolded random coil tau protein has been reported to form fibrils with a regularly aligned β-pleated sheet configuration (von Bergen et al., 2005). The tau fibrils, which are found mainly within neuronal cytoplasm, are the main components of the NFTs which disrupt the normal function of neurons, similar to Aβ (Michael et al., 2014).

Although the TEM appearance alone cannot confirm the hydrophobic nature of the tau peptides, there is some evidence to suggest that twisted, stacked fibrillar morphologies are consistent with lateral association of protofilaments, which could be driven by lateral hydrophobic packing, steric-zipper interfaces and van der Waals interactions (Taylor &

Staniforth 2022; van Gils et al., 2020; Liberta et al., 2019). However, as multiple forces (including electrostatic interactions, salt screening and PTMs) modulate fibril morphology, the TEM observation seen in this study does not determine the mechanistic contribution of hydrophobicity in our tau peptide system.

### 6.4.1 Challenges, strengths and limitations

As far as the author is aware, this was the first study which analysed both non-phosphorylated and phosphorylated tau peptides utilising Congo red and birefringence assays. It proved to be challenging attempting to mount and bond the tau peptides onto the glass slides. Peptide density could have been optimised in order to more effectively attach to the glass slides. This could not be done in the present study as there were limited amounts of tau peptide remaining at this final stage of the experimentation.

Historically, the primary diagnostic criterion for amyloidosis is the identification of so-called ‘apple-green birefringence’ in Congo red -stained tissue sections using a polarising optical microscope (Sipe and Cohen 2000, Rosenblum 2002, Hawkins et al. 1990). However, the visual characterisation of amyloid is not an exact science despite the assay's endurance (Hawkins, et al. 1990). At the stage of specimen preparation, Congo red staining can be technically sensitive as it can be prone to discrepancies in staining intensity and quality due to variations in amyloid amount (Yang et al. 2024). Plastic coverslips can scatter light and inconsistently polarise in a pattern that can be detrimental to examination under cross polarised light. This technique can also exhibit some inter-observer variability (El-Maenawy et al. 2019). However, this was mitigated by the fact that this work was outsourced to a very experienced colleague, with whom the author had maintained close communication and collaboration with regards to the standardization of procedures and interpretation.

The methodology could have been improved by including a positive and negative control i.e. slides containing known amyloid and unstained peptides. This could have confirmed the specificity of the staining. False positives can occur when staining tissues, however this was not a concern in this study due to the use of the peptides. Alternatively, Congo red fluorescence microscopy could have been considered as it has been reported to have a higher sensitivity. It has been suggested that the bright fluorescence may make it easier to identify amyloid deposits (Song et al. 2024).

### 6.4.2 Clinical relevance

Neuronal axons have the highest concentration of functional tau, which aids in microtubule assembly, and is necessary for both axonal transport and the structural integrity of neurons (Goedert et al., 1989). Hyperphosphorylated tau undergoes additional post-translational changes in pathological circumstances, which impairs microtubule interaction, resulting in aggregation into intracellular amyloid deposits (Gong & Iqbal, 2008; Wesseling et al., 2020). Tau amyloid fibrils serve as seeds that trigger other tau monomers to aggregate to produce amyloid (Clavaguera et al., 2009; Frost et al., 2009). This seeding effect can spread to functionally-connected neurons to continue the clustering of tau (Frost et al., 2009).

This study has shown that NFTs, composed of hyperphosphorylated tau protein, demonstrated birefringence and confirmed the presence of intracellular amyloid-β. This is in line with assertions by previous researchers that Aβ can accumulate in neurons before the formation of extracellular Aβ plaques. This can potentially act as a precursor to plaque formation and neuronal damage (Bi et al., 2019; Kobro-Flatmoen et al., 2023). This adds to our understanding

of the complex relationship between Aβ and tau. This is essential for developing effective therapies for AD, as interventions which have targeted Aβ or tau individually have not achieved substantial breathroughs (Zhang et al., 2021).

### 6.4.3 Future work

Due to the multiple and complex mechanisms involved in the interaction between Aβ and tau protein, further research may focus on the co-localisation of monomeric, oligomeric Aβ and $A\beta_{1\text{-}42}$ as well as phosphorylated tau via immunofluorescence analyses. Laboratory techniques which can accurately characterise the proximity of molecules such as Fluorescence Resonance Energy Transfer (FRET) microscopy can be considered for human brain tissue-based research. In fact, the next generation of FRET-based biosensor cells has been proposed as a novel tool to study tau seeding activity in AD, which may shed light on early tau-related pathological events (Lathuiliere et al., 2023).

## 6.5 CONCLUSION

The study attempted to evaluate the birefringence properties of tau *in vitro*. The tau peptides investigated clearly demonstrated birefringence at the polarizing light wavelength which was similar to that of insoluble Aβ. The hypothesis is accepted in this instance.

# CHAPTER 7

# GENERAL DISCUSSION

# GENERAL DISCUSSION

## 7.1 Rationale for research: AD and Recognised Risk Factors

There is a misconception that dementia is a natural part of aging. Although aging is a major risk factor for AD, it is not an inevitable outcome and multiple modifiable as well as non-modifiable factors have been implicated in AD pathogenesis (Peters 2006). The recognition of modifiable risk factors which include lifestyle and health-related considerations is crucial for developing effective preventive strategies. A recent Lancet Commission report expanded the list of modifiable risk factors for dementia from the original 12 to 14; quality of education in early life, social isolation, air pollution, traumatic brain injury, hearing loss, depression, high blood pressure, diabetes, obesity, physical inactivity, smoking, excessive alcohol consumption, uncorrected vision loss and high cholesterol (Figure 7.1). This report revealed that 45% of cases of dementia could potentially be delayed or decreased, with appropriate interventions targeted at specific risk factors, which marked a 5% increase from their 2020 findings (Livingston et al. 2024).

'Dental disease' and 'Infection and systemic inflammation' were considered potential risk factors with insufficient evidence to be included. The authors stated that there was a paucity of consistent, high-quality evidence linking oral disease to dementia due to the life-course accumulation of dementia risk, and the extended presymptomatic build-up of pathology which would necessitate large-scale longitudinal epidemiological studies (Livingston et al. 2024). It is not surprising that a recent search of the Alzheimer's organisations confirmed that oral health is not considered a risk factor for AD; Alzheimer's Society (https://www.alzheimers.org.uk/), Alzheimer's Association (https://www.alz.org/),

Alzheimer's Disease International (https://www.alzint.org/about/), Alzheimer's Research UK (https://www.alzheimersresearchuk.org/) and Alzheimer Europe (https://www.alzheimer-europe.org/). The lack of recognition of oral health as a risk factor for AD has long-term implications on public health and policies. Ignoring preventable oral disease can perpetuate existing health inequalities as oral health problems disproportionately impact vulnerable and lower socio-economic populations. The lack of awareness of the bidirectional links with AD mean preventive measures and early interventions may not be put into action by policymakers nor the public (Patel et al. 2021). This is one of the growing concerns in the dental fraternity as the bidirectional relationship of poor oral health and multiple systemic diseases (including diabetes, cardiovascular disease, MetS, adverse pregnancy outcomes and AD) has been overlooked in healthcare (Ocbe et al. 2025).

The first researchers to detect *P. gingivalis* LPS in post-mortem AD brains were Poole et al. (2013), led by Dr Sim Singhrao from the University of Central Lancashire. In their study, brain tissue from age-matched individuals with and without AD were obtained from the Brains for Dementia Research network (provided by the Newcastle Brain Tissue Resource). Immunolabeling and immunoblotting detected the presence of LPS from *P. gingivalis* in 4 out of 10 AD subjects, however, no evidence of LPS from *P. gingivalis* was identified in the non-AD control tissues. Six years later, the landmark study by Dominy et al. (2019), reported *P. gingivalis* Kgp (lysine-specific gingipain) and Rgp (arginine-specific gingipain) antigens in post-mortem AD brain tissues. Although, this study also found lower amounts of gingipains in the control brain tissues. These were the studies which influenced and shaped the scope of this original research. The experimental work has been carried out to strengthen the evidence which highlights the role of periodontal and endodontic infections in the pathogenesis of AD.

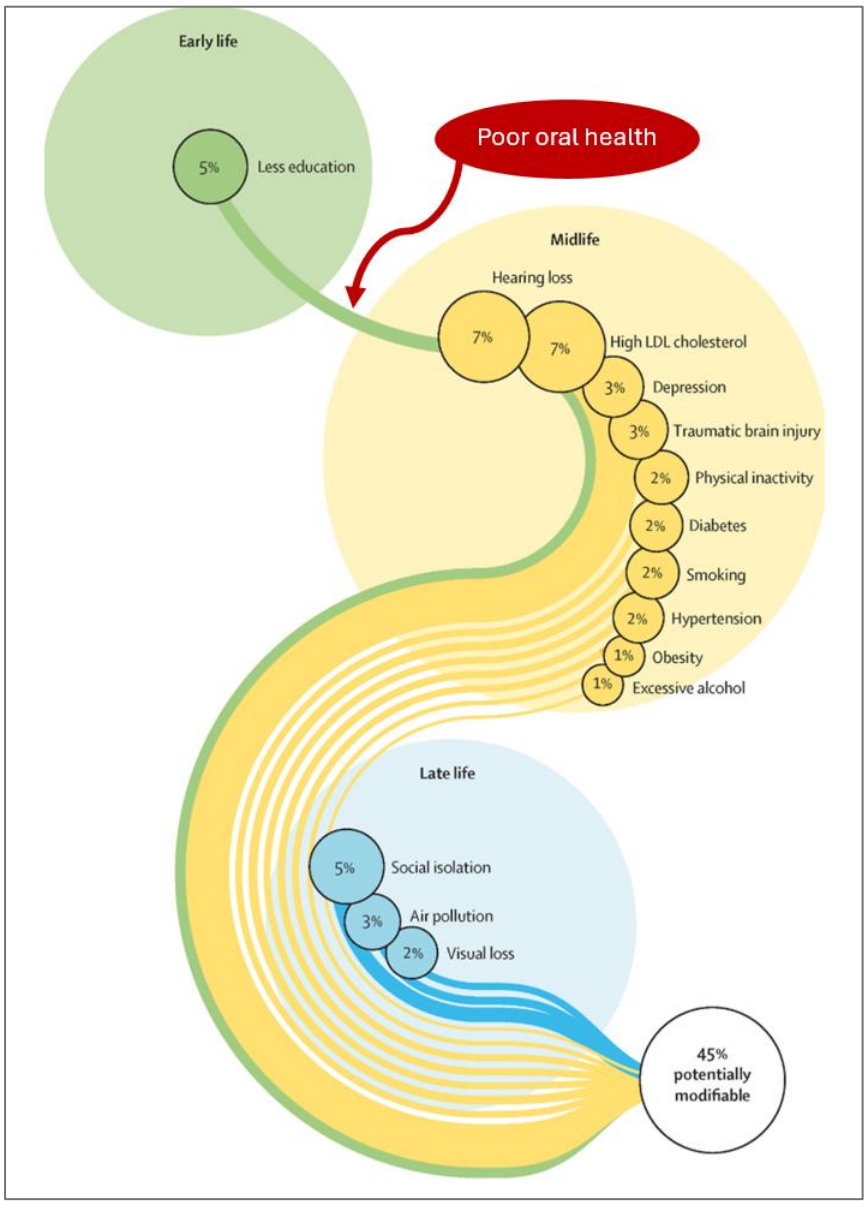


**Figure 7.1:** Potentially modifiable risk factors for dementia which have expanded from 12 factors to 14, with the addition of vision loss and high cholesterol as potentially modifiable risk factors, irrespective of the APOE genetic status. The percentages shown represent a reduction in cases of dementia if the risk factor was eliminated. Based on the present study results and accumulated evidence thus far, the link to oral disease has been included (Image adapted from Livingston et al. 2024).

## 7.2 Aβ expression in human oral tissues

Aβ aggregates are the main constituents of AD senile plaques. Aβ peptide plays a significant role in the onset and progression of AD, with a continued focus on 'Amyloid Cascade Hypothesis'. Although Aβ can be produced in healthy subjects, under certain conditions, this molecule can undergo aggregation and instigate disease progression (Zhang et al. 2023). Aβ oligomers are considered neurotoxic as it can directly disrupt synaptic function through various mechanisms, including oxidative stress, excitotoxicity (overstimulation of neurons caused by excessive stimulation of glutamate receptors leading to an influx of calcium) and mitochondrial dysfunction (Nordengen et al. 2019). Numerous cell types, including neurons, astrocytes, neuroblastoma cells, hepatoma cells, fibroblasts, and platelets, can produce Aβ (Figure 7.2).

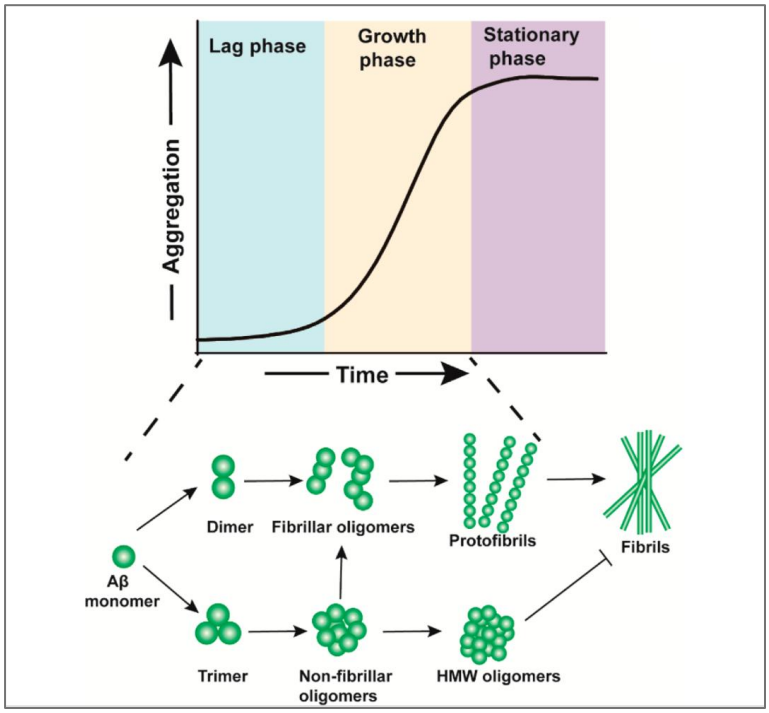


**Figure 7.2:** Schematic drawing shows Aβ aggregation involving three phases from Aβ monomers to mature fibrils: an initial lag phase, followed by a growth phase and then a final stationary phase. Aβ oligomers undergoing fibril generation, mainly exist in the lag and growth phases. Some Aβ fibrillar oligomers, can form Aβ dimers, followed by protofibrils and mature fibrils. Aβ trimers (termed non-fibrillar oligomers), are structurally different from fibrillar aggregates, but can form fibrils via structural conversion (Image and legend adapted from Huang and Liu 2020).

More evidence is emerging on the duality Aβ's role as an Antimicrobial Peptide (AMP). Moir et al. (2018) discussed this eloquently by referring to the 'antimicrobial protection hypothesis of AD'. The pathogenesis of Aβ is reframed in the antimicrobial protection paradigm as dysregulated innate immune response rather than aberrant stochastic or unpredictable behaviour. Researchers have previously reported that Aβ functions as an AMP as part of the innate immune defence mechanism against microbial pathogens (Soscia et al. 2010, Kumar et al. 2016). Not only does Aβ resemble human cathelicidin AMP (LL-37), but it has also been shown to inhibit bacterial growth of gram positive and negative bacteria, *C. albicans* as well as viruses e.g. influenza A and Herpes Simplex Type1 (Soscia et al. 2010, White et al. 2014, Bourgade et al. 2016). As such, it is not surprising that immune challenges would activate the central nervous system antimicrobial response, leading to upregulation of Aβ (Moir et al.2018). Aβ oligomers mediate binding, anti-adhesion, agglutination and entrapment activities against pathogens (Kumar et al. 2016). As an AMP, Aβ can also modulate the adaptive immune pathway and induce cytokines and regulators of host cell differentiation (Mansour et al. 2014). It is also believed that dysregulation of AMP immunomodulatory activity contributes to the pathophysiology of numerous chronic inflammatory diseases, especially linked to neurodegenerative diseases (Moir et al. 2018). Interestingly, peripheral tissues may be involved in the brain's and its vasculature's circulating amyloid pool, contributing to AD pathogenesis, as Aβ can bind to a variety of plasma and membrane proteins. Aβ deposition can occur in non-neural tissues and blood vessels of AD patients, including their skin, subcutaneous tissue, skeletal muscle and intestines (Joachim et al. 1989, Roher et al. 2010).

The results presented in Chapter 2 reported the detection of Aβ in human tooth tissues and naturally formed plaque biofilm for the first time (Kanagasingam et al. 2022). In line with Moir et al. (2018) 'antimicrobial protection hypothesis of AD', the host appears to have responded to the periodontal and endodontic infection by releasing Aβ as an innate immune response, not observed in the healthy teeth. The serial histological sections acted as their own controls in a way, as immunolocalisation of the insoluble Aβ consistently coincided with infected regions of the tooth tissue. Prior to our publication, Japanese researchers had confirmed the expression of Aβ Precursor Protein (APP) in macrophages from inflamed gingival tissue samples collected during periodontal flap surgery and tooth extraction (Kubota et al. 2014).

Similar to the Chapter 2 study, all subjects from the Kubota et al. (2014) study were systemically healthy, however, in our study, the inclusion criteria were patients between 50-90 years old, whereas the Kubota et al. (2014) had a mixed age range including 35 year-old subjects. Their microarray analyses and the Quantitative Reverse Transcription Polymerase Chain Reaction (qRT-PCR) observed upregulation of transcripts for APP (p, C1QA (gene that codes for the A-chain polypeptide of the complement system component, C1q) and IL-1β in infected periodontal soft tissues. This suggests that genes which are commonly elevated in periodontitis and AD were expressed in the infected gingival samples. The authors made the case that the increase in APP expression in diseased gingival tissues in healthy individuals implies a pathological as well as a physiological role, including antimicrobial (Otsuka et al. 1991, Kummer et al. 2002, Kubota et al. 2014). The detection of both APP (a protein which is cleaved by β-secretase, followed γ-secretase to release Aβ) and Aβ in oral tissues suggests that a similar immunological response may be involved in both periodontitis and AD (Kubota et al. 2014, Kanagasingam et al. 2020, Kanagasingam et al. 2022).

## 7.3 *P. gingivalis*, cytokines and amyloidogenic processing

Due to limitations imposed by the IRAS/ethical approval, the experimental procedures in Chapter 2 could not employ PCR techniques to identify the bacteria within the infected teeth and dental plaque. It could only be surmised via morphological analysis using SEM and the Gram stains that *P. gingivalis* (a Gram-negative, rod or coccobacillus, anaerobic bacteria) may have been present. *P. gingivalis* is not only a keystone pathogen in periodontitis but also has a high prevalence in primary endodontic infections (Siqueira et al. 2008, Hajishengallis et al. 2012). Considering the previous findings of APP and Aβ detection within infected oral tissues (Kubota et al. 2014, Kanagasingam et al. 2022), it was important to assess if *P. gingivalis* virulence factors had the ability to modulate amyloidogenic processing in neuronal cells to produce Aβ.

Keeping with the Amyloid Cascade Hypothesis, APP processing and cleavage can occur via amyloidogenic and non-amyloidogenic pathways. The non-amyloidogenic pathway involves APP cleavage by α-secretase in the middle of the Aβ domain, producing soluble APPα (sAPPα), C-terminal fragment (CTα or C83) and p3(a truncated Aβ peptide), considered an innate mechanism. This pathway does not generate the full length Aβ peptides which are associated with AD amyloid plaque formation (Patterson et al. 2008). Conversely, the amyloidogenic pathway generates a long secreted form of APP (sAPPβ), C-terminal fragments (CTFβ and C99) and Aβ(40 and 42). Of the two Aβ isomers, Aβ-42 is more prone to aggregation, form fibrils leading to AD amyloid plaques (Shen et al. 2023).

The shared molecular mechanisms across AD and periodontitis involve dysregulation of pathways of inflammatory mediators, immune response, oxidative stress as well as changes to the extracellular matrix (Martinez-Garcia et al. 2024). The elements of inflammatory mediators

and immune response were further investigated in the cell culture laboratory study in Chapter 3, whereby the human neuroblastoma SH-SY5Y CRL-2266$^{TM}$ cell line was used to determine the effects of *P. gingivalis* conditioned medium containing virulence factors, in the presence and absence of cytokines. The cytokines chosen, IL-1β, IL-6, and TNF-α were shown to be more prevalent in the gingival crevicular fluid of patients with periodontitis (Neurath and Kesting 2024). The SH-SY5Y cell line was exposed to *P. gingivalis* growth medium which contained the virulence factors, specifically the proteolytic enzyme, gingipains which cleave APP to generate Aβ. In combination with the cytokines TNF-α and IL-1β, the results showed that APP breakdown was accelerated. Western blotting was carried out to detect the resultant fragments after APP cleavage. The cytokines appeared to have amplified the detection of the C99 and C83 fragmentation.

C83 is membrane-bound fragment, generated after cleavage of APP by α-scretase and is generally considered non-toxic. Researchers have confirmed the neuroprotective effect of sAPPα and some have proposed that C83 may have similar effects and could decrease the levels of C99. By producing β-secretase, C99 is a key intermediate in the production of Aβ (Capone et al. 2021). Its accumulation can disrupt mitochondrial function, contribute to endosomal and lysosomal dysfunction, neuroinflammation and cognitive impairments (Vaillant-Beuchot et al. 2020). Chapter 3 demonstrated that infection and inflammation can both lead to an excessive accumulation of Aβ1-40/42, leading to AD amyloid plaque formation (Kanagasingam et al. 2022).

Acute short-lived neuroinflammation has been reported to have no long-term effects on neuronal health, as moderate microgliosis can have beneficial effects in removing neurotoxins,

cellular debris and necrotic cells. On the other hand, chronic neuroinflammation in AD involves persistent activation of microglia and release of inflammatory mediators. In a constant microgliosis and astrogliosis, the inflammatory cycle is perpetuated, leading to further elevated levels of cytokines and chemokines (Rogers et al. 2002, Rivest 2009, Dzamba et al. 2016, Domingues et al. 2017). Cytokines and chemokines promoters or suppressors disease. They can impact APP proteolytic processing by affecting secretase enzyme activities, Aβ production and its deposition into senile plaques (Figure 7.3).

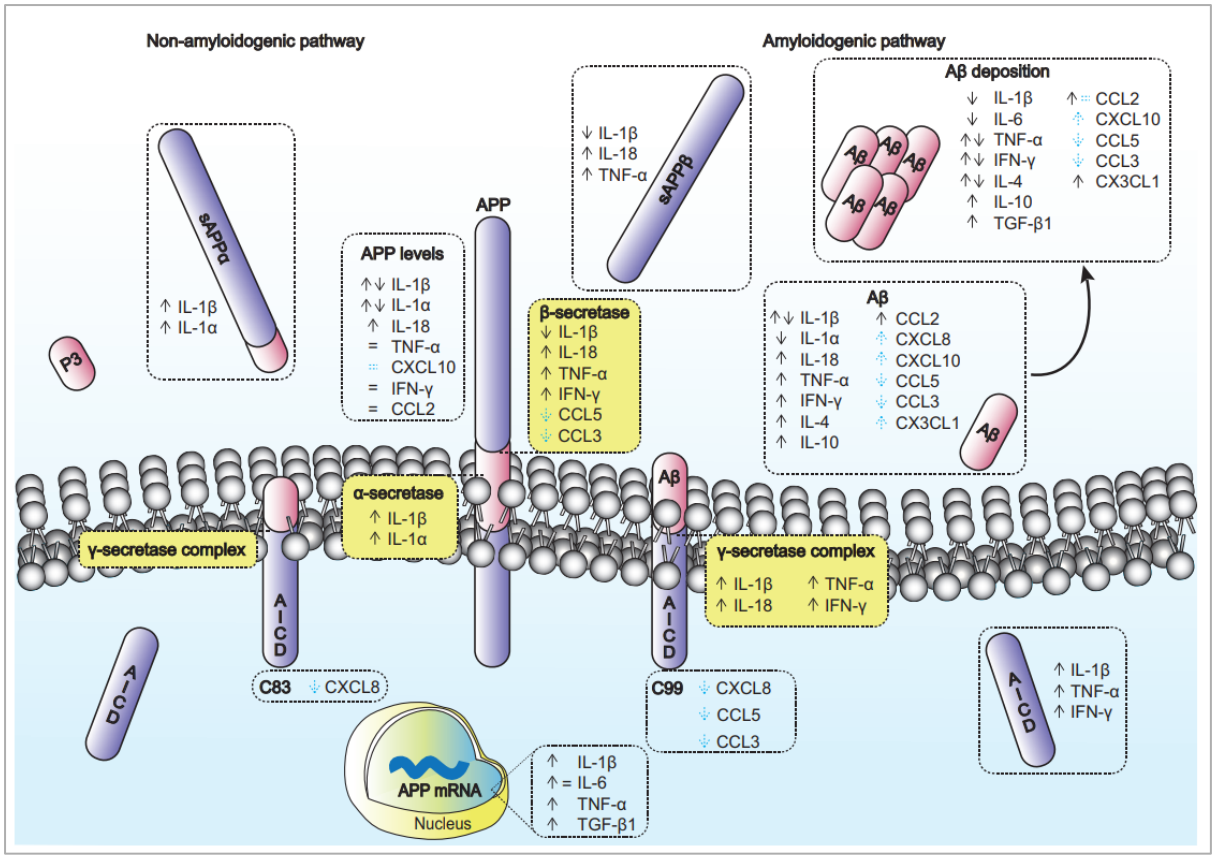


**Figure 7.3:** The impact of chemotactic and pro-inflammatory cytokines is shown on APP and Aβ peptide, including both non-amyloidogenic and the amyloidogenic pathways, which can lead to Aβ production. The arrows and equal symbol represent the various effects of cytokines and chemokines on APP, fragments produced by APP cleavage (e.g. sAPPα, sAPPβ and APP intracellular domain, AICD), APP secretases (α-secretase, β-secretase and γ-secretase) and on Aβ and its deposition. The light blue dashed arrows and equal symbol represent the putative effects based on chemokines receptor KO/deficiency data (Image from Domingues et al., 2017).

## 7.4 Periodontitis, AD and associated comorbidities

Evidence continues to build to strengthen links between periodontitis various systemic inflammatory conditions including cardiovascular disease, diabetes, respiratory diseases, rheumatoid arthritis, adverse pregnancy outcomes and AD (Grossi and Genco 1998, Preshaw et al. 2012, Martinez-Garcia et al. 2024). A recent integrative bioinformatics study conducted a comprehensive literature and biological database mining to systematically identify diseases sharing associated genes, proteins or molecular pathways with periodontitis. The authors reported significant molecular overlaps between periodontal disease and systemic conditions, such as cardiovascular disease, diabetes mellitus, rheumatoid arthritis, and inflammatory bowel disease. Hub genes revealed in the periodontitis comorbidity network such as TNF, IL6, IL10 and NOS3 were shown to be highly implicated (Martinez-Garcia et al. 2024). Another *in silico* analysis integrated experimental transcriptomic data from AD and periodontitis revealed shared molecular linkages including six crosstalk genes; C4A, C4B, CXCL12, FCGR3A, IL1B, and MMP3, as well as the 'Mitogen-activated protein kinase'(MAPK) pathway. The MAPK signalling pathway is the upstream signalling intermediate to cytokines such as TNF-α, IL-1β and IL-6 (Chi et al. 2006). These immune-inflammatory mediators are considered primary links between periodontal disease and AD, which have been substantiated by experimental data from Chapter 3 as well as other studies (Gu et al. 2020, Fu et al. 2023).

In order to investigate the comorbidities associated with both periodontitis and AD, a mouse model was utilised as reported in Chapter 4. The effect of *P. gingivalis* (W83) oral infection on the development of AD pathophysiology were investigated in obese, diabetic (db/db) mice. Although Aβ and NFTs were not detected via methamine silver impregnation, which was opposed to the findings of Illievski et al. (2018) and D´ıaz-Zu´niga et al. (2020),

neuroinflammation was consistently observed across the experimental groups in our study. It would have been interesting to quantify the microglial cells using densitometric analysis (Khakpour et al. 2022), however, a qualitative approach identified consistent findings of astrogliosis and microgliosis. The mice in our study were sacrificed at 16 weeks, whereas Illievski et al. (2018) culled the mice at 23 weeks. Our study induced periodontitis with $10^9$ CFU/ml of *P. gingivalis* W38, similar to Illievski et al. (2018), however, they carried out 'chronic application', specifically 2 x 50 µl, 3 times per week for 22 weeks. It may be surmised that by increasing the bacterial load and frequency of application, as well as allowing more time for 'aging' and continuous chronic inflammation, Aβ and NFTs deposition may occur. The addition of *F. nucleatum* made our study unique as antibodies to this 'orange complex' bacteria have been reported to be significantly higher in serum from AD patients compared to healthy controls (Sparks Stein et al., 2012).

Epidemiological and experimental evidence have established the bidirectional relationships between periodontitis, diabetes, and obesity (Suvan et al. 2015, D'Aiuto et al. 2018, Marruganti et al. 2023), which points to a multimorbid three-way relationship. This interplay is seen to overlap with risk factors for AD, sustained by systemic inflammation, insulin resistance and metabolic dysfunction as well as lifestyle-related risk factors (Ebrahimpour et al. 2020). Based on the available evidence, preventive measures aimed at tackling the modifiable risk factors can lower the risk of neuroinflammation in individuals with comorbidities, which could decrease their risk of developing AD (Greenberg et al. 2012).

## 7.5 *P. gingivalis* and Tau peptides

Historically, the Amyloid Hypothesis has been the focus of AD research and therapeutic strategies (Hardy and Selkoe 2002). The extensive neuropathological data from sporadic AD

postmortem brains and the modest outcomes of anti-amyloid treatments have provoked debate on alternative aetiological factors (Braak and Del Tredici 2015, Huang et al. 2020). In AD, Aβ plaques accumulate extracellularly from aggregated Aβ peptides released from neurons, whereas tau, which are part of the neuron's cytoskeleton, accumulates intracellularly. Hyperphosphorylation of tau causes disassociation from microtubules, clumps together to form NFTs, resulting in neuronal death (Hardy and Selkoe 2002, Kametani and Hasegawa 2018).

It is interesting to note that tau pathology arises much earlier than Aβ plaques, even within the first few decades of life. Aβ pathology appears to appear later in life, peaking after 60 years of age (Figure 7.4a and b). A multi-centre study of 1431 participants across the AD clinical spectrum had tau positron emission tomography (PET) scans, which were compared to MRI and Amyloid PET markers, including the Mini-Mental State Examination (MMSE) evaluation. Tau PET tracers demonstrated accurate prognostic utility, meaning tau may have potential use as a prognostic marker during the prodromal and preclinical stages of AD (Ossenkoppele et al. 2021). This is in line with Braak and Braak (1991) reporting that tau pathology correlates better than Aβ to the clinical stages of AD.

Chapter 5 builds on the existing evidence by focussing on the impact of tau fragments cleaved by gingipains on the activities of *P. gingivalis*. Gingipains' crucial contribution to *P. gingivalis* virulence including tissue adhesion, degradation of host immune proteins (e.g. CD14), pro-inflammatory effects and disruption of apoptotic cell clearance are well established in the literature (Grenier et al. 2003, Guo et al. 2010, Kinane et al. 2012). Questions arose regarding the possibility of gingipains digesting host proteins to form amino acids which could be a source of nutrients to the bacterium as described by Imamura (2003). Dominy et al. (2019) provided significant pieces to the puzzle, as they were the first to convincingly demonstrate

that gingipains could cleave tau peptides in SH-SY5Y cells, with some of the released peptides forming NFTs. Our study sought to firstly, confirm if gingipains fragmented tau peptides would inhibit or enhance the growth of *P. gingivalis* via antibacterial assays. Secondly, it was important to assess the structure of the tau peptides to confirm if they would form helical twists, linked to PHF and SF which could lead to NFT formation.

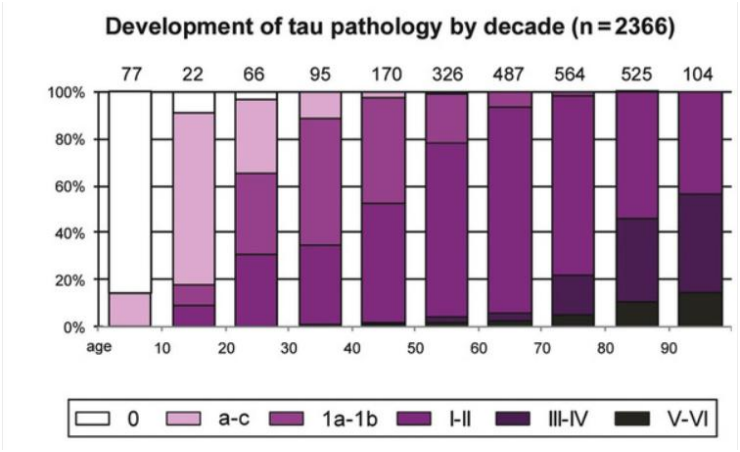


(a)

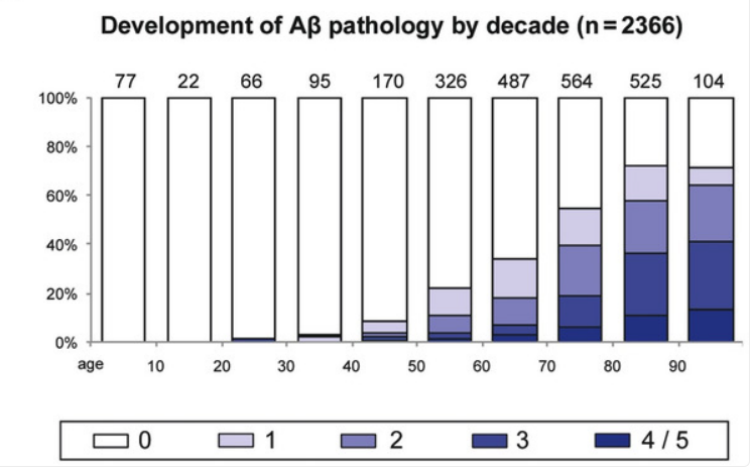


(b)

**Figure 7.4:** The bar charts show the frequency of fibrillar tau pathology in the human brain across the decades of lifespan. White columns indicate an absence of abnormal tau. The colour-coded key and columns in purple shades show the frequency of cases at all stages of AT8-positive tau lesions (a). The number of cases are presented directly above the columns for each decade of life. The frequency of Aβ pathology are shown in columns in blue shading, which show the frequency of subjects at various Aβ plaque phases (Image credit: Braak and Del Tredici 2015, Arnsten et al. 2020).

At the time of writing, our study was the only experimental work which reported on the antimicrobial influence of phosphorylated and non-phosphorylated tau peptides and *P. gingivalis*. All non-phosphorylated tau peptides showed no significant effects on the growth of *P. gingivalis*. Phosphorylated tau peptides A and B, without the hexapeptide motif and with VQIINK motif respectively, were found to be cytotoxic to *P. gingivalis*. Phosphorylated tau peptide C, which also had the similar VQIINK motif showed no antimicrobial effects. These results rejected Imamura's suggestion that gingipain cleaved proteins may provide nutrition to P. gingivalis. Our results agreed with Kobayashi et al. (2008), whose research team synthesised tau peptides derived from inter-repeat binding domains and proline rich regions, which are important for microtubule interactions. Significant inhibition of *Staphylococcus aureus a*nd *Escherichia coli* were demonstrated. Both bacteria are known to be associated with oral diseases, particularly periodontal disease (Lamont and Hajishengallis 2015). Interestingly, the addition of salt, cations, or serum (which simulated the natural environment present in blood) did not affect the antimicrobial action of the tau-derived peptides (Kobayashi et al. 2008). Taken together, our results and Kobayashi et al. (2008) makes the case for tau's role as antimicrobial peptides, including implications to the sporadic AD pathophysiological timeline.

Circular dichroism results for tau peptide A in both phosphorylated and non-phosphorylated forms revealed a conformation consisting of mainly β-type structures. Tau assemblies which are abundant in β-sheet-rich filaments is necessary for toxicity, which corroborates the antibacterial assay results for tau peptide A (Passarella and Goedert 2018). It was unfortunate that the aforementioned peptide could not be examined under TEM. The ultrastructural investigations of phosphorylated and non-phosphorylated tau peptides B-F short fibrils with helical repeats or twists. These results were in agreement with previous TEM studies (Terry 1963, Kidd 1964).

A final investigation was carried out to assess if tau peptides would demonstrate birefringence via polarising light microscopy (Louros et al. 2024). As detailed in Chapter 6, tau peptides B, C, D, E and F in their non-phosphorylated and phosphorylated forms produced apple green birefringence through crossed polarisers over a wavelength range of 455 to 600 nm. Hyperphosphorylated tau undergoes additional post-translational changes in pathological circumstances, which impairs microtubule interaction, resulting in aggregation into intracellular amyloid-like deposits (Gong and Iqbal 2008, Wesseling et al. 2020). Al Mammeri et al. (2023) studied the molecular basis of tau assembly, recognising its intrinsically disordered characteristic which stabilises microtubules, as well as its propensity for clumping into cross–β amyloid fibrils.

## 7.6 Clinical implications of research findings

The experimental studies carried out in this thesis have addressed the roles of *P. gingivalis*, Aβ and tau in the pathogenesis of AD. Based on the findings linking Aβ, tau and gingipains, combination therapy may be more effective than monotherapy. Early trials focussed on Aβ clearance or reduction yielded limited results. Although more recent Aβ- targeted medication such as lecanemab and donanemab have been reported to slow down cognitive decline in patient populations with low-medium levels of tau protein, long term effects have not been confirmed (Chopade et al. 2022).

Given this study findings that *P. gingivalis* infection triggers neuroinflammation, the protease inhibitor against gingipains, Atuzaginstat (COR388) was anticipated to have therapeutic effects by modulating or inhibiting neuroinflammation. In the first quarter of 2022, the U.S. Food and Drug Administration (FDA) had placed a full clinical hold on Atuzaginstat (COR388). The

decision meant that Cortexyme had to halt the clinical trials of COR388. The decision was made due to hepatic adverse events. In the meantime, Cortexyme will be prioritizing the development of a safer therapeutic agent named, COR588 for mild to moderate AD (Sabbagh and Decourt 2022).

Keeping in mind the complex aetiology and risk factors, it would make sense to consider 'combination' disease-modifying therapy for AD. The benefits include the ability to target a wide range of pathways to produce additive effects as well as the opportunity to use smaller and safer doses of medication (Salloway et al. 2020).

As part of a holistic preventive and management strategy, blending pharmaceutical and lifestyle interventions such as those that target comorbidities for both periodontitis and AD may be the way forward. As presented in Figure 7.1, many modifiable risk factors have been identified for dementia, which overlap with periodontal disease. The implementation of a common risk factor approach will require screening, early diagnosis and treatment, in both dental and medical settings. The opportunistic screening for systemic diseases in dental practices could identify individuals at increased risk and engage with those who are unaware of their heightened risk or susceptibility. For example, dental professionals play a pivotal role in raising awareness of the links between obesity, diabetes, periodontitis and AD. This well aligned to NHS England's 'Making Every Contact Count (MECC): Consensus Statement. 2016' (www.england.nhs.uk). Similarly, medical professionals should also signpost patients with periodontitis to dental practitioners. The dental and medical teams can certainly advocate for periodontal treatment, maintenance of optimal oral health as well as consistent lifestyle interventions (Figure 7.5).

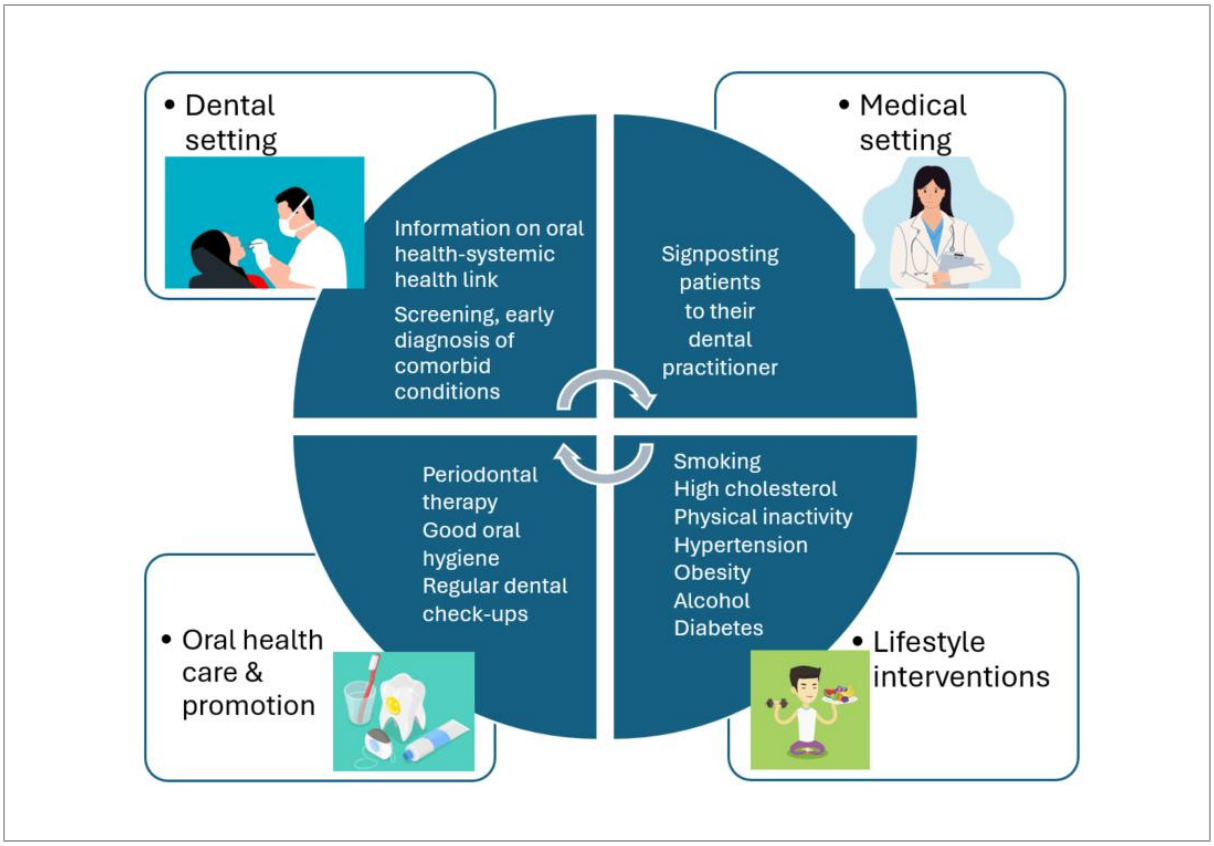


**Figure 7.5:** Proposed strategies to address the challenges of multi-morbidity in periodontitis and AD, by engaging with medical and dental professionals in both settings.

## 7.7 Future directions

Funding for further research should prioritise modifiable risk factors, including maintenance of oral health and lifestyle interventions in the dental setting. Proving a causal link between periodontitis and AD will require establishing correlation, identification of a credible biological mechanism and evidence of periodontal therapy modifying the severity of AD (Cerajewska et al., 2016).

Future investigations may include longitudinal epidemiologic cohort studies which observe a population and measure their periodontal and cognitive status from the prodromal state till the onset of AD (middle age to 70s) to confirm correlation. It would be difficult to exclude the

impact of existing comorbidities. Clinician variability, lack of standardisation of diagnostic procedures and delivery of periodontal therapy would need to be minimised. For ethical reasons, it would not be possible to withhold periodontal treatment, which precludes the opportunity to observe periodontal disease progression over time to establish links to AD.

Clinical trials aimed assessing the effects of periodontal management on inflammatory biomarkers, symptoms, progression and quality of life of those suffering from AD would be valuable to strengthen the bidirectional relationship. Sufficient sample sizes would be challenging to achieve, necessitating a multi-centre approach.

Mammalian model studies are important to ascertain how periodontal pathogens enter the brain, their capacity to form biofilms in the brain upon crossing the BBB as well as the mechanisms for the immune and inflammatory response which could induce the pathological changes associated with AD. The tau hypothesis can be further validated with the use of non-transgenic animal models (or wild type) which can recreate the molecular events occurring in the human brain. Due to limitations with the mouse model, non-human primates (e.g. rhesus, mouse lemure, marmosets and cynomolgus macaques) may be considered for this research as they are genetically, anatomically and physiologically more similar to humans. As they age, they naturally exhibit Aβ deposits, tau pathology and cognitive deficits (Jiang et al. 2024). Having said this, the standards for ethics, the requirements for responsible research practices, animal welfare and high cost may prove to be a hindrance.

## 7.7 Thesis Conclusion

According to a bibliometric study of periodontitis and AD, which implemented a search period from January 2018 to May 2024, a total of 507 papers were included with an annual growth rate of 6.8. The University of Central Lancashire (UCLAN) produced the most output with 17 publications with a total of 313 citations. It was interesting to note the changing trends over the years i.e. from 2018 to 2020, biomarkers and periodontitis, from 2021 onwards, a shift in theme was observed to *P. gingivalis* and neuroinflammation. From the list of authors with the highest scientific production, again UCLAN emerged at the top, represented by Dr Sim Singhroa (Matta-Pacheco et al. 2024).

The experimental work presented in this PhD thesis has contributed to the evidence-base linking periodontitis and AD. Both soluble and insoluble Aβ fibrils were detected within the EPS of periodontal and endodontic natural biofilm. The immunolocalisation of the insoluble Aβ coincided with infected regions within dentinal tubules. Periodontal and endodontics pathogens were shown to give rise to insoluble Aβ experimentally, which may behave in a similar manner to prions. This means there is a potential for Aβ cross seeding to the brain from the periodontal and endodontic lesions, which may increase the risk of AD development later in life.

The neuroblastoma cell line, SH-SY5Y demonstrated neuroinflammation upon exposure to *P. gingivalis* conditioned medium containing virulence factors. This outcome was also observed when the cell line was exposed to cytokines, TNF-α and IL-1β. *P. gingivalis* virulence factors accelerated APP cleavage, increasing the production of the C99 fragment, which was further amplified when combined with cytokines (TNF-α and IL-1β). All three cytokines (TNF-α, IL-

1β, and IL-6) increased the production of the C83 fragment. As a result of P. *gingivalis* infection and pro-inflammatory cytokines, an excessive accumulation of Aβ1-40/42 was observed.

*P. gingivalis* W83 induced periodontal disease in db/db mice provided a disease co-morbidity model with the potential to reproduce AD pathophysiology. Although Aβ and NFTs were not detected, the mouse model demonstrated astrogliosis and microgliosis. This study highlighted the increased risk of neuroinflammation in subjects with comorbidities of obesity and diabetes, when exposed to chronic periodontal disease. This may lead to a heightened risk of developing AD.

The phosphorylated peptide A reduced *P. gingivalis* viability, and CD spectroscopy demonstrated the phosphorylated and the non-phosphorylated peptide A predominantly formed from β sheet structures in aqueous solution with potential antimicrobial activity. Phosphorylation of tau peptides physically changed their tertiary structure into PHFs with potential for self-aggregation and binding to the NFT lesion. These findings align with a sinister relationship between periodontal disease and AD.

Antibacterial assays revealed that phosphorylated tau peptides A (without the hexapeptide motif) and B (containing the VQIINK motif) were shown to inhibit the growth of *P. gingivalis*. The tertiary structure of tau peptides B and C (in both non-phosphorylated and phosphorylated forms) confirm physical changes caused by post-translational modification. TEM investigations of tau peptides B, C, D, E and F appeared to have the ability to self-aggregate and become incorporated to form longer fibers. Phosphorylated tau peptide C were observed to have clear stacking and twisting of the fibers, which may suggest hydrophobicity on the external part of the fiber, which may contribute to further aggregation of PHF or SF to produce

larger aggregates and bundles of filaments, eventually leading to formation of NFTs. Tau Peptides B, C, D, E and F in both non-phosphorylated and phosphorylated forms exhibited mainly β-sheet type structures. A potential link with tau, as a substrate for gingipains, is strengthened via the *in vitro* formation of PHF and SF, which leads to NFT formation. The present study highlights the plausibility of free tau being released, by gingipains, from microtubules which can lead to neuronal death. Further birefringence analysis of tau peptides showed that NFTs, composed of hyperphosphorylated tau protein, demonstrated positive birefringence, confirming the presence of intracellular Aβ. This can potentially act as a precursor to plaque formation and neuronal damage.

Overall, the experimental studies carried out have improved the understanding of the complex relationship between periodontitis, *P. gingivalis* and AD, although causality has yet to be proven. This finding may impact the development of effective therapies for AD, as interventions which have targeted Aβ or tau individually have not achieved significant outcomes. Strategies for preventive measures may include the removal of the potential causative agent (*P. gingivalis* or its gingipains) at the primary oral site, which could impact periodontitis and AD pathogenesis. A paradigm shift is needed to change the way we view AD, from a ‘single-disease’ to a ‘multiple-disease’ framework, exemplified by an integrated multidisciplinary approach, including targeting multimorbid periodontitis as well as other lifestyle interventions.

# REFERENCES


Abbott, P.V. and Salgado, J.C. (2009). Strategies for the endodontic management of concurrent endodontic and periodontal diseases. *Australian Dental Journal*, 54(1), pp.70-85.

Aggidis, A., Devitt, G., Zhang, Y., Chatterjee, S., Townsend, D., Fullwood, N.J., Ortega, E.R., Tarutani, A., Hasegawa, M., Cooper, A., Williamson, P., Mendoza-Oliva, A., Diamond, M.I., Mudher, A. and Allsop, D. (2024). A novel peptide-based tau aggregation inhibitor as a potential therapeutic for Alzheimer's disease and other tauopathies. *Alzheimer's & Dementia*, 20(11), pp.7788-7804

Agholme, L., Lindström, T., Kågedal, K., Marcusson, J. and Hallbeck, M. (2010). An in vitro model for neuroscience: differentiation of SH-SY5Y cells into cells with morphological and biochemical characteristics of mature neurons. *Journal of Alzheimer's disease*, 20(4), pp.1069-1082.

Ahn, S.M., Byun, K., Cho, K., Kim, J.Y., Yoo, J.S., Kim, D., Paek, S.H., Kim, S.U., Simpson, R.J. and Lee, B. (2008). Human microglial cells synthesize albumin in brain. *PLoS One*, 3(7), e2829.

Akl, S., Ranatunga, M., Long, S., Jennings, E. and Nimmo, A. (2021). A systematic review investigating patient knowledge and awareness on the association between oral health and their systemic condition. *BMC Public Health*, 21(1), 2077.

Akiyama, H., Barger, S., Barnum, S., Bradt, B., Bauer, J., Cole, G.M., Cooper, N.R., Eikelenboom, P., Emmerling, M., Fiebich, B.L., Finch, C.E., Frautschy, S., Griffin, W.S., Hampel, H., Hull, M., Landreth, G., Lue, L., Mrak, R., Mackenzie, I.R., McGeer, P.L., O'Banion, M.K., Pachter, J., Pasinetti, G., Plata-Salaman, C., Rogers, J., Rydel, R., Shen, Y., Streit, W., Strohmeyer, R., Tooyoma, I., Van Muiswinkel, F.L., Veerhuis, R., Walker, D., Webster, S., Wegrzyniak, B., Wenk, G. and Wyss-Coray, T. (2000). Inflammation and Alzheimer's disease. *Neurobiology of Aging*, 21(3), pp.383-421.

Al-Abdulla, N., Bakhsh, A., Mannocci, F., Proctor, G., Moyes, D. and Niazi, S.A. (2023). Successful endodontic treatment reduces serum levels of cardiovascular disease risk biomarkers-high-sensitivity C-reactive protein, asymmetric dimethylarginine, and matrix metalloprotease-2. *International Endodontic Journal*, 56(12), pp.1499-1516.

Aldridge, G.M., Podrebarac, D.M., Greenough, W.T. & Weiler, I.J., (2008) The use of total protein stains as loading controls: an alternative to high-abundance single-protein controls in semi-quantitative immunoblotting. Journal of Neuroscience Methods, 172(2), pp.250-254.

Aleksijević, L.H., Aleksijević, M., Škrlec, I., Šram, M., Šram, M., and Talapko, J. (2022). Porphyromonas gingivalis virulence factors and clinical significance in periodontal disease and coronary artery diseases. *Pathogens*, 11(10), 1173.

Alonso, A.C., Grundke-Iqbal, I. and Iqbal, K. (1996). Alzheimer's disease hyperphosphorylated tau sequesters normal tau into tangles of filaments and disassembles microtubules. *Nature Medicine*, 2(7), pp.783-787.

Alonso, R., Pisa, D., Aguado, B. and Carrasco, L. (2017). Identification of fungal species in brain tissue from Alzheimer's disease by next-generation sequencing. *Journal of Alzheimer's Disease*, 58(1), pp.55-67.
Alzheimer's Disease Facts and Figures. (2024). *Alzheimer's & Dementia,* 20(5), pp.3708-3821.

Anthony, J.C., Breitner, J.C., Zandi, P.P., Meyer, M.R., Jurasova, I., Norton M.C. and Stone, S.V. (2000). Reduced prevalence of AD in users of NSAIDs and H2 receptor antagonists: The Cache County study. *Neurology*, 54(11), pp. 2066-2071.

Arana-Chavez, and V.E., Castro-Filice, L.S. (2019). Transmission Electron Microscopy (TEM) and Scanning Electron Microscopy (SEM) for the Examination of Dental Hard Tissues. *Methods in Molecular Biology*, 1922, pp325-332.

Arnsten, A.F.T., Datta, D., Del Tredici, K. and Braak, H. (2021). Hypothesis: Tau pathology is an initiating factor in sporadic Alzheimer's disease. *Alzheimer's & Dementia,* 17(1), pp.115-124.

Armitage, G.C., Dickinson, W.R., Jenderseck, R.S., Levine, S.M. and Chambers, D.W. (1982). Relationship between the percentage of subgingival spirochetes and the severity of periodontal disease. *Journal of Periodontology*, 53(9), pp.550-556.

Arriagada, P.V., Growdon, J.H., Hedley-Whyte, E.T. and Hyman, B.T. (1992). Neurofbrillary tangles but not senile plaques parallel duration and severity of Alzheimer's disease. *Neurology*, 42(3), pp.631-639.

Arrivé, E., Letenneur, L., Matharan, F., Laporte, C., Helmer, C., Barberger-Gateau, P., Miquel, J.L. and Dartigues, J.F. (2012). Oral health condition of French elderly and risk of dementia: a longitudinal cohort study. *Community Dentistry and Oral Epidemiology*, 40(3), pp.230-238.

Avlund, K., Holm-Pedersen, P., Morse, D.E., Viitanen, M. and Winblad, B. (2004). Tooth loss and caries prevalence in very old Swedish people: the relationship to cognitive function and functional ability. *Gerodontology*, 21(1), pp.17-26.

Azarpazhooh, A. and Fillery, E.D. (2008). Prion disease: The implications for dentistry. *Journal of Endodotics*, 34(10), pp. 1158-1166.

Bachrach, G., Altman, H., Kolenbrander, P.E., Chalmers, N.I., Gabai-Gutner, M., Mor, A., Friedman, M. and Steinberg, D. (2008). Resistance of Porphyromonas gingivalis ATCC 33277 to direct killing by antimicrobial peptides is protease independent. *Antimicrobial Agents* and *Chemotherapy*, 52(2), pp.638-642.

Bahar, B., Kanagasingam, S., Tambuwala, M.M., Aljabali, A.A.A., Dillon, S.A., Doaei, S., Welbury, R., Chukkapalli, S.S. and Singhrao, S.K. (2021). *Porphyromonas gingivalis* (W83) infection induces Alzheimer's disease-like pathophysiology in obese and diabetic mice. *Journal of Alzheimers Disease*, 82(3), pp.1259-1275.

Bahar, B. and Singhrao, S.K. (2021). An evaluation of the molecular mode of action of trans-resveratrol in the Porphyromonas gingivalis lipopolysaccharide challenged neuronal cell model. *Molecular Biology Reports*, 48(1), pp.147-156.

Bajaj, J.S., Matin, P., White, M.B., Fagan, A., Deeb, J.G., Acharya, C., Dalmet, S.S., Sikaroodi, M., Gillevet, P.M. and Sahingur, S.E. (2018). Periodontal therapy favorably modulates the oral-gut-hepatic axis in cirrhosis. *The American Journal of Physiology-Gastrointestinal and Liver Physiology,* 315(5), pp.G824-G837.

Balan, P., Gogineni, S.B., Kumari, S.N., Shetty, V., Lakshman Rangare, A., Castelino, R.L. and Areekat K.F. (2015). Candida Carriage Rate and Growth Characteristics of Saliva in Diabetes Mellitus Patients: A Case-Control Study. *Journal of Dental Research, Dental Clinics, Dental Prospects.* 9(4), pp.274-279.

Bale, B.F., Doneen, A.L. and Vigerust, D.J. (2017). High-risk periodontal pathogens contribute to the pathogenesis of atherosclerosis. *Postgraduate Medical Journal*, 93(1098), pp.215-220.

Balin, B.J., Little, C.S., Hammond, C.J., Appelt, D.M., Whittum-Hudson, J.A., Gerard, H.C. and Hudson, A.P. (2008). Chlamydophila ´pneumoniae and the etiology of late-onset Alzheimer's disease. *Journal of Alzheimer's Disease*, 13(4), pp.371-380.

Ballatore, C., Lee, V.M.Y. and Trojanowski, J.Q. (2007). Tau-mediated neurodegeneration in Alzheimer's disease and related disorders. *Nature Reviews Neuroscience,* 8, pp.663-672.

Barreto-Santamaría, A., Arévalo-Pinzón, G., Patarroyo, M.A. and Patarroyo, M.E. (2021). How to Combat Gram-Negative Bacteria Using Antimicrobial Peptides: A Challenge or an Unattainable Goal? *Antibiotics (Basel)*, 10(12), 1499.

Beach, T.G. (2022). A history of senile plaques: from Alzheimer to amyloid imaging. *Journal of Neuropathology & Experimental Neurology,* 81(6), pp.387-413.

Becerra, S.C., Roy, D.C., Sanchez, C.J., Christy, R.J. and Burmeister, D.M. (2016). An optimized staining technique for the detection of Gram positive and Gram negative bacteria within tissue. *BMC Research Notes*, 9, 216.

Belyaev, N.D., Kellett, K.A., Beckett, C., Makova, N.Z., Revett, T.J., Nalivaeva, N.N., Hooper, N.M. and Turner, A.J. (2010). The transcriptionally active amyloid precursor protein (APP) intracellular domain is preferentially produced from the 695 isoform of APP in a {beta}-secretase-dependent pathway. *Journal of Biological Chemistry*, 285(53), pp.41443-41454.

Bender, I.B., Seltzer, S. and Yermish, M. (2003). The incidence of bacteremia in endodontic manipulation: preliminary report. 1960. *Journal of Endodontics*, 29(11), pp.697-700.

Beutler, B. (2000). Endotoxin, toll-like receptor 4, and the afferent limb of innate immunity. *Current Opinion in Microbiology,* 3(1), pp.23-28.

Beydoun, M.A., Beydoun, H.A., Hossain, S., El-Hajj, Z.W., Weiss, J. and Zonderman, A.B. (2020). Clinical and bacterial markers of periodontitis and their association with incident all-cause and Alzheimer's disease dementia in a large national survey. *Journal of Alzheimer's Disease*, 75(1), pp.157-172.

Bi, C., Bi, S. and Li, B. (2019). Processing of mutant β-Amyloid precursor protein and the clinicopathological features of familial Alzheimer's disease. *Aging and Disease,* 10(2), pp.383-403.

Bils, R.F. and Hall, C.E. (1962). Electron microscopy of wound-tumor virus. *Virology,* 17(1), pp.123-130.

Blasko, I., Veerhuis, R., Stampfer-Kountchev, M., Saurwein-Teissl, M., Eikelenboom, .P and Grubeck-Loebenstein, B. (2000). Costimulatory effects of interferon-gamma and interleukin-1beta or tumor necrosis factor alpha on the synthesis of Abeta1-40 and Abeta1-42 by human astrocytes. *Neurobiology of Disease,* 7(6B), pp.682-689.

Boyer, E., Leroyer, P., Malherbe, L., Fong, S.B., Loreal, O., Mallet, M.B. and Meuric V. (2020). Oral dysbiosis induced by Porphyromonas gingivalis is strain-dependant in mice. *Journal of Oral Microbiology,* 12(1), 1832837.

Bokhari, S.A.H., Khan, A.A., Butt, A.K., Azhar, M., Hanif, M., Izhar, M. and Tatakis, D.N. (2012). Non-surgical periodontal therapy reduces coronary heart disease risk markers: a randomized controlled trial. *Journal of Clinical Periodontology,* 39(11), pp.1065-1074.

Botelho, J., Mascarenhas, P., Viana, J., Proença, L., Orlandi, M., Leira, Y., Chambrone, L., Mendes, J.J. and Machado, V. (2022). An umbrella review of the evidence linking oral health and systemic noncommunicable diseases. *Nature Communications,* 13(1), 7614.

Bourgade, K., Le Page, A., Bocti, C., Witkowski, J.M., Dupuis, G., Frost, E.H. and Fülöp, T.Jr. (2016). Protective effect of Amyloid-β peptides against herpes simplex virus-1 infection in a neuronal cell culture model. *Journal of Alzheimer's Disease,* 50(4), pp.1227-1241.

Braak, H., Alafuzoff, I., Arzberger, T., Kretzschmar, H. and Del Tredici, K. (2006). Staging of Alzheimer disease-associated neurofibrillary pathology using paraffin sections and immunocytochemistry. *Acta Neuropathologica,* 112(4), pp.389-404.

Braak, H. and Braak, E. (1991). Neuropathological stageing of Alzheimer-related changes. *Acta Neuropathologica,* 82(4), pp.239-259.

Braak H, Thal DR, Ghebremedhin E, Del Tredici K. (2011). Stages of the pathologic process in Alzheimer disease: Age categories from 1 to 100 years. *Journal of Neuropathology & Experimantal Neurology,* 70(11), pp.960–969.

Breitner, J.C., Welsh, K.A., Helms, M.J., Gaskell, P.C., Gau, B.A., Roses, A.D., Pericak-Vance, M.A. and Saunders, A.M. (1995). Delayed onset of Alzheimer's disease with nonsteroidal anti-inflammatory and histamine H2 blocking drugs. *Neurobiology of Aging,* 6(4), pp.523-530.

Brion, J.P. (1998). Neurofibrillary Tangles and Alzheimer's Disease. *European Neurology,* 40(3), pp.130-140.

Brion, J.P. (2006). Immunological demonstration of tau protein in neurofibrillary tangles of Alzheimer's disease. *Journal of Alzheimer's Disease,* 9(s3), pp.177-185.

Brosseron, F., Krauthausen, M., Kummer, M. and Heneka M.T. (2014). Body fluid cytokine levels in mild cognitive impairment and Alzheimer's disease: a comparative overview. *Molecular Neurobiology*, 50(2), pp.534-544.

Callahan, L.M., Vaules, W.A. and Coleman, P.D. (1999). Quantitative decrease in synaptophysin message expression and increase in cathepsin D message expression in Alzheimer disease neurons containing neurofibrillary tangles. *Journal of Neuropathology & Experimental Neurology,* 58(3), pp.275–287.

Campus, G., Salem, A., Uzzau, S., Baldoni, E. and Tonolo, G. (2005). Diabetes and periodontal disease: a case-control study. *Journal of Periodontology.* 76(3), pp.418-425.

Capone, R., Tiwari, A., Hadziselimovic, A., Peskova, Y., Hutchison, J.M., Sanders, C.R. and Kenworthy, A.K. (2021). The C99 domain of the amyloid precursor protein resides in the disordered membrane phase. *Journal of Biological Chemistry*, 296, 100652.

Castellani, R.J., Plascencia-Villa, G. and Perry, G. (2019). The amyloid cascade and Alzheimer's disease therapeutics: theory versus observation. *Laboratory Investigations,* 99(7), pp.958-970.

Caton, J.G., Armitage, G., Berglundh, T., Chapple, I.L.C., Jepson, S., Kornman, K.S., Mealey, B.L., Papapanou, P.N., Sanz, M. and Tonetti, M.S. (2018). A new classification scheme for periodontal and peri-implant diseases and conditions - Introduction and key changes from the 1999 classification. *Journal of Clinical Periodontology*, 45(20), pp.1-8.

Cerajewska, T.L., Davies, M. and West, N.X. (2015). Periodontitis: a potential risk factor for Alzheimer's disease. *British Dental Journal*, 218(1), pp.29-34.

Cetin, S., Knez, D., Gobec, S., Kos, J. and Pislar, A. (2022). Cell models for Alzheimer's and Parkinson's disease: At the interface of biology and drug discovery. *Biomedicine and Pharmacotherapy*, 149, 112924.

Chapman, M.R., Robinson, L.S., Pinkner, J.S., Roth, R., Heuser, J., Hammar, M., Normark, S. and Hultgren, S.J. (2002). Role of Escherichia coli curli operons in directing amyloid fiber formation. *Science*, 295, pp.851-855.

Chaffee, B.W. and Weston, S.J. (2010). Association between chronic periodontal disease and obesity: a systematic review and meta-analysis. *Journal of Periodontology*, 81(12), pp.1708-1724.

Chapple, I.L.C. and Genco, R.; working group 2 of the joint EFP/AAP workshop. (2013). Diabetes and periodontal diseases: consensus report of the Joint EFP/AAP Workshop on Periodontitis and Systemic Diseases. *Journal of Periodontology,* 84(45), pp.106-112.

Chapple, I.L.C., Mealey, B.L., Van Dyke, T.E., Bartold, P.M., Dommisch, H., Eickholz, P., Geisinger, M.L., Genco, R.J., Glogauer, M., Goldstein, M., Griffin, T.J., Holmstrup, P., Johnson, G.K., Kapila, Y., Lang, N.P., Meyle, J., Murakami, S., Plemons, J., Romito, G.A., Shapira, L., Tatakis, D.N., Teughels, W., Trombelli, L., Walter, C., Wimmer, G., Xenoudi, P. and Yoshie, H. (2018). Periodontal health and gingival diseases and conditions on an intact and

a reduced periodontium: Consensus report of workgroup 1 of the 2017 World Workshop on the Classification of Periodontal and Peri-Implant Diseases and Conditions. *Journal of Clinical Periodontology*, 45 (20), pp.68-77.

Chen, C.K., Wu, Y.T. and Chang, Y.C. (2017). Association between chronic periodontitis and the risk of Alzheimer's disease: a retrospective, population-based, matched-cohort study. *Alzheimer's Research and Therapy*, 9(1), 56.

Chhabra, A., Solanki, S., Saravanabawan, P., Venkiteswaran, A., Nimmathota, N. and Modi, N.M. (2024). A systematic review of the efficacy and safety of anti-amyloid beta monoclonal antibodies in treatment of Alzheimer's disease. *Expert Opinion on Biological Therapy*, 24(11), pp.1261-1269.

Chi, H., Barry, S.P., Roth, R.J., Wu, J.J., Jones, E.A., Bennett, A.M. and Flavell, R.A. (2006). Dynamic regulation of pro- and anti-inflammatory cytokines by MAPK phosphatase 1 (MKP-1) in innate immune responses. *Proceedings of the Natioanl Academy of Sciences (PNAS)*, 103(7), pp.2274-2279.

Chiu, H.C., Fu, M.M.J., Yang,T.S., Fu, E., Chiang, C.Y., Tu, H.P., Chin, Y.T., Lin, F.G. and Shih, K.C. (2016). Effect of high glucose, Porphyromonas gingivalis lipopolysaccharide and advanced glycation end-products on production of interleukin-6/-8 by gingival fibroblasts. *Journal of Periodontal Research*, 52(2), pp.268-276.

Chopade, P., Chopade, N., Zhao, Z., Mitragotri, S., Liao, R, and Chandran Suja, V. (2022). Alzheimer's and Parkinson's disease therapies in the clinic. *Bioengineering & Translational Medicine*, 8(1), e10367.

Cicciu, M., Matacena, G., Signorino, F., Brugaletta, A., Cicciu, A. and Bramanti, E. (2013). Relationship between oral health and its impact on the quality life of Alzheimer's disease patients: a supportive care trial. *International Journal of Clinical and Experimental Medicine*, 6(9), pp.766–772.

Ciccotosto, G.D., Mohammed, A.I., Paolini, R., Bijlsma, E., Toulson, S., Holden, J., Reynolds, E.C., Dashper, S.G., and Butler,C.A. (2024). Chronic Oral Inoculation of Porphyromonas gingivalis and Treponema denticola Induce Different Brain Pathologies in a Mouse Model of Alzheimer Disease. *The Journal of Infectious Diseases*, 230(2), pp.109-116.

Cieplik, F., Zaura, E., Brandt, B.W., Buijs, M.J., Buchalla, W., Crielaard, W., Laine, M.L., Deng, D.M. and Exterkate, R.A.M. (2018). Microcosm biofilms cultured from different oral niches in periodontitis patients. *Journal of Oral Microbiology*, 11(1), 1551596.

Clavaguera, F., Bolmont, T., Crowther, R.A., Abramowski, D., Frank, S., Probst, A., Fraser, G., Stalder, A.K., Beibel, M., Staufenbiel, M., Jucker, M., Goedert, M. and Tolnay, M. (2009). Transmission and spreading of tauopathy in transgenic mouse brain. *Nature Cell Biology*, 11(7), pp.909-13.

Cohen, A.S. (1967). Amyloidosis. *The New England Journal of Medicine*, 277(10), pp.522-530.

Collins, J.R., Arredondo, A., Roa, A., Valdez, Y., León, R. and Blanc, V. (2016). Periodontal pathogens and tetracycline resistance genes in subgingival biofilm of periodontally healthy and diseased Dominican adults. *Clinical Oral Investigations*, 20(2), pp.349-356.

Cope, T.E., Rittman, T., Borchert, R.J., Jones, P.S., Vatansever, D., Allinson, K., Passamonti, L., Vazquez Rodriguez, P., Bevan-Jones, W.R., O'Brien, J.T. and Rowe, J.B. (2018). Tau burden and the functional connectome in Alzheimer's disease and progressive supranuclear palsy. *Brain*, 141(2), pp.550–567.

Corder, E.H., Saunders, A.M., Strittmatter, W.J., Schmechel, D.E., Gaskell, P.C., Small, G.W., Roses, A.D., Haines, J.L. and Pericak-Vance, M.A. (1993). Gene dose of apolipoprotein E type 4 allele and the risk of Alzheimer's disease in late onset families. *Science*, 261(5123), pp.921-923.

Costa, T.H.R., de Figueiredo Neto, J.A., de Oliveira, A.E.F., Lopes e Maia, M.de.F, de Almeida, A.L. (2014). Association between chronic apical periodontitis and coronary artery disease. *Journal of Endodontics,* 40(2), pp.164-167.

Curtis, M.A., Diaz, P.I. and Van Dyke, T.E. (2020). The role of the microbiota in periodontal disease. *Periodontology 2000*, 83(1), pp.14-25.

D'Aiuto, F., Gkranias, N., Bhowruth, D., Khan, T., Orlandi, M., Suvan, J.E., Masi, S., Tsakos, G., Hurel, S., Hingorani, A.D., Donos, N. and Deanfield, J.E.; TASTE Group. (2018). Systemic effects of periodontitis treatment in patients with type 2 diabetes: a 12 month, single-centre, investigator-masked, randomised trial. *The Lancet Diabetes & Endocrinology,* 6(12), pp.954-965.

D'Aiuto, F., Orlandi, M. and Gunsolley, J.C. (2013). Evidence that periodontal treatment improves biomarkers and CVD outcomes. *Journal of Clinical Periodontology,* 40(14), pp.85-105.

Das, A.C., Sahoo, S.K., Parihar, A.S., Bhardwaj, S.S., Babaji, P. and Varghese, J.G. (2020). Evaluation of role of periodontal pathogens in endodontic periodontal diseases. *Journal of Family Medicine and Primary Care,* 9(1), pp.239-242.

Dávila-Bouziguet, E., Targa-Fabra, G., Ávila, J., Soriano, E. and Pascual, M. (2019). Differential accumulation of Tau phosphorylated at residues Thr231, Ser262 and Thr205 in hippocampal interneurons and its modulation by Tau mutations (VLW) and amyloid-β peptide. *Neurobiology of Disease*, 125, pp.232-244.

Debelian, G.J., Olsen, I. and Tronstad, L. (1995). Bacteremia in conjunction with endodontic therapy. *Endodontics & Dental Traumatology*, 11(3), pp.142-149.

de Bont, N., Netea, M.G., Demacker, P.N., Verschueren, I., Kullberg, B.J., van Dijk, K.W., van der Meer, J.W. and Stalenhoef, A.F. (1999). Apolipoprotein E knock-out mice are highly susceptible to endotoxemia and Klebsiella pneumoniae infection.
*Journal of Lipid Research*, 40(4), pp.680–685.

DeFina, P.A., Moser, R.S., Glenn, M., Lichtenstein, J.D. and Fellus, J. (2013). Alzheimer's Disease Clinical and Research Update for Health Care Practitioners. *Journal of aging research,* 207178.

de la Torre, J.C. (2006). How do heart disease and stroke become risk factors for Alzheimer's disease? *Neurological Research*, 28(6), pp.637-644.

DeLeon-Pennell, K.Y., de Castro Brás, L.E. and Lindsey, M.L. (2013). Circulating *Porphyromonas gingivalis* lipopolysaccharide resets cardiac homeostasis in mice through a matrix metalloproteinase-9-dependent mechanism. *Physiological reports,* 1(5), e00079.

Demmer, R.T., Norby, F.L., Lakshminarayan, K., Walker, K.A., Pankow, J.S., Folsom, A.R., Mosley, T., Beck, J. and Lutsey, P.L. (2020). Periodontal disease and incident dementia: The Atherosclerosis Risk in Communities Study (ARIC). *Neurology*, 95(12), pp.e1660-e1671.

d'Errico, P., Ziegler-Waldkirch, S., Aires, V., Hoffmann, P., Mezö, C., Erny, D., Monasor, L.S., Liebscher, S., Ravi, V.M., Joseph, K., Schnell, O., Kierdorf, K., Staszewski, O., Tahirovic, S., Prinz, M. and Meyer-Luehmann, M. (2022). Microglia contribute to the propagation of Aβ into unaffected brain tissue. *Nature Neuroscience*, 25(1), pp.20-25.

Diaz, P.I., Hoare. A. and Hong, B.Y. (2016). Subgingival microbiome shifts and community dynamics in periodontal diseases. *Journal of the California Dental Association*, 44(7), pp.421-435.

Diaz-Zuniga, J., More, J., Melgar-Rodriguez, S., Jimenez-Union, M., Villalobos-Orchard, F., Munoz-Manriquez, C., Monasterio, G., Valdes, J.L., Vernal, R. and Paula-Lima, A. (2020). Alzheimer's disease-like pathology triggered by Porphyromonas gingivalis in wild type rats is serotype dependent. *Frontiers in Immunology*, 11, 588036.

DiCarlo, G., Wilcock, D., Henderson, D., Gordon, M. and Morgan, D. (2001). Intrahippocampal LPS injections reduce Abeta load in APP+PS1 transgenic mice. *Neurobiology of Aging,* 22(6), pp.1007-1012.

Dillon, A., Singhrao, S.K., Achilles-Day, U., Pearce, M., Glyn Morton, L.H. and Crean, S.J. (2014). Vermamoeba vermiformis does not propagate Legionella pneumophila subsp. pascullei in a simulated laboratory dental-unit waterline system. *International Biodeterioration and Biodegradation,* 90, pp.1-7.

Ding, Y., Ren, J., Yu, H., Yu, W. and Zhou, Y. (2018). Porphyromonas gingivalis, a periodontitis causing bacterium, induces memory impairment and age-dependent neuroinflammation in mice. *Immunity and Ageing*, 15, 6.

Ding X, Zhang S, Jiang L, Wang L, Li T, Lei P. Ultrasensitive assays for detection of plasma tau and phosphorylated tau 181 in Alzheimer's disease: a systematic review and meta-analysis. Transl Neurodegener. 2021 Mar 12;10(1):10

Dixon, D.R. and Darveau, R.P. (2005). Lipopolysaccharide Heterogeneity: Innate Host Responses to Bacterial Modification of Lipid A Structure. *Journal of Dental Research,* 84(7), pp.584-595.

Doody, R.S., Thomas, R.G., Farlow, M., Iwatsubo, T., Vellas, B., Joffe, S., Kieburtz, K., Raman, R., Sun, X., Aisen, P.S., Siemers, E., Liu-Seifert, H. and Mohs, R. Alzheimer's Disease Cooperative Study Steering Committee; Solanezumab Study Group. (2014). Phase 3 trial of Solanezumab for mild to moderate Alzheimer's disease. *The New England Journal of Medicine*, 370(4), pp.311-321.

Dominy, S.S., Lynch, C., Ermini, F., Benedyk, M., Marczyk, A., Konradi, A., Nguyen, M., Haditsch, U., Raha, D., Griffin, C., Holsinger, L.J., Arastu-Kapur, S., Kaba, S., Lee, A., Ryder, M.I., Potempa, B., Mydel, P., Hellvard, A., Adamowicz, K., Hasturk, H., Walker, G.D., Reynolds, E.C., Faull, R.L.M., Curtis, M.A., Dragunow, M. and Potempa, J. (2019). Porphyromonas gingivalis in Alzheimer's disease brains: Evidence for disease causation and treatment with small-molecule inhibitors. *Science Advances*, 5(1), eaau3333.

Dunn, B., Stein, P. and Cavazzoni, P. (2021). Approval of aducanumab for Alzheimer disease-The FDA's perspective. *JAMA Internal Medicine*, 181(10), pp.1276-1278.

Dunn, N., Mullee, M., Perry, V.H. and Holmes, C. (2005) Association between dementia and infectious disease: Evidence from a case-control study. *Alzheimer Disease & Associated Disorders*, 19(2), pp.91-94.

Duong, S., Patel, T. and Chang, F. (2017). Dementia. What pharmacists need to know. *Canadian Pharmacists Journal*, 150(2), pp.118-129.

Dwane, S., Durack, E. and Kiely, P.A. (2013). Optimising parameters for the differentiation of SH-SY5Y cells to study cell adhesion and cell migration.
*BMC Research Notes*, 6, 366.

Dzamba, D., Harantova, L., Butenko, O. and Anderova, M. (2016). Glial Cells - the key elements of Alzheimer´s disease. *Current Alzheimer Research*, 13(8), pp.894-911.
Ebrahimpour, S., Zakeri, M. and Esmaeili, A. (2020). Crosstalk between obesity, diabetes, and alzheimer's disease: Introducing quercetin as an effective triple herbal medicine. *Ageing Research Reviews*, 62, 101095,

Ehnevid, H., Jansson, L., Lindskog, S. and Blomlof, L. (1993). Periodontal healing in teeth with periapical lesions. A clinical retrospective study. *Journal of Clinical Periodontology*, 20(4), pp.254-258.

Eisenberg, D.S. and Sawaya, M.R. (2017). Structural studies of amyloid proteins at the molecular level. *Annual Review of Biochemistry*. 86, pp.69-95.

El Mammeri, N., Duan, P., Dregni, A.J. and Hong, M. (2023). Amyloid fibril structures of tau: Conformational plasticity of the second microtubule-binding repeat. *Science Advances*, 9(28), eadh4731.

Emery, D.C., Shoemark, D.K., Batstone, T.E., Waterfall, C.M., Coghill, J.A., Cerajewska, T.L., Davies, M., West, N.X. and Allen, S.J. (2017). 16S rRNA next generation sequencing analysis shows bacteria in Alzheimer's post-mortem brain. *Frontiers in Aging Neuroscience*, 9, 195.

Fan, L., Mao, C., Hu, X., Zhang, S., Yang, Z., Hu, Z., Sun, H., Fan, Y., Dong, Y., Yang, J., Shi, C. and Xu, Y. (2020). New insights into the pathogenesis of Alzheimer's disease. *Frontiers in Neurology*, 10, 1312.

Fandrich, M. (2007). On the structural definition of amyloid fibrils and other polypeptide aggregates. *Cellular and Mollecular Life Sciences*, 64(16), pp.2066-2078.

Fani, L., Ahmad, S., Ikram, M.K., Ghanbari, M. and Ikram, M.A. (2021). Immunity and amyloid beta, total tau and neufilament light chain: Findings from a community-based cohort study. *Alzheimer's & Dementia*, 17(3), pp.446-456.

Farrer, L.A., Cupples, L.A., Haines, J.L., Hyman, B., Kukull, W.A., Mayeux, R., Myers, R.H., Pericak-Vance, M.A., Risch, N. and van Duijn, C.M. (1997). Effects of age, sex, and ethnicity on the association between apolipoprotein E genotype and Alzheimer disease. A meta-analysis. APOE and Alzheimer Disease Meta Analysis Consortium. *JAMA*, 278(16), pp.1349-1356.

Feng, X., Deng, T., Zhang, Y., Su, S., Wei, C. and Han, D. (2011). Lipopolysaccharide inhibits macrophage phagocytosis of apoptotic neutrophils by regulating the production of tumour necrosis factor α and growth arrest-specific gene 6. *Immunology*, 132(2), pp.287-295.

Fichou, Y., Al-Hilaly, Y.K., Devred, F., Smet-Nocca, C., Tsvetkov, P.O., Verelst, J., Winderickx, J., Geukens, N., Vanmechelen, E., Perrotin, A., Serpell, L., Hanseeuw, B.J., Medina, M., Buée, L. and Landrieu, I. (2019). The elusive tau molecular structures: can we translate the recent breakthroughs into new targets for intervention?
*Acta Neuropathologica Communications*, 7(1), 31.

Foguem, C. and Manckoundia, P. (2018). Lewy body disease: Clinical and pathological "overlap syndrome" between synucleinopathies (Parkinson disease) and tauopathies (Alzheimer's disease). *Current Neurology and Neuroscience Reports*, 18(5), 24.

Fowler, D.M., Koulov A.V., Balch W.E., Kelly J.W. (2007) 'Functional amyloid – from bacteria to humans', Trends in Biochemical Sciences, 32(5), pp. 217–224.

Fratiglioni, L., Ahlbom, A., Viitanen, M. and Winblad, B. (1993). Risk factors for late-onset Alzheimer's disease: a population-based, case-control study. *Annals of Neurology*, 33(3), pp.258–266.

Friedland, R.P. (2015). Mechanisms of molecular mimicry involving the microbiota in neurodegeneration. *Journal of Alzheimer's Disease*, 45(2), pp.349-362.

Frost, B. and Diamond, M.I. (2009). The expanding realm of prion phenomena in neurodegenerative disease. *Prion*, 3(2), pp.74-77.

Frost, B., Jacks, R.L. and Diamond, M.I. (2009). Propagation of tau misfolding from the outside to the inside of a cell. *Journal of Biological Chemistry*, 284(19), pp.12845–12852.

Fu, K.L., Chiu, M.J., Wara-Aswapati, N., Yang, C.N., Chang, L.C., Guo, Y.L., Ni, Y.H. and Chen, Y.W. (2023). Oral microbiome and serological analyses on association of Alzheimer's disease and periodontitis. *Oral Diseases*, 29(8), pp.3677-3687.

Gatz, M., Mortimer, J.A., Fratiglioni, L., Johansson, B., Berg, S., Reynolds, C.A. and Pedersen, N.L. (2006). Potentially modifiable risk factors for dementia in identical twins. *Alzheimer's & Dementia*, 2(2), pp.110-117.

Gendron, T.F. and Petrucelli, L. (2009). The role of tau in neurodegeneration. *Molecular Neurodegeneration*, 4, 13.

Genco, R.J. and Van Dyke, T.E. (2010). Prevention: reducing the risk of CVD in patients with periodontitis. *Nature Reviews Cardiology*, 7(9), pp.479-480.

Gerson, J.E., Sengupta, U., Lasagna-Reeves, C.A., Guerrero-Muñoz, M.J., Troncoso, J. and Kayed, R. (2014). Characterization of tau oligomeric seeds in progressive supranuclear palsy. *Acta Neuropathologica Communications,* 2, 73.

Giannakopoulos, P., Herrmann, F.R., Bussière, T., Bouras, C., Kövari, E., Perl, D.P., Morrison, J.H., Gold, G. and Hof, P.R. (2003). Tangle and neuron numbers, but not amyloid load, predict cognitive status in Alzheimer's disease. *Neurology*, 60(9), pp.1495-1500.

Gil-Montoya, J.A., Barrios, R. and Santana, S., Sanchez-Lara, I., Pardo, C.C., Fornieles-Rubio, F., Montes, J., Ramirez, C., Gonzalez-Moles, M.A. and Burgos, J.S. (2017). Association between periodontitis and amyloid-B peptide in elderly people with and without cognitive impairment. *Journal of Periodontology*, 88(10), pp.1051-1058.

Glenner, G.G. and Wong, C.W. (1984). Alzheimer's disease: initial report of the purification and characterization of a novel cerebrovascular amyloid protein. *Biochemical and Biophysical Research Communications,* 120(3), pp.885-890.

Goedert, M., Klug, A. and Crowther, R.A. (2006). Tau protein, the paired helical filament and Alzheimer's disease. *Journal of Alzheimer's Disease,* 9(s3), pp.195-207.

Goedert, M., Spillantini, M.G., Jakes, R., Rutherford, D. and Crowther, R.A. (1989). Multiple isoforms of human microtubule-associated protein tau: sequences and localization in neurofibrillary tangles of Alzheimer's disease. *Neuron,* 3(4), pp.519-526.

Goldner, J. (1938). A modification of the Masson trichrome technique for routine laboratory purposes. *The American Journal of Pathology*, 14(2), pp.237-243.

Gomes, B.P.F.A., Berber, V.B., Kokaras, A.S., Chen, T. and Paster, B.J. (2015). Microbiomes of endodontic-periodontal lesions before and after chemomechanical preparation. *Journal of Endodontics*, 41(12), pp.1975–1984.

Gomes, C.C., Guimarães, L.S., Pinto, L.C.C., Camargo, G.A.D.C.G., Valente, M.I.B., and Sarquis, M.I.M. (2017). Investigations of the prevalence and virulence of Candida albicans in periodontal and endodontic lesions in diabetic and normoglycemic patients. *Journal of Applied Oral Science,* 25(3), pp.274-281.

Gong, C.X. and Iqbal, K. (2008). Hyperphosphorylation of microtubule-associated protein tau: a promising therapeutic target for Alzheimer disease. *Current Medicinal Chemistry,* 15(23), pp.2321–2328.

Goto, T., Kuramoto, E., Dhar, A., Wang, R.P.H., Seki, H., Iwai, H., Yamanaka, A., Matsumoto, S.E., Hara, H., Michikawa, M., Ohyagi, Y., Leung, W.K. and Chang, R.C.C. (2020). Neurodegeneration of trigeminal mesencephalic neurons by the tooth loss triggers the progression of Alzheimer's disease in 3×Tg-AD model mice. *Journal of Alzheimer's Disease,* 76(4), pp.1443-1459.

Gralle, M. and Ferreira, S.T. (2007). Structure and functions of the human amyloid precursor protein: The whole is more than the sum of its parts. Progress in Neurobiology, 82(1), pp.11-32.

Greenberg, B.L. and Glick, M. (2012). Assessing systemic disease risk in a dental setting: a public health perspective. *Dental Clinics of North America,* 56(4), pp.863-874.

Greenlee-Wacker, M.C. (2016). Clearance of apoptotic neutrophils and resolution of inflammation. *Immunological reviews,* 273(1), pp.357-370.

Grenier, D., Roy, S., Chandad, F., Plamondon, P., Yoshioka, M., Nakayama, K. and Mayrand, D. (2003). Effect of inactivation of the Arg- and/or Lys-gingipain gene on selected virulence and physiological properties of Porphyromonas gingivalis. *Infectection and Immunity,* 71(8), pp.4742-4748.

Grossi, S.G. and Genco, R.J. (1998). Periodontal disease and diabetes mellitus: a two-way relationship. *Annals of Periodontology,* 3(1), pp.51-61.

Grundke-Iqbal, I., Iqbal, K., Quinlan, M., Tung, Y.C., Zaidi, M.S. and Wisniewski, H.M. (1986). Microtubule-associated protein tau. A component of Alzheimer paired helical filaments. *Journal of Biological Chemistry,* 261(13), pp.6084-6089.

Gu, L. and Guo, Z. Alzheimer's Aβ42 and Aβ40 peptides form interlaced amyloid fibrils. (2013). *Journal of Neurochemistry,* 126(3), pp.305-311.

Gu, Y., Wu, Z., Zeng, F., Jiang, M., Teeling, J.L., Ni, J. and Takahashi, I. (2020). Systemic exposure to lipopolysaccharide from Porphyromonas gingivalis induces bone loss-correlated Alzheimer's disease-like pathologies in middle-aged mice. *Journal of Alzheimer's Disease,* 78(1), pp.61-74.

Guo, Y., Nguyen, K.A. and Potempa, J. (2000). Dichotomy of gingipains action as virulence factors: from cleaving substrates with the precision of a surgeon's knife to a meat chopper-like brutal degradation of proteins. *Periodontology 2000,* 54(1), pp.15-44.

Gupta, S., Kapoor, P., Chaudhary, K., Gautam, A., Kumar, R.; Open Source Drug Discovery Consortium; Raghava, G.P.S. (2013). In silico approach for predicting toxicity of peptides and proteins. *PLoS One,* 8(9), e73957.

Haass, C., Schlossmacher, M.G., Hung, A.Y., Vigo-Pelfrey, C., Mellon, A., Ostaszewski, B.L., Lieberburg, I., Koo, E.H., Schenk, D. and Teplow, D.B. (1992). Amyloid beta-peptide is produced by cultured cells during normal metabolism. *Nature,* 359, pp.322–325.

Haditsch, U., Roth, T., Rodriguez, L., Hancock, S., Cecere, T., Nguyen, M., Arastu-Kapur, S., Broce, S., Raha, D., Lynch, C.C., Holsinger, L.J., Dominy, S.S. and Ermini, F. (2020). Alzheimer's disease-like neurodegeneration in *Porphyromonas gingivalis* infected neurons with persistent expression of active gingipains. *Journal of Alzheimer's Disease,* 75(4), pp.1361-1376.

Hajishengallis, G. and Chavakis, T. (2021). Local and systemic mechanisms linking periodontal disease and inflammatory comorbidities. *Nature Reviews Immunology,* 21(7), pp.426-440.

Hajishengallis, G., Darveau, R.P. and Curtis, M.A. (2012). The keystone-pathogen hypothesis. *Nature Reviews Microbiology,* 10(10), pp.717-725.

Hajishengallis, G. and Lamont, R.J. (2016). Dancing with the stars: how choreographed bacterial interactions dictate nososymbiocity and give rise to keystone pathogens, accessory pathogens, and pathobionts. *Trends in Microbiology,* 24(6), pp.477-489.

Hajishengallis, G., Kajikawa, T., Hajishengallis, E., Maekawa, T., Reis, E.S., Mastellos, D.C., Yancopoulou, D., Hasturk, H. and Lambris, J.D. (2019). Complement-dependent mechanisms and interventions in periodontal disease. *Frontiers in Immunology,* 10, 406.

Hanger, D.P., Hughes, K., Woodgett, J.R., Brion, J.P. and Anderton, B.H. (1992). Glycogen synthase kinase-3 induces Alzheimer's disease-like phosphorylation of tau: Generation of paired helical filament epitopes and neuronal localisation of the kinase. *Neuroscience Letters,* 147(1), pp.58-62.

Hanger, D.P., Byers, H.L., Wray, S., Leung, K-Y., Saxton, M.J., Seereeram, A., Reynolds, C.H., Ward, M.A. and Anderton, B.H. (2007). Novel phosphorylation sites in tau from Alzheimer brain support a role for casein kinase 1 in disease pathogenesis. *Journal of Biological Chemistry,* 282(32), pp.23645-23654.

Harding, A., Gonder, U., Robinson, S.J., Crean, S.J. and Singhrao, S.K. (2017). Exploring the association between Alzheimer's disease, oral health, microbial endocrinology and nutrition. *Frontiers in Aging Neuroscience,* 9, 398.

Harding, A., Robinson, S., Crean, S.J and Singhrao, S.K. (2017). Can better management of periodontal disease delay the onset and progression of Alzheimer's disease? Journal of Alzheimer's Disease, 58(2), pp.337-348.

Harding, A. and Singhrao, S.K. (2022). Periodontitis and dementia: a bidirectional relationship? *Journal of Dental Research,* 101(3), pp.245-246.

Hardy, J. and Allsop, D. (1991). Amyloid deposition as the central event in the aetiology of Alzheimer's disease. *Trends in Pharmacological Sciences,* 12(10), pp.383-388.

Hardy, J. and Selkoe, D.J. (2002). The Amyloid hypothesis of Alzheimer's Disease: progress and problems on the road to therapeutics. *Science* 297(5580), pp.353-356.

Harris, F., Dennison, S.R. and Phoenix, D.A. (2012). Abberant action of amyloidogenic host defense peptides: a new paradigm to investigate neurodegenerative disorders? The *FASEB Journal*, 26(5), pp.1776-1781.

Hasegawa, Y. and Nagano, K. (2021). Porphyromonas gingivalis FimA and Mfa1 fimbriae: Current insights on localization, function, biogenesis, and genotype. *Japanese Dental Science Review*, 57, pp.190–200.

Hatipoglu, M.G., Kabay, S.C. and Guven, G. (2011). The clinical evaluation of the oral status in Alzheimer-type dementia patients. *Gerodontology*, 28(4), pp.302–306.

Hawkins, P.N., Lavender, J.P. and Pepys, M.B. (1990). Evaluation of systemic amyloidosis by scintigraphy with 123I-labeled serum amyloid P component. *The New England Journal of Medicine*, 323(8), pp.508-513.

Hawrani, A., Howe, R.A., Walsh, T.R. and Dempsey, C.E. (2010). Thermodynamics of RTA3 peptide binding to membranes and consequences for antimicrobial activity. *Biochimica et Biophysica Acta (BBA)*, 1798(6), pp.1254-1262.

Heneka, M.T., Golenbock, D.T. and Latz, E. (2015), Innate immunity in Alzheimer's disease. Nature Immunology, 16(3), pp.229-236.

Heneka, M.T., Carson, M.J., El Khoury, J., Landreth, G.E., Brosseron, F., Feinstein, D.L., Jacobs, A.H., Wyss-Coray, T., Vitorica, J., Ransohoff, R.M., Herrup, K., Frautschy, S.A., Finsen, B., Brown, G.C., Verkhratsky, A., Yamanaka, K., Koistinaho, J., Latz, E., Halle, A., Petzold, G.C., Town, T., Morgan, D., Shinohara, M.L., Perry, V.H., Holmes, C., Bazan, N.G., Brooks, D.J., Hunot, S., Joseph, B., Deigendesch, N., Garaschuk, O., Boddeke, E., Dinarello, C.A., Breitner, J.C., Cole, G.M., Golenbock, D.T. and Kummer, M.P. (2015). Neuroinflammation in Alzheimer's disease. *The Lancet Neurology*, 14(4), pp.388-405.

Herrera, D., Retamal-Valdes, B., Alonso, B. and Feres, M. (2018). Acute periodontal lesions (periodontal abscesses and necrotizing periodontal diseases) and endo-periodontal lesions. *Journal of Periodontology*, 89(1), pp.85–102.

Hewitt, S.M., Baskin, D.G., Frevert, C.W., Stahl, W.L. and Rosa-Molinar, E. (2014). Controls for immunohistochemistry: the Histochemical Society's standards of practice for validation of immunohistochemical assays. *Journal of Histochemistry & Cytochemistry*, 62(10), pp.693-697.

Holt, S.C., Kesavalu,. L., Walker, S. and Genco, C.A. (1999). Virulence factors of Porphyromonas gingivalis. *Periodontology 2000*, 20, pp.168-238.

Holmes, C. and Cotterell, D. (2009). Role of infection in the pathogenesis of Alzheimer's disease: implications for treatment. *CNS Drugs*, 23(12), pp.993-1002.

How, K.Y., Song, K.P. and Chan, K.G. (2016). *Porphyromonas gingivalis*: An Overview of Periodontopathic Pathogen below the Gum Line. *Frontiers in Microbiology*, 7, 53.

Howard, J. and Pilkington, G.J. (1992). Fibronectin staining detects micro-organisms in aged and Alzheimer's disease brain. *Neuroreport*, 3(7), pp.615-618.

Howie, A.J. (2019). Origins of a pervasive, erroneous idea: The "green birefringence" of Congo red-stained amyloid. *International Journal of Experimantal Pathology*, 100(4), pp.208-221.

Huang, L.K., Chao, S.P. and Hu, C.J. (2020). Clinical trials of new drugs for Alzheimer disease. *Journal of Biomedical Science*, 27(1), 18.

Huang, Y.R. and Liu, R.T. (2020). The toxicity and polymorphism of β-Amyloid oligomers. *International Journal of Molecular Sciences*, 21(12), 4477.

Hubacek, J.A., Peasey, A., Pikhart, H., Stavek, P., Kubinova, R., Marmot, M. and Bobak, M. (2010). APOE polymorphism and its effect on plasma C-reactive protein levels in a large general population sample. *Human Immunology*, 71(3), pp.304-308.

Hugo, F.N., Hilgert, J.B., Bertuzzi, D., Padilha, D.M.P. and De Marchi. R.J . (2007). Oral health behaviour and socio-demographic profile of subjects with Alzheimer's disease as reported by their family caregivers. *Gerodontology*, 24(1), pp.36-40.

Hung, S.L., Lee, N.G., Chang, L.Y., Chen, Y.T. and Lai, Y.L. (2014). Stimulatory effects of glucose and *Porphyromonas gingivalis* lipopolysaccharide on the secretion of inflammatory mediators from human macrophages. *Journal of Periodontology,* 85(1), pp.140-149.

Hyman, B.T., Phelps, C.H., Beach, T.G., Bigio, E.H., Cairns, N.J., Carrillo, M.C., Dickson, D.W., Duyckaerts, C., Frosch, M.P., Masliah, E., Mirra, S.S., Nelson, P.T., Schneider, J.A., Thal, D.R., Thies, B., Trojanowski, J.Q., Vinters, H.V. and Montine, T.J. (2012). National Institute on Aging–Alzheimer's Association guidelines for the neuropathologic assessment of Alzheimer's disease. *Alzheimer's & Dementia,* 8(1), pp.1-13.

Ide, M., Harris, M., Stevens, A., Sussams, R., Hopkins, V., Culliford, D., Fuller, J., Ibbett, P., Raybould, R., Thomas, R., Puenter, U., Teeling, J., Perry, V.H. and Holmes, C. (2016). Periodontitis and cognitive decline in Alzheimer's disease. *PLOS One*, 11(3).

Igboin, C.O., Griffen, A.L. and Leys, E.J. Porphyromonas gingivalis strain diversity. (2009). *Journal of Clinical Microbiology*, 47(10), pp.3073-3081.

Ilievski, V., Zuchowska, P.K., Green, S.J., Toth, P.T., Ragozzino, M.E., Le, K., Alijewar, H.W., O'brien-Simpson, N.M., Reynolds, E.C. and Watanabe, K. (2018). Chronic oral application of a periodontal pathogen results in brain inflammation, neurodegeneration and amyloid beta production in wild type mice. *PLOS One*, 13(10), e0204941.

Imamura, T. (2003). The role of gingipains in the pathogenesis of periodontal disease. *Journal of Periodontology*, 74(1), pp.111-118.

Imamura, T., Tanase, S., Hamamoto, T., Potempa, J. and Travis, J. (2001). Activation of blood coagulation factor IX by gingipains R, arginine-specific cysteine proteinases from Porphyromonas gingivalis. *Biochemical Journal*, 353(2), pp.325-331.

Insel, P.S., Donohue, M.C., Berron, D., Hansson, O. and Mattsson-Carlgren. N. (2021). Time between milestone events in the Alzheimer's disease amyloid cascade. *NeuroImage*, 227, 117676.

Ishida, N., Ishihara, Y., Ishida, K., Tada, H., Funaki-Kato, Y., Hagiwara, M., Ferdous, T., Abdullah, M., Mitani, A., Michikawa, M. and Matsushita, K. (2017). Periodontitis induced by bacterial infection exacerbates features of Alzheimer's disease in transgenic mice. *NPJ Aging and Mechanisms of Disease*, 3, 15.

Isola G, Polizzi A, Serra S, Boato M, Sculean A. Relationship between periodontitis and systemic diseases: A bibliometric and visual study. Periodontol 2000. 2025 Jan 8. doi: 10.1111/prd.12621. Epub ahead of print. PMID: 3977596

Jack, C.R.Jr., Bennett, D.A., Blennow, K., Carrillo, M.C., Dunn, B., Haeberlein, S.B., Holtzman, D.M., Jagust, W., Jessen, F., Karlawish, J., Liu, E., Molinuevo, J.L., Montine, T., Phelps, C., Rankin, K.P., Rowe, C.C., Scheltens, P., Siemers, E., Snyder, H.M. and Sperling, R. (2018). NIA-AA Research Framework: Toward a biological definition of Alzheimer's disease. *Alzheimer's & Dementia,* 14(4), pp.535-562.

Jacobs, S., Lie, D.C., DeCicco, K.L., Shi, Y., DeLuca, L.M., Gage, F.H. and Evans, R.M. (2006). Retinoic acid is required early during adult neurogenesis in the dentate gyrus. *The Proceedings of the National Academy of Sciences USA*, 103(10),pp.3902-3907.
Jaeger, L.B., Dohgu, S., Sultana, R., Lynch, J.L., Owen, J.B., Erickson, M.A., Shah, G.N., Price, T.O., Fleegal-Demotta, M.A., Butterfiled, D.A. and Banks, W.A. (2009). Lipopolysaccharide Alters the Blood-brain Barrier Transport of Amyloid Beta Protein: A Mechanism for Inflammation in the Progression of Alzheimer's Disease. *Brain, Behaviour, and Immunity,* 23(4), pp.507-517.

Jia, L., Han, N., Du, J., Guo, L., Luo, Z. and Liu, Y. (2019). Pathogenesis of Important Virulence Factors of *Porphyromonas gingivalis* via Toll-Like Receptors. *Frontiers in Cellular and Infection Microbiology*, 9, 262.

Jiang, Z., Wang, J., Qin, Y., Liu, S., Luo, B., Bai, F., Wei, H., Zhang, S., Wei, J., Ding, G., Ma, L., He, S., Chen, R., Sun, Y., Chen, Y., Wang, L., Xu, H., Wang, X., Chen, G. and Lei, W. (2024). A nonhuman primate model with Alzheimer's disease-like pathology induced by hippocampal overexpression of human tau. *Alzheimer's Research & Therapy,* 16(1), 22.

Jiang, Z., Wang, J., Qin, Y. et al. A nonhuman primate model with Alzheimer's disease-like pathology induced by hippocampal overexpression of human tau. Alz Res Therapy 16, 22 (2024). https://doi.org/10.1186/s13195-024-01392-0

Jimenez, J., Guijarro, J.I., Orlova, E., Zurdo, J., Dobson, C.M., Sunde, M. and Saibil, H.R. (1999). Cryo-electron microscopy structure of an SH3 amyloid fibril and model of the molecular packing. The *EMBO Journal*, 18(4), pp.815-821.

Jin, L.J., Lamster, I.B., Greenspan, J.S., Pitts, N.B., Scully, C. and Warnakulasuriya, S. (2016). Global burden of oral diseases: emerging concepts, management and interplay with systemic health. *Oral Diseases,* 22(7), pp.609-619.

Jin, L.W., Claborn, K.A., Kurimoto, M., Geday, M.A., Maezawa, I., Sohraby, F., Estrada, M., Kaminksy, W. and Kahr, B. (2003). Imaging linear birefringence and dichroism in cerebral amyloid pathologies. *Proceedings of the National Academy of Sciences (PNAS),* 100(26), pp.15294-15298.

Jin, Y.P., Østbye, T., Feightner, J.W., Di Legge, S. and Hachinski, V. (2008). Joint effect of stroke and APOE E4 on dementia risk: the Canadian Study of Health and Aging. *Neurology*, 70(1), pp.9-16.

Joachim, C.L., Mori, H. and Selkoe, D.J. (1989). Amyloid betaprotein deposition in tissues other than brain in Alzheimer's disease. *Nature*, 341(6239), pp.226–230.

Jung, H.H., Yang, S.T., Sim, J.Y., Lee, S., Lee, J.Y., Kim, H.H., Shin, S.Y. and Kim, J.I. (2010). Analysis of the solution structure of the human antibiotic peptide dermcidin and its interaction with phospholipid vesicles. *BMB Reports*, 43(5), pp.362-368.

Kaci, G., Goudercourt, D., Dennin, V., Pot, B., Doré, J., Ehrlich, S.D., Renault, P., Blottière, H.M., Daniel, C. and Delorme, C. (2014). Anti-Inflammatory Properties of Streptococcus salivarius, a Commensal Bacterium of the Oral Cavity and Digestive Tract. *Applied and Environmental Microbiology*, 80(3), pp.928-934.

Kamer, A.R., Pirraglia, E., Tsui, W., Rusinek, H., Vallabhajosula, S., Mosconi, L., Yi, L., McHugh, P., Craig, R.G., Svetcov, S., Linker, R., Shi, C., Glodzik, L., Williams, S., Corby, P., Saxena, D. and de Leon, M.J. (2015). Periodontal disease associates with higher brain amyloid load in normal elderly. *Neurobiology of Aging*, 36(2), pp.627-633.

Kametani, F. and Hasegawa, M. (2018). Reconsideration of Amyloid Hypothesis and Tau Hypothesis in Alzheimer's Disease. *Frontiers in Neuroscience*, 12, 25.

Kametani, M., Nagasawa, Y., Usuda, M., Kaneki, A., Ogawa, M., Shojima, K., Yamazaki, H., Tokumoto, K., Matsuoka, D., Suehara, K., Suehiro, Y., Akitomo, T., Mitsuhata, C., Misaki, T., Ito, S., Naka, S., Matsumoto-Nakano, M., Nakano, K., Kishimoto, H., Shinmura, K. and Nomura, R. (2024). Relationship between the presence of red complex species and the distribution of other oral bacteria, including major periodontal pathogens in older Japanese individuals. *International Journal of Molecular Sciences*, 25(22), 12243.

Kanagasingam, S., Chukkapalli, S.S., Welbury, R. and Singhrao, S.K. (2020). Porphyromonas gingivalis is a strong risk factor for Alzheimer's disease. *Journal of Alzheimer's Disease*, 4(1), pp.501-511.

Kanagasingam, S., von Ruhland, C., Welbury, R. and Singhrao, S.K. (2022b). Antimicrobial, polarizing light, and paired helical filament properties of fragmented tau peptides of selected putative gingipains. *Journal of Alzheimer's Disease*, 89(4), pp.1279-1291.

Kanagasingam, S., von Ruhland, C., Welbury, R., Chukkapalli, S.S. and Singhrao, S.K. (2022a). Porphyromonas gingivalis conditioned medium induces amyloidogenic processing of the amyloid-B protein upon in vitro infection of SH-SY5Y cells. *Journal of Alzheimer's Disease Reports*, 6(1), pp.577-587.

Karran, E. and De Strooper, B. (2022). The amyloid hypothesis in Alzheimer disease: new insights from new therapeutics. *Nature Reviews Drug Discovery*, 21(4), pp.306-318.

Kassebaum, N.J., Bernabé, E., Dahiya, M., Bhandari, B., Murray, C.J.L. and Marcenes, W. (2014). Global burden of severe periodontitis in 1990-2010: A systematic review and meta-regression. *Journal of Dental Research,* 93(11), pp.1045-1053.

Kendlbacher, F.L., Bloch, S., Hager-Mair, F.F., Schäffer, C. and Andrukhov, O. (2024). Red-complex bacteria exhibit distinctly different interactions with human periodontal ligament stromal cells compared to Fusobacterium nucleatum. *Archives of Oral Biology,* 164, 106004

Kent, S.A., Spires-Jones, T.L. and Durrant, C.S. (2020). The physiological roles of tau and Aβ: implications for Alzheimer's disease pathology and therapeutics. *Acta Neuropathologica,* 140(4), pp.417-447.

Khlistunova, I., Biernat, J., Wang, Y., Pickhardt, M., von Bergen, M., Gazova, Z., Mandelkow, E. and Mandelkow, E.M. (2006). Inducible expression of Tau repeat domain in cell models of tauopathy: aggregation is toxic to cells but can be reversed by inhibitor drugs. *Journal of Biological Chemistry,* 281(2), pp.1205-1214.

Kinane, J.A., Benakanakere, M.R., Zhao, J., Hosur, K.B. and Kinane, D.F. (2012). Porphyromonas gingivalis influences actin degradation within epithelial cells during invasion and apoptosis. *Cellular Microbiology,* 14(7), pp.1085-1096.

Kirst, M.E., Li, E.C., Alfant, B., Chi, Y.Y., Walker. C., Magnusson, I. and Wang, G.P. (2015). Dysbiosis and alterations in predicted functions of the subgingival microbiome in chronic periodontitis. *Applied and Environmental Microbiology*, 81(2), pp.783-793.

Kidd, M. (1964). Alzheimer's disease. An electron microscopical study. *Brain,* 87(2), pp.307-320.

Kleinert, M., Clemmensen, C., Hofmann, S.M., Moore, M.C., Renner, S., Woods, S.C., Huypens, P., Beckers, J., de Angelis, M.H., Schürmann, A., Bakhti, M., Klingenspor, M., Heiman, M., Cherrington, A.D., Ristow, M., Lickert, H., Wolf, E., Havel, P.J., Müller, T.D. and Tschöp, M.H. (2018). Animal models of obesity and diabetes mellitus. *Nature Reviews Endocrinology*, 14(3), pp.140-162.

Knopman, D.S., Amieva, H., Petersen, R.C., Chételat, G., Holtzman, D.M., Hyman, B.T., Nixon, R.A. and Jones, D.T. (2021). Alzheimer disease. *Nature Reviews Disease Primers,* 7(1), 33.

Kobayashi, N., Masuda, J., Kudoh, J., Shimizu, N. and Yoshida, T. (2008). Binding sites on tau proteins as components for antimicrobial peptides. *Biocontrol Science,* 13(2), pp.49-56.

Kobayashi, T., Hayashi, A., Yoshikawa, R., Okuda, K. and Hara, K. (1990). The microbial flora from root canals and periodontal pockets of non-vital teeth associated with advanced periodontitis. *International Endodontic Journal,* 23(2), pp.100-106.

Kobro-Flatmoen, A., Hormann, T.M. and Gouras, G. (2023). Intracellular Amyloid-β in the normal rat brain and human subjects and its relevance for Alzheimer's disease. *Journal of Alzheimer's Disease,* 95(2), pp.719-733.

Kubota, T., Maruyama, S., Abe, D., Tomita, T., Morozumi, T., Nakasone, N., Saku, T., and Yoshie, H. (2014). Amyloid beta (A4) precursor protein expression in human periodontitis-affected gingival tissues. *Archives of Oral Biology*, 59(6), pp.586-594.

Kulatunga, D.C.M., Ranaraja, U., Kim, E.Y., Kim, R.E., Kim, D.E., Ji, K.B and Kim, M.K. (2024). A novel APP splice variant-dependent marker system to precisely demarcate maturity in SH-SY5Y cell-derived neurons. *Scientific Reports*, 14(1), 12113.

Kumar, D.K.V., Choi, S.H., Washicosky, K.J., Eimer, W.A., Tucker, S., Ghofrani, J., Lefkowitz, A., McColl, G., Goldstein, L.E., Tanzi, R.E. and Moir, R.D. (2016). Amyloid-β peptide protects against microbial infection in mouse and worm models of Alzheimer's disease. *Science Translational Medicine*, 8(340), p.340ra72.

Kumar, P.S., Leys, E.J., Bryk, J.M., Martinez, F.J., Moeschberger. M.L. and Griffen, A.L. (2006). Changes in periodontal health status are associated with bacterial community shifts as assessed by quantitative 16S cloning and sequencing. *Journal of Clinical Microbiology*, 44(10). pp.3665-3673.

Kummer, C., Wehner, S., Quast, T., Werner, S. and Herzog, V. (2002). Expression and potential function of beta-amyloid precursor proteins during cutaneous wound repair. *Experimental Cell Research*, 280(2), pp.222-232.

Kurihara, H., Kobayashi, Y., Francisco, I.A., Isoshima, O., Nagai, A. and Murayama, Y. (1995). A microbiological and immunological study of endodontic-periodontic lesions. *Journal of Endodontics*, 21(12), pp.617-621.

Lačević, A., Foschi, F., Pojskić, L., Pojskić, N., Bajrović, K. and Izard, J. (2015). Correlation of periodontal pathogens in concurrent endodontic-periodontal diseases. *Oral Biology and Dentistry*, 3, pp.51-56.

Lal, S., Pearce, M., Achilles-Day, U.E.M., Day, J.G., Morton, L.H.G., Crean, S.J and Singhrao, S.K. (2017). Developing an ecologically relevant heterogeneous biofilm model for dental-unit waterlines. *Biofouling* 33(1), pp.75-87.

Lambert, J.C. and Amouyel, P. (2011). Genetics of Alzheimer's disease: new evidences for an old hypothesis? *Current Opinion in Genetics & Development*, 21(3), pp.295-301.

Lamont R,J. and Hajishengallis, G. (2015). Polymicrobial synergy and dysbiosis in inflammatory disease. *Trends in Molecular Medicine*, 21(3), pp.172-183.

Lamont, R.J and Jenkinson, H.F. (1998). Life Below the Gum Line: Pathogenic Mechanisms of *Porphyromonas gingivalis*. *Microbiology and Molecular Biology Reviews*, 62(4), 1244-1263.

Lathuiliere, A., Jo, Y., Perbet, R., Donahue, C., Commins, C., Quittot, N., Fan, Z., Bennett, R.E. and Hyman, B.T. (2023). Specific detection of tau seeding activity in Alzheimer's disease using rationally designed biosensor cells. *Molecular Neurodegeneration*, 18(1), 53.

Laurance, S., Lemarié, C.A., Blostein, M.D. (2012). Growth arrest-specific gene 6 (gas6) and vascular hemostasis. *Advances in Nutrition*, 3(2), pp.196-203.

Lee, D.C., Rizer, J., Selenica, M.B., Reid, P., Kraft, C., Johnson, A., Blair, L., Gordon, M.N., Dickey, C.A. and Morgan, D. (2010). LPS- induced inflammation exacerbates phospho-tau pathology in rTg4510 mice. *Journal of Neuroinflammation* 7, 56.

Lee, H.J., Seo, H.I., Cha, H.Y., Yang, Y.J., Kwon, S.H. and Yang, S.J. (2018). Diabetes and Alzheimer's disease: mechanisms and nutritional aspects. *Clinical Nutrition Research.* 7(4). pp.229-240.

Lee, S.H., Kang, J., Ho, A., Watanabe, H., Bolshakov, V.Y. and Shen, J. (2020). APP family regulates neuronal excitability and synaptic plasticity but not neuronal survival. *Neuron,* 108(4), pp.676-690.

Lee, Y.L., Hu, H.Y., Huang, L.Y., Chou, P. and Chu, D. (2017). Periodontal disease associated with higher risk of dementia: population-based cohort study in Taiwan. *Journal of the American Geriatrics Society*, 65(9), pp.1975-1980.

Lei, S., Li, J., Yu, J., Li, F., Pan. Y., Chen, X., Ma, C., Zhao, W. and Tang, X. (2023). Porphyromonas gingivalis bacteremia increases the permeability of the blood-brain barrier via the Mfsd2a/Caveolin-1 mediated transcytosis pathway. *International Journal of Oral Science*,15(1), 3.

Li, B., Chohan, M.O., Grundke-Iqbal, I. and Iqbal, K. (2007). Disruption of microtubule network by Alzheimer abnormally hyperphosphorylated tau. *Acta Neuropathologica*, 113(5), pp.501-511.

Li, H., Guan, R., Sun, J. and Hou, B. (2014). Bacteria community study of combined periodontal-endodontic lesions using denaturing gradient gel electrophoresis and sequencing analysis. *Journal of Periodontology*, 85(10), pp.1442–1449.

Li, L., Cavuoto, M., Biddiscombe, K, and Pike, K.E. (2020). Diabetes mellitus increases risk of incident dementia in APOEε4 carriers: A meta-analysis. *Journal of Alzheimer's Disease*, 74(4), pp.1295-1308.

Li, N. and Collyer, C.A. (2011). Gingipains from Porphyromonas gingivalis - Complex domain structures confer diverse functions. *European Journal of Microbiology and Immunology*, 1(1), pp.41-58.

Li, P., Fung, Y.M.E, Yin, X., Seneviratne, C.J., Che, C.M. and Jin, L. (2018). Controlled cellular redox, repressive hemin utilization and adaptive stress responses are crucial to metronidazole tolerance of Porphyromonas gingivalis persisters. *Journal of Clinical Periodentology*, 45(10), pp.1211-1221.

Liberta F, Loerch S, Rennegarbe M, Schierhorn A, Westermark P, Westermark GT, Hazenberg BPC, Grigorieff N, Fändrich M, Schmidt M. (2019) Cryo-EM fibril structures from systemic AA amyloidosis reveal the species complementarity of pathological amyloids. Nat Commun. Mar 7;10(1):1104.

Lin, J.W., Chang, C.H. and Caffrey, J.L. (2020). Examining the association between oral health status and dementia: A nationwide nested case-controlled study. *Experimental Biology and Medicine*, 245(3), pp.231-244.

Liu, M., Sui, D., Dexheimer, T., Hovde, S., Deng, X., Wang, K.W., Lin, H.L., Chien, H.T., Kweon, H.K., Kuo, N.S., Ayoub, C.A., Jimenez-Harrison, D., Andrews, P.C., Kwok, R., Bochar, D.A., Kuret, J., Fortin, J., Tsay, Y.G. and Kuo, M.H. (2020). Hyperphosphorylation renders tau prone to aggregate and to cause cell death. *Molecular Neurobiology,* 57(11), pp.4704-4719.

Liu, Y., Wu, Z., Nakanishi, Y., Ni, J., Hayashi, Y., Takayama, F., Zhou, Y., Kadowaki, T. and Nakanishi, H. (2017). Infection of microglia with Porphyromonas gingivalis promotes cell migration and an inflammatory response through the gingipain-mediated activation of protease-activated receptor-2 in mice. *Scientific Reports*, 7(1), 11759.

Livingston, G., Huntley, J., Liu, K.Y., Costafreda, S.G., Selbæk, G., Alladi, S., Ames, D., Banerjee, S., Burns, A., Brayne, C., Fox, N.C., Ferri, C.P., Gitlin, L.N., Howard, R., Kales, H.C., Kivimäki, M., Larson, E.B., Nakasujja, N., Rockwood, K., Samus, Q., Shirai, K., Singh-Manoux, A., Schneider, L.S., Walsh, S., Yao ,Y., Sommerlad, A. and Mukadam, N. (2024). Dementia prevention, intervention, and care: 2024 report of the Lancet standing Commission. *The Lancet,* 404(10452), pp.572-628.

Löe, H. (1993.) Periodontal disease. The sixth complication of diabetes mellitus. *Diabetes Care*, 16(1), pp.329-334.

Louros, N., Wilkinson, M., Tsaka, G., Ramakers, M., Morelli, C., Garcia, T., Gallardo, R., D'Haeyer, S., Goossens, V., Audenaert, D., Thal, D.R., Mackenzie, I.R., Rademakers, R., Ranson, N.A., Radford, S.E., Rousseau, F. and Schymkowitz, J. (2024). Local structural preferences in shaping tau amyloid polymorphism. *Nature Communications,* 15(1), 1028.

Love, R.M. (2001). Enterococcus faecalis – a mechanism for its role in endodontic failure. International Endodontic Journal, 34(5), pp.399-405.

Luchsinger, J.A., Tang, M.X., Stern, Y., Shea, S. and Mayeux, R. (2001). Diabetes mellitus and risk of Alzheimer's disease and Dementia with stroke in a multiethnic cohort. *American Journal of Epidemiology,* 154(7), pp.635–641.

Lutz, T.A. and Woods, S.C. (2012). Overview of animal models of obesity. *Current Protocols in Pharmacology,* 5, 61.

Ma, K.S., Hasturk, H., Carreras, I., Dedeoglu, A., Veeravalli, J.J., Huang, J.Y., Kantarci, A. and Wei, J.C. (2022). Dementia and the risk of periodontitis: A population-based cohort study. *Journal of Dental Research,* 101(3), pp.270-277.

Macedo, A.C., Tissot, C., Therriault, J., Servaes, S., Wang, Y.T., Fernandez-Arias, J., Rahmouni, N., Lussier, F.Z., Vermeiren, M., Bezgin, G., Vitali, P., Ng, K.P., Zimmer, E.R., Guiot, M.C., Pascoal, T.A., Gauthier, S. and Rosa-Neto, P. (2023). The use of tau PET to stage Alzheimer disease according to the Braak staging framework. *The Journal of Nuclear Medicine,* 64(8), pp.1171-1178.

Makiura, N., Ojima, M., Kou, Y., Furuta, N., Okahashi, N., Shizukuishi, S. and Amano, A. (2008). Relationship of Porphyromonas gingivalis with glycemic level in patients with type 2

diabetes following periodontal treatment. *Oral Microbiology and Immunology*, 23(4), pp.348-351.

Mansour, S.C., Pena, O.M. and Hancock, R.E.W. (2014). Host defense peptides: front-line immunomodulators. *Trends in Immunology,* 35(9), pp.443-450.

Marques, S.C.F, Oliveira, C.R., Outeiro, T.F. and Pereira, C.M.F. (2010). Alzheimer's disease: the quest to understand complexity. *Journal of Alzheimer's Disease,* 21(2), pp.373-383.

Matta-Pacheco, J., Tsukamoto-Jaramillo, A., Tinedo-López, P.L., Espinoza-Carhuancho, F., Pacheco-Mendoza, J. and Mayta-Tovalino, F. (2024). Bibliometric study of periodontitis and Alzheimer's disease: trends, collaboration, and emerging patterns. *The Journal of Contemporary Dental Practice,* 25(9), pp.863-868.

Mayeda, E.R., Glymour, M.M., Quesenberry, C.P., Johnson, J.K., Perez-Stable, E.J. and Whitmer, R.A. (2017). Survival after dementia diagnosis in five racial/ethnic groups. *Alzheimer's & Dementia,*13(7), pp.761-769.

Mazgaeen, L. and Gurung, P. (2020). Recent advances in lipopolysaccharide recognition systems. *International Journal of Molecular Science*, 21(2), 379.

McAvoy, T., Lassman, M.E., Spellman, D.S., Ke, Z., Howell, B.J., Wong, O., Zhu, L., Tanen, M., Struyk, A. and Laterza, O.F. (2014). Quantification of tau in cerebrospinal fluid by immunoaffinity enrichment and tandem mass spectrometry. *Clinical Chemistry*, 60(4), pp.683–689.

McGeer, P.L. and McGeer, E.G. (2002). Local neuroinflammation and the progression of Alzheimer's disease. *Journal of Neurovirology*, 8(6), pp.529-538.

McLean, C.A., Cherny, R.A., Fraser, F.W., Fuller, S.J., Smith, M.J., Beyreuther, K., Bush, A.I. and Masters, C.L. (1999). Soluble pool of Abeta amyloid as a determinant of severity of neurodegeneration in Alzheimer's disease. *Annals of Neurology*, 46(6), pp.860-866.

Merchant, A.T., Georgantopoulos, P., Howe, C.J., Virani, S.S., Morales, D.A. and Haddock, K.S. (2016). Effect of long-term periodontal care on hemoglobin A1c in type 2 diabetes. *Journal of Dental Research,* 95(4), pp.408-415.

Meurman, J.H. and Bascones-Martinez, A. (2021). Oral infections and systemic health - more than just links to cardiovascular diseases. *Oral Health and Preventive Dentistry*, 19, pp,441-448.

Meyle, J., Dommisch, H., Groeger, S., Giacaman, R.A., Costalonga, M. and Herzberg, M. (2017). The innate host response in caries and periodontitis. Journal of Clinical Periodontology, 44(12), pp.1215-1225.

Michael, R., Otto, C., Lenferink, A., Gelpi, E., Montenegro, G.A., Rosandić, J., Tresserra, F., Barraquer, R.I. and Vrensen, G.F. (2014). Absence of amyloid-beta in lenses of Alzheimer patients: a confocal Raman microspectroscopic study. *Experimental Eye Research*, 119, pp.44-53.

Miklossy, J. (1993). Alzheimer's disease - a spirochetosis. *Neuroreport,* 4(7), pp.841-848.

Miles, A.A, Misra, S.S and Irwin, J.O. (1938). The estimation of the bactericidal power of the blood. *Journal of Hygiene,* 38(6), pp.732-749.

Miles, A.J., Janes, R.W. and Wallace, B.A. (2021). Tools and methods for circular dichroism spectroscopy of proteins: a tutorial review. *Chemical Society Reviews*, 50(15), pp.8400-8413.

Minter, M.R., Zhang, C., Leone, V., Ringus, D.L., Zhang, X., Oyler-Castrillo, P., Musch, M.W., Liao, F., Ward, J.F., Holtzman, D.M., Chang, E.B., Tanzi, R.E. and Sisodia, S.S. (2016). Antibiotic-induced perturbations in gut microbial diversity influences neuro-inflammation and amyloidosis in a murine model of Alzheimer's disease. *Scientific Reports*, 6, 30028.

Mocanu, M.M., Nissen, A., Eckermann, K., Khlistunova, I., Biernat, J., Drexler, D., Petrova, O., Schönig, K., Bujard, H., Mandelkow, E., Zhou, L., Rune, G. and Mandelkow, E.M. (2008). The potential for beta-structure in the repeat domain of tau protein determines aggregation, synaptic decay, neuronal loss, and coassembly with endogenous Tau in inducible mouse models of tauopathy. *The Journal of Neuroscience,* 28(3), pp.737-748.

Moir, R.D., Lathe, R. and Tanzi, R.E. (2018). The antimicrobial protection hypothesis of Alzheimer's disease. *Alzheimer's & Dementia*, 14(12), pp.1602-1614.

Monasterio, G., Fernández, B., Castillo, F., Rojas, C., Cafferata, E.A., Rojas, L., Alvarez, C., Fernández, A., Hernández, M., Bravo, D. and Vernal, R. (2019). Capsular-defective Porphyromonas gingivalis mutant strains induce less alveolar bone resorption than W50 wild-type strain due to a decreased Th1/Th17 immune response and less osteoclast activity. *Journal of Periodontology,* 90(5), pp.522-534.

Moretti, E.W., Morris, R.W., Podgoreanu, M., Schwinn, D.A., Newman, M.F., Bennett, E., Moulin, V.G., Mba, U.U. and Laskowitz, D.T. Perioperative Genetics and Safety Outcomes Study (PEGASUS) Investigative Team. (2005). APOE polymorphism is associated with risk of severe sepsis in surgical patients. *Critical Care Medicine,* 33(11), pp.2521-2526.

Mulhall, H., Huck, O. and Amar, S. (2020). Porphyromonas gingivalis, a Long-Range Pathogen: Systemic Impact and Therapeutic Implications. *Microorganisms*, 8(6), 869.

Multhaup, G., Huber, O., Buee, L. and Galas, M.C. (2015). Amyloid precursor protein (APP) intracellular fragment (AICD), Aβ42, and tau in nuclear roles. *Journal of Biological Chemistry,* 290(39), pp.23515–23522.

Murray, D.A., and Wilton, J.M.A. (2003). Lipopolysaccharide from the Periodontal Pathogen *Porphyromonas gingivalis* Prevents Apoptosis of HL60-Derived Neutrophils In Vitro. *Infection and Immunity,* 71(12), pp.7232-7235.

Mysak, J., Podzimek, S., Sommerova, P., Lyuya-Mi, Y., Bartova, J., Janatova, T., Prochazkova, J. and Duskova, J. (2014). *Porphyromonas gingivalis*: Major Periodontopathic Pathogen Overview. *Journal of Immunology Research,* 476068.

Naito, M., Hirakawa, H., Yamashita, A., Ohara, N., Shoji, M., Yukitake, H., Nakayama, K., Toh, H., Yoshimura, F., Kuhara, S., Hattori, M., Hayashi, T. and Nakayama, K. (2008). Determination of the genome sequence of Porphyromonas gingivalis strain ATCC 33277 and genomic comparison with strain W83 revealed extensive genome rearrangements in P. gingivalis. *DNA Research,* 15(4), pp.215-225.

Nazir, M.A. (2017). Prevalence of periodontal disease, its association with systemic diseases and prevention. *International Journal of Health Sciences*, 11(2), pp.72-80.

Nelson, R., Sawaya, M.R., Balbirnie, M., Madsen, A.O., Riekel, C., Grothe, R., and Eisenberg, D. (2005). Structure of the cross-spine of amyloid-like fibrils. *Nature*, 435(7043), pp.773-778.

Neurath, N. and Kesting, M. (2024). Cytokines in gingivitis and periodontitis: from pathogenesis to therapeutic targets. *Frontiers in Immunology*, 15, 1435054.

Newman, G.R. and Hobot, J.A. (1987). Modern acrylics for post-embedding immunostaining techniques. *Journal of Histochemistry and Cytochemistry*, 35(9), pp.971-981.

Newman, G.R. and Jasani, B. (1998). Silver development in microscopy and bioanalysis: A new versatile formulation for modern needs. *Journal of Histochemistry and Cytochemistry*, 30(9), pp.635-645.

Ng, A., Tam, W.W., Zhang, M.W., Ho, C.S., Husain, S.F., McIntyre, R.S. and Ho, R.C. (2018). IL-1β, IL-6, TNF- α and CRP in Elderly Patients with Depression or Alzheimer's disease: Systematic Review and Meta-Analysis. *Scientific Reports*, 8(1), 12050.

Niazi, S.A., Clarke, D., Do, T., Gilbert, S.C., Mannocci, F. and Beighton, D. (2010). Propionibacterium acnes and Staphylococcus epidermidis isolated from refractory endodontic lesions are opportunistic pathogens. *Journal of Clinical Microbiology*, 48(11), pp.3859-3869.

Niazi, S.A. and Bakhsh, A. (2022). Association between endodontic infection, its treatment and systemic health: a narrative review. *Medicina,* 58(7), 931.

Nichols, F.C. and Rojanasomsith, K. (2006). Porphyromonas gingivalis lipids and diseased dental tissues. *Oral Microbiology and Immunology,* 21(2), pp.84-92.

Nie, R. Wu, Z. Ni, J. Zeng, F. Yu, W. Zhang, Y. Kadowaki, T. Kashiwazaki, H. Teeling, J.L. and Zhou, Y. (2019). Porphyromonas gingivalis Infection Induces Amyloid-β Accumulation in Monocytes/Macrophages. *Journal of Alzheimer's Disease*, 72(2), pp.479-494.

Nonaka, S., Okamoto, R., Katsuta, Y., Kanetsuki, S. and Nakanishi, H. (2024). Gingipain-carrying outer membrane vesicles from Porphyromonas gingivalis cause barrier dysfunction of Caco-2 cells by releasing gingipain into the cytosol. *Biochemical and Biophysical Research Communications*, 707, 149783.

Nordengen, K., Kirsebom, B.E., Henjum, K., Selnes, P., Gísladóttir, B., Wettergreen, M., Torsetnes, S.B., Grøntvedt, G.R., Waterloo, K.K., Aarsland, D., Nilsson, L.N.G. and Fladby, T. (2019). Glial activation and inflammation along the Alzheimer's disease continuum. *Journal of Neuroinflammation,*16(1), 46.

O'Brien, R.J. and Wong, P.C. (2011). Amyloid precursor protein processing and Alzheimer's disease. *Annual Review of Neuroscience*, 34, pp.185-204.

Öçbe, M., Çelebi, E. and Öçbe, Ç.B. (2025). An overlooked connection: oral health status in patients with chronic diseases. *BMC Oral Health*, 25(1), 314.

Olsen, I, and Potempa, J. (2014). Strategies for the inhibition of gingipains for the potential treatment of periodontitis and associated systemic diseases. *Journal of Oral Microbiology*, 6(1).

Olsen, I. and Singhrao, S.K. (2015). Can oral infection be a risk factor for Alzheimer's disease? *Journal of Oral Microbiology*, 7(1), 29143.

Olsen, I. and Singhrao, S.K. (2018). Importance of heterogeneity in *Porphyromonas gingivalis* lipopolysaccharide lipid A in tissue specific inflammatory signaling. *Journal of Oral Microbiology*, 10(1), 1440128.

Olsen, I. and Singhrao, S.K. (2019). Is there a link between genetic defects in the complement cascade and Porphyromonas gingivalis in Alzheimer's disease? *Journal of Oral Microbiology*, 12(1), 167648.

Olsen, I., Taubman, M.A. and Singhrao, S.K. (2016). Porphyromonas gingivalis suppresses adaptive immunity in periodontitis, atherosclerosis and Alzheimer's disease. *Journal of Oral Microbiology*, 8, 33029.

Onyango, I.G., Jauregui, G.V., Čarná, M., Bennett Jr, J.P. and Stokin, G.B. (2021). Neuroinflammation in Alzheimer's Disease. *Biomedicines*, 9(5), 524.

Orlandi, M., Graziani, F. and D'Aiuto, F. (2020). Periodontal therapy and cardiovascular risk. *Periodontology 2000*, 83(1), pp.107-124.

Ossenkoppele, R., Smith, R., Mattsson-Carlgren, N., Groot, C., Leuzy, A., Strandberg, O., Palmqvist, S., Olsson, T., Jögi, J., Stormrud, E., Cho, H., Ryu, Y.H., Choi, J.Y., Boxer, A.L., Gorno-Tempini, M.L., Miller, B.L., Soleimani-Meigooni, D., Iaccarino, L., La Joie, R., Baker, S., Borroni, E., Klein, G., Pontecorvo, M.J., Devous, M.D.Sr., Jagust, W.J., Lyoo, C.H., Rabinovici, G.D. and Hansson, O. (2021). Accuracy of Tau positron emission tomography as a prognostic marker in preclinical and prodromal Alzheimer disease: A head-to-head comparison against amyloid positron emission tomography and magnetic resonance imaging. *JAMA Neurology*,78(8), pp.961-971.

O'Toole, P.J., Morrison, I.E. and Cherry, R.J. (2000). Investigations of spectrin-lipid interactions using fluoresceinphosphatidylethanolamine as a membrane probe. *Biochimica et Biophysica Acta*, 1466(1-2), pp.39-46.

Otsuka, N., Tomonaga, M. and Ikeda K. (1991). Rapid appearance of beta-amyloid precursor protein immunoreactivity in damaged axons and reactive glial cells in rat brain following needle stab injury. *Brain Research*, 568(1-2), pp.335-338.

Paganini-Hill, A,. White, S.C. and Atchison, K.A. (2012). Dentition, dental health habits, and dementia: the Leisure World Cohort Study. Journal of the American Geriatric Society, 60(8), pp.1556-1563.

Palmeri, A., Ricciarelli, R., Gulisano, W., Rivera, D., Rebosio, C., Calcagno, E., Tropea, M.R., Conti, S., Das, U., Roy, S., Pronzato, M.A., Arancio, O., Fedele, E. and Puzzo, D. (2017). Amyloid-β Peptide Is Needed for cGMP-Induced Long-Term Potentiation and Memory. *The Journal of Neuroscince*, 37(29), pp.6926-6937.

Panza, F., Lozupone, M., Logroscino, G and Imbimbo, B.P. (2019). A critical appraisal of amyloid-β-targeting therapies for Alzheimer disease. *Nature Reviews Neurology*, 15(2), pp.73-88.

Papapanou, P.N. (1996). Periodontal diseases: Epidemiology. *Annals of Periodontology*, 1(1), pp.1-36.

Parahitiyawa, N.B., Jin, L.J., Leung, W.K., Yam, W.C. and Samaranayake, L.P. (2009). Microbiology of odontogenic bacteremia: beyond endocarditis. *Clinical Microbiology Reviews*, 22(1), pp.46-64

Paris, I., Savage, J.C., Escobar, L., Abiega, O., Gagnon, S., Hui, C.W., Tremblay, M.E., `Sierra, A. and Valero, J. (2018). ProMoIJ: A new tool for automatic three-dimensional analysis of microglial process motility. *GLIA*, 66(4), pp.828-845.

Park, J., Kim, S., Lee, S.M., Baek, H. and Shin, D.S. (2025). Rapid detection of Lys-gingipain using fluorogenic peptide substrate for diagnosis of periodontitis. *Journal of Dental Sciences*, 20(2), pp.802-810.

Park, D.H., Tak, E.J., Park, OJ. et al. (2025) Association between root canals and gingival sulci microbiota in secondary and persistent endodontic infections. Sci Rep 15, 11253.

Passarella, D. and Goedert, M. (2018). Beta-sheet assembly of Tau and neurodegeneration in Drosophila melanogaster. *Neurobiology of Aging*, 72, pp.98-105.

Paster, B.J., Olsen, I., Aas, J.A. and Dewhirst, F.E. (2006). The breadth of bacterial diversity in the human periodontal pocket and other oral sites. *Periodontology 2000*, 42(1), pp.80-87.

Patel, J., Wallace, J., Doshi, M., Gadanya, M., Ben Yahya, I., Roseman, J. and Srisilapanan, P. (2021). Oral health for healthy ageing. *The Lancet Healthy Longevity*, 2(8), e521-e527.

Patterson, C., Feightner, J.W., Garcia, A., Hsiung, G.Y.R., MacKnight, C. and Sadovnick, A.D. (2008). Diagnosis and treatment of dementia: 1. Risk assessment and primary prevention of Alzheimer disease. *Canadian Medical Association Journal*, 178(5), pp.548-556.

Paula-Lima, A.C., Melgar-Rodriguez, S. and Carrillo, B. (2022). Gingival crevicular fluid as biomarker's source for Alzheimer's disease. *Odovtos International Journal of Dental Sciences*, 24(1), pp.156-176.

Pérez, M., Valpuesta, J.M., Medina, M., Montejo de Garcini, E. and Avila, J. (1996). Polymerization of tau into filaments in the presence of heparin: the minimal sequence required for tau-tau interaction. *Journal of Neurochemistry*, 67(3), pp.1183-1190.

Perry, G., Kawai, M., Tabaton, M., Onorato, M., Mulvihill, P., Richey, P., Morandi, A., Connolly, J.A. and Gambetti, P. (1991). Neuropil threads of Alzheimer's disease show a marked alteration of the normal cytoskeleton. The *Journal of Neuroscience*, 11(6), pp.1748-1755.

Peters, R. (2006). Ageing and the brain. *Postgraduate Medical Journal*, 82(964), pp.84-88.

Pfundstein, G., Nikonenko, A.G. and Sytnyk, V. (2022). Amyloid precursor protein (APP) and amyloid β (Aβ) interact with cell adhesion molecules: Implications in Alzheimer's disease and normal physiology. *Frontiers in Cell and Developmental Biology*, 10, 969547.

Pisa, D., Alonso, R., Rabano, A., Rodal, I. and Carrasco, L. (2015). Different brain regions are infected with fungi in Alzheimer's disease. *Scientific Reports*, 5, 15015.

Pisa, D., Alonso, R., Juarranz, A., Rábano, A. and Carrasco, L. (2015). Direct visualization of fungal infection in brains from patients with Alzheimer's disease. *Journal of Alzheimer's Disease*, 43(2), pp.613-624

Plattner, F., Angelo, M. and Giese, K.P. (2006). The roles of cyclin-dependent kinase 5 and glycogen synthase kinase 3 in tau hyperphosphorylation. *Journal of Biological Chemistry*, 281(35), pp.25457-25465.

Poole, S., Singhrao, S.K., Kesavalu, L., Curtis, M.A. and Crean, S.J. (2013). Determining the presence of periodontopathic virulence factors in short-term post-mortem Alzheimer's disease brain tissue. *Journal of Alzheimer's Disease*, 36(4), pp.665.677.

Poole, S., Singhrao, S.K., Chukkapalli, S., Rivera, M., Velsko, I., Kesavalu, L. and Crean, S.J. (2015). Active infection of Porphorymonas gingivalis and infection-induced complement activation in ApoE-/-mice brains. Journal of Alzheimer's Disease, 43(1), pp.67-80.

Preshaw, P.M., Alba, A.L., Herrera, D., Jepsen, S., Konstantinidis, A., Makrilakis, K. and Taylor, R. (2012). Periodontitis and diabetes: a two-way relationship. *Diabetologia*, 55(1), pp.21-31.

Prince, M., Ali, G.C., Guerchet, M., Prina, A.M., Albanese, E. and Wu, Y.T. (2016). Recent global trends in the prevalence and incidence of dementia, and survival with dementia. *Alzheimer's Research & Therapy,* 8(1), 23.

Puzzo, D., Privitera, L., Fa', M., Staniszewski, A., Hashimoto, G., Aziz, F., Sakurai, M., Ribe, E.M., Troy, C.M., Mercken, M., Jung, S.S., Palmeri, A. and Arancio, O. (2011). Endogenous amyloid-β is necessary for hippocampal synaptic plasticity and memory. *Annals of Neurology*, 69(5), pp.819-830.

Qiu, C., Kivipelto, M. and von Strauss, E. (2009). Epidemiology of Alzheimer's disease: occurrence, determinants, and strategies toward intervention. *Dialogues in Clinical Neuroscience,* 11(2), pp.111-128.

Quan, B.D., and Sone, E.D. (2013). Cryo-TEM analysis of collagen fibrillar structure. *Methods Enzymol*, 532, pp.189-205.

Quinn, J.P., Corbett, N.J., Kellett, K.A.B. and Hooper, N.M. (2018). Tau Proteolysis in the Pathogenesis of Tauopathies: Neurotoxic Fragments and Novel Biomarkers. *Journal of Alzheimer's Disease*, 63(1), pp.13-33.

Rangarajan M, Aduse-Opoku J, Hashim A, Paramonov N, Curtis MA. Characterization of the α- and β-mannosidases of Porphyromonas gingivalis (2013) *Journal of Bacteriology* Dec;195(23):5297-307.

Relvas, M., Mendes-Frias, A., Gonçalves, M., Salazar, F., López-Jarana, P., Silvestre, R. and Viana da Costa, A. (2024). Salivary IL-1β, IL-6, and IL-10 Are Key Biomarkers of Periodontitis Severity. *International Journal of Molecular Sciences*, 25(15), 8401.

Reynolds, E.S. (1963). The use of lead citrate at high pH as an electron opaque stain in the electron microscopy. *Journal of Cell Biology*, 17(1), pp.208-212.

Rhodius-Meester, H.F.M., Tijms, B.M., Lemstra. A.W., Prins. N.D., Pijnenburg, Y.A.L., Bouwman, F., Scheltens. P. and van der Flier, W.M. (2019). Survival in memory clinic cohort is short, even in young-onset dementia. *Journal of Neurology, Neurosurgery & Psychiatry*, 90(6), pp.726-728.

Ribeiro, G.R., Costa, J.L.R., Ambrosano, G.M.B. and Garcia, R.C.M.R. (2012). Oral health of the elderly with Alzheimer's disease. *Oral Surgery Oral Medicine Oral Pathology Oral Radiology*, 114(3), pp.338-343.

Ricciarelli, R. and Fedele, E. (2017). The amyloid cascade hypothesis in Alzheimer's disease: it's time to change our mind. *Current Neuropharmacology*, 15(6), pp.926-935.

Ricucci, D. Siqueira, J.F.Jr., and Rôças, I.N (2021). Pulp response to periodontal disease: novel observations help clarify the processes of tissue breakdown and infection. *Journal of Endodontics*, 47, pp.740-754.

Riegerová, P., Brejcha, J., Bezděková, D., Chum, T., Mašínová, E,. Čermáková. N., Ovsepian, S.V., Cebecauer, M. and Štefl M. (2021). Expression and Localization of AβPP in SH-SY5Y Cells Depends on Differentiation State. *Journal of Alzheimer's Disease*, 82(2), pp.485-491.

Rocas, I.N., Siqueira, J.F.Jr. and Santos, K.R.N. (2004). Association of Enterococcus faecalis with different forms of periradicular diseases. *Journal of Endodontics*, 30(5), pp.315-320.

Roda, A.R., Serra-Mir, G., Montoliu-Gaya, L., Tiessler, L. and Villegas, S. (2022). Amyloid-beta peptide and tau protein crosstalk in Alzheimer's disease. *Neural Regeneration Research*, 17(8), pp.1666-1674.

Rogers, J., Strohmeyer, R., Kovelowski, C.J. and Li, R. (2002). Microglia and inflammatory mechanisms in the clearance of amyloid beta peptide. *GLIA*, 40(2), pp.260-269.

Rokad, F., Moseley, R., Hardy, R.S., Chukkapalli, S., Crean, S.J., Kesavalu, L. and Singhrao, S.K. (2017). Cerebral oxidative stress and microvasculature defects in TNF-a expressing transgenic and Porphyromonas gingivalis-infected ApoE–/–mice. *Journal of Alzheimer's Disease*, 60(3), pp.359-369.

Rolim, T.de.S., Fabri, G.M.C., Nitrini, R., Anghinah, R., Teixeira, M.J., Siqueira, J.T., Cesari, J.A.F. and Siqueira, S.R.D. (2014). Evaluation of patients with Alzheimer's disease before and after dental treatment. *Arquivos de Neuro-Psiquiatria (Archives of Neuropsychiatry)*, 72(12), pp.919-24.

Rosen, J., Sancheti, P., Fierlinger, A., Niazi, F., Johal, H. and Bedi, A. (2017). Response to: important considerations when determining the cost-effectiveness of viscosupplements in the treatment of knee osteoarthritis. *Advances in Therapy*, 33(12), pp.2273-2276.

Rosenblum, W.I. (2002). Structure and location of amyloid beta peptide chains and arrays in Alzheimer's disease: new findings require reevaluation of the amyloid hypothesis and of tests of the hypothesis. *Neurobiology of Aging,* 23(2), pp.225-230.

Rossjohn, J., Cappai, R., Feil, S.C., Henry, A., McKinstry, W.J., Galatis, D., Hesse, L., Multhaup, G., Beyreuther. K., Masters, C.L. and Parker, M.W. (1999). Crystal structure of the N-terminal, growth factor-like domain of Alzheimer amyloid precursor protein. *Nature Structural & Molecular Biology*, 6(4), pp.327-331.

Rupf, S., Kannengießer, S., Merte, K., Pfister, W., Sigusch, B. and Eschrich, K. (2000). Comparison of profiles of key periodontal pathogens in periodontium and endodontium. *Dental Traumatology*, 16(6), pp.269–275.

Ryder, M.I. (2020). *Porphyromonas gingivalis* and Alzheimer disease: Recent findings and potential therapies. *Journal of Periodontology*, 91(1), pp.45-49.

Sabbagh, M.N. and Decourt, B. (2022). COR388 (atuzaginstat): an investigational gingipain inhibitor for the treatment of Alzheimer disease. *Expert Opinion on Investigational Drugs*, 31(10), pp.987-993.

Salehi, A., Ashford, J.W. and Mufson, E.J. (2016). The link between Alzheimer's disease and Down syndrome. A historical perspective. *Current Alzheimer Research*, 13(1), pp.2-6.

Salloway, S.P., Sevingy, J., Budur, K., Pederson, J.T., DeMattos, R.B., Von Rosenstiel, P., Paez, A., Evans, R., Weber, C.J., Hendrix, J.A., Worley, S., Bain, L.J. and Carrillo, M.C. (2020). Advancing combination therapy for Alzheimer's disease. *Alzheimer's & Dementia,* 6(1), e12073.

Sandros, J., Papapanou, P.N., Nannmark, U. and Dahlén, G. (1994). Porphyromonas gingivalis invades human pocket epithelium in vitro. *Journal of Periodontal Research*, 29(1), pp.62-69.

Sansores-Espana, L.D., Melgar-Rodriguez, S., Olivares-Sagredo, K., Cafferata, E.A., Martinez-Aguilar, V.M., Vernal, R., Paula-Lima, A.C. and Diaz-Zuniga, J. (2021). Oral-gut-brain axis in experimental models of periodontitis: Associating gut dysbiosis with neurodegenerative diseases. *Frontiers in Aging*, 2, 781582.

Schedin-Weiss S, Winblad B, Tjernberg LO. (2014)The role of protein glycosylation in Alzheimer disease. *Federation of European Biochemical Societies Journal*, 281(1):46-62.

Serrano-Pozo, A., Das, S. and Hyman, B.T. (2021). APOE and Alzheimer's disease: advances in genetics, pathophysiology, and therapeutic approaches. The Lancet Neurology, 20(1), pp.68-80.

Shafiei, S.S., Guerrero-Munoz, M.J. and Castillo-Carranza, D.L. (2017). Tau oligomers: cytotoxicity, propagation, and mitochondrial damage. *Frontiers in Aging Neuroscience,* 9, 83.

Shaftel, S.S., Kyrkanides, S., Olschowka, J.A., Miller, J.H., Johnson, R.E. and O'Banion, M.K. (2007). Sustained hippocampal IL-1 beta overexpression mediates chronic neuroinflammation and ameliorates Alzheimer plaque pathology. *Journal of Clinical Investigation*, 117(6), pp.1595-1604.

Sharma, A.N., Elased, K.M., Garrett, T.L. and Lucot, J.B. (2010). Neurobehavioral deficits in db/db diabetic mice. *Physiology & Behaviour*, 101(3), pp.381-388.

Shen, H., Jiang, Y., Qiu, C., Xie, X., Zhang, H., He, Z., Song, Z. and Zhou, W. (2024). Abnormal amyloid precursor protein processing in periodontal tissue in a murine model of periodontitis induced by Porphyromonas gingivalis. *Journal of Periodontal Research*, 59(2), pp.395-407.

Sheng, J.G., Bora, S.H., Xu, G., Borchelt, D.R., Price, D.L. and Koliatsos, V.E. (2003). Lipopolysaccharide-induced-neuroinflammation increases intracellular accumulation of amyloid precursor protein and amyloid beta peptide in APPswe transgenic mice. *Neurobiology of Disease*, 14(1), pp.133-145.

Shipley, M.M., Mangold, C.A. and Szpara, M.L. (2016). Differentiation of the SH-SY5Y Human Neuroblastoma Cell Line. *Journal of Visualized Experiments*, (108), 53193.

Siddiqui, H., Eribe, E.R.K., Singhrao, S.K., and Olsen, I. (2019). High throughput sequencing detect gingivitis and periodontal oral bacteria in Alzheimer's disease autopsy brains. *Neuro Research*, 1(1)3.

Silhavy, T.J., Kahne, D., and Walker, S. (2010). The bacterial cell envelope. *Cold Spring Harbor Perspectives in Biology*, 2(5).

Simon, J.H., Glick, D.H. and Frank, A.L. (1972). The relationship of endodontic-periodontic lesions. *Journal of Periodontology*, 43(4), pp.202-208.

Singh, A., Rouxel, P., Watt, R.G. and Tsakos, G. (2013). Social inequalities in clustering of oral health related behaviors in a national sample of British adults. *Preventive Medicine*, 57(2), pp.102-106.

Singhrao, S.K., Chukkapalli, S., Poole, S., Velsko, I., Crean, S.J. and Kesavalu, L. (2017). Chronic *Porphyromonas gingivalis* infection accelerates the occurrence of age-related granules in ApoE– / – mice brains. *Journal of Oral Microbiology.* 9(1). 1270602.

Singhrao, S.K., Cole, G., Henderson, W.J. and Newman, G.R. (1990). LR White embedding allows a multi-method approach to the analysis of brain tissue from patients with Alzheimer's disease. *Journal of Histochemistry,* 22(5), pp.257-268.

Singhrao, S.K., Consoli, C., Dennison, S.R., Kanagasingam, S. and Welbury, R. (2024). Porphyromonas gingivalis LPS and actinomyces naeslundii conditioned medium enhance the release of a low molecular weight, transcriptionally active, fragment of glycogen synthase-3 kinase in IMR-32 cell line. *Journal of Alzheimer's Disease Reports*, 8(1), pp.1055-1067.

Singhrao, S.K. and Olsen, I. (2018). Are *Porphyromonas gingivalis* outer membrane vesicles, microbullets for sporadic Alzheimer's disease manifestation? *Journal of Alzheimer's Diseases Reports*, 2(1), pp.219-228.

Sipe, J.D. and Cohen, A.S. (2000). Review: history of the amyloid fibril. *Journal of Structural Biology*, 130(2-3), pp.88-98.

Siqueira, J.F.Jr. (2001). Strategies to treat infected root canals. *Journal of the California Dental Association*, 29(12), pp.825-837.

Siqueira, J.F.Jr. and Rocas, I.N. (2009). Diversity of endodontic microbiota revisited. *Journal of Dental Research*, 88(11), pp.969-981.

Siqueira, J.F.Jr. and Rocas, I.N. (2022). A critical analysis of research methods and experimental models to study the root canal microbiome. *International Endodontic Journal*, 55(1), pp.46-71.

Siqueira JF Jr, Rôças IN. Present status and future directions: Microbiology of endodontic infections. Int Endod J. 2022 May;55 Suppl 3:512-530

Siqueira, J.F.Jr, Rocas, I.N. and Silva, M.G. (2008). Prevalence and clonal analysis of Porphyromonas gingivalis in primary endodontic infections. *Journal of Endodontics*, 34(11), pp.1332-1336.

Sleutel, M., Pradhan, B., Volkov, A.N. and Remaut, H. (2023). Structural analysis and architectural principles of the bacterial amyloid curli. *Nature Communications*, 14(1), pp.2822.

Sleutel M, Remaut H. (2025) Structural insights into Escherichia coli CsgA amyloid fibril assembly revisited. mBio. Aug 13;16(8):e0079525

Smalley, J.W. and Olczak, T. (2017). Heme acquisition mechanisms of Porphyromonas gingivalis - Strategies used in a polymicrobial community in a heme-limited host environment. *Molecular Oral Microbiology*, 32(1), pp.1-23.

Socransky, S.S., Haffajee, A.D., Cugini, M.A., Smith, C. and Kent, R.L.Jr. (1998). Microbial complexes in subgingival plaque. *Journal of Clinical Periodontology*, 25(2), 134-144.

Song, I.S., Han, K., Park, Y.M., Ji, S., Jun, S.H., Ryu, J.J. and Park, J.B. (2016).
Severe Periodontitis Is Associated with Insulin Resistance in Non-abdominal Obese Adults. *The Journal of Clinical Endocrinology & Metabolism*, 101(11), pp.4251-4259.

Song, H., Cheng, Y., Wang, X., Hong, X., Guo, Z., Li, H., Li, L. and Wang, P. (2025). The evaluation of Congo red staining combined with fluorescence microscopy in the diagnosis of primary cutaneous amyloidosis. *The Journal of Dermatology*, 52(2), pp.281-290.

Sonntag, D. and Peters, O.A. (2007). Effect of prion decontamination protocols on nickel-titanium rotary surfaces. *Journal of Endodontics*, 33(4), pp. 442-446.

Soscia, S.J., Kirby, J.E., Washicosky, K.J., Tucker, S.M., Ingelsson, M., Hyman, B., Burton, M.A., Goldstein, L.E., Duong, S., Tanzi, R.E. and Moir, R.D. (2010). The Alzheimer's disease-associated amyloid b-protein is an antimicrobial peptide. *PLoS One*, 5(3), e9505.

Soto, C. and Satani, N. (2011). The intricate mechanisms of neurodegeneration in prion diseases. *Trends Mol Med*, 17(1), pp.14-24.

Sparks Stein, P., Steffen. M.J., Smith, C., Jicha, G., Ebersole, J.L., Abner, E. and Dawson D 3rd. (2012). Serum antibodies to periodontal pathogens are a risk factor for Alzheimer's disease. *Alzheimer's & Dementia*, 8(3), pp.196-203.

Sperling, R.A., Aisen, P.S., Beckett, L.A., Bennett, D.A., Craft, S., Fagan, A.M., Iwatsubo, T., Jack, C.R.Jr., Kaye, J., Montine, T.J., Park, D.C., Reiman, E.M., Rowe, C.C., Siemers, E., Stern, Y., Yaffe, K., Carrillo, M.C., Thies, B., Morrison-Bogorad, M., Wagster, M.V. and Phelps, C.H. (2011). Toward defining the preclinical stages of Alzheimer's disease: recommendations from the National Institute on Aging-Alzheimer's Association workgroups on diagnostic guidelines for Alzheimer's disease. *Alzheimer's & Dementia*, 7(3), pp.280-292.

Spitzer, P., Condic, M., Herrmann, M., Oberstein, T.J., Scharin-Mehlmann, M., Gilbert, D.F., Friedrich, O., Grömer, T., Kornhuber, J., Lang, R. and Maler, J.M. (2016). Amyloidogenic amyloid-β-peptide variants induce microbial agglutination and exert antimicrobial activity. *Scientific Reports*, 6, 32228.

Sreerama, N., Venyaminnov, S.Y. and Woody, R.W. (1999). Estimation of the number of alpha-helical and beta-strand segments in proteins using circular dicroism spectroscopy. *Protein Science*, 8(2), pp.370-380.

Sreerama, N. and Woody, R.W. (1993). A self-consistent method for the analysis of protein secondary structure from circular dicroism. *Analytical Biochemistry*, 209(1), pp.32-44.

Stashenko, P., Teles, R. and D'Souza, R. (1998). Periapical inflammatory responses and their modulation. *Critical Reviews in Oral Biology & Medicine*, 9(4), pp.498-521.

Stein, P.S., Desrosiers, M., Donegan, S.J., Yepes, J.F. and Kryscio, R.J. (2007). Tooth loss, dementia and neuropathy in the Nun study. *The Journal of the American Dental Association*, 138(10), pp.1314-1322.

Stein, P.S., Steffen, M.J., Smith, C., Jicha, G., Ebersole, J.L., Abner, E. and Dawson, D.3rd. (2012). Serum antibodies to periodontal pathogens are a risk factor for Alzheimer's disease. *Alzheimer's & Dementia*, 8(3), pp.196-203.

Sunde, M., Serpell, L.C., Bartlam, M., Fraser, P.E., Pepys, M.B. and Blake, C.C. (1997). Common core structure of amyloid fibrils by synchrotron x-ray diffraction. *Journal of Molecular Biology*, 273(3), pp.729-739.

Sundqvist, G. (1994). Taxonomy, ecology, and pathogenicity of the root canal flora. *Oral Surgery, Oral Medicine, Oral Pathology and Oral Radiology*, 78(4), pp.522-530.

Suvan, J.E., D'Aiuto, F., Moles, D.R., Petrie, A. and Donos, N. (2011). Association between overweight/obesity and periodontitis in adults. A systematic review. *Obesity Reviews*, 12(5), pp.e381-e404.

Suvan, J.E., Petrie, A., Nibali, L., Darbar, U., Rakmanee, T., Donos, N. and D'Aiuto, F. (2015). Association between overweight/obesity and increased risk of periodontitis. *Journal of Clinical Periodontology*, 42(8), pp.733-739.

Swardfager, W., Lanctot, K., Rothenburg, L., Wong, A., Cappell, J. and Herrmann N. (2010). A meta-analysis of cytokines in Alzheimer's disease. *Biological Psychiatry*, 68(10), pp.930-941.

Sweeney, M.D., Sagare, A.P. and Zlokovic, B.V. (2018). Blood-brain barrier breakdown in Alzheimer disease and other neurodegenerative disorders. *Nature Reviews Neurology*. 14(3), pp.133-150.

Syrjälä, A.M.H., Ylöstalo, P., Ruoppi, P., Komulainen, K., Hartikainen, S., Sulkava, R. and Knuuttila, M. (2012). Dementia and oral health among subjects aged 75 years or older. *Gerodontology*, 29(1), pp.36-42.

Taglialegna, A., Matilla-Cuenca, L., Dorado-Morales, P., Navarro, S., Ventura, S., Garnett, J.A., Lasa, I. and Valle, J. (2020). The biofilm-associated surface protein Esp of Enterococcus faecalis forms amyloid-like fibers. *NPJ Biofilms and Microbiomes*, 6(1), 15.

Takemura, N., Noiri, Y., Ehara, A., Kawahara, T., Noguchi, N. and Ebisu, S. (2004). Single species biofilm-forming ability of root canal isolates on gutta-percha points. *European Journal of Oral Sciences*, 112(6), pp.523-529.

Taylor, C.G. and Staniforth, R.A. (2022) General principles underpinning amyloid structure. Frontiers in Neuroscience, 16, p.878869.

Terry, R.D. (1963). The fine structure of neurofibrillary tangles in Alzheimer's disease. *Journal of Neuropathology & Experimental Neurology*, 22(4), pp.629-642.

Tomás, I., Diz, P., Tobías, A., Scully, C. and Donos, N. (2012). Periodontal health status and bacteraemia from daily oral activities: systematic review/meta-analysis. *Journal of Clinical Periodontology*, 39(3), pp.213-228.

Tonetti, M.S., D'Aiuto, F., Nibali, L., Donald, A., Storry, C., Parkar, M., Suvan, J., Hingorani, A.D., Vallance, P. and Deanfield, J. (2007). Treatment of periodontitis and endothelial function. *The New England Journal of Medicine*, 356(9), pp.911-920. Erratum in: *The New England Journal of Medicine*, Jun 2018, 378(25), 2450.

Troseid, M., Nestvold, T.K., Rudi, K., Thoresen, H., Nielsen, E.W. and Lappegard, K.T. (2013). Plasma lipopolysaccharide is closely associated with glycemic control and abdominal obesity: evidence from bariatric surgery. *Diabetes care*, 36(11), pp.3627-3632.

Tsoi, L.M., Wong, K.Y., Liu, Y.M. and Ho, Y.Y. (2007). Apoprotein E isoform-dependent expression and secretion of pro-inflammatory cytokines TNF-alpha and IL-6 in macrophages. *Archives of Biochemistry and Biophysics*, 460(1), pp.33-40.

Vaillant-Beuchot, L., Mary, A., Pardossi-Piquard, R., Bourgeois, A., Lauritzen, I., Eysert, F., Kinoshita, P.F., Cazareth, J., Badot, C., Fragaki, K., Bussiere, R., Martin, C., Mary, R., Bauer, C., Pagnotta, S., Paquis-Flucklinger, V., Buée-Scherrer, V., Buée, L., Lacas-Gervais, S., Checler, F. and Chami, M. (2021). Accumulation of amyloid precursor protein C-terminal fragments triggers mitochondrial structure, function, and mitophagy defects in Alzheimer's disease models and human brains. *Acta Neuropathologica*, 141(1), pp.39-65.

van der Lee, S.J., Wolters, F.J., Ikram, M.K., Hofman, A., Ikram, M.A., Amin. N. and van Duijn, C.M. (2018). The effect of APOE and other common genetic variants on the onset of Alzheimer's disease and dementia: a community-based cohort study. *The Lancet Neurology*, 17(5), pp.434-444.

van Gils, M., Jumde, V.R., Haldar, S., Preet, S. and Höök, F. (2020) The hydrophobic effect characterises the thermodynamic signature of amyloid fibril growth. Communications Biology, 3(1), p.302.

Varghese, S.S., Thomas, H., Jayakumar, N.D., Sankari, M., Lakshmanan, R. (2015). Estimation of salivary tumor necrosis factor-alpha in chronic and aggressive periodontitis patients. *Contemporary Clinical Dentistry*, 6(1), pp.152-156.

Vernal, R., Diaz-Guerra, E., Silva, A., Sanz, M. and Garcia-Sanz, J.A. (2014). Distinct human T-lymphocyte responses triggered by Porphyromonas gingivalis capsular serotypes. *Journal of Clinical Periodontology*, 41(1), pp.19-30.

Vernal, R., Leon, R., Silva, A., van Winkelhoff, A.J., Garcia-Sanz J.A. and Sanz, M. (2009). Differential cytokine expression by human dendritic cells in response to different porphyromonas gingivalis capsular serotypes. *Journal of Clinical Periodontology*, 36(1), pp.823-829.

Villar, A., Paladini, S. and Cossatis, J. (2024). Periodontal disease and Alzheimer's: insights from a systematic literature network analysis. *The Journal of Prevention of Alzheimer's Disease*, 11(4), pp.1148-1165.

Von Bergen, M., Friedhoff, P., Biernat, J., Heberle, J., Mandelkow, E.M. and Mandelkow, E. (2000). Assembly of tau protein into Alzheimer paired helical filaments depends on a local sequence motif ((306)VQIVYK(311)) forming beta structure. *Proceedings of the National Academy of Sciences (PNAS)*, 97(10), pp.5129-5134.

Vulders, R.C.M., van Hoogenhuizen, R.C., van der Giessen, E. and van der Zaag, P.J. (2021). Clearing-induced tissue shrinkage: A novel observation of a thickness size effect. *PLoS One*, 16(12), e0261417.

Walker, J.T., Dickinson, J., Sutton, J.M., Raven, N.D. and Marsh, P.D. (2007). Cleanability of dental instruments - implications of residual protein and risks from Creutzfeldt-Jakob disease. *British Dental Journal*, 203(7), pp.395-401.

Wall, J., Golding, C.A., Van Veen, M. and O'Shea, P. (1995) The use of fluoresceinphosphatidylethanolamine (FPE) as a real-time probe for peptide-membrane interactions. *Molecular Membrane Biology*, 12(2), pp.183-192.

Wan, J. and Fan, H. (2023). Oral Microbiome and Alzheimer's Disease. *Microorganisms*, 11(10), pp.2550.

Wan, L., Nie, G., Zhang, J. and Zhao, B. (2012). Overexpression of Human Wild-Type Amyloid-β Protein Precursor Decreases the Iron Content and Increases the Oxidative Stress of Neuroblastoma SH-SY5Y Cells. *Journal of Alzheimer's Disease*, 30(3), pp.523-530.

Wang, C., Cheng, T., Li, X. and Jin, L. (2020). Metronidazole-treated Porphyromonas gingivalis persisters invade human gingival epithelial cells and perturb innate responses. *Antimicrobial Agents and Chemotherapy*, 64(6), e02529-19.

Wang, J., Jiang, Y., Chen, W., Zhu, C. and Liang, J. (2012). Bacterial flora and extraradicular biofilm associated with the apical segment of teeth with post-treatment apical periodontitis. *Journal of Endodontics*, 38(1), pp.954-959.

Wang, J.H. and Sung, T.Y. (2024). ToxTeller: Predicting Peptide Toxicity Using Four Different Machine Learning Approaches. *ACS Omega*, 9(29), pp.32116-32123.

Wang, J.Z., Grundke-Iqbal, I. and Iqbal, K. (2007). Kinases and phosphatases and tau sites involved in Alzheimer neurofibrillary degeneration. *European Journal of Neuroscience*, 25(1), pp.59-68

Wang, Q., Nie, L., Zhao, P., Zhou, X., Ding, Y., Chen, Q. and Wang, Q. (2021). Diabetes fuels periodontal lesions via GLUT1-driven macrophage inflammaging. *International Journal of Oral Science*, 13(1), 11.

Watts, A., Crimmins, E.M. and Gatz, M. (2008). Inflammation as a potential mediator for the association between periodontal disease and Alzheimer's disease. *Neuropsychiatric Disease and Treatment*, 4(5), pp.865-876.

Weingarten, M.D., Lockwood, A.H., Hwo, S.Y. and Kirschner, M.W. (1975). A protein factor essential for microtubule assembly. *The Proceedings of the National Academy of Sciences (PNAS)*, 72(5), pp.1858-1862.

Weiss, E.I., Shaniztki, B., Dotan, M., Ganeshkumar, N., Kolenbrander, P.E. and Metzger, Z. (2000). Attachment of Fusobacterium nucleatum PK1594 to mammalian cells and its coaggregation with periodontopathogenic bacteria are mediated by the same galactose-binding adhesin. *Oral Microbiology and Immunology*, 15(6), pp.371-377.

Wesseling, H., Mair, W., Kumar, M., Schlaffner, C.N., Tang, S., Beerepoot, P., Fatou, B., Guise, A.J., Cheng, L., Takeda, S., Muntel, J., Rotunno, M.S., Dujardin, S., Davies, P., Kosik, K.S., Miller, B.L., Berretta, S., Hedreen, J.C., Grinberg, L.T., Seeley, W.W., Hyman, B.T.,

Steen, H. and Steen, J.A. (2020). Tau PTM profiles identify patient heterogeneity and stages of Alzheimer's disease. *Cell,* 183(6), pp.1699-1713.

White, M.R., Kandel, R., Tripathi, S., Condon, D., Qi, L., Taubenberger, J. and Hartshorn, K.L. (2014). Alzheimer's associated β-amyloid protein inhibits influenza A virus and modulates viral interactions with phagocytes. *PLoS One,* 9(7), e101364.

Whitmore, L. and Wallace, B.A. (2004). DICHROWEB, an online server for protein secondary structure analyses from circular dichroism spectroscopic data. *Nucleic Acids Research,* 32(2), pp.668-673.

Whitmore, L. and Wallace, B.A. (2008). Protein secondary structure analyses from circular dichroism spectroscopy: Methods and reference databases. *Biopolymers*, 89(5), pp.392-400.

Whitmore, L., Woollett, B., Miles, A.J., Janes, R.W. and Wallace, B.A. (2010). The protein circular dichroism data bank, a Web-based site for access to circular dichroism spectroscopic data. *Structure*, 18(10), pp.1267-1269

WHO/CDS/CSR/APH/2000, Centers for Disease Control and Prevention. (2003). Guidelines for infection control in dental health-care settings. *Morbidity and Mortality Weekly Report (MMWR),* 52.

WHO consultation. (1999). WHO infection control guidelines for transmissible spongiform encephalopathies. *World Health Organization Communicable Disease Surveillance and Control*, Geneva, Switzerland.

Witman, G.B., Cleveland, D.W., Weingarten, M.D. and Kirschner, MW. (1976). Tubulin requires tau for growth onto microtubule initiating sites. *The Proceedings of the National Academy of Sciences (PNAS)*, 73(11), pp. 4070-4074.

World Alzheimer Report 2018. The state of the art of dementia research: new frontiers. *Alzheimer's Disease International,* pp.1-48.

Wozniak, M.A., Mee, A.P. and Itzhaki, R.F. (2009). Herpes simplex virus type 1 DNA is located within Alzheimer's disease amyloid plaques. *The Journal of Pathology*, 217(1), pp.131-138.

Wu, L., Zhang, S.Q., Zhao, L., Ren, Z.H. and Hu, C.Y. (2022). Global, regional, and national burden of periodontitis from 1990 to 2019: Results from the Global Burden of Disease Study 2019. *Journal of Periodontology*, 93(10), pp.1445-1454.

Wu, Z., Ni, J., Liu, Y., Teeling, J.L., Takayama, F., Collcutt, A., Ibbett, P. and Nakanishi, H. (2017). Cathepsin B plays a critical role in inducing Alzheimer's disease-like phenotypes following chronic systemic exposure to lipopolysaccharide from Porphyromonas gingivalis in mice. *Brain, Behaviour and Immunity*, 65, pp.350-361.

Xia, Y., Prokop, S., Gorion, K.M., Kim, J.D., Sorrentino, Z.A., Bell, B.M., Manaois, A.N., Chakrabarty, P., Davies, P. and Giasson, B.I. (2020). Tau Ser208 phosphorylation promotes aggregation and reveals neuropathologic diversity in Alzheimer's disease and other tauopathies. *Acta Neuropathologica Communications*, 8(1), 88.

Xu, W., Zhou, W., Wang, H. and Liang, S. (2020). Roles of Porphyromonas gingivalis and its virulence factors in periodontitis. *Advances in Protein Chemistry and Structural Biology*, 120, pp.45–84.

Yáñez, L., Soto, C., Tapia, H., Pacheco, M., Tapia, J., Osses, G., Salinas, D., Rojas-Celis, V., Hoare, A., Quest, A.F.G., Díaz-Elizondo, J., Pérez-Donoso, J.M. and Bravo, D. (2024). Co-Culture of P. gingivalis and F. nucleatum Synergistically Elevates IL-6 Expression via TLR4 Signaling in Oral Keratinocytes. *International Journal of Molecular Sciences*, 25(7), 3611.

Yang, X., Bai, B., Zhang, Y., Aydin, M., Li, Y., Selcuk, S.Y., Casteleiro Costa, P., Guo, Z., Fishbein, G.A., Atlan, K., Wallace, W.D., Pillar, N. and Ozcan, A. (2024). Virtual birefringence imaging and histological staining of amyloid deposits in label-free tissue using autofluorescence microscopy and deep learning. *Nature Communications*, 15(1), 7978.

Yi, M., Li, T., Niu, M., Zhang, H., Wu, Y., Wu, K. and Dai, Z. (2024). Targeting cytokine and chemokine signaling pathways for cancer therapy. *Signal Transduction and Targeted Therapy* 9(1), 176.

Yiannopoulou, K.G., Anastasiou, A.I., Zachariou, V. and Pelidou, S.H. (2019). Reasons for failed trials of disease-modifying treatments for Alzheimer disease and their contribution in recent research. *Biomedicines*, 7(4), 97.

Yilmaz, Ö., Verbeke, P., Lamont, R.J. and Ojcius, D.M. (2006). Intercellular spreading of Porphyromonas gingivalis infection in primary gingival epithelial cells. *Infection and Immunity*, 74(1), pp.703-710.

Yoneda, M., Naka, S., Nakano, K., Wada, K., Endo, H., Mawatari, H., Imajo, K., Nomura, R., Hokamura, K., Ono, M., Murata, S., Tohnai, I., Sumida, Y., Shima, T., Kuboniwa, M., Umemura, K., Kamisaki, Y., Amano, A., Okanoue, T., Ooshima, T. and Nakajima, A. (2012). Involvement of a periodontal pathogen, Porphyromonas gingivalis on the pathogenesis of non-alcoholic fatty liver disease. *BMC Gastroenterology*, 12, 16.

Yoneyama, T., Yoshida, M., Ohrui, T., Mukaiyama, H., Okamoto, H., Hoshiba, K., Ihara, S., Yanagisawa, S., Ariumi, S., Morita, T., Mizuno, Y., Ohsawa, T., Akagawa, Y., Hashimoto, K. and Sasaki, H. (2002). Oral Care Working Group. Oral care reduces pneumonia in older patients in nursing homes. *Journal of the American Geriatrics Society*, 50(3), pp.430-433.

Zehnder, M., Gold, S.I. and Hasselgren, G. (2002). Pathologic interactions in pulpal and periodontal tissues. *Journal of Clinical Periodontology*, 29(8), pp.663-671.

Zeng, F., Liu, Y., Huang, W., Qing, H., Kadowaki, T., Kashiwazaki, H., Ni, J. and Wu, Z. (2021). Receptor for advanced glycation end products up-regulation in cerebral endothelial cells mediates cerebrovascular-related amyloid accumulation after Porphyromonas gingivalis infection. Journal of Neurochemistry, 158(3), pp.724-736.

Zhan, X., Stamova, B., Jin, L.W., DeCarli, C., Phinney, B. and Sharp, F.R. (2016). Gram-negative bacterial molecules associate with Alzheimer disease pathology. Neurology, 87(22), pp.2324- 2332.

Zhan, X., Stamova, B. and Sharp, F.R. (2018). Lipopolysaccharide associates with amyloid plaques, neurons and oligodendrocytes in Alzheimer's disease brain: A review. *Frontiers in Aging Neuroscience*, 10, 42.

Zhang, D., Hu, X., Qian, L., O'Callaghan, J.P. and Hong, J.S. (2010). Astrogliosis in CNS pathologies: is there a role for microglia? *Molecular Neurobiology*, 41(2-3), pp.232-41.

Zhang, H., Wei, W., Zhao, M., Ma, L., Jiang, X., Pei, H., Cao, Y. and Li, H. (2021). Interaction between Aβ and tau in the pathogenesis of Alzheimer's disease. *International Journal of Biological Sciences*, 17(9), pp.2181-2192.

Zhang, J., Yu, C., Zhang, X., Chen, H., Dong, J., Lu, W., Song, Z. and Zhou, W. (2018). Porphyromonas gingivalis lipopolysaccharide induces cognitive dysfunction, mediated by neuronal inflammation via activation of the TLR4 signaling pathway in C57BL/6 mice. *Journal of Neuroinflammation*, 15, 37.

Zhang, Y., Chen, H., Li, R., Sterling, K. and Song, W. (2023). Amyloid β-based therapy for Alzheimer's disease: challenges, successes and future. *Signal Transduction and Targeted Therapy*, 8(1), 248.

Zhang, Z., Liu, D., Liu, S., Zhang, S. and Pan, Y. (2021). The Role of Porphyromonas gingivalis Outer Membrane Vesicles in Periodontal Disease and Related Systemic Diseases. *Frontiers in Cellular and Infection Microbiology*, 10, 585917.

Zhao, M., Wang, Y., Shen, Y., Wei, C., Zhang, G. and Sun, L. (2024). A review of the roles of pathogens in Alzheimer's disease. *Frontiers in Neuroscience*, 18, 1439055.